Assistive System Based on Autonomous Attendant Model for Attendant Propelled Wheelchairs

学位授与平成２６年３月
関西大学審査学位論文

Assistive System Based on Autonomous Attendant Model for Attendant Propelled Wheelchairs

Thesis submitted to Kansai University for the degree of
Doctorate of Engineering

Tatsuto Suzuki

Department of Mechanical Engineering

March 2014

Table of contents

Abstract

This study focused on the individual propelling performance by force velocity relationship, and validated a proposed assisting control method based on the individual force velocity relationship. The force velocity relationship is well used to evaluate individual exercising performances, especially cycling. This study defined the individual force velocity relationship as the sustainable physical performance that an attendant maximises operating force under minimising subjective hardness.

A proposed assistive controller in this study generates assistive forces when the attendant propelling force exceeds an assist boundary force defined by the individual force velocity relationship. From this assisting rule, the proposed assistive system uses attendant propelling power up to the assist boundary force. The assist boundary force is easy to adjust to the individual propelling performance. Also by using assistive forces only when it is needed, the energy consumption in this system is reduced, and further, the attendant is able to use pushing the wheelchair as a form of moderate, controlled exercise to keep healthy. The main objectives in this studies were below.

1) Investigate the actual propelling load in the attendant propelled wheelchair on flat surface and longitudinal slopes, by operating forces, wheelchair velocity, walking pattern and each joint load. (Chapter 2)

2) Investigate the autonomous force velocity relationship in propelling on a motorised treadmill, by operating forces, walking velocity, walking pattern, postures, and heart rate. (Chapter 3)

3) Develop and validate an attendant-wheelchair model to design the assist controller. (Chapter 4)

4) Design and validate the assist as needed control with a powered attendant propelled wheelchair on real environments. (Chapter 5)

With findings of autonomous individual force velocity relationships, this study successfully showed desired performance of the proposed assist controller based on the force velocity relationship. From the summarised results, the proposed assistive system worked well in line with the control rule that the assistive system generates assistive forces as the attendant needed propelling force over the assist boundary force. This feature provides superior low energy consumption in the proposed assistive system compared with the common proportional assist controls, because the propelling force by attendants under the assist boundary force can continues under light subjective hardness similar to walking. The actual feelings by attendants with the proposed assistive system were similar

to the proportional assist control.

The proposed assist control in this study would be very useful to add an assistive system to the attendant propelled wheelchair as well as manual wheelchairs, hand cycles, and rehabilitation systems to control patients's load in line with rehabilitation progress.

Chapter 1 Introduction

The average life span becomes twice longer in the world in recent 200 years. At some countries, population ratio over 65 years old almost reaches 20% now. The welfare states in the world societies tries to keep aged people healthy and improve quality of life of them, despite the rapid increase of aged population. There are many reasons to drop the mortality rates. One is widespread of promotions of healthcare; such as encouraging exercises, improving nutrition and stopping bad habit like much drinking and smoking. Also the new treatment technologies are developed one by one. Under this situation, the aged people get longer life however a part of the aged people suffer physical disabilities from many diseases, in addition many of them are predicted to meet further disabilities. In countries with life prediction over 70 years old, people spend on average about eight years or 11.5 percent of their life span, living with disabilities. Guralnik 1995[1] found that about 85% of the aged over 70 years old in poor mobility suffers from walking disability.

In old age, decreased muscle strength and poor balance caused by ageing leads aged people to functional limitations and disability (Sakari-Rantala 1998[2]). Minimum levels of lower-extremity strength and the ability to maintain postural stability in the upright position are necessary for walking. The aged people are easy to be fatigued by prolonged gait, and the fatigue increases fall risks in elderly people because of loosing muscle strength in fatigue. Pereira 2011[3] found that the 20min walking in the treadmill are enough to induce fatigue in elderly people. Weakened muscle strength by ageing causes walking disability. For a mobility investigation to follow up four years on over 65 year aged, the 15% of follow-up participants with good mobility becomes walking disability. The mobility performances consisted of walking speed, rising from a chair and standing balance.

Also many diseases related to ageing cause walking disabilities. About 25% of people, who suffer from cerebrovascular diseases and osteoarthritis, needs to use mobility devices because of their poor mobility (Kaye 2000[4]). In rheumatoid arthritis, global pain and disease activity are related to walking disability during the first eight years, van der Leeden 2010[5] studied. And knee or hip osteoarthritis causes walking disability, which should focus on effective treatment of cardiovascular risk factors.(Nuesch 2011[6])

The situation that the walking disabilities in aged people increased by ageing and

diseases, attentions to public because of concerning the increase of health care cost.

Participating in social activities for aged people increases the quality of life as well as helps to preserve cognitive function, Glei reported in 2005[7]. The social activities are, for example, to see and help someone for exchange opinions and ideas, and to touch with nature for refreshment in mind. Also in-house mobility is very important in daily life, for example, go to toilet, bathroom, bed for sleep, dining room for having foods and talking with families. People have a right to go everywhere they want, and the independence improves quality of life in walking disabilities. Also Fries 1994[8] reports that older persons who engaged in aerobic activities have lower mortality and slower development of disabilities. This is probably associated with increased strength and organ reserve by physical loads in exercises. In other words, the aged people need some physical load to keep their health condition.

Walking disabilities use wheelchairs as mobility devices to assist moving. Wheelchairs are developed in old age, now its very common to use in our society. Some in-house activities in short distance is not easy for walking disabilities, but there are many possibilities to do because many ideas to move short distance away from a wheelchair are available, for example, using handrails and walkers. Changing the plan of a house also would improve it, for example, to place a bed room to near bathroom, or the portable toilet can be set near a bed. The distance, which walking disabilities can move by themselves, depends on the conditions of disability level in lower extremity. However, going outside is very difficult for walking disabilities, so the attendant uses the mobility devices to assist moving, such as wheelchairs.

The wheelchair propelled by attendant is called as the attendant-propelled wheelchairs, which have two straight bars in the back for driving by an attendant. The attendant-propelled wheelchairs generally have two small front casters and two rear wheels, which does not have hand rims in some types, because the occupant with severe walking disability is likely not to be able to push hand rims by hands. The attendant propelled wheelchairs with an attendant play a key role to support improved accessibility for walking disabilities.

The attendant propelled wheelchair is very useful to move and transfer people with walking disability. Basically the caster and wheels of the attendant-propelled wheelchairs reduce the load of propelling, however, the wheelchair weight with a disabled occupant

increase actual propelling load for the attendant. This is because the resistance force in wheelchairs by road surfaces is determined by the total wheelchair weight, which is distributed to normal forces at each caster and wheel.(van der Woulde 2003[9]) In addition, the gravity forces work toward downward direction on slopes, and the attendant have to exert operating forces against the gravity forces. Depends on the occupant weight, the total weight of the wheelchair with an occupant is likely to be over 100Kg, or even greater if the occupant is obese. From this point, the effort needed by an attendant to propel the wheelchair with the disabled occupant is very hard, especially attendant in weak physical performance. By the hardness of propelling the attendant propelled wheelchairs, some aged attendant could not use it, or avoid assisting with each other, though using the attendant propelled wheelchairs increases opportunities of aged social activities. The large propelling load limits the time and distance in using the attendant propelled wheelchairs. Some cases the attendant might face dangerous possibilities in accidents with other traffics and pedestrians, because of hard manoeuvrability. The attendant strong intension to keep the occupant safety in the attendant propelled wheelchairs might increase possibilities in overexertion, which can result in pain to an attendant's back or shoulders and elbows joints.

With a demographic transition by the balance change between decline of birth rates and falling death rates, the average age of the population increases and the distribution of young working people to retired individuals' shifts to favour the retirees, there is an increasing deficit of young attendants. Recent ageing society faces a problem of the deficit in younger attendants, so the case one of aged spouse help to travel a disabled partner, can be seen sometimes. From view of privacy and varieties of assisting activities, the spousal attendant is better than non-spousal attendants for older people.(Finlayson 2008[10]) Therefore, frequently the spouses of those with mobility impairments work as attendants for loved ones in many cases; these people are often themselves elderly.

From these back grounds mentioned above, it is strongly desired to reduce the propelling load in the attendant propelled wheelchairs. The most effective method is to reduce the total wheelchair weight including a disabled occupant (Abel 1991[11]), however, the occupant weight is account for around 80% of the total weight. This means that the reduction of road resistance by the decreased wheelchair body weight would be limited. An another solution is to adjust the handle hight in order to minimise attendant

pushing performance.(Al-Eisawi 1999[12]) Many studies reveal that the handle height to maximise pushing performance at stand still is around shoulder height.(Hoozemans 2004[13]) However, the increased pushing force by adjusted handle height is very small within 15%, and the shoulder height is not the best position in pulling from previous studies. In addition, the higher handle height for applied pushing force tends to cause the forward falling of wheelchairs, because front casters stuck by some obstacle or gap become a fulcrum and the high handle height easily creates rotational moment of the wheelchair to forward falling.

One of solutions to solve these problem is the powered attendant propelled wheelchair. (Abel 1991[14]) The power attendant propelled wheelchair (PAPW) generates assistive forces by electrical motors, and the amount of the assistive force is determined by the controller with the operating forces measured by load cells at handle. The simple controller like a proportional controller generates the assistive force from the production of assist gain around 1 and measured operating force. Some PAPW products with simple controller are available in the market, however, the controllers need to be optimised to attendant characteristics, especially aged attendants. Also the reduction of energy consumption, which provide driving for long distance, is strong demands from attendants.

This study proposed an assist as needed control to include three features below. Then, the developed attendant-propelled wheelchair with this controller was tested on flat surfaces and longitudinal slopes with different weight conditions.

1) Assist if the attendant propelling is insufficient over natural attendant propelling capability at high propelling load.

2) Use natural individual attendant propelling capability at low propelling load in order to reduce energy consumption as well as to keep attendants' health for aged.

3) Easily adjust the controller to fit individual capability.

The hypotheses in this study are below.

1) Human has autonomous propelling capability to continue long time under low subjective hardness, and use it as the natural attendant propelling capability.

2) The assistive system to use the autonomous propelling capability as an assisting boundary, provides sufficient assistive force as well as the reduction of energy consumption.

For testing the hypotheses above, the objectives in this studies are below.

1) Investigate the actual propelling load in the attendant propelled wheelchair on flat surface and longitudinal slopes, by pushing and pulling force, wheelchair velocity, walking pattern and each joint load. (Chapter 2)

2) Investigate the autonomous propelling capability on a motorised treadmill, by pushing and pulling force, walking velocity, walking pattern, postures, and heart rate. (Chapter 3)

3) Develop and validate an attendant-wheelchair model to design assist controls and to discuss the stabilities. (Chapter 4)

4) Design and validate the assist as needed control with a powered attendant propelled wheelchair on real environments. (Chapter 5)

The proposed assist control based on individual propelling capability for the attendant propelled wheelchair, provides sufficient assist forces with lower energy consumption, meanwhile reduces possibilities of injuries at long distance driving. Eventually, the burden to use the attendant propelled wheelchair by aged attendants eases for long driving, so the aged attendants would easily use the attendant propelled wheelchair to go out for disabled occupants. These features increase the quality of life in the disabled occupant and aged attendant together.

References

[1]Jack M. Guralnik, Luigi Ferrucci, Eleanor M. Simonsick, Marcel E. Salive, and Robert B. Wallace, Lower-Extremity Function in Persons over the Age of 70 Years as a Predictor of Subsequent Disability, *N Engl J Med*, vol.332, pp.556-562, 1995

[2]Sakari-Rantala R, Era P, Rantanen T, Heikkinen E., Associations of sensory-motor functions with poor mobility in 75- and 80-year-old people., *Scand J Rehabil Med*, vol. 30, no. 2, pp.121-127, 1998

[3]M. P. Pereira and M. Gonçalves, "Effects of Fatigue Induced by Prolonged Gait When Walking on the Elderly," *Human Movement*, vol. 12, no. 3, pp. 242–247, Sep. 2011.

[4]H. Stephen Kaye, Taewoon Kang, Mitchell P. LaPlante, Mobility Device Use in the United States, National Institute on Disability and Rehabilitation Research, *US Department of Education*, June 2000

[5]Marike van der Leeden, Rutger Dahmen, Jennie Ursum, Leo D. Roorda, Prediction of Walking Disability by Disease-Related Factors in Patients with Rheumatoid Arthritis , *J Rehabil Med*, vol. 42, pp.506–510, 2010

[6]Eveline Nüesch, Paul Dieppe, Stephan Reichenbach, Susan Williams, Samuel Iff, Peter Jüni, All cause and disease specific mortality in patients with knee or hip osteoarthritis: population based cohort study, *BMJ*, vol. 342, pp.1-8, Published 8 March 2011

[7]D. A. Glei, "Participating in social activities helps preserve cognitive function: an analysis of a longitudinal, population-based study of the elderly," *International Journal of Epidemiology*, vol. 34, no. 4, pp. 864–871, Apr. 2005

[8] J. Fries, G. Singh, and D. Morfeld, "Running and the Development of Disability with Age," *Annals of Internal medicine*, vol. 121, no. 7, pp. 502–509, 1994.

[9]L. Van der Woude, C. Geurts, H. Winkelman, and H. Veeger, "Measurement of wheelchair rolling resistance with a handle bar push technique," *Journal of Medical Engineering & Technology*, vol. 27, no. 6, pp. 249-258, 2003.

[10]M. Finlayson and C. Cho, "A descriptive profile of caregivers of older adults with MS and the assistance they provide," *Disabil Rehabil*, vol. 30, no. 24, pp.1848-1857, 2008.

[11]Abel E.W. and Frank T.G., "The design of attendant propelled wheelchairs," Prosthetics and orthotics international, 15, pp.38-45, 1991

[12]Al-Eisawi K. W., Kerk C. J., Congelton J. J., Amendola A. A., Jenkins O. C., and Gaines W., "Factors affecting minimum push and pull forces of manual carts," Applied

Ergonomics, 30, pp235-245, 1999

[13]M. J. M. Hoozemans, P. P. F. M. Kuijer, I. Kingma, J. H. van Dieen, W. H. K. de Vries, L. H. V. van der Woude, D. J. H. E. J. Veeger, A. J. van der Beek, and M. H. W. Frings-Dresen, "Mechanical loading of the low back and shoulders during pushing and pulling activities," *Ergonomics*, vol. 47, no. 1, pp. 1–18, Jan. 2004.

[14]E. Abel, T. Frank, G. Boath, and N. Lunan, "An Evaluation of Different Designs of Providing Powered Propulsion For Attendant Propelled Wheelchairs," *Proceedings of the Annual International Conference of the IEEE Engineering in Medicine and Biology Society*, vol. 13, pp. 1863–1864, 1991

Chapter 2 Attendant load of propelling a wheelchair

2-1 Introduction

The purpose of this chapter is to investigate attendant propelled wheelchair loads in pushing and pulling on a level and longitudinal slopes. In this study, we defined a required capability as the minimum level of the physical strength to propel an attendant-propelled wheelchair. The attendants naturally cope with the propelling load by increasing muscle strength, adjusting postures, and maximising walking velocity. The required capability in pushing and pulling needs to be investigated to improve the propelling load of attendant-propelled wheelchairs and to develop assistive control system.

The propelling activities in industries impose high load on workers when load objects are very heavy over 400kg, so some studies related to the propelling activities in workplaces are carried out for prevention of many injuries caused by overexertion. There are previous studies about the pushing load in hand carts for material handling, which are similar to the case of attendant propelling.

Many investigations in maximum pushing and pulling forces in usage of industrial carts were reported. Theses cases were tested on a level with very heavy weight over 100kg up to 450kg. These studies focused on the pushing and pulling force, and compression and shear forces in lamber spine L5/S1, which causes the back pain. Resnick 1995[1] studied force exertions involved in cart pushing, to predict the peak performance of workers and biomechanical stresses. Four participants pushed carts with loads from 45 to 450kg at several heights. The results showed the peak push forces reached 500N for make participants. Calculated static compression forces at the L5/S1 spinal disc were consistently over the NIOSH limit 3400N for strong participant when the cart load reached 225kg. Jansen 2002[2] investigated the pushing force of cart with vertical push bar and large diameter caster. Al-Eisawi 1999[3] measured the three dimensional hand forces in initial pushing and pulling a cart with 73kg and 181kg weight and three different handle heights; knuckle, elbow, and shoulder. The diameter of cart wheels was 15.24cm (6inch), and the floor was covered with carpet tiles on level. Al-Eisawi found that the minimum horizontal force were appeared at shoulder height in pushing and pulling, and minimum vertical forces were appeared at shoulder height in pushing and knuckle height in pulling. Al-Eisawi 1999[4] also investigated the factors for minimum pushing force of cart such as weight, wheel width, diameter and orientation. Ciriello 2001[5] investigated horizontal and vertical components of maximum acceptable initial and sustained forces while performing push cart tasks on high and low coefficient of friction floors. The results

revealed maximum acceptable weights of the push cart tasks on the low coefficient of friction floor were significantly lower (31%) than the maximum acceptable weights on the high coefficient of friction floor. Ergonomic strategies should include the maintenance of sufficient coefficient of friction on floors to maximise the psychophysical pushing capabilities of the industrial workers, Ciriello concluded. Jung 2005[6] reviewed the articles in pushing and pulling carts. The review introduced previous studies focused on four-wheel cart and discussed wheel design, handle height, load weight, moving direction, motion phase, and floor types. Jung concluded the systematic classification of manual vehicles is necessary to make specific ergonomic recommendation for cart usages. Jung 2006[7] evaluated the wheeled luggage-pulling task in terms of kinematics and perceived exertion to identify the degree of physical load on luggage users. The results show that the user height along with luggage-pulling speed is the most significant variable to affect all body parts kinematics, and the pulling luggage is considered to be light work with moderate stress. Bennett studied the biomechanical responses in the form of hand forces during dynamic submaximal trolley pushing and pulling with up to 300kg load on a level. Bennett found the significant differences in hand forces between 100kg and 200/300kg load. Lin 2010[8] studied the force exertions and muscle activities for operating a manual guided vehicle used to transfer panel glasses about 240kg in the TFT-LCD manufacturing workplace. Lin tested three handle heights around shoulder height 88cm, and two types of caster diameters 153mm and 203mm. The results showed that the heights of 115cm and 153mm were the lowest force in the tested conditions. Kwong 2010[9] studied aged customer's view on shopping trolleys by questionnaire, and the results show that aged shoppers expect the lightness, easy pushing and pulling, the use of the stairs, and an adjustable handle height.

Some researcher focused on the cart pushing and pulling in longitudinal slopes. Raison 2007[10] studied a methodology to determine joint efforts in the human body during maximum ramp pushing. The methodology was based on multibody dynamics. From the results the proposed method was accurate to determine the joint effort in dynamic conditions. Ger 2007[11] analysed the load on the lumbar spine of flight attendants during trolley handling aboard aircraft regarding posture and exerted forces. The results showed the lumbar load varied respective to handling mode(push/pull), floor gradient, trolley type and loading, and individual execution technique. In the same study, Glitsch 2007[12] found that the greatest physical workload of flight attendant when pushing/pulling trolleys aboard, was to be expected the beginning of services: The trolleys are fully laden, and the cabin floor can still be inclined up to 8 degree.

The pushing load depends on type of wheels. Two wheel container pushing and pulling were investigated. Schibye 2001[13] investigated the mechanical load on the low back and shoulders during pushing and pulling of two-wheeled waste containers in the tasks of

lifting and carrying of bags and bins. The results showed the compression at L4/L5 was from 605 to 1445N during pushing and pulling. The shoulder load was between 1 and 38Nm. The results suggest that the torques at the low back and shoulders are low during pushing and pulling, and no relation exists between the amount of the external force and the torque at the low back and shoulder. Laursen 2002[14] investigated the Net torques at the shoulder joint and the lumbar spine as well as the compression and share forces in the lumbar spine at the L4/L5 level, while seven waste collectors pushed and pulled a two wheeled container on three different surfaces; flag stones, paving stones, and grass. The results showed the lumbar spine compression force was below 1800N and the shear force was below 200N in all situations. The shoulder torque was up to 80N in pulling with one hand. The results suggest that the container weight affects the magnitude of the push/pull forces and the load on the shoulders, but not the load on the lumbar spine. Kingma 2003[15] studied the joint loading by design factors of two wheeled carts, such as centre of mass (COM) and handle location. Kingma investigated the handle forces and joint loading during two handed steady pushing and pulling. The results showed backward displacement of the COM increased low back loading, and forward displacement of the COM increased shoulder and elbow loading. A 0.1m increase of the handle height slightly reduced the required vertical force. The results suggest the design of the two wheeled containers can be improved by moving the COM in the direction of the wheel axis, and by raising the height of the handles.

The gender difference was discussed in pushing and pulling cart case. Van der Beek 2000[16] studied the gender differences regarding exerted forces and physiological load during pushing and pulling of wheeled cages by postal workers. Van Der Beek tested the force direction in pushing and pulling four wheeled cages with from 130 up to 550kg weight. Exerted force and physiological load were heigh at the cart weight 400 and 550kg. Gender differences were significant for all extracted parameters.

Different from these studies in maximal exerted forces and propelling force for carts, the attendants of wheelchairs must delicately regulate own force and walking velocity respective to the propelling load for occupant's safety in wheelchairs. This study focuses on the light propelling load of the attendant-propelled wheelchairs, in which the total weight of the wheelchair is within 100kg.

Some investigations in attendant propelling were carried out, especially the pushing forces of the attendant propelled wheelchair on a level. Abel 1991[17] studied design of handles and understanding of biomechanical factors associated with wheelchair pushing. Abel showed preferred handle position is 0.75 of shoulder height, 1.14 times shoulder width. The preferred position did not correspond to minimum level of resultant pushing forces or lower levels of moment in upper joints. Van der Woude 1995[18] analysed the

external forces and biomechanical loading on the musculoskeletal system during wheelchair pushing with different push handle heights. Using higher pushing height, net moments in shoulders, elbows, and wrists were lower as well as the compression and shear forces at L5-S1 were also lower. From experiment results, a pushing at 86.5% of shoulder height was most favourable.

The number of aged attendants recently increase to help their spouses with the attendant propelled wheelchair, and the physical strength of the aged attendants is much weaker than workers in industries. Among the aged attendants, the demand to reduce the propelling load of the attendant-propelled wheelchair is rising now, even if the total weight of the attendant wheelchair is lighter than that in industries.

One solution is an assisting system, which has motors delivering auxiliary driving force. For the design of this powered system, it is important to investigate how much attendants naturally exert pushing force with walking in daily life. The attendants adjust propelling force by the propelling load, and maximise the walking velocity naturally. The mechanism to adapt the pushing/pulling during walking against the propelling load is not known well.

In this chapter, the ascending and descending an attendant propelled wheelchair on longitudinal slopes were investigated about the points below.

1. How to cope with the increased propelling load for attendants? This study investigate this point with an instrumented attendant-propelled wheelchair on different conditions by wheelchair weight and slope angle. The analysis was done based on operating forces, walking velocity, walking pattern, and propelling posture.

2. How large is the joint load in ascending and descending an attendant propelled wheelchair? The joint load was analysed with a seven-link model in sagittal plane. The physical strength in upper extremity is weaker than that in lower extremity. The main driver to generate propelling force is lower extremity, so upper extremity need to support the force from lower extremity to the wheelchair. Weak participants suffered shoulder and elbow pain, so this study focused on the joint load in shoulder and elbow. In addition, the knee joint load was analysed because some part of the aged participants generally suffer from knee pain, which is main trouble by osteoarthritis in lower extremity by ageing.

The instrumented attendant propelled wheelchair had six-axis load cells in both straight grips and velocity encoders in both rear wheels. Three different horizontal slopes 6.5%(3.6deg.), 9.0%(5.0deg.), 12.1%(6.9deg.), and flat surface, which are made of concrete tiles, are used as the slope conditions. The measured parameters for the investigation were the horizontal and vertical forces at each grip, wheelchair velocity, the time of foot on and off, and joint positions in sagittal plane. With seven-link model in sagittal plane, the joint torques in ascending and descending were calculated. From the

results of the investigations above, the required capability in ascending and descending of the attendant-propelled wheelchair on longitudinal slopes are discussed.

2-2 Methodology to investigage propelling a wheelchair on a slope

The instrumented wheelchair in Fignure 2-2 was developed for this study. The base wheelchair was NHS standard attendant-propelled wheelchairs in UK. The wheelchair has two polyurethane front casters (diameter:190mm), and two polyurethane rear wheels (diameter:310mm). The wheelbase between front casters and rear wheels was 380mm. This wheelchair was specialised for attendant propulsion, so there is no hand rim on the rear wheels. The attendant controls the movement of the wheelchair using two grips set behind of a seat. The hight and width of the two grips were 950mm and 440mm respectively, and the grips were placed in parallel with the ground surface. Six-axis load cell (AMTI model MC3A-6-250) was placed the stem point at each grip, and detected the operating force produced by the attendant. The six-axis signals from each load cell were treated by a strain amplifier (AMTI model MSA-6), then the amplifier outputted three translational force signals Fx, Fy, Fz, and three moment signals Mx, My, Mz. The force signal Fx was set to cross direction(+:right, -: left), Fy was set to forward direction(+: front, -:back), and Fz was set to vertical direction(+:upward, -:down ward). The moment signals Mx, My, and Mz were also measured, however, these forces were not utilised because the moments of grips contributed less to the wheelchair forward movement in ascending and descending on the longitudinal slopes. Wheelchair velocity measured from each wheel rotation detected by a rotary encoder 500p/r, under the assumption that no slips happened between rear wheel and tested surfaces. The pulley, which directly drives the rotary encoder, contacted to the polyurethane part of the rear wheel. The rotational resistance by the pulley was minimised and very smaller than the total road resistance of the wheelchair. An embedded signal processing unit converted the output pulse of the encoder to the dc voltage in proportion to wheel rotational velocity. The total weight of the instrumented wheelchair was 35.3kg. This study used steel weights instead of an occupant because the aim of this study was to investigate the attendant behaviour by the propelling load determined by the total wheelchair weight. The weight conditions in this study were implemented with rounded steal weights placed on the seat of the wheelchair. Each steal weight was about 10kg. The detail of the relationship between propelling load in wheelchairs on the slopes is discussed in the Appendix A. The detected forces and velocities were simultaneously recorded with 100Hz sampling by LabView (National Instruments Inc.). The LabView code was originally developed before this study.

Five sagittal joint positions, shoulder, elbow, hip, knee and ankle of a participant were measured while the participant was ascending and descending in the middle of the longitudinal slope on each trial. The measurement of joint position was done by a video camera with reflective markers, and its frame rate is 30Hz. The camera position was well

calibrated before this study by the reflective markers and flat board 1.8m(W) x 2m(H), which cover with the area from ankle to shoulder heigh and almost of two steps. The reflective markers (diameter: 40mm) were adhered on the skin near the centre of each joints. In ascending trials, the markers were placed on the left side of shoulder, elbow, hip, and both knees and ankles. In descending trials, the markers were placed on the right side of the joint as the same way in ascending. To enhance the reflection by the markers, the 500W light was placed from the side of wheelchair travels, and the participant wore black tight clothes. The video recordings were done by a PC based software and were synchronised with force and velocity recordings in the instrumented wheelchair. Recorded marker positions were tracked by the MaxTraq2D software (Innovation systems Inc.), and converted actual length (mm) with calibrated scale in the screen. The knee and ankle positions in the far side from the video camera disappeared during the leg in the near side hided far side in walking, however, this happens in very short time within three frames , and we interpolated the missing knee and ankle positions in the far side by velocity estimation and spline function in the MaxTraq2D.

This study used three longitudinal slopes and a flat lane in the Pedestrian Accessibility Movement Environment Laboratory(PAMELA) facility of University College London. The PAMELA platform has 57 of surface modules, which can reproduce various height and oriented slopes by five oil cylinders to support the surface 1200mm x 1200m from the ground. The surface material can be replaced to many types of real kerbs and road surfaces. In this study, typical concrete pavers in UK footway, which consists of 400mm x 400mm tiles, was used as the surface material.

The three slopes 3.6deg. (6.5%), 5.0deg.(9.0%), and 6.9deg.(12.1%) in Figure 2-2 were set in the PAMELA platform, and the length in slopes were 4.8m, 3.6m, and 2.4m respectively to adjust the potential energy at each slope was the same. The length of 2.4m at 6.9deg. was enough because the wheelchair velocity became steady before middle of the slope.

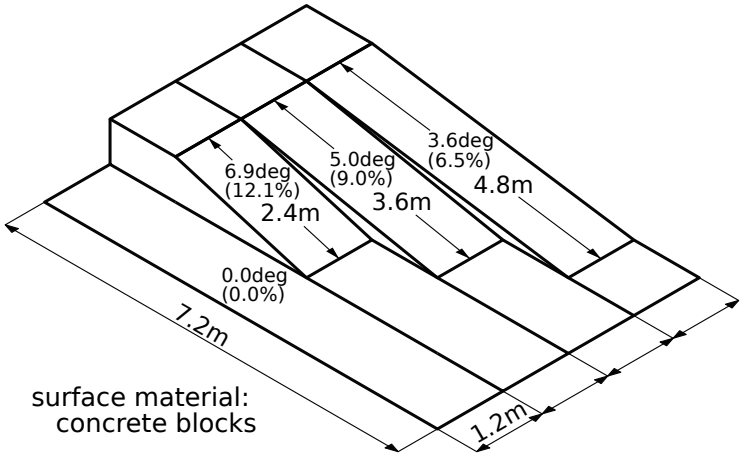

Figure 2-1 Three longitudinal slopes and a flat lane for this study

The measurements of the attendant propelling in ascending and descending were carried out on four weight conditions W (+0.00, +20.35, +40.70, and +61.05kg), and four slope angles θ (0, 3.6, 5.0 and 6.9deg.). The base weight M of the instrumented wheelchair was 35.30kg, so maximum weight condition in the wheelchair was 96.35kg. The additional resistance loads over the flat condition were calculated from the equation (2-1). From the equation (2-1), the additional resistance loads F_{RA} in this study are shown in the table 2-1.

$$F_{RA} = (M + W)g\sin\theta \qquad (2\text{-}1)$$

Here, g is the gravity acceleration 9.81m/s, and θ is the slope angle. The increase of the wheelchair weight M+W increases the road resistance. (Lemaire, 1991) On the steady wheelchair velocity, the attendant in ascending or descending must generate pushing or pulling force equivalent to the resistance load by the total wheelchair weight M+W and the slope angle θ.

Table 2-1 The additional resistance load F_{RA} by weight W and slope angle θ

Additional resistance load F_{RA} [N]	**Slope angle θ [deg. (%)]**			
Additional weight W [kg]	0 (0)	3.6 (6.5)	5.0 (9.0)	6.9 (12.1)
0.00	0	21.7	20.2	41.6
20.35	0	34.2	47.5	65.5
40.70	0	46.8	64.9	89.5
61.05	0	59.3	82.3	113.4

Before each trial, the wheelchair was placed on the flat level which the front casters were positioned at the edge between the slope and level surface. The orientations of the front casters were set straight toward heading into a traveling lane. The participant waited with slightly gripping the both straight bars behind of the wheelchair, then started to propel after a "go" sign, which was made after starting the recording. Before all of trials, the participant was asked to ascend or descend naturally at steady speed, not vigorously as if a person was sitting the wheelchair and you were in charge of transferring an occupant safely. After finishing ascending or descending, the participant stopped and stand still without gripping the bars until the recording was stopped. The day 1 for each participant was for ascending, and day 2 was for descending. Minimising the effect of fatigue, the order of the combination of the weight W and the slope angle θ was from heaviest and steepest first, then reduced the weigh W by about 20kg to zero, then reduced the slope

angle and started the weight W = 60kg to zero again. Each combination has three trials from start point. All combinations for one participant was finished when both the weight W and the slope angle θ were zero.

Five participants in aged from 27 to 44 without any movement disorders took part in this study after agreement with informed consent. Three of five participant were male, and remaining two were female. The averaged height of all participant was 172cm, and averaged weight was 69 kg.

2-3 Attendant Model for joint torque investigation

From measuring the joint positions and the horizontal and vertical propelling force in the sagittal plane, the joint torques were calculated with an attendant model in Figure 2-2 (a) and each link model in (b). For this study, the attendant movements in ascending and descending mainly occurred in the sagittal plane, so the two dimensional model for joint analysis was used.

The attendant model consisted of seven links; forearm, upper arm, trunk, left thigh, left leg, right thigh, and right leg. The links of forearm and upper arm included both left and right hands because both hands work together in the same way while propelling the wheelchair in straight. In Figture 2-2(b), each link in the model had centre of mass m_i, which place is determined by length L_i and length ratio L_{R_i} / L_i. Each mass m_i and its displacement length L_{R_i} were solved from previous cadaver studies from measured participant's weight and each link length L_i.(Winter, 1990[19]) The masses of forearm and upper arm links, were used doubled mass of single arm in this study. To simplify the calculation of the joint torques, this study assumed that all of joints were revolute joints in the sagittal plane. Each torque were calculated with equations based on multi-body dynamics.(Nikravesh, 1988[20]) A basic equation for each link in Figure 2-2(b) is below.

$$M_i r_i - \Phi_{q_i} \lambda_i = f_i \tag{2-2}$$

where

System mass matrix: $$M_i = \begin{bmatrix} m_i & 0 & 0 \\ 0 & m_i & 0 \\ 0 & 0 & \mu_i \end{bmatrix}$$

System state vector: $$r_i = \begin{bmatrix} x_i \\ y_i \\ \phi_i \end{bmatrix}$$

External force vector: $$f_i = \begin{bmatrix} f^e_{x_i} \\ f^e_{y_i} - m_i g \\ f^e_{n_i} \end{bmatrix}$$

Jacobian matrix: $$\Phi_{q_i} = \begin{bmatrix} 1 & 0 \\ 0 & 1 \\ -(y^{P_a} - y_i) & (x^{P_a} - x_i) \end{bmatrix}$$

Reaction force vector by constraint: $$\lambda_i = \begin{bmatrix} \lambda_{x_i} \\ \lambda_{y_i} \end{bmatrix}$$

Here, g is the gravity acceleration $9.81\,\mathrm{m/s^2}$. The Jacobian matrix Φ_{q_i} was solved from revolute constraint between two connected links. The external force vector f_i was described next equation.

$$\begin{aligned} f_{x_i}^e &= f_{x_i} - \lambda_{x_{(i-1)}} \\ f_{y_i}^e &= f_{y_i} - \lambda_{y_{(i-1)}} \\ f_{n_i}^e &= \tau_a - \tau_b + \left(r^{P_b} - r_i\right) \times \begin{bmatrix} f_{x_i} \\ f_{y_i} \end{bmatrix} \end{aligned} \tag{2-3}$$

Here, the subscript i of each variables is link number shown in Figure 2-1(a). r_i shows a position vector at link i. The operator $\times$ shows cross product between two vectors. $f_{x_i}^e$ and $f_{y_i}^e$ are external forces to apply at the joint position P_b. τ_a is the joint torque which we finally solve. τ_b is the counter torque at the joint position P_b

The calculations for the joint torques were carried out by an originally developed MALAB code for this study. The joint torques only during single support phases in walking were calculated. The double support phases have unknown two boundary conditions while both feet contact on the ground, so it is impossible to solve the equation (2-2) systematically. While single support phase, the calculation steps to solve joint torques were following.

1. Calculate the system state vector $\ddot{r}_i$ from the measured joint positions P_X. The subscript letter X shows joint position; X=p (shoulder), e (elbow), w (wrist), h (hip), Lk (left knee), La (left ankle), Rk (left knee), and Ra (right ankle).

2. Calculate the external force vector f_i from $\ddot{r}_i$ with total horizontal force fx1 and vertical force fy1 measured from the both grips.

3. Calculate the joint torque τ_a from the elbow to the hip one by one, then calculate τ_a from the right ankle to the hip with the same step.

4. Calculate the hip torque from the results of the step three above, then calculate the joint torque τ_a from the left knee to the left ankle.

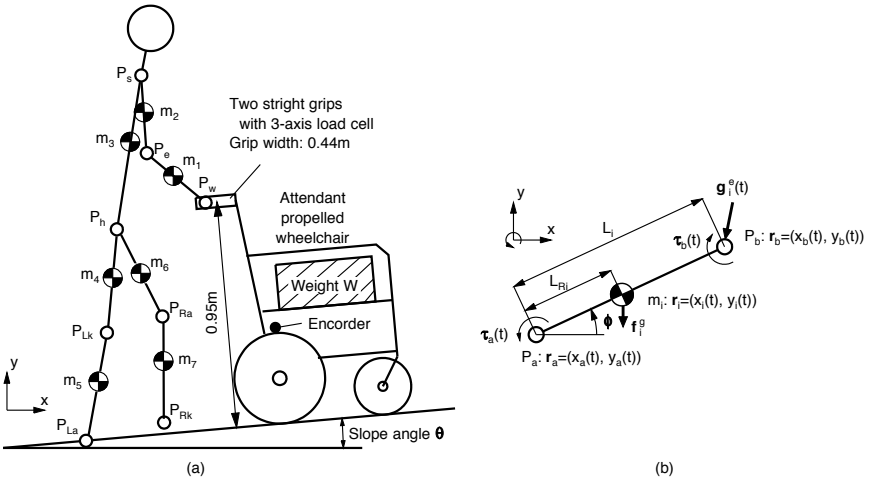

Figure 2-2 Attendant model for the investigation of joint torque.
(a) Overview of 7-link model and a attendant propelled wheelchair
(b) The definition at each link by multi-body dynamics

2-4 Propelling force and velocity

Figure 2-3 (a) shows typical propelling force and wheelchair velocity in ascending at the weight W=60kg (Participant 1). In the beginning, the participant pushed hard about 100N(0, 3.5, and 5.0deg.) to increase wheelchair acceleration from starting to one second passed. After getting enough wheelchair acceleration, usually three seconds passed from start, the participant reduced and roughly regulated the propelling forces at constant level with steady velocity. On the slope angle θ = 6.9deg., the initial acceleration force reached 138N. In the steady state, the averaged pushing force increased from 29N to 136N with the increase of the slope angle θ in order to cope with the increased resistance load. Simultaneously, the averaged wheelchair velocity decreased from 0.66m/s to 0.42m/s. The periodic changes in the pushing force appeared in the slope cases, and the magnitude of the frequency components increased in proportion to the increase of the slope angle θ.

Figure 2-3 (b) shows time series propelling force and wheelchair velocity in descending cases on the weight W=60kg (Participant 1). For comparison, the propelling with pushing at a level surface is included. The initial push in the propelling force and the wheelchair velocity until one second from the starting were similar to the ascending cases because of getting acceleration to start, however the propelling force changed from pushing to pulling to prevent from accelerating the wheelchair rapidly in downward slopes. Similar with the ascending cases, the steady state can be seen in the descending cases after around three seconds passed from start. In the steady state, the averaged pulling force increased from -43N to -84N in order to cope with the downward gravity force of the wheelchair by the increase of the slope angle θ. Simultaneously, the averaged wheelchair velocity decreased from 0.66m/s to 0.57m/s. The frequency components of the pulling force were lower than of the pushing force in the ascending cases. These propelling styles in ascending and descending by Figure 2-3 (a) and (b) were the similar of other participants.

This study focused on the steady state after three seconds passed from start. In the steady state, the period in two seconds was used for the analysis in this study because it was enough to cover for two steps. For investigating the outlined propelling behaviours in ascending and descending, this study extracted averaged propelling force, wheelchair velocity, step length, and cadence from time series data including foot switch outputs.

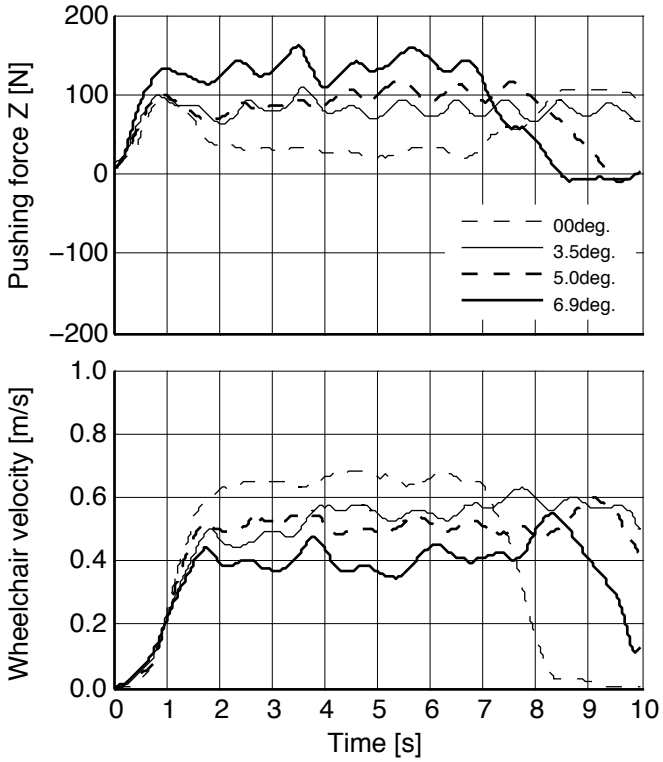

(a) Ascending case

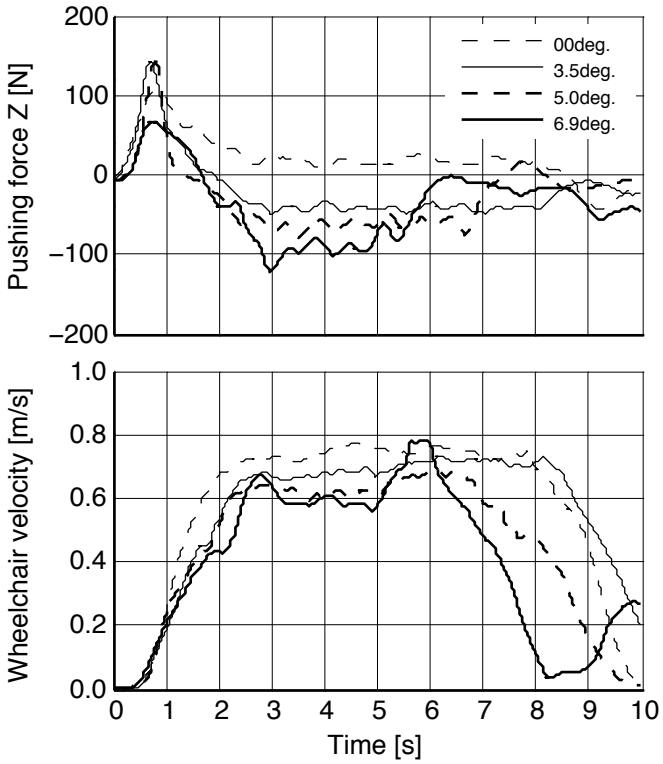

(b) Descending case

Figure 2-3 Propelling force from start in ascending and descending cases at the weight W=60kg. (Participant 1)

Figure 2-4 shows the propelling force and the wheelchair velocity in steady state under the four weight and four slope conditions. The propelling forces in (a)horizontal Fx and

(b)vertical Fy were averaged sum of both left and right forces during steady velocity period in two seconds. The upper graph shows the pushing forces in ascending, including pushing the wheelchair at a level, and the lower graph shows the pulling forces in descending. In the steady state, the resistance load is theoretically equal to the horizontal force Fx.

In the lower resistance loads by the weight W =00kg and the slope angle θ=00deg. in ascending in Figure 2-4(a), the wheelchair velocity V_W at each participant was highest in the range between 0.75m/s and 1.08m/s. With the increased resistance load in the ascending, the wheelchair velocity V_W decreased proportionally to the range between 0.42m/s and 0.61m/s in the highest resistance load by the weight W =60kg and the slope angle θ=6.9deg. The pushing forces Fx in all participant at the highest resistance load were similar in the range between 127N and 135N. The trend which the decrease of the wheelchair velocity with the increase of the resistance load was common in all participant in the ascending. The calculated spearman rank correlations in ascending were r=-0.876 ($p<0.001$)[participant one], r=-0.753($p<0.001$)[participant two], r=-0.941($p<0.001$) [participant three], r=-0.694($p<0.01$)[[participant four], and r=-0.806($p<0.001$)[participant five]. Estimated 1st order linear functions for these trends were Fx=214-266V_W (participant one), Fx=186-215V_W (two), Fx=189-233V_W (three), Fx=160-145V_W (four), and Fx=171-161V_W (five). And the averaged estimated function of five participants was Fx=184-204V_W.

In the descending cases shown by the lower graph, the pulling force Fx was in the range between -17N and -39N at the different wheelchair velocities by participants in the lower resistance load by the weight W =00kg and the slope angle θ=3.6deg. With the increased resistance load, the pulling force increased up to about -107N at the different wheelchair velocities V_W in range between 0.43m/s and 1.11m/s. The trend of the relationship between the pulling force Fx and the wheelchair velocity V_W in descending was different in participants. The participant one and three showed the similar trend, in which the wheelchair velocity V_W decreased and the pulling force increased with the increase of the load resistance. This trend was an opposite trend to the ascending cases. The remaining participants two, four and five, however, showed the different tread, in which the wheelchair velocity V_W was roughly constant and the pulling force increased. The calculated spearman rank correlations in descending were r=0.930 ($p<0.001$) [participant one], r=0.098($p=0.76$)[participant two], r=0.545($p=0.07$)[participant three], r=-0.490($p=0.11$)[[participant four], and r=-0.140($p=0.66$)[participant five].

The vertical force Fy in Figure 2-4(b) shows the force generated by the participant when push up(positive value) or down(negative value) the grips. In the ascending cases

shown in the upper graph, most participants except participant three showed the trend of the increased vertical up force with the increased resistance load. At the lower resistance load by the weight W =00kg and the slope angle θ=00deg., the vertical force Fy of most participants showed negative value around -50N. With the increase of the resistance load, the negative vertical force comes to near zero. The participant four and five showed positive value around 50N in the vertical force when the resistance load was very high at the weight W =60kg and the slope angle θ=6.9deg. In the descending cases, the trend of the relationship between the vertical force Fy and wheelchair velocity V_W was different with the participant. In the lower resistance load, vertical force were nearly zero in all participant, however, the vertical force appeared under the higher resistance load. At the maximum resistance load by the weight W =60kg and the slope angle θ=6.9deg., the participant one and three generated positive vertical forces, and the participant two and four generated negative vertical forces. The participant five generated around zero vertical forces.

To summarise the relationship between horizontal force Fx and vertical force Fy, the force efficiency ξ defined by the equation (2-4), shows in Figure 2-5.

$$\xi = \frac{F_x}{\sqrt{F_x^2 + F_y^2}} \times 100 \ [\%] \qquad (2\text{-}4)$$

In the ascending cases of all participants, the force efficiency ξ in higher walking velocity under lower resistance load, were mainly lower than 40%, which means that large force losses appeared under lower resistance. In the higher resistance load, the force efficiency ξ became high around 100% because the vertical forces were very smaller than the horizontal forces. It means the participants generated propelling force effectively. In the descending cases, the force efficiency ξ were nearly 100% under lower resistance load, however the increased resistance load reduced the force efficiency to about 80%.

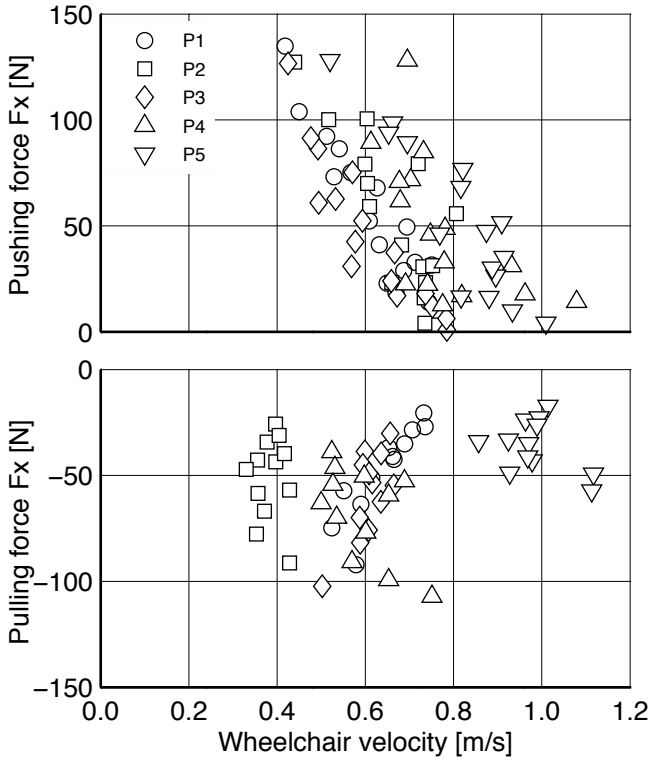

(a) Horizontal force Fx

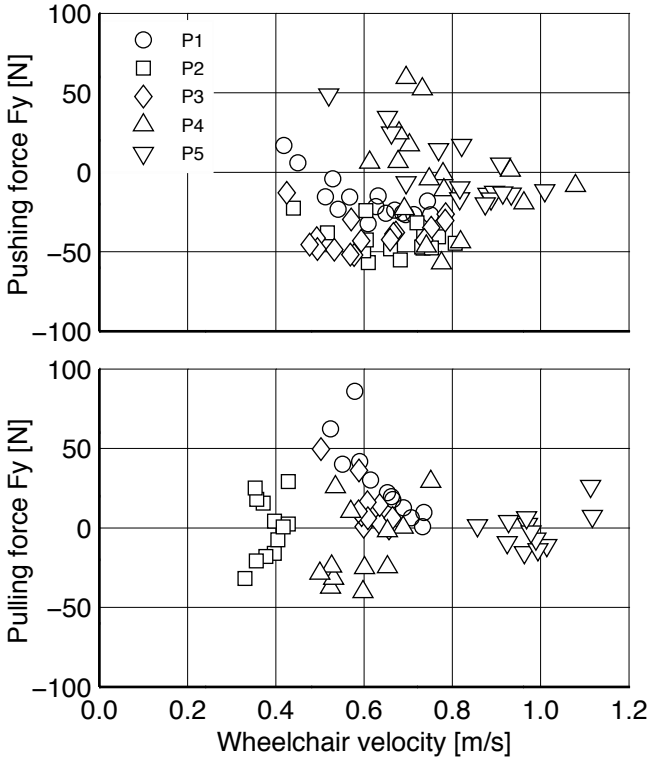

(b) Vertical force Fy

Figure 2-4 Horizontal and vertical force in upward and downward slopes

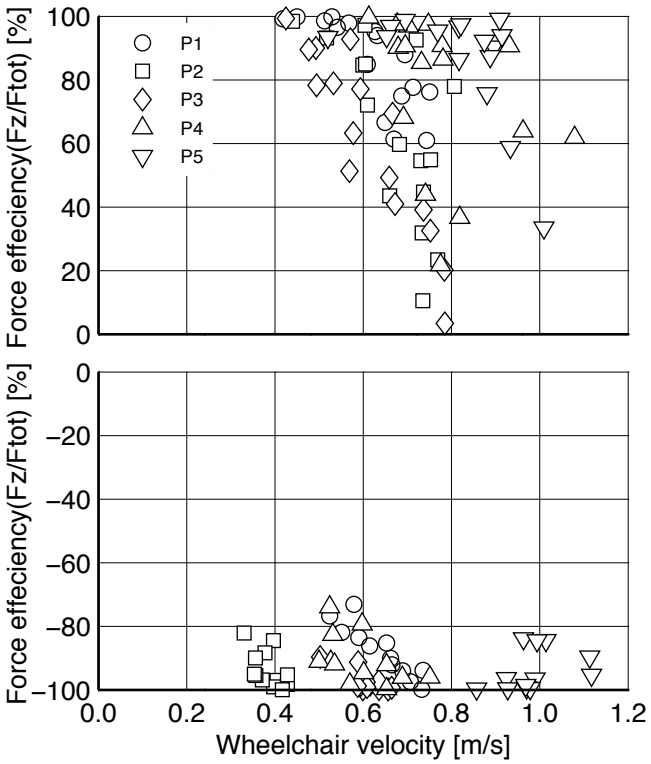

Figure 2-5 Efficiency of the total force for propelling

Figure 2-6 shows the averaged mechanical power P in ascending (upper graph) and descending (lower graph). The averaged mechanical powers were calculated by the multiplication between the averaged horizontal force Fx and the wheelchair velocity V_W because the work in ascending/descending a wheelchair is done by only the horizontal force Fx, and the averaged attendant walking velocity is equal to the averaged wheelchair velocity under steady state.

In the ascending cases, the mechanical power P in the low resistant load were very lower than 20W because of low horizontal force Fx, though the wheelchair velocity V_W was higher than in other resistance loads. With the increase of the resistance load, the mechanical power P increased up to around 60W at the high resistance load by the weight W =60kg and the slope angle θ=6.9deg. This trend was similar in all participant cases. In the descending cases in the lower graph of Figure 2-6, the different trends were shown by each participant. All of participants, excluding two have a similar trend, which the mechanical power P increased up to the range between 51W and 64W with the increased resistance load. However, the participant two showed maximum mechanical power about 27W. The maximum mechanical powers were different by each participant case.

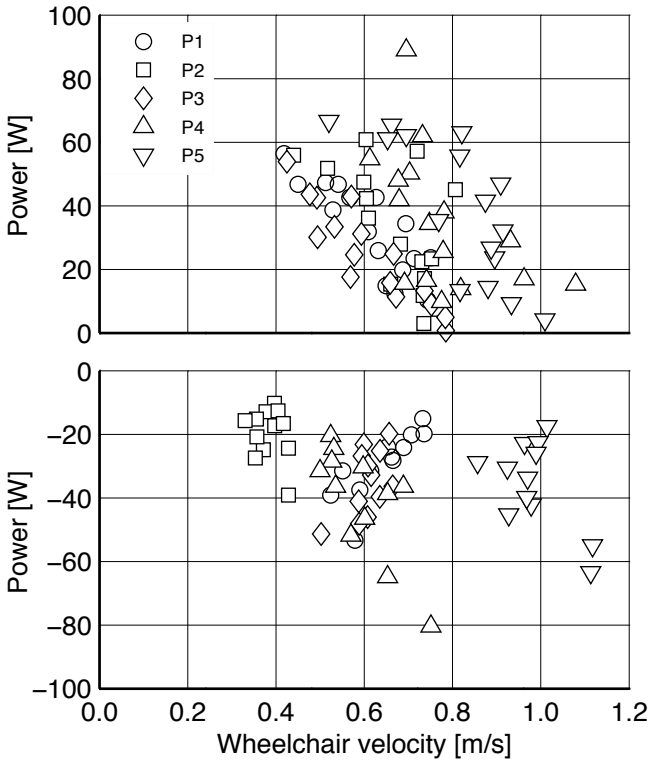

Figure 2-6 Averaged mechanical power in pushing/pulling on the slopes

2-5 Propelling postures on slopes and walking pattern

Figure 2-7 shows the propelling postures of the participant one in (a) propelling at a level , (b) in ascending on the slope angle θ=5.0deg., and (c) in descending on θ=5.0deg. All weight conditions were W =60kg. These stick pictures were shown in the period from the beginning of stance phase to the end. The frame time in these stick pictures was 25% of each stance phase period. In the case of propelling at a level(a), the participant propelled the wheelchair at nearly straight posture. In the ascending case (b) , the participant inclined to the wheelchair to generate large pushing force. The step length in ascending was the similar length at a level pushing from the comparison with the case (a) and (b). In the descending cases, the participant leaned backward to cope with large pulling force. The step length in descending was shorter than the length at a level pushing. The important difference in postures between ascending and descending was the upper limb posture, which was changed by the propelling styles. This is because the distance between shoulder and grip positions was narrower by forward leaned pushing in ascending, and wider by backward leaned pulling in descending.

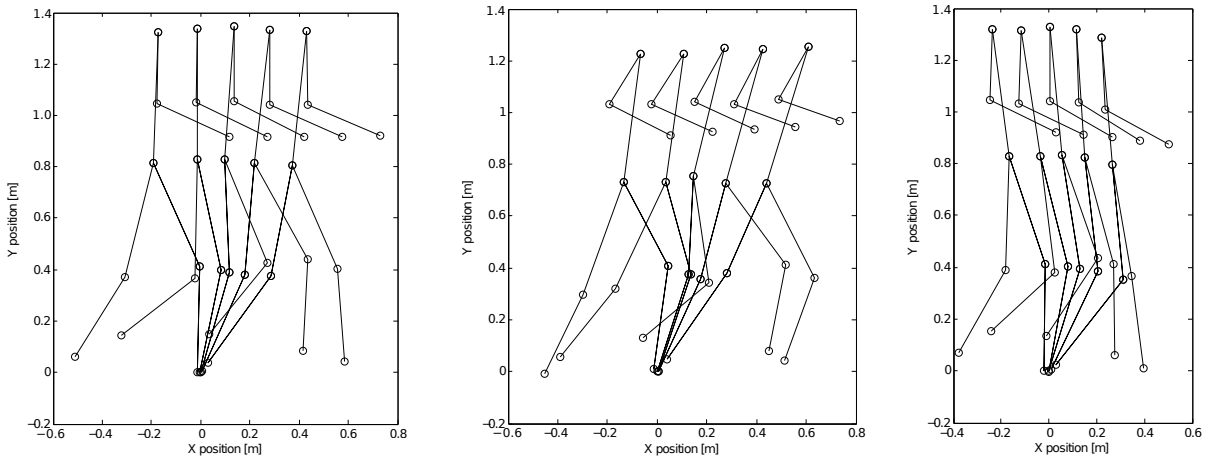

(a) (b) (c)

Figure 2-7 Whole body postures in (a)propelling at a level, (b)ascending, and (c)descending.
The slope angle is 5.0deg. and weight condition is W=60kg.

Figure 2-8 shows the cadence in the ascending (upper graph) and descending (lower graph) cases. The cadence was calculated from the time at foot on and off detected by switches in both shoe sides. In the ascending and descending, the cadences of all participants were almost along with a monotonic increasing curve against the wheelchair velocity, even though the range of the wheelchair velocity was different with the participants. The cadence curve started from about 30step/min at the wheelchair velocity

0.42m/s by the high resistance load in participant one and three. With the increase of the resistance load, the cadence slightly increased up to around 42step/min at the wheelchair velocity 0.9m/s by the lower resistance load in the participant five. The cadence curve in the descending was slightly higher than in the ascending.

Figure 2-9 shows the step length in the ascending (upper graph) and descending(lower graph) cases. The step length of all participants were calculated from the averaged cadence in Figure 2-7 and the averaged wheelchair velocity V_W, because the averaged participant walking velocity is equal to the averaged wheelchair velocity under the steady state. The step length showed the similar manner with the cadence. The step length curve by the resistance load showed monotonic increasing in the ascending cases and descending cases. The step length curve started from 0.7m at the wheelchair velocity around 0.4m/s to around 1.2m at the wheelchair velocity 0.9m/s in the end. The step length curve in the ascending cases was slightly higher than in the descending cases.

Figure 2-10 shows that walking ratio defined by the ratio of the step length by the cadence. The walking ratios were constant around 0.03m/(step/min) in ascending and around 0.02m/(step/min) in descending against the wheelchair velocity by the resistance load, even though the ranges of the walking velocity in the participants were different.

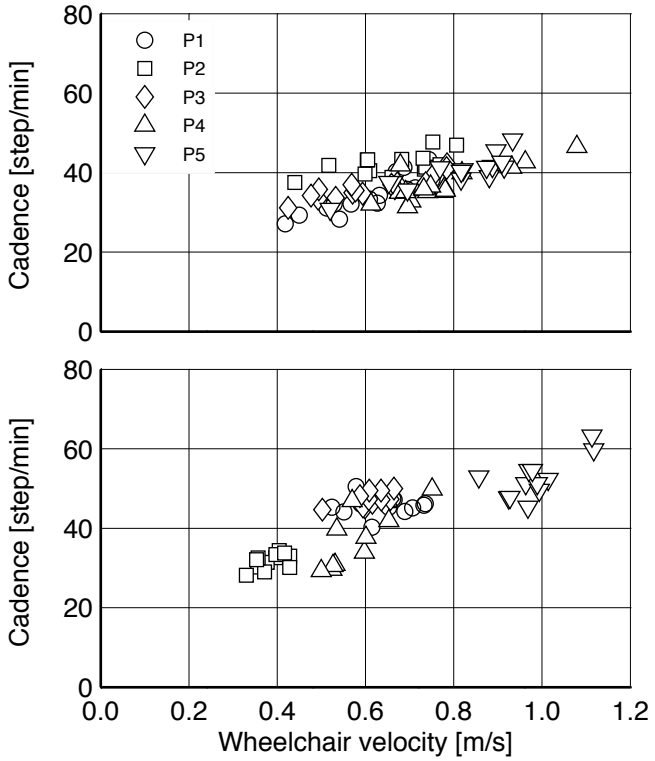

Figure 2-8 Cadence in ascending and descending

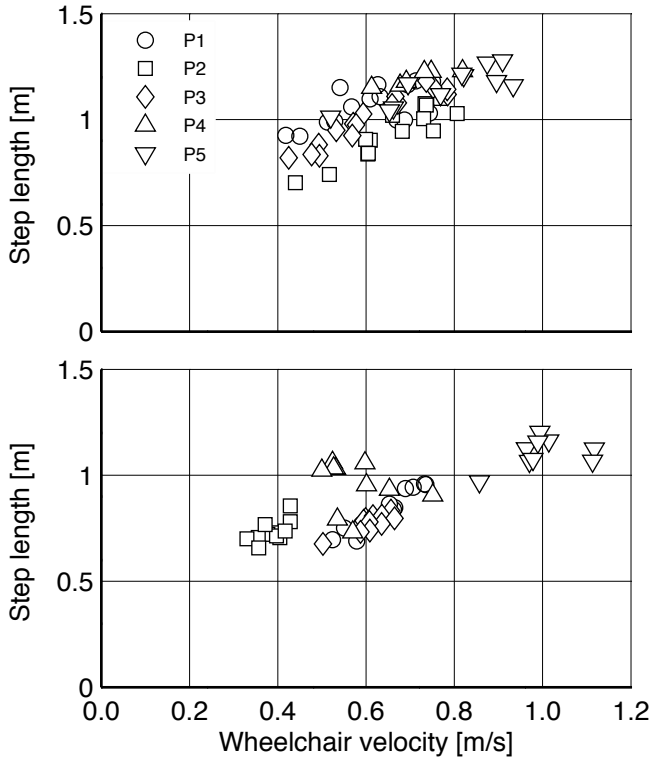

Figure 2-9 Step length in ascending and descending

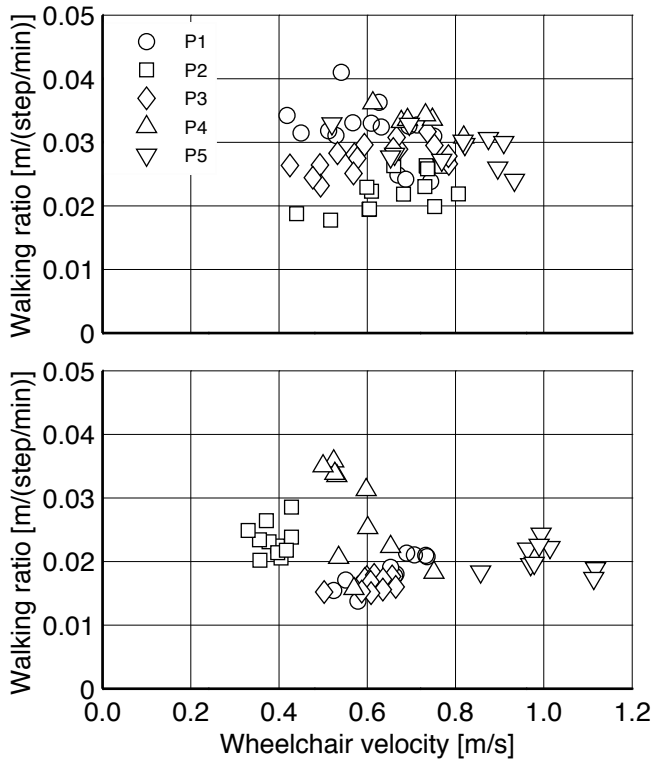

Figure 2-10 Walking ratio in ascending and descending

Figure 2-11 shows the averaged shoulder angle (upper graph) and the elbow angle (lower angle) in ascending and descending. The horizontal axis in Figure 2-11 is the horizontal propelling force Fx, which is equal to the resistance load under steady state. The positive horizontal propelling force Fx is pushing force in ascending and negative

values is pulling force in descending. In the ascending cases by all participants, including pushing at a level, the shoulder angle decreased to about -25deg. at the horizontal pushing force Fx=129N, from about -0.2deg. in pushing at a level on the lighter resistance load by the weight W=00kg. Simultaneously, the elbow angle by all participant except participant five, increased to 107deg. at the force Fx=129N from about 64deg. at the force nearly zero on the lightest resistance load at a level.

In the descending cases by all participants except participant two, the shoulder angle decreased to around -8.4deg at the horizontal force Fx= -94N, from -0.2deg. at Fx=-27N on the lighter resistance load. The elbow angles by all participants except participant two simultaneously keep constant angle about 61deg. with the increased pulling force Fx. The participant two showed constant lower averaged elbow angle about 38deg.

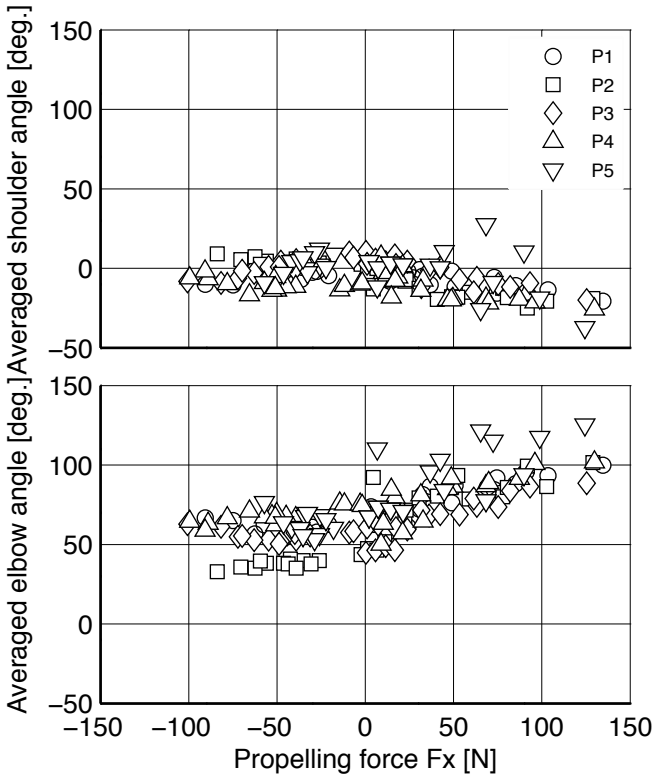

Figure 2-11 Averaged angle of shoulder and elbow

2-6 Joint torque in propelling a wheelchair

Figure 2-12 shows the time series plot of calculated joint torques in a stance phase of the participant one in ascending and descending under the resistance load by the weight W=60kg and the slope angle θ=5.0deg. The stance phase in horizontal axis is normalised by each stand phase in ascending and descending. The upper graph shows the joint torques in the upper extremity, such as shoulder, elbow, and trunk. The lower graph shows the joint torques in the lower extremity, such as knee and ankle. The joint torque in the ascending and descending shows continuous line and dotted line respectively. From the comparison of the range in joint torques between upper and lower extremity, the joint torques in lower extremity were about six times higher than in the upper extremity. In the ascending case, the ankle and knee torques started from -111Nm at the ankle and -139Nm at the knee in the beginning of the stance phase, then increased to 136Nm at the ankle and 61Nm at the knee in the end of the stance phase. Simultaneously, the trunk torque changed periodically from -25Nm at the beginning, then increased to the maximum value around 37Nm, then decreased and repeated new cycle. The shoulder and elbow torques were kept 28Nm and 10Nm respectively. The ankle and knee joint torques in the descending showed a similar curve in the ascending cases. However, the descending ankle and knee torques in the beginning of the stance phase were about 60Nm lower than the torque in ascending. In the end of the stance phase, the ankle torques in both ascending and descending took a similar about 130Nm, however, the knee torque in ascending was about 50Nm larger than the torque in descending. The trend of the trunk torque in descending was similar to the trend in ascending, however, the magnitude of periodical changes in descending was roughly half of the ascending cases. The shoulder torque in the ascending was positive about 28Nm, however, the shoulder torque in descending was negative about -7Nm. The elbow torques in both ascending and descending were almost same about 10Nm.

From the time series of the joint torques, this study focused on the maximum and minimum joint torques at ankle, knee, and trunk, and also focused on the averaged joint torque at shoulder and elbow.

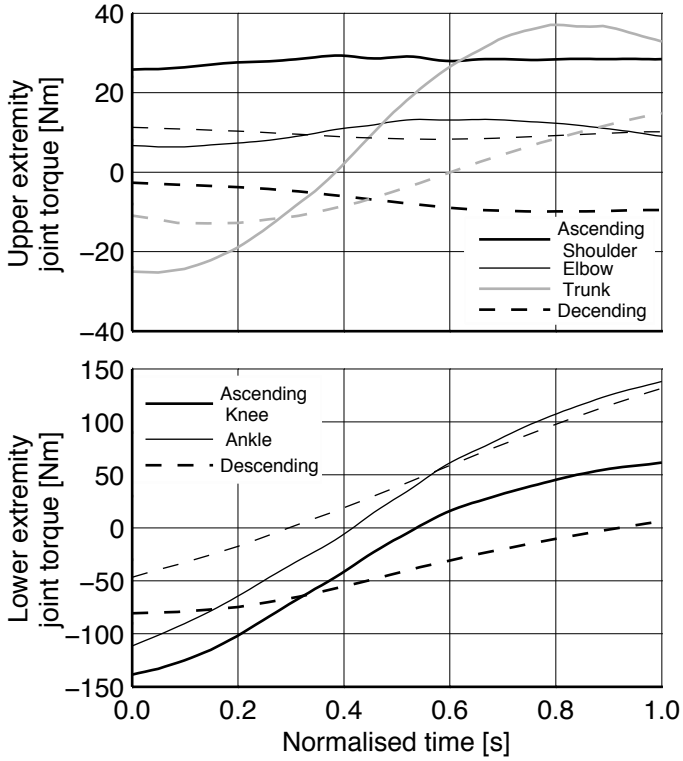

Figure 2-12 Time series plot of joint torques (Participant one)
the weight W=60kg, and the slope angle theta = 5.0deg.

Figure 2-13 shows the averaged shoulder and elbow torques in a stance phase of the ascending and descending. In the ascending cases, the averaged shoulder torque in the upper graph proportionally increased to about 23N at the pushing force Fx=129N from 2Nm at about Fx=6N. This proportional trend in ascending by the resistance load was similar in all of participants. In the descending cases, the averaged shoulder torque decreased with the increase of the pulling force Fx, however, the decline of the averaged shoulder torque by each participant was different. For example, participant one showed nearly constant the shoulder torque about -2Nm, but participant four showed sharp drop up to -40Nm by the resistance load. The shoulder torques were generated in flexion direction in ascending, and extension direction in descending.

The elbow torque in ascending proportionally increased to about 14Nm in flexion at the pushing force Fx=129N from about 2Nm at the lightest resistance load of flat propelling with the weight W=00kg. This trend was the same in all participant, except the participant four, who generated slight larger elbow torques around 23Nm than others. The elbow torque in descending was different with the participant. The participant one generated the elbow torque about 18Nm in flexion with the increased pulling force Fx=-90N. The other participants showed around 0Nm under the large pulling force Fx=-100N.

Figure 2-14 shows the calculated trunk torque in the ascending and descending cases. The trunk torque changed periodically in the time series result in Figure 2-12, so the

maximum and minimum trunk torque were focused. In the ascending cases, the trend in the maximum trunk torque by all participants proportionally increased in the range of the pushing force under 40N, and the trunk torque was kept roughly constant in the pushing force over 40Nm. The participant one, three five generated smaller maximum trunk torque around 40Nm than other participants two and four, who generated large maximum trunk force about 66Nm and 75Nm respectively. In the descending case, the maximum trunk toque were roughly constant at 18Nm(participant one), -1.5Nm(two), 10Nm(three), 33Nm(four), and 14Nm(five).

The trends of the minimum trunk torques in the ascending were different with the participant. The participant one, three and five generated constant minimum trunk torque around -20Nm. The participant two and four in ascending generated almost constant positive minimum trunk torque about 5Nm and 13Nm respectively. In the descending cases, the minimum trunk torque increased to 0Nm from flexion torque around -20Nm, with the increase of the pulling force Fx up to -100N.

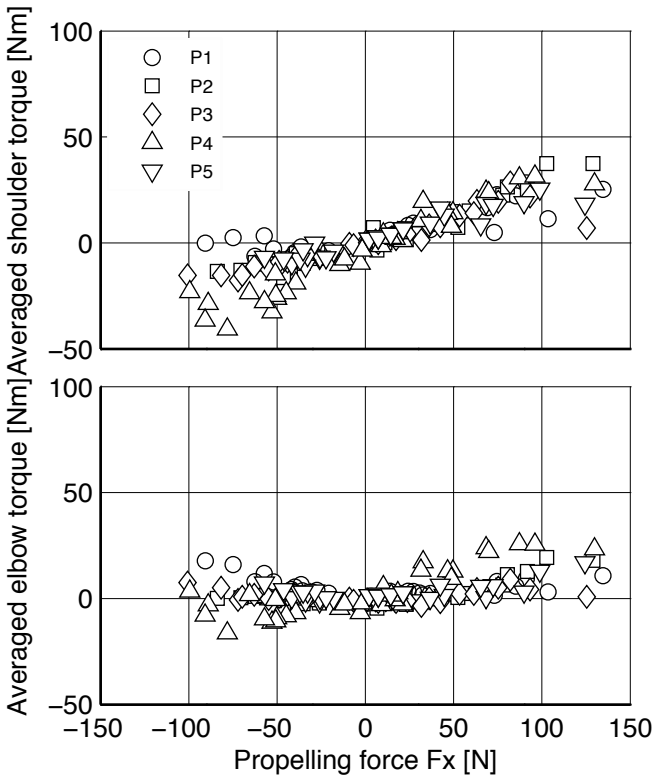

Figure 2-13 Averaged shoulder and elbow torque

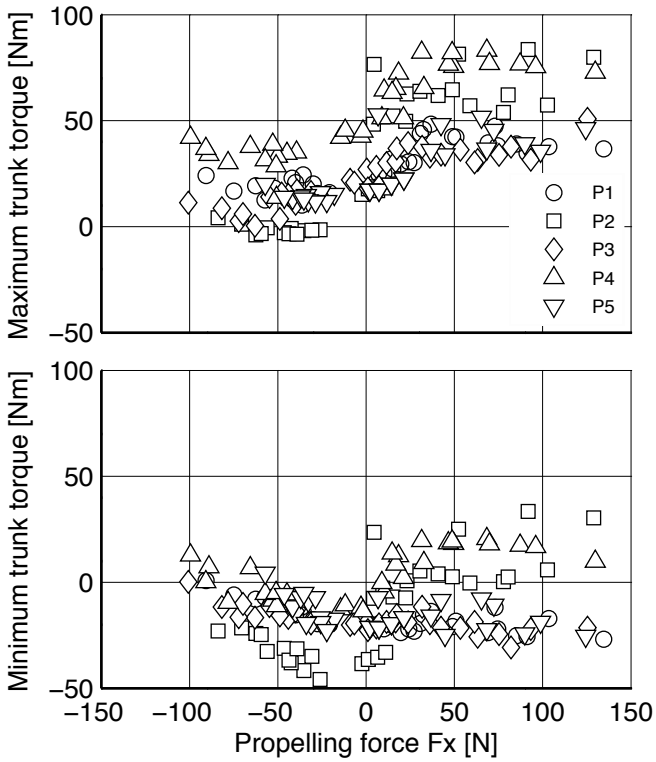

Figure 2-14 Maximum and minimum trunk torque

The maximum and minimum torques at knee and ankle on stance phase show in Figure 2-15(knee) and Figure 2-16(ankle). In Figure, the upper graph shows the maximum torques, and the lower graph shows the minimum torques. In ascending, the maximum ankle torques of all participants were constant about 205Nm(participant one), 243Nm(two), 172Nm(three), 252Nm(four), and 178Nm(five) in plantar flexion with the horizontal pushing force Fx. Also the minimum ankle toques were constant about around -129Nm(participant one), -127Nm(two), -136Nm(three), -169Nm(four), and -130Nm(five) in dorsiflexion. In the descending cases, the maximum ankle torque in participant one and four slightly decreased to 187Nm and 196Nm respectively with the increase of the pulling force. The maximum ankle torques by remaining participants two, three and five were almost constant at 168Nm(two), 147Nm(three), and 166Nm(five). The minimum ankle torques, however, largely decreased to about -51Nm(participant one), -111Nm(two), -52Nm(three), -96Nm(four), and -20Nm(five) with the increase of the pulling force. The torque values in maximum and minimum ankle were depends on each participant, however, the outlined tread by the horizontal propelling force Fx showed similar to all participant. The maximum knee torques in ascending were almost constant about 96Nm(participant one), 109Nm(two), 55Nm(three), 121Nm(four), and 91Nm(five) in flexion, and the minimum knee torques in descending proportionally increased to around -157Nm in extension at the pushing force Fx=129N. The trends of ankle maximum and minimum torques in ascending were similar to all participants. In the descending cases, the maximum knee torque proportionally dropped to around -7Nm with the increase

of the pulling force Fx. The minimum knee torques were almost constant at -81Nm(participant one), -78Nm(two), -69Nm(three), -84Nm(four), and -53Nm(five) in extension. These trends of the knee torque in descending were similar to all participant.

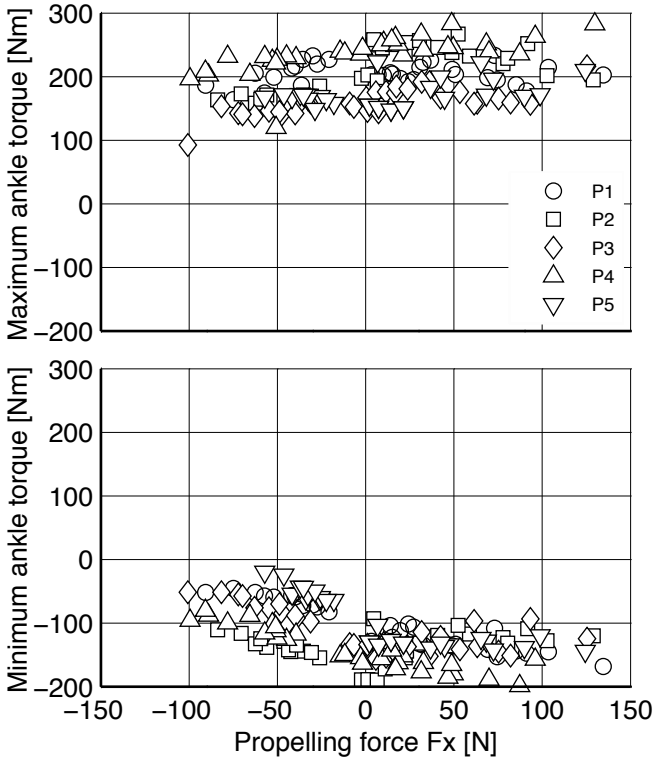

Figure 2-15 Maximum and minimum ankle torque

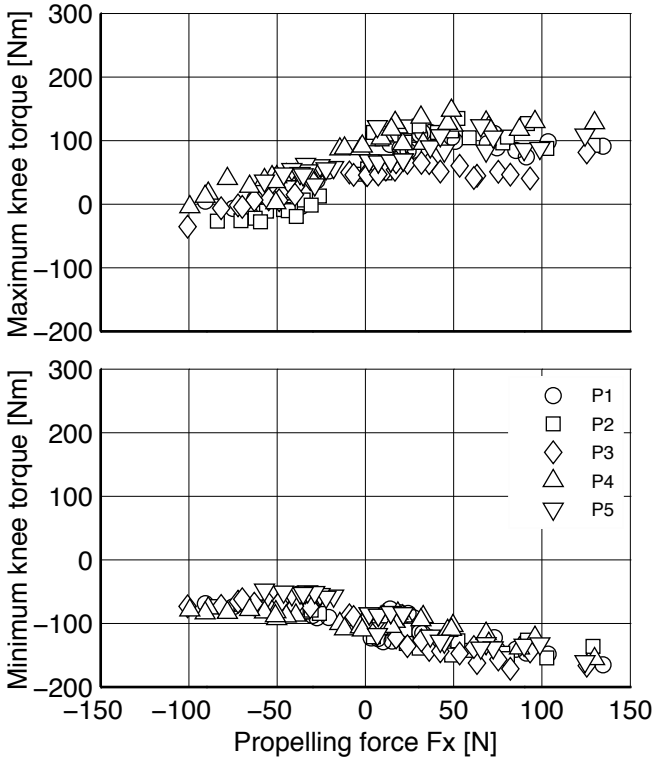

Figure 2-16 Maximum and minimum knee torque

2-7 Discussions

Push forces by wheelchair velocity in ascending

This study investigated required capability of propelling an attendant-propelled wheelchair in ascending and descending on slopes, against the resistance load by the wheelchair weight and the slope angle. The participants need to exert pushing/pulling force equivalent to the resistance load under steady wheelchair velocity. The participants choose wheelchair velocity to match individual physical strength. In ascending cases, the wheelchair velocity at low resistance load was faster than at high resistance load. The relationship between horizontal pushing force and wheelchair velocity by all participants in Figure 2-4(a) are identified as monotonic function by spearman's rank correlation. From this finding, this study estimated these force velocity relationships in ascending as a linear function, and the estimated liner functions for all participants have similar trend. This means that required capability of propelling an attendant-propelled wheelchair in ascending would be estimated with simple function.

The monotonic decrease trend of the relationship between pushing force and walking velocity are consistent with previous studies related to industrial cart pushing under several typical weight conditions. This trend would based on the force velocity relationship in human muscles.(Hill 1939) The force velocity relationship in human muscles shows hyperbolic curve, so further investigation why the pushing force - walking velocity relationship shows linearity, is needed.

The pushing force velocity relationship depends on subjective hardness.(Suzuki 2008) All participant finished to ascend in all trials, however, the subjective hardness were different. Based on the feeling after finishing trials, the participant five, who is the weakest in this study, showed her hardness feeling, even though her pushing force - walking velocity relationship was similar to others. The natural provided capability in forward propelling at a level by Suzuki 2008[21] was around one-third of the pushing force velocity relationship in this study. This point suggests that individual hardness should be estimated based on individual capability in ascending.

Pull forces by wheelchair velocity in descending

In descending, the participant two, four and five almost kept the wheelchair velocity constant with the increase of the resistance load. The wheelchair accelerates automatically downward by the gravity force along with downward slopes. These participant would intended to keep the walking velocity constant. Only participant one clearly shows a

monotonic decrease in the pulling force - walking velocity relationship, and it supported by spearman's rank correlation. The participant five was too weak to pull the wheelchair on the downward slopes, so only she can do was to follow the wheelchair under the minimum velocity control she could do. The participant two and four could control the wheelchair at constant velocity with enough physical strength. The participant five was following wheelchair in the descending cases, so she didn't need to generate large horizontal force to cope with the gravity force by the wheelchair weight. It is because the participant five's vertical forces were almost zero under all of conditions.

The trend of the force velocity relationship in descending is different from in ascending, because the descending style is strongly based on individual physical strength and preferences.

Mechanical power

The mechanical power can be used as an index of the hardness because the increase of the mechanical power means the increase of the instant mechanical energy to propel a wheelchair. In the ascending cases, the mechanical power increased with the increase of the resistance load, and the maximum mechanical powers by most participants were about 60W at the highest resistance load. This might suggest that the human has some implicit rule to regulate output power under natural condition. This topics should be investigated to prove in future works.

In the descending cases, the maximum powers were around 50W by some participant. The participant doesn't need to pull hard the wheelchair, because the gravity component of the slope accelerate wheelchair without attendant forces. The participant two regulated the wheelchair velocity low around 0.4m/s, because he has high physical strength. In other hand, the participant five has very weak strength, so she followed wheelchair rolling with minimum effort in pulling the wheelchair. The individual preference in descending would be a reason for the different maximum mechanical power.

Posture change

With the increase of the resistance load in the ascending, the participants lean forward to the wheelchair and adjust the direction of the total pushing force to horizontal. The force efficiency in Figure 2-5 suggest that the participant adjusted their posture to generate effectively pushing force without losses. This is supported by the decrease of negative vertical force Fy with the increase of the resistance load in Figure 2-4(b). The participant four and five are lower hand position, so pushing up the grip at the higher load resistance is found from the positive vertical force. The results of the force efficiency in Figure 2-5

suggest that higher grip bar height would be suitable against low resistance load, however lower grip height would be better for high resistance load in ascending. In descending, almost zero vertical force suggests that the participants can generate light pulling force easily at heigh grip positions. In the higher resistance load, however the participants cannot generate large pulling force at high grip position, because the participant needs lower grip position to balance the backward leaned posture in pulling. These results suggest the grip height should be designed based on the resistance load in ascending and descending.

In ascending, all participant shows the decreased shoulder angle and the increased elbow angle with the increase of the horizontal pushing force. This means that the attendant moved shoulder slightly backward, and folding their elbow sharply. This posture in the upper extremity is enable to narrow the distance between the hand at the grips and attendant body by learning toward the wheelchair. The relationship between the distance and the pushing force suggest that the arms works as a spring to store kinematic energy. The attendant would use both arms as a mechanical cushioning in order to cover some deficit of pushing force.

In descending, the posture in both arms are almost same with the increase of the pulling force. The shoulder angle decreased slightly to 15deg., and the elbow angle was kept around 60deg. This means that the participant pulls the wheelchair with leaning backward, and the both arms are kept the same posture.

Walking pattern

The results in the cadence and the step length in Figure 2-8 and 2-9, show all participant were almost along with the monotonic increased curve against the wheelchair velocity in the ascending and descending. This means that the cadence and the step length are not affected by the wheelchair weight and the slope angle, but only the wheelchair velocity, which is equal to the walking velocity under steady state. From the results that the wheelchair velocity decreased with the increase of the resistance load in Figure 2-3, the attendant need to reduce the cadence and the step length to secure the stable walking under generating large propelling forces in pushing or pulling. The cadences in descending were slightly higher than in ascending, and the step lengths in descending were slightly smaller than in ascending. This means that the attendants need smaller step length in higher cadence to cope with the large pulling force in the descending.

The walking ratio defined by the ratio of the step length by the cadence in Figure 2-10, showed almost constant around 0.03m/(step/min). This means all participant reduce the cadence and the step length in the same manner against the increased resistance load. Also the results that the walking ratio in descending was smaller than in ascending, support the

different walking style in ascending and descending. In addition, the walking style of the attendants is not affected by the slope angle. Only the walking velocity by the resistance load, change the walking style. This means that the generating large pushing or pulling force in walking needs longer foot contact period in the ground. This topics discuss in the chapter 3 again.

Joint torque

In the comparison between the joint torque in the upper and lower extremity, the pushing force in ascending and the pulling force in descending are mainly generated by the ankle and knee. This is because the attendant obtain the reaction force from the ground for pushing/pulling, and the grip is the only point to transfer generated leg force to the wheelchair to propel. The ankle torque is roughly equal to the torque by the multiplication of the pushing/pulling force at the grips and the length from the ground to the grips, from the definition of the torque in physics. From this point, higher grip position needs more ankle torque, however too lower grip position is difficult for pushing/pulling because of difficulty to adjust propelling postures. From previous push/pull studies, shoulder hight is one of the best height to maximise pushing/pulling forces.

The participant in ascending generated to positive shoulder and elbow torque in flexion to support the horizontal pushing force to the wheelchair. The positive shoulder torque in flexion were mainly generated to push the wheelchair, and the negative torque in extension were mainly generated to pull the wheelchair in descending cases. The elbow in ascending generated the pushing force. The elbow in descending, however, contributes less to large pull forces, because the elbow angle were around 60deg.

In the ascending cases, the negative minimum trunk torque contributes to generate the horizontal pushing force in the beginning of stance phase in Figure 2-12. This means that the participant two and four did not use effectively the trunk torque for the pushing force. In stead of using the trunk torque, the participant two and four leaned their upper body forward to the wheelchair, so that they could use the body weight for the pushing force. In the descending cases, positive maximum trunk torque contributes to generate the horizontal pulling force. In the large pulling cases at around -100N, the minimum trunk torque becomes around zero. This means that the participant did not need to rotate their upper body for leaning forward, because the reactive force from the wheelchair pull their upper body with large pulling force.

In the ascending cases, the main contributors to the pushing force are negative minimum ankle and knee torques in the first part of the stance phase. The knee hardness increased proportionally to the pushing force, however, the ankle hardness was the same. In the case of the large pushing force, the knee torques were almost equal to the ankle

toques, so the hardness at knee was too high in the ascending. In descending cases, the main contributors for pulling force are positive ankle and knee torques in the end of the stance phase. The positive points of the ankle torque in the ascending were almost same to the ankle torque in the descending.

Limitation of this study

The resistance loads were generated by the increased wheelchair weight and longitudinal slope angle. The propelling postures between at a level and on slopes were different. To estimate generalised required capability in propelling needs more number of participant in further studies. The maximum pushing force 135N and pulling force -100N in the condition of the weight W =60kg and the slope angle =6.9deg. were different. Theoretically, these value are the same, however, actual vertical load distribution in the front casters and the rear wheels are different by the slope angle θ and the vertical force Fy. This points should be discussed in the future works. Also the difference in the resistance load between ascending and descending would depend on the distribution of vertical load in the front casters and rear wheels of the wheelchair. Also the vertical propelling force Fy affects the distribution because the generated vector position of Fy is near the contact points of the rear wheel to the ground. The details of road resistance are shown in the Appendix A and these topics are for future works.

2-8 Conclusions

This study investigated required capability of propelling an attendant-propelled wheelchair in ascending and descending on longitudinal slopes, against the resistance load by the wheelchair weight and the slope angle. The participants need to exert pushing/ pulling force equivalent to the resistance load under steady wheelchair velocity. The participants choose wheelchair velocity to match individual physical strength. In the comparison between the joint torque in the upper and lower extremity, the pushing force in ascending and the pulling force in descending are mainly generated by the ankle and knee.

From the estimated relationship between the pushing force and the wheelchair velocity, this study can easily estimate the attendant load from the mechanical power and energy on the ascending works. The descending cases were vary, so we would need to investigate pulling cases deeply in future experiments with increased number of participants.

References

[1]M. L. Resnick and D. B. Chaffin, “An ergonomic evaluation of handle height and load in maximal and submaximal cart pushing,” *Applied Ergonomics*, vol. 26, no. 3, pp. 173–178, Jan. 1995.

[2]Jansen J.P., Hoozemans M.J., van der Beek A.J., and Frings-Dresen M.H., “Evaluation of ergonomic adjustments of catering carts to reduce external pushing forces,” Applied Ergonomics, 33, pp117-127, 2002

[3]K. W. Al-Eisawi, C. J. Kerk, J. J. Congleton, A. A. Amendola, O. C. Jenkins, and W. G. Gaines, “The effect of handle height and cart load on the initial hand forces in cart pushing and pulling,” *Ergonomics*, vol. 42, no. 8, pp. 1099–1113, Aug. 1999

[4]Al-Eisawi, K. W., Kerk, C. J., Congelton, J. J., Amendola, A. A., Jenkins, O. C., Gaines, W., 1999, "Factors affecting minimum push and pull forces of manual carts," Applied Ergonomics, 30, pp235-245

[5]V. Ciriello and R. McGorry, “Maximum acceptable horizontal and vertical forces of dynamic pushing on high and low coefficient of friction floors,” *International journal of industrial Erogonomics*, vol. 27, pp. 1–8, 2001.

[6]M.-C. Jung, J. M. Haight, and A. Freivalds, “Pushing and pulling carts and two-wheeled hand trucks,” *International Journal of Industrial Ergonomics*, vol. 35, pp. 79–89, Jan. 2005.

[7]M.-C. Jung, J. M. Haight, and A. Freivalds, “Luggage-pulling task evaluation by kinematics and subjective ratings,” *Journal of SH&E Research*, vol. 3, no. 1, pp. 1–34, Jan. 2006.

[8]C.-L. Lin, M.-S. Chen, Y.-L. Wei, and M.-J. J. Wang, “The evaluation of force exertions and muscle activities when operating a manual guided vehicle,” *Applied Ergonomics*, vol. 41, pp. 313–318, Jan. 2010.

[9]E. W. Y. Kwong, C. K. Y. Lai, E. Spicciolato, and M. C. M. Wong, “Views of Adults on Shopping Trolleys: Implications for the Development of a Shopping Trolley,” *The Ergonomics Open Journal*, vol. 3, pp. 32–37, Jan. 2010.

[10]M. Raison, C. Gaudez, S. Le Bozec, and W. P. y, “Determination of joint efforts in the human body during maximum ramp pushing efforts,” *J Biomech*, vol. 40, no. 3, pp. 627–633, 2007.

[11]M. J. Ger, K. Sawatzki, U. Glitsch, R. Ellegast, H. J. R. Ottersbach, K. Schaub, G. Franz, and A. Luttmann, “Load on the lumbar spine of flight attendants during pushing and pulling trolleys aboard aircraft,” *International Journal of Industrial Ergonomics*, vol. 37, pp. 863–876, Jan. 2007.

[12]U. Glitsch, H. J. R. Ottersbach, R. Ellegast, K. Schaub, G. Franz, and M. J. ger,

"Physical workload of flight attendants when pushing and pulling trolleys aboard aircraft," *International Journal of Industrial Ergonomics*, vol. 37, pp. 845–854, Jan. 2007.

[13]B. Schibye, K. Sùgaard, D. Martinsen, and K. Klausen, "Mechanical load on the low back and shoulders during pushing and pulling of two-wheeled waste containers compared with lifting and carrying of bags and bins," *Clinical Biomechanics*, vol. 16, pp. 549–559, Jan. 2001.

[14]B. Laursen, "The effect of different surfaces on biomechanical loading of shoulder and lumbar spine during pushing and pulling of two-wheeled containers," *Applied Ergonomics*, vol. 33, no. 2, pp. 167–174, Mar. 2002.

[15]I. Kingma, P. Kuijer, and M. Hoozemans, "Effect of design of two-wheeled containers on mechanical loading," *International journal of industrial ergonomics*, vol. 31, pp. 73–86, 2003.

[16]A. J. Van Der Beek, B. D. R. Kluver, M. H. W. Frings-Dresen, and M. J. M. Hoozemans, "Gender differences in exerted forces and physiological load during pushing and pulling of wheeled cages by postal workers," *Ergonomics*, vol. 43, no. 2, pp. 269–281, Feb. 2000.

[17]Abel E.W. and Frank T.G.,"The design of attendant propelled wheelchairs," Prosthetics and orthotics international, 15, pp.38-45, 1991

[18]L. H. Van Der Woude, C. M. Van Koningsbruggen, A. L. Kroes, and I. Kingma, "Effect of push handle height on net moments and forces on the musculoskeletal system during standardized wheelchair pushing tasks," *Prosthet Orthot Int*, vol. 19, no. 3, pp. 188–201, 1995.

[19]Winter D.A., "Biomechanics and Motor Control of Human Movement, Second edition," John Wiley & Sons, 1990

[20]Nikravesh P.E., 1988, "Computer-Aided Analysis of Mechanical Systems," Prentice-hall

[21]Tatsuto S. and Hinonobu U, "Investigation of the Light Load in Propelling a Handcart on Various Road Resistances," Journal of Biomechanical Science and Engineering, 4(3), pp.423-433, 2009

Chapter 3 Attendant autonomous capability in propelling a wheelchair

3-1 Introduction

This chapter focuses on investigating an autonomous provided capability of propelling attendant-propelled wheelchair with an occupant. Attendants propel the attendant-propelled wheelchair to support traveling of a patient with walking disabilities. In the most of traveling time, the attendants propel the attendant-propelled wheelchair under natural effort. The attendants can propel hard to drive the wheelchair at fast speed, however, the fast driving makes attendant tired and fatigued easily. So the attendant unconsciously minimises the propelling force and maximises the walking velocity in order to drive the wheelchair to prevent from fatigue as long as possible. In this study, we define this unconsciously regulated propelling activity as an autonomous provided capability in propelling.

The autonomous provided capability in propelling is needed for the design of the assist as needed control in powered attendant-propelled wheelchairs. The minimised attendant's propelling performance appears in the most part of the travelling time, so the design of the assist control must be treat the autonomous provided capability in propelling as the standard propelling performance of the attendant.

In the previous studies about push and pull activities, the investigations focused about the factors, such as maximum condition of push/pull forces, joint loading, isometric or isokinetic, posture, foot position and floor friction, in order to prevent from occupational musculoskeletal injuries in industrial factories.

In early days, the maximum pushing and pulling forces were focused. About the pushing and pulling performance at standing, Ayoub 1974[1] studied maximum push and pull force under standing positions. Chaffin 1983[2] analysed optimal postures for exerting maximum force. Snook 1991[3] stipulated the approximate limits on occasional pushing and pulling activities.

Most of previous studies were carried out under maximal exertion because many injuries on pushing cart likely happen in industries and warehouses. The main health problem among industrial workers was back pain, so the compression and shear forces at lamber spine were investigated well. Andres 1991[4] proposed and validated a sagittal plane with a dynamic biomechanical model in order to predict L5/S1 compressive force and required coefficient of friction during dynamic cart pushing and pulling. The results showed the biodynamic model holds promise as a tool for analysis of actual industrial pushing and pulling tasks, when carefully applied. Kumar 1994[5] investigated low back

pain caused by maximal push and pull tasks. Lee 1991 estimated lower back loading in cart pushing and pulling with six subjects at three different forces(98N, 196N, and 294N), three different heights(660mm, 1090mm, and 1520mm), and two different speeds(0.5m/s and 1m/s). The results suggested that the low back loading in pushing a cart was lesser than in pulling. The participant weight affected the lower back loading more significantly in pulling(50% increase) than in pushing(25% increase). The handle height 1090mm in pushing was better than other heights, and the handle height 1520mm reduced mostly the lower-back loading in pulling. Hoozemans 2004[6] studied the mechanical load on the low back and shoulder during pushing and pulling in combination with three task constraints; the use of one or two hands, three cart weights, and two handle height. Hoozemans used a biomechanical model to estimate mechanical loading at the low back and shoulder joint. From their results, Hoozemans recommended to maintain low cart weight and to push or pull at shoulder height. Lett 2006[7] studied to assess several mechanical issues related to low back loading during pushing and pulling tasks. The results showed that the main contributors to the forces produced on the low back were the quantity of the load being pushed or pulled, handle height, experience level and technique. Marras 2009[8] investigated the low back loading and risk associated with pushing activities in various physical factors, such as load magnitude, speed of push, required control, and handle height. Marras found the greatest anterior/posterior shear loads at the upper levels of the lumbar spine, and the anterior/posterior shear load was influenced by all physical factors in the experiments.

The joint loading at pushing and pulling was also reported. Gagnon 1992[9] evaluated muscular moments and mechanical work at all body joints, and spinal loading at L5/S1 while pushing a 22kg box onto shelves of different heights. The results showed that the working height was an important factor for upper limbs, and its involvement increases at the higher level.

Kumar 1995[10] investigated the difference between isometric and isokinetic pushing and pulling under the handle to be fixed and moved at constant speed. Kumar tested two handed push-pull strength in sagittal plane at heights of 25cm, 100cm, and 150cm in isometric and isokinetic conditions under stabilised lower extremity; hip, knees, and ankles. Both male and female participants exerted strongest force in pulling at medium height 100cm in isometric mode. The isometric pushing strength for male participants ranged from 41% to 68% of the maximum pulling forces, and from 27% to 44% for female participants. The isokinetic strengths were significantly lower than isometric strengths.

The force directions in pushing and pulling were investigated. Looze 2000[11] studied how force direction changes as handle height and force level change, and investigated the load on shoulder and low back. Looze carried out experiments that eight participants

pushed or pulled a stationary bar or movable carts at various height and horizontal force levels while walking on a treadmill. Looze found that the pushing force direction changed from 45deg. downward to near horizontal with the increase of the horizontal force level and handle height, and the pulling force direction changed from 14deg upward to near horizontal.

Also the foot position and floor friction about pushing and pulling were investigated. MacKinnon 2002[12] examined the effects of standardised foot positions during the execution of a submaximal pulling task. MacKinnon focused on how experimentally controlled foot positions could affect the parameters of a load. The results showed the load velocities and forces were not affected by standardised foot positions. Boocock 2006[13] tested the hypothesis whether differences in the frictional properties of a floor surface affect the kinematics and kinetics of pushing and pulling. The results showed that the handlers involved in the pushing and pulling of trolleys were capable of adjusting posture and the direction of hand and foot forces in order to compensate for reduced levels of floor friction.

The posture in pushing and pulling, including arm posture and orientation were investigated. MacKinnon 1998[14] investigated the differences in maximal isometric pull forces in the sagittal plane. Eight participants produced maximum isometric horizontal pulls on three different postural conditions; free standing, fixed standing, and seated. MacKinnon found that the largest horizontal forces were produced at near elbow height in standing posture and slightly lower elbow height in the sitting posture. Herring 2007[15] studied the effect of distance and height on maximal isometric push and pull strength with reference to manual transmission truck drivers. The results showed that the furthest distance 45cm and the middle height 64.3cm from the edge of a chair were optimal positions to generate push/pull forces to the shift knob under minimum muscle activities. Okunribido 2008[16] investigated arm posture and hand force during bi-manual pushing. Okunribido found that the forearm posture was important to exert force, and the balance in forces was important. Seo 2010[17] evaluated the biomechanical models for the effects of handle orientation, handle material, gloves and arm posture on maximum push/pull force. Seo found that the push/pull force with a perpendicular handle was 10% larger than the force with a parallel handle, and the decrease of the friction between handle and hand further decreased the push/pull forces in the parallel handle.

There is no previous study to investigate natural provided capability in pushing and pulling the attendant-propelled wheelchair on the slope. So, this study focuses on the autonomous provided capability in propelling the wheelchair with a force velocity relationship as an indicator of the provided capability in propelling. Hill 1938[18] shows the force velocity relationship in contraction performance of muscles. Also torque angular velocity relationship is used to show the performance of rotational prime motors, such as,

electric motors and combustion engines. In previous studies, there are many cases to use the force velocity relationship and the torque angular velocity relationship as the indicator of the physical performance by human.

In early stage of the previous studies, some researchers focused on pedalling, cranking and running exercises under maximum effort, in order to estimate human performance as the prime motors. Vandewalle 1987[19] investigated the force velocity relationship and maximum power of pedalling on a cycle ergometer. Vandewalle observed the maximum anaerobic power in athletes from evaluated force-velocity relationship. Vandewalle 1989[20] also investigated the force-velocity relationship and maximum power of cranking in young swimmers. Vandewalle's purpose is to study the effect of growth upon maximal anaerobic power of the upper and lower limbs. Jaskólska 1999[21] studied treadmill measurement of the force-velocity relationship and power output in subjects with different maximal running velocities. Jaskólska's purpose is to estimate the gross body force-velocity (F-V) relationship on a newly developed motorised treadmill in subjects who differed in their predicted maximal running velocity calculated from the F-V relationship. With 32 subjects, the F- V relationships during running were obtained from all-out sprints against different resistance settings that were 5%, 8%, 10%, 13%, 15% and 20% of the maximal value the treadmill could produce. The F-V relationship fitted a linear regression in the subjects. Jaskólska concluded that the linear F- V relationship measured on the treadmill was independent of the subject's maximal running speed. The subjects with a higher maximal speed also developed higher power on the tested resistance range. Rahmani 2001[22] studied the force velocity relationship during maximal dynamic and isometric squat exercises with masses ranging from 60 to 180kg on the shoulders. The results showed the forces produced during the squat exercise in ascending were linearly related to the velocity in each participants, and the highest power was produced against lightest load 60kg. Hintzy 2003[23] determined the relationship between force and velocity parameters during a specific multi-articular upper limb movement - hand rim propulsion on a wheelchair ergometer. Seventeen healthy able-bodied female participant performed nice maximal sprints in 8s with friction torque varying from 0 to 4Nm. Individual force velocity relationship were established for peak force and velocity from nine sprints. The results shows the force velocity relationships were linear in all participants. The results shows the maximum power in average was about 90W at velocity about 1.6m/s. Toji 2007[24] investigated the effect of ageing on muscular power development by determining the force velocity relationship in the elbow flexors. The results shows the maximum powers by participants in their 70s were significantly lower than in other groups in their 50s and 20s. The ratio of the maximum power in their 70s by in their 20s was about 70%. Dorel 2009[25] investigated the contribution of each

functional sector to the power-velocity relationship of lower-limb extensor muscles in maximal cycling exercises. Dorel investigated the muscle function in downstroke while pedalling and the flextor muscle's ability to pull on the pedal during the upstroke. Raj 2010[26] found that ageing was associated with a downward and leftward shift of the force velocity curve due the lower muscle strength across all contraction speed.

This study focuses on the autonomous provided capability in propelling. The maximum provided capability in propelling can be obtained from the measurement of the maximum pushing force on the motorised treadmill at constant belt velocity. Under natural exercises, however, human regulates output forces by subjective hardness to continue exercises for long time. This means that the attendants would take unconsciously and steadily autonomous propelling against a load resistance after few minutes passed from start. And the attendants maximise the propelling force and the walking velocity with minimised subjective hardness, which can be determined by the exercising heart rate (EHR).

The aim of this chapter is to obtain this autonomous capability in propelling under minimised subjective hardness. In the exercises, people feel subjective hardness as the increase of their heart rate from the resting heart rate. This study uses this relative heart rate from rest as the indicator of subjective hardness. The relative heart ratio is commonly used as the Exercise Heart Rate (EHR) to assess the subjective hardness by heart rate by Karvonen 1957[27].

From daily experiences about propelling attendant propelled wheelchair, the attendant would propel a wheelchair under the steady propelling force and walking velocity against a certain constant propelling load by environment if propelling continues long time. This study defined this steady propelling condition as an operating point in propelling. The propelling load is mainly determined by the wheelchair weight, the materials of front casters and rear wheels, road surfaces, and slope angles. If the propelling load is changed by environments, the attendants adapt their operating point against the changed propelling load. This similar phenomenon can be seen a prime motor-load system. The prime motor under the operating point stably drives a load under the condition that the motor torque is equal to the resistant torque. The motor performance curve can be estimated from the steady operating points by various constant load conditions. From the analogy between the prime motor-load system and the attendant wheelchair system, the hypotheses in this chapter are following.

1. The natural(autonomous) provided capability in propelling is obtained from the measurement of the steady operating points by various constant propelling load. This means that the attendant autonomously maximises the propelling force and the walking velocity with minimising the subjective hardness, in order to propel long time against

propelling loads.

2. The force-velocity relationship of the autonomous provided capability in propelling is a monotonic decreasing function. The attendant generates large propelling force under low walking velocity, however, the propelling force decreases under the increased walking velocity.

3. The provided capability in propelling is determined by the subjective hardness. The attendant can increase the propelling capability in propelling if bearable subjective hardness is increased.

In the first part of this chapter, we confirmed that the methodology to assess the autonomous provided capability in propelling was effective from an outlined attendant-wheelchair model. From the confirmation of the methodology, the developed apparatus to assess the autonomous propelling is introduced. With the simulated wheelchair weight 100kg under the apparatus, we solved the autonomous propelling behaviour responding to varying propelling loads, at a level and longitudinal slopes from -8 degree to +8 degree. On the propelling the wheelchair, the autonomous provided capability is shown as the relationship of the propelling force and the wheelchair velocity. Three able-bodied subject without any musculoskeletal disorders joined this study. Also the generated forces in single leg, which contributes the main propelling force, are estimated from walking pattern.

3-2 Autonomous provided capability in propelling

This section proves the methodology how to assess the autonomous provided capability in propelling, using outlined attendant-wheelchair model in Figure 3-1.

Attendants propel against the propelling load by an attendant-propelled wheelchair, mainly based on wheelchair weight and road resistance. In the attendant propelling, main physical parameters are operating force, walking velocity and wheelchair velocity. The attendants exert the pushing force to keep wheelchair velocity suitable for attendants, and also involuntarily adjust the relative velocity and distance between the attendant and the wheelchair, to follow the wheelchair. The attendants carry out propelling activity under bearable subjective hardness, based on attendant's characteristics, such as physical, sensory, motor, psychomotor, personality, training and experience and health status so on. From this detailed view in the attendant propelling, this study proposed the outlined model about the attendant-wheelchair system.

Figure 3-1 shows the outlined signal model of attendant-wheelchair system. Left side in Figure 3-1 is an attendant part, and right side is a wheelchair part. This study assumes that all elements in the model are linear. The attendant part consisted of a brain part $G_{BR}(s)$ and a body components $G_H(s)$. The wheelchair system $G_W(s)$ consists of the weight including an occupant, and resistance load by road surface and slope angles.

In the model, the brain $G_{BR}(s)$ in the attendant part determines a planned pushing force $F(t)$ from the walking speed $v(t)$, and the planned force $F(t)$ by the walking velocity $v(t)$ is regulated by subjective hardness described by exercising heart rate (EHR). The EHR is the response of circulatory system $G_C(s)$ by exercises of whole body. This study defined the relationship between the planned force $F(t)$ and the walking velocity $v(t)$ as an equation (3-1)

$$F(t) = \varphi\{v(t)\} \tag{3-1}$$

This study assumed that the function by the equation (3-1) was a 1st order monotonic decreasing function, because the increase of the walking velocity $v(t)$ generally needs more kinetic energy, and this phenomena causes the decrease of the planned force $F(t)$. The curve shape of $F(t) = \varphi\{v(t)\}$ is determined by attendant's physical strength against exercise loads and the performance of the circulatory system described by the transfer function $G_C(s)$. With the planned force $F(t)$ by the walking velocity $v(t)$, the lower extremity of the attendant generates the driving force $f_D(t)$ through a muscle dynamics $G_M(s)$.

$$f_d(t) = L^{-1}\{G_M(s)F(s)\} \tag{3-2}$$

Here, the symbol L^{-1} shows inverse Laplace transform and the s shows Laplace operator. The walking velocity $v(t)$ is generated by the difference of forces between the driving force $f_D(t)$ and the operating force $f_W(t)$.

$$v(t) = L^{-1}\left[G_H(s)\left\{F_D(s) - F_W(s)\right\}\right] \tag{3-3}$$

The operating force $f_W(t)$ is transferred by the arm function $G_{AM}(s)$, based on the relative velocity between the attendant $v(t)$ and the wheelchair $v_W(t)$.

$$f_W(t) = L^{-1}\left[G_{AM}(s)\left\{V(s) - V_W(s)\right\}\right] \tag{3-4}$$

From the equation 3-2 to 3-4, the operating force $F_W(s)$ and the wheelchair velocity $v_W(t)$ are solved as equations below.

$$F_W(s) = \frac{G_{AM}(s)G_H(s)G_M(s)}{1 + G_{AM}(s)G_H(s)}F(s) + \frac{G_{AM}(s)}{1 + G_{AM}(s)G_H(s)}V_W(s) \tag{3-5}$$

$$V(s) = \frac{G_{AM}(s)G_H(s)}{1 + G_{AM}(s)G_H(s)}V_W(s) + \frac{G_H(s)G_M(s)}{1 + G_{AM}(s)G_H(s)}F(s) \tag{3-6}$$

In general, the production of $G_{AM}(s)G_H(s)$ is assumed greater than 1. From this assumption, the equations 3-5 and 3-6 are simplified.

$$F_W(s) = G_M(s)F(s) - \frac{1}{G_H(s)}V_W(s) \tag{3-7}$$

$$V(s) = V_W(s) + \frac{G_M(s)}{G_{AM}(s)}F(s) \tag{3-8}$$

This study focuses on the outputs at steady state. Before using final value theorem, the transfer function of the body movement is assumed $G_H(s) = 1/ms$, here the m is an attendant weight. And the transfer function of the arm function is also assumed $G_{AM}(s) = c + k/s$, here the c is a damping coefficient and the k is a stiffness in the attendant's arm. And the gain of $G_M(s)$ is assumed as 1 because human has proportionality that planned movements correspond to actual body movements. From these assumption, the outputs of the equations 3-7 and 3-8 at steady state are solved with the final value theorem.

$$[f_W(\infty), v_W(\infty)] = [F(t), V(t)]_{t=\infty} \tag{3-9}$$

This equation means the walking velocity $v(t)$ follows the wheelchair velocity $v_W(t)$ without offset. The wheelchair velocity $v_W(t)$ is generated by the operating force $f_W(t)$ with the wheelchair dynamics $G_W(s)$.

$$v_W(t) = L^{-1}\left\{G_W(s)F_W(s)\right\} \tag{3-10}$$

The attendant keeps propelling with updating [F(t), V(t)] until the attendant-wheelchair system is in steady state. Under steady state after enough time passed, the planned force and the walking velocity become F_S and V_S in the brain respectively. From the equation 3-9, the attendant-wheelchair system satisfies an equation below.

$$[F(\infty),V(\infty)]=[f_W(\infty),v_W(\infty)]=[F_S,V_S] \tag{3-11}$$

The equation 3-11 means that the attendant autonomously determine the wheelchair velocity $v_W(t)$ at steady state from $[F(\infty),V(\infty)]=[F_S,V_S]$. The operating point $[F_S,V_S]$, which is determined by subjective hardness EHR of the propelling activity, is an extreme important factor in the model. So this study focuses on and simplify the relationship between the wheelchair velocity $v_W(t)$ and the operating point $[F_S,V_S]$.

The wheelchair dynamics $G_W(s)$ can be described by 1st order lag element in the equation 3-12, because the wheelchair dynamics $G_W(s)$ mainly depends on its total mass M including an occupant, and road resistance. The road resistance is generally assumed as $Rv_W(t)$, here R is a proportional road resistance coefficient to the wheelchair velocity $v_W(t)$.

$$G_W(s)=\frac{V_W(s)}{F_W(s)}=\frac{1}{Ms+R}=\frac{\frac{1}{R}}{\frac{M}{R}s+1} \tag{3-12}$$

Here, the time constant is $T=M/R$, and the gain is $K=1/R$. The next equation is obtained from the simplified equation 3-12 with the final value theorem.

$$f_W(\infty)=Rv_W(\infty) \tag{3-13}$$

With the equation 3-11 and 3-13, the relationship between the wheelchair velocity $v_W(t)$ and the operating point $[F_S,V_S]$ is shown in next equations.

$$\begin{cases} v_W(\infty)=V_S \\ v_W(\infty)=\dfrac{F_S}{R} \end{cases} \tag{3-14}$$

Finally, the equation 3-14 provides the proof that the force velocity relationship of $F(t)=\varphi\{v(t)\}$ is solved by the operating point $[F_S,V_S](=[f_W(\infty),v_W(\infty)])$ with varying the resistance load coefficient R. This R describes a ratio of the road resistance force by the wheelchair velocity.

This study defines the propelling situation by an attendant at the $[F_S,V_S]$ as autonomous propelling. In this chapter 3, this study provides the results of autonomous propelling in attendant propelled wheelchair. The simplified solution for autonomous propelling is shown in Figure 3-2. On this solution, enough smoothing in both signals of the operating force $f_W(t)$ and the wheelchair velocity $v_W(t)$ is needed because both

signals contain periodic changes caused by two leg walking. The performance of this method to solve the relationship $F(t)=\varphi\{v(t)\}$ relies on 1st order element which has large lag time compared with the response time by all of transfer functions in the attendant part.

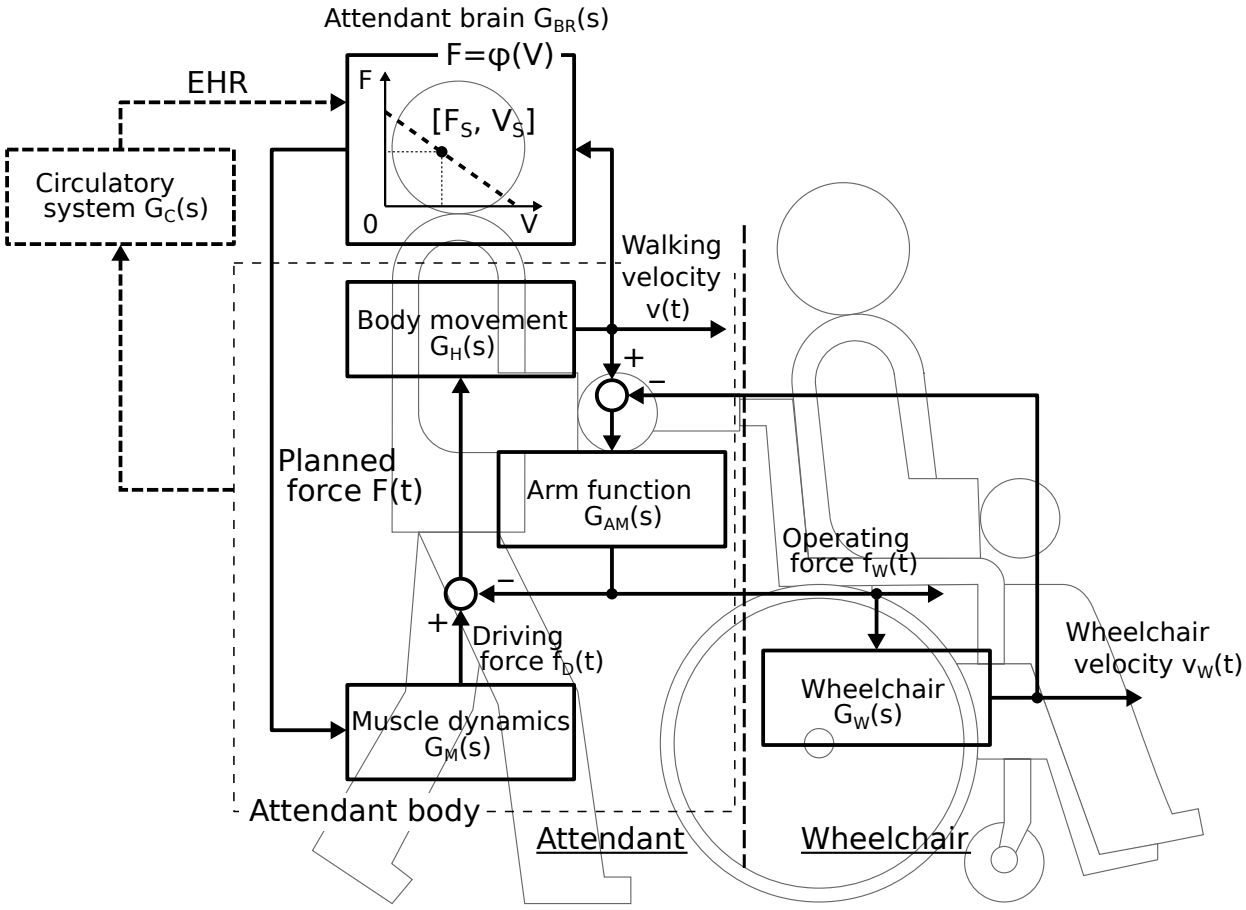

Figure 3-1 Outlined block diagram of attendant-wheelchair system

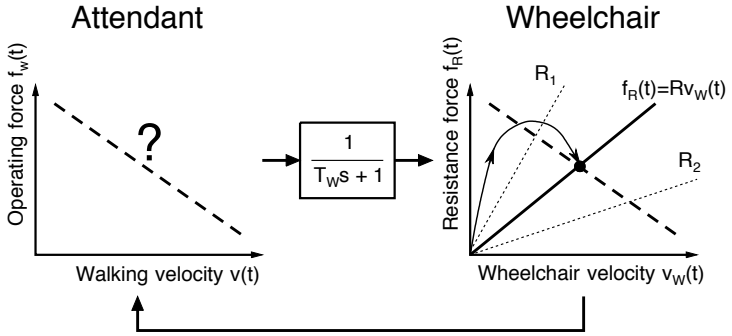

Figure 3-2 Solution of autonomous propelling

According to the methodology to assess the autonomous provided capability in Figure 3-2, this study developed experimental devices to investigate the autonomous capability in propelling, the autonomous pushing wheelchair(Appendix A), and hand cranking(Appendix B). These devices have signal processing system to simulate the

various resistance loads. At the case of attendant-propelling, the motorised treadmill device with two straight bars was developed. This chapter mainly focus on the attendant propelling first, and later introduce the case of wheelchair pushing and occupant-cranking with a developed motorised apparatuses in the Appendix A and B.

The coefficient of road resistance R determines the propelling loads. The investigation with the stable R at each trial gives reproducible results, so this system can separate between nonlinearity and noises caused by various disturbances which real systems have. The increase of R provides the increased propelling load in proportion to the wheelchair velocity. The time constant T_W, which regulates smoothing time of signals, reduces the rapid change of the wheelchair velocity caused by sudden irregular changes in the operating force.

3-3 Methodology for investigating autonomous propelling

Based on the section 3-2, which showed the idea of searching the operating points at steady state, new experimental device in Figure 3-1 was developed to investigate the autonomous provided capability in propelling by attendants. This device was built on a motorised treadmill and added two straight grips placed on the same position of the attendant propelled wheelchairs. The treadmill system is suitable for investigating the detailed analysis in walking for long time under steady state. From the comparison between the walking in overground and treadmill, Alton 1998[28] showed that the kinematics in both conditions are almost same. From this view, this study used a treadmill as a base experiments condition. The belt surface dimension for walking was 1450mm(length) x 470mm(wide) and it was enough to walk with pushing and pulling the grips freely. Also the treadmill can be tilted to reproduce the propelling in ascending and descending. The belt of the treadmill was driven by the driver roller (ϕ=60mm) with the 3.5kW AC servomotor (Mitsubishi HA-SE352). The belt velocity $v_t(t)$ measured by the encoder in the servomotor, was feedback controlled by a motor driver with input velocity signals. The belt was tensioned well to prevent from any slip between the surface of the driver roller and the back of the belt.

The straight grip had a 1-axis load cell, which measured range was from -200N in pulling and +200N in pushing, with the time constant 0.6s. Total pushing force $f_W(t)$ was measured from the sum of both propelling force $f_{WL}(t)$ and $f_{WR}(t)$.

The attendant position $d(t)$ from the grips on the treadmill was measured by the ultrasonic sensor placed in front of the participants. Also the detailed joint movements were recorded by a video camera at the frame rate 30Hz with reflective markers adhered to each joint; shoulder, elbow, wrist, hip, both knees and ankles. The walking pattern was measured from foot on and off detected by a switch fixed to the side of each shoe. The heart rate of the participants measured by a strap type of a heart rate monitor (Polar Inc.)

This device has signal processing system along with the methodology of Figure 3-2. From Equation (3-12), the $G_W(s)$ is virtual wheelchair component and also has functions for searching the operating points $[F_S, V_S]$. The gain $K_W = 1/R$ of the $G_W(s)$ provides the ideal linear propelling load without disturbance. The range of the R was used in 1.2 - 1250 N/(km/h)[=4.3 - 4500N/(m/s)] in this investigation. The time constant $T_W(=M/R)$ was used in the range 5 - 8sec. The wheelchair element $G_W(s)$ calculated the wheelchair velocity from the total operating force $f_W(t)$, then the motor driver controlled the belt

velocity of the treadmill to correspond to the calculated wheelchair velocity.

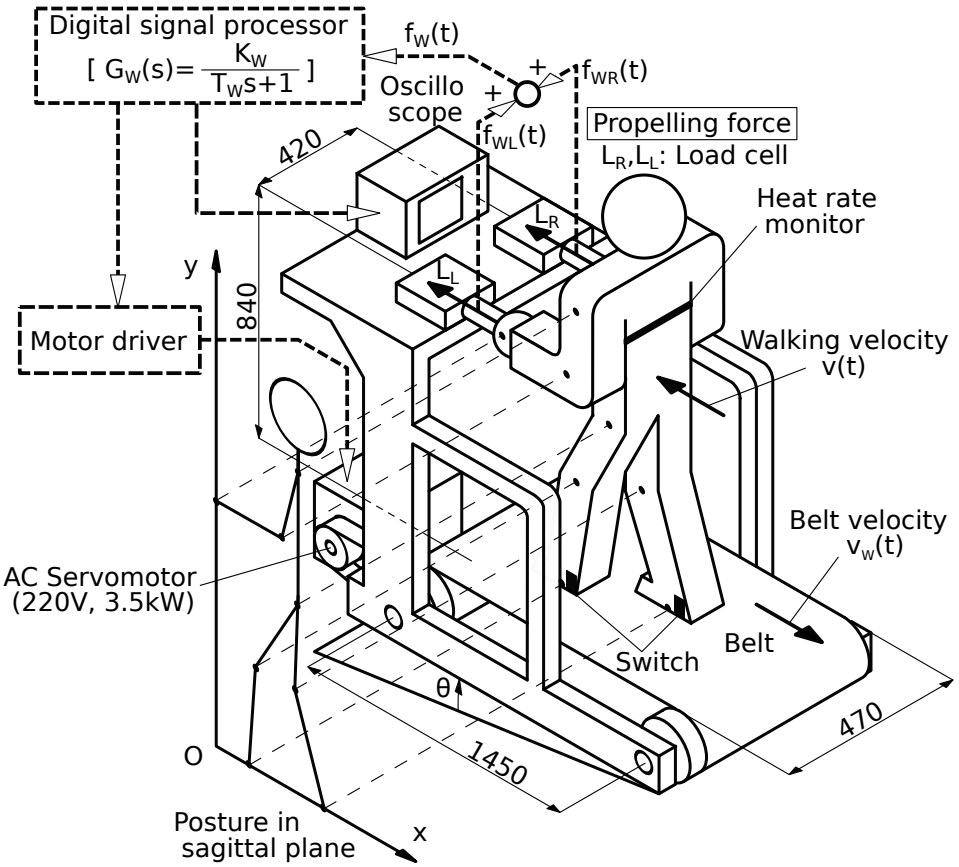

Figure 3-3 Motorised treadmill with grips

This study focused on the walking pattern and the generated force by a single leg under propelling a wheelchair at steady state, because attendants walk by two legs and both leg forces mainly contribute to generate the pushing force $f_W(t)$. In this study, the walking pattern was described by the defined parameters in Figure 3-4, based on the assumption that the movements of both legs were symmetry. The defined walking pattern, which has a strong relationship with the walking velocity $v(t)$, consists of step length L_S, stride time D_P, standing period D_t, swing period D_w and double support period $D_b[=D_{b1}+D_{b2}]$. The MS of the vertical axis in Figure 3-4 shows the foot state in contact with the ground; zero is foot on and one is foot off. The stride time D_P is the period from a foot on to a next foot on in the same side. The step length L_S was calculated from the settled walking velocity V_S and the stride time D_P with an equation below.

$$L_S = V_S D_P \tag{3-15}$$

Under steady state walking, the body mass of the attendant faintly cause the change of the pushing force $f_W(t)$ because of slight horizontal body acceleration. Based on this condition, the pushing force $f_W(t)$ was assumed to be generated when each leg stood on the ground. From Figure 3-4, a left leg stands in the period $D_w + D_{b1} + D_{b2}$, and a right leg stands in the period D_t. The averaged single-leg generated force F_L, which was assumed the same in both side, was calculated from the settled pushing force F_S with the stride time D_P.

$$F_L = F_S \frac{1}{\frac{D_w + D_t + D_{b1} + D_{b2}}{D_P}} = F_S \frac{1}{1 + \frac{D_b}{D_P}} \tag{3-16}$$

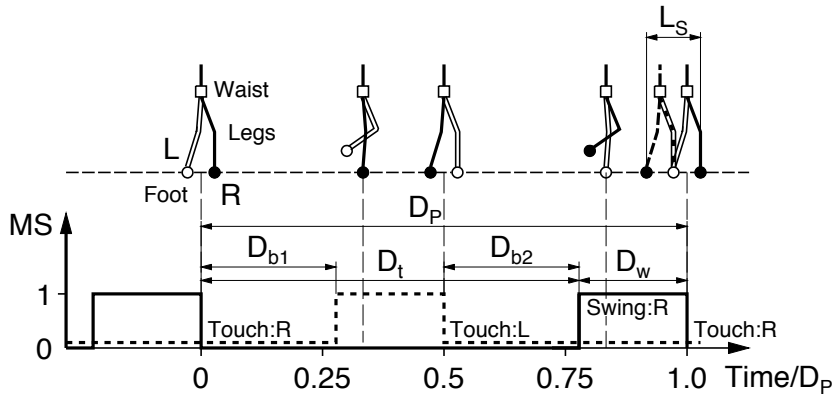

Figure 3-4 Definition of walking parameters

The procedure of trials was following; a participant had stood on the treadmill with gripping slightly the straight bars before a start sign showed. Then, the participant started to propel on the treadmill naturally, and continued to propel for 20 minutes at steady state. The participant was asked this procedure before all trials. In each trial, the operating point $[f_W(t),\ v_t(t)]$ was recorded from well smoothed pushing force $f_W(t)$ and the treadmill belt velocity $v_t(t)$. Also, the distance $d(t)$ from the grips to the participant, and the foot contacting state were simultaneously recorded. After one trial, the participant had rested on a chair for 10 minutes or more until the participant's heart rate returned to stable condition, then the resistant load R in the range of 0.33 - 347 N/(m/s) was randomly selected and carried out next trial. In the trial of maximum pushing, the belt velocities were manually controlled and the participant continued propelling until he or she could not keep propelling in maximum state.

In the exercises, subjective hardness is defined as the increase of heart rate from resting

state. This study used the relative heart rate from rest as the indicator of subjective hardness. The relative heart ratio is commonly used as the Exercise Heart Rate (EHR) to assess the subjective hardness using heart rate. The EHR is defined with the equation below. (Karvonen 1957[27])

$$EHR = \frac{HR - HR_{REST}}{HR_{MAX} - HR_{REST}}[\%] \tag{3-17}$$

Here, the HR is the heart rate under exercises, the HR_{MAX} is the maximum heart rate, which can be estimated by the formula: 220 - age, and the HR_{REST} is the heart rate at rest.

Three participants in around 23year old joined this study. All participant were healthy males without any disorders as representation. The participant's descriptions show in Table 3-1. In advance, we explained well the detailed procedure in the trials and received all subject's agreements to take part in our experiments. The trials were prepared to stop immediately when the participant claimed their wrong feeling or fatigue thorough experiments. The maximum time of experiments for each participant at the same day was limited in three hours.

Table 3-1 Description of participants

Subject (age)	A (24)	B (23)	C (23)
Height [cm]	169	168	178
Weight [kg]	75	56	90
Grip force [N] (average of both side)	333	368	456
Back force [N]	1254	696	1544
Leg length [cm]	78	78	79
Arm length [cm]	58	57	65
Natural Walking speed [m/s]	1.19	1.14	1.11
Sports activity	Occasionally	Sometimes	None

3-4 Results of autonomous propelling on the treadmill

Time series propelling behaviour

Figure 3-5 shows the time series of the pushing force $f_W(t)$, distance $d(t)$, and foot contact condition under steady propelling on a level, and Figure 3-6 shows the posture at the time in Figure 3-5. Both plots were the results of the participant A. The resistance load in a plot (a) and (b) were R=44N/(m/s) and R=1.39N/(m/s), and the settled walking velocities were V_S=0.14m/s, and V_S=1.25m/s respectively. The horizontal axes in both graphs were normalised by the single stride time from right foot on to next right foot on at each resistance load R. The numbers with circles in Figure 3-5 and Figure 3-6 show the time division by five, and show the same normalised moment in both graphs.

In the case that the resistance load R is heavy in Figure 3-5(a), the pushing force $f_W(t)$ was around 90N with periodic changes, and the distance $d(t)$ was changed periodically around 300mm, while the double support phase $D_{b1}+D_{b2}$ was accounted for large part of the stride time D_P. The periodic change in the pushing force $f_W(t)$ and the distance $d(t)$ were synchronised by feet's movement, and the phase between the pushing force $f_W(t)$ and the distance $d(t)$ was opposite that the maximised pushing force $f_W(t)$ occurred at the minimised distance $d(t)$. The amplitude of frequency component in the pushing force $f_W(t)$ and the distance $d(t)$ were around 15N and 30mm respectively. In the case that the resistance load R was light in Figure 3-5(b), the pushing force $f_W(t)$ became around 20N, lower than the $f_W(t)$ in the heavy resistance load R, and also the distance d(t) was around 380mm, longer than the $d(t)$ in the heavy R. Both the pushing force $f_W(t)$ and the distance $d(t)$ had periodic frequency components, and its amplitudes were around 12N and 30mm respectively. The double support phase $D_{b1}+D_{b2}$ was almost disappeared in the stride time D_P. The phase between the pushing force $f_W(t)$ and the distance $d(t)$ was opposite that the maximised pushing force occurred at the minimised distance $d(t)$.

This study focused on averaged and settled pushing force F_S, treadmill velocity V_S, the exercising heart ratio, the mechanical power of propelling, the posture difference against the resistance load R, the frequency components in the pushing force $f_W(t)$, the distance $d(t)$, and the walking pattern consisted of stance, swing and double support phase.

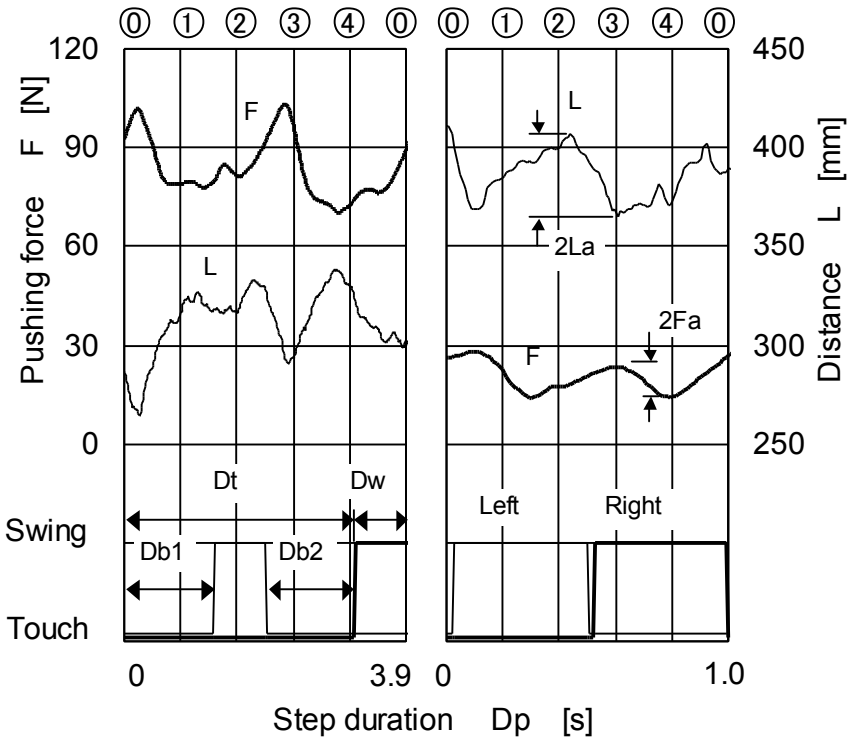

(a) R=160N/(km/h) (b) R=5N/(km/h)

Figure 3-5 Propelling behaviour at steady state

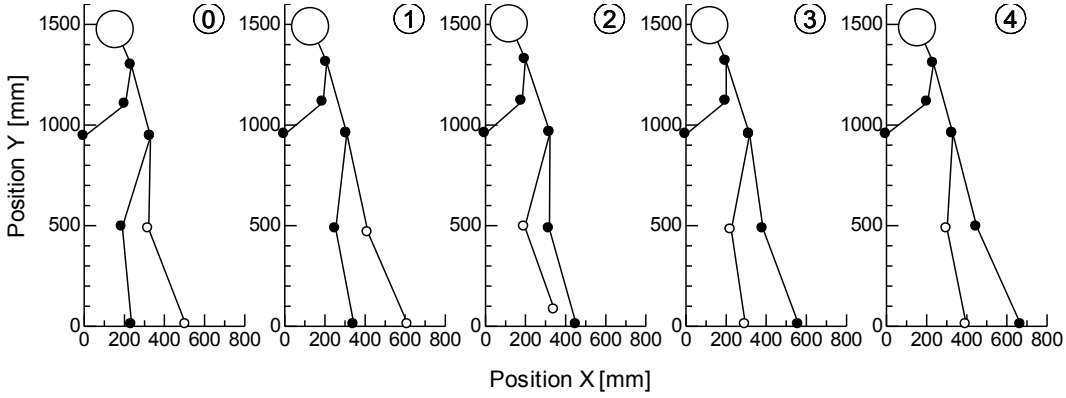

(a) R=160N/(km/h) (V = 0.5km/h)

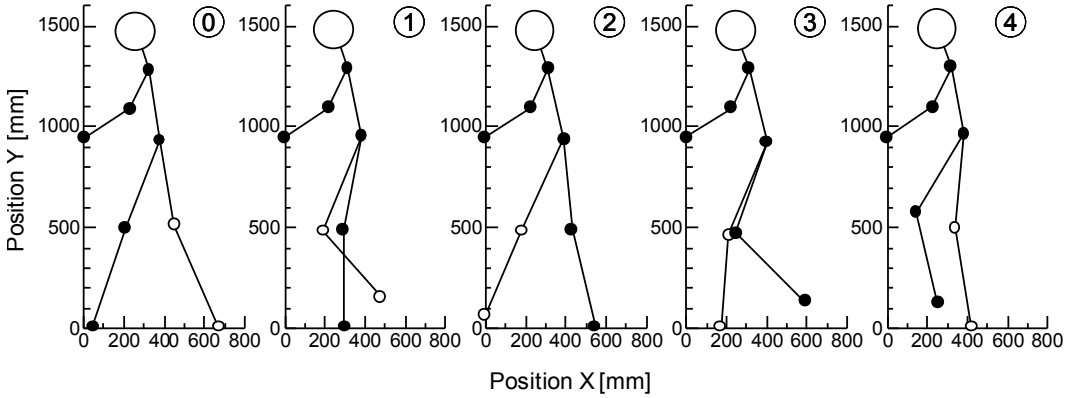

(b) R=5N/(km/h) (V = 4.5km/h)

Figure 3-6 Propelling posture on a level

Autonomous provided capability in propelling

We carried out the examination for solving the propelling activity at flat surface (θ=0) on the device in Figure 3-3. The results of propelling activity show in Figure 3-7(a) about autonomous propelling and in Figure 3-4(b) about maximum propelling. The trajectory in Figure 3-4(a) shows a transient response of the participant A's $f_W(t)$ and $v_t(t)$ from start to steady state at R=1.4N/(m/s). Just after starting to propel, the trajectory was transient, then 30 - 50 seconds passed, the trajectory had limit cycles at steady state. The time behaviours of the $f_W(t)$ and $v_t(t)$ at steady state, oscillated by two leg walking(Uchiyama 2007), but plotted circles on Figure 3-4(a) show well averaged $[f_a(\infty), v_t(\infty)] = [F_S, V_S]$, which can be organised by the relationship of $f_W(t)$=φ{ $v_t(t)$ } on steady state. The circle's colours in the plot describe the result at each participant; white is the participant A, black is B, and grey is C. The meaning of marker's colours thorough this chapter is the same. The dotted thin lines in the Figure 3-7(a) are typical resistant load R in the experiments. The employed ranges of R at each participant were different to cover the wide area of the settled operating point $[F_S, V_S]$.

At the low resistance load R around 1.4N/(m/s), all participants propelled under near natural walking velocity with the pushing force about 20N. With the increase of the resistance load R, the walking velocity decreased and the pushing force increased in all participants. Over R=22N/(m/s), the walking velocity became nearly zero with the pushing forces around 80N. From the comparison between maximum and autonomous propelling, the maximum pushing force F_m at very slow walking was over three times higher than autonomous force F_S, and the ratio against nearly natural walking was about 10 times. The drop of the pushing force between over R=22N/(m/s) and around R=1.4N/(m/s) was about 60N in both F_m and F_S. The drop trend of the walking velocity under the increased pushing force by the resistance load R, was similar to all participants.

The maximum propelling in Figure 3-7(b) was difficult to continue over four minutes because of its hardness. On the contrary, the propelling tasks under condition in Figure 3-7(b) was easy to continue in 20minutes.

Figure 3-8 is calculated results of mechanical power P in the autonomous provided capability in pushing by all participants. The mechanical power was calculated to multiply the pushing force F_S and the wheelchair velocity V_S. In this study, the maximum mechanical power under the autonomous propelling was about 40W by the relative strong participant A. The other participants generated 20 - 30W. In the participant A case, the mechanical power P proportionally increased on the range of the walking velocity V_S <

2.5km/h(0.69m/s), and slightly decreased over the range V_S > 2.5km/h(0.69m/s).

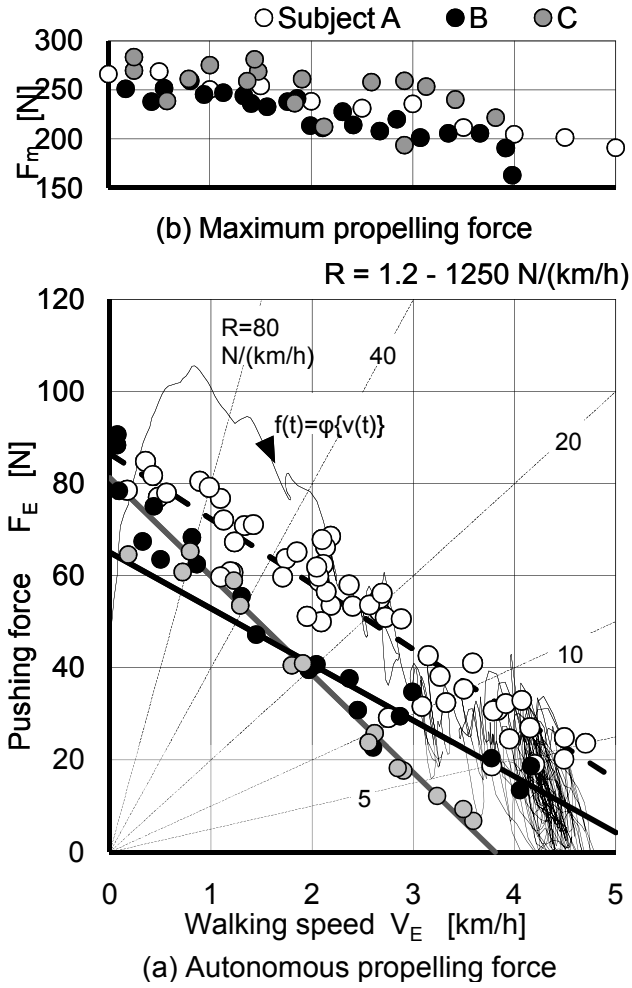

Figure 3-7 Autonomous and maximum propelling force

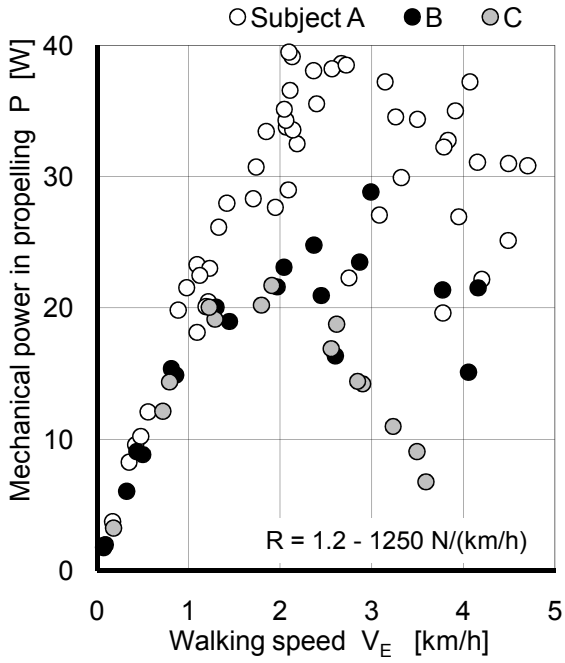

Figure 3-8 Mechanical power of the provided capability in propelling

Subjective hardness by exercising heart rate

Figure 3-9 shows the time behaviour of the Exercising Heart Rate (*EHR*). The indicated experimental conditions in Figure 3-9 were that a pushing force *Fd* was 40N, and the walking velocities *v* were 1km/h(0.28m/s), 3km/h(0.83m/s), and 5km/h(1.39m/s). In this experiments, the pushing force *Fd* was indicated to participant by an oscilloscope, and the participant adjusted the actual pushing force to the indicated pushing force while walking on the treadmill. The belt velocity of the treadmill was controlled to the indicated walking velocity by the electric motor . The *EHR* was calculated by the equation 3-17 with the measured heart rate during the trial. The *EHR*s until about four minutes in the beginning were similar to the rested condition at stand still, then the *EHR*s started to rise. This means that circulatory system has dead time delay elements. After about 10 minutes passed, the increased *EHR*s were stable at constant, and the increased *EHR*s by propelling were in proportion to the walking velocity *v*. In this chapter, this study used the averaged *EHR* in three minutes after 10 minutes passed.

Figure 3-10 shows the *EHR* under the experiments in the Figure 3-7(a). The time behaviours of *EHR* became steady after 10 minutes passed from beginning in each trial. The *EHR* in all participants increased slightly from around 20% against the increase of the resistance load coefficient *R*, which caused the decrease of the walking speed. Most of the results, however, were nearly constant value under 30%.

Figure 3-11 shows the *EHR* on various the pushing forces *Fd* and the walking velocities *V* on the motorised treadmill. The range of the indicated pushing force *Fd* was from 0 to 80N, and the walking velocity *V* was from 0km(0m/s) to 5km/h(1.39m/s). The upper graph in Figure 3-6 shows the measured *EHR* at each propelling condition, and lower graph shows the linear interpolated distribution of *EHR* in propelling condition on the plane by the pushing forces and the walking velocities. The *EHR* at stand still(the pushing force *Fd*=0 and the walking velocity *V*=0) was about 10%, and increased with the increase of the pushing force *Fd* and the walking velocity *V*. In the condition in walking without pushing (the pushing force *Fd*=0), the *EHR* in natural walking speed around 4km/ h(1.11m/s) was about 20%. This results suggest that the people get used to the light exercises on the subjective hardness around *EHR*=20% with long time. That is the reason why the EHR on the long time propelling at the treadmill in Figure 3-4 was about 20%.

Figure 3-12 shows the mechanical power in pushing with walking. The circled results were calculated mechanical power from the measured pushing forces and walking velocities under autonomous condition in Figure 3-7(a). The mechanical power in autonomous propelling likely has a peak around 2.5km/h(0.69m/s). The dashed power curves shows the mechanical power by the subjective hardness *EHR* =10%, 20% and 30%. These power curves were calculated from the liner approximated relationship

between the pushing force and the walking velocity on the lower graph in Figure 3-11. This results show the provided capability in propelling increases by the increased subjective hardness.

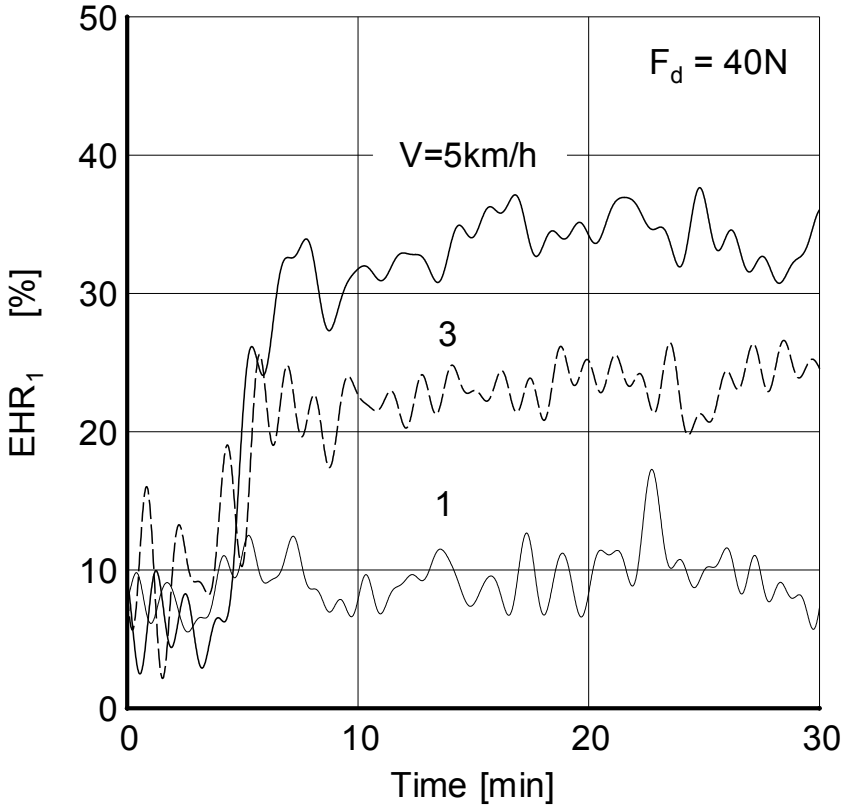

Figure 3-9 Time behaviour of EHR on pushing with walking

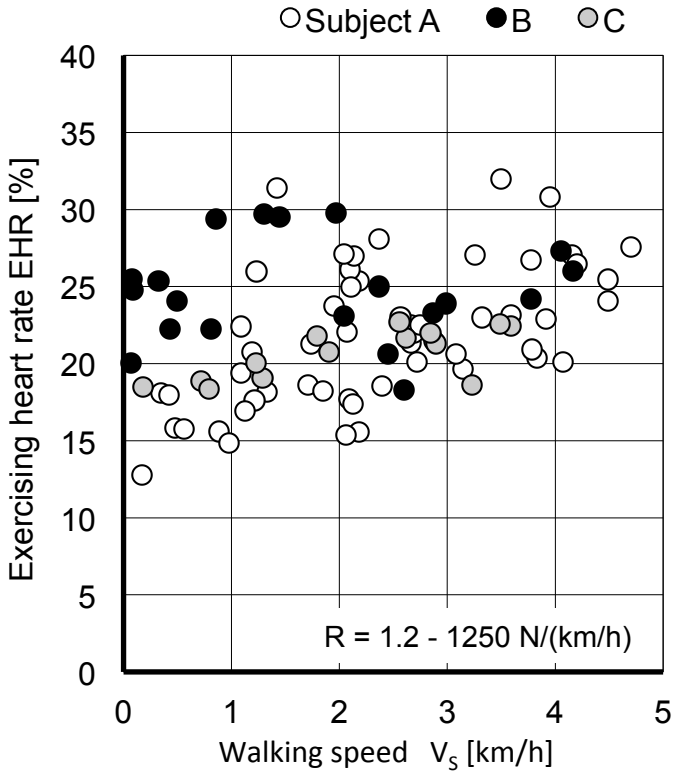

Figure 3-10 Exercising Heart Rate

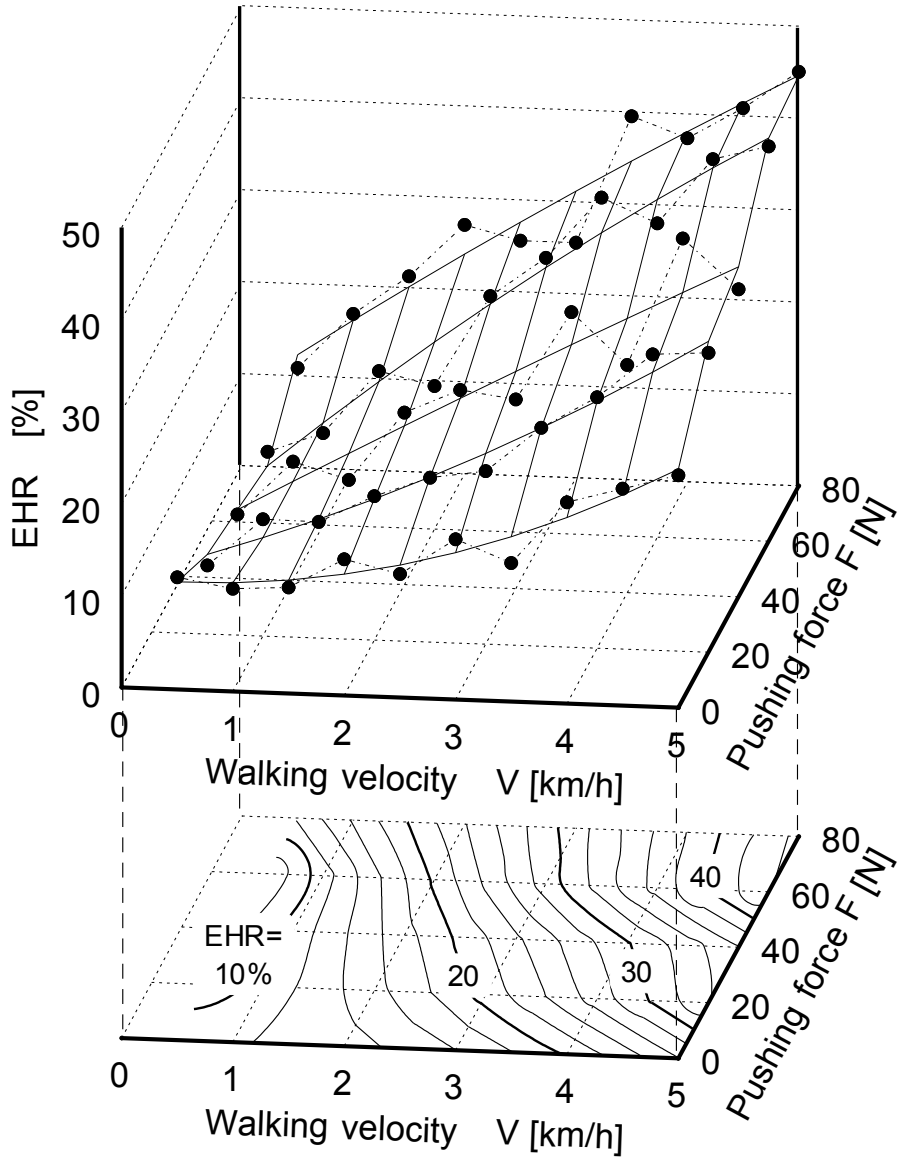

Figure 3-11 EHR on various pushing forces and walking velocities

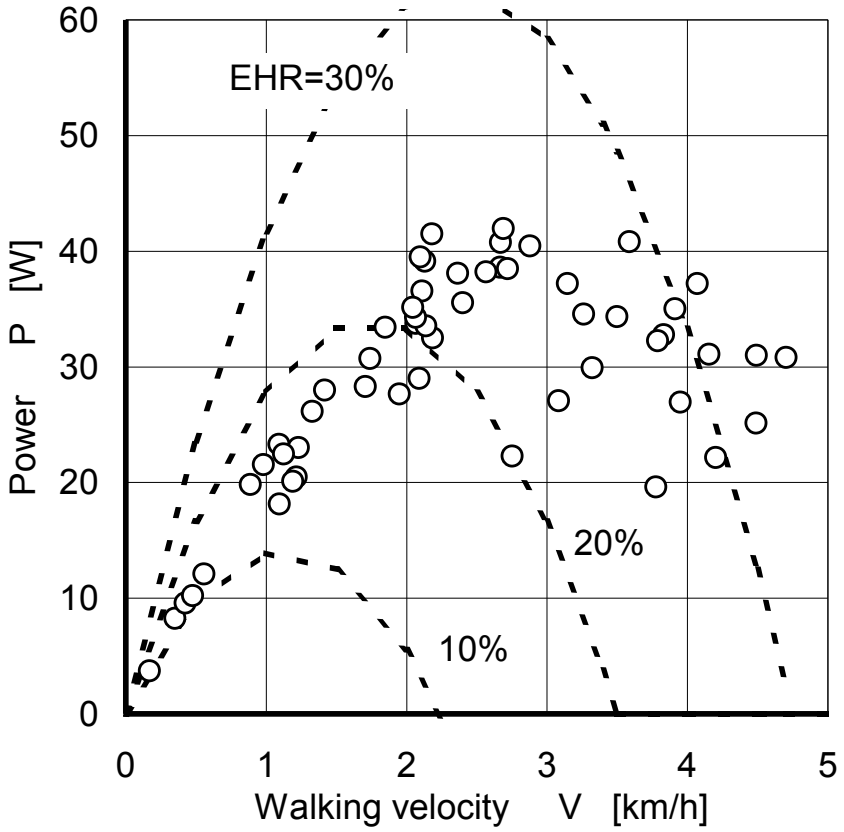

Figure 3-12 Mechanical power in pushing with walking

Figure 3-13 shows the amplitude of the frequency components in the pushing force $f_W(t)$ and the distance $d(t)$. The frequency f in the pushing force $f_W(t)$ and the distance $d(t)$ was the same and the f corresponded to the cadence in Figure 3-13. In the settled walking velocity V_S>0.4m/s, the amplitude F_{AP} of the pushing force and D_{AP} of the distance were almost constant 5N and 13mm respectively. In the low walking velocity under 0.4m/s at high resistance load R, both amplitude F_{AP} and D_{AP} increased drastically.

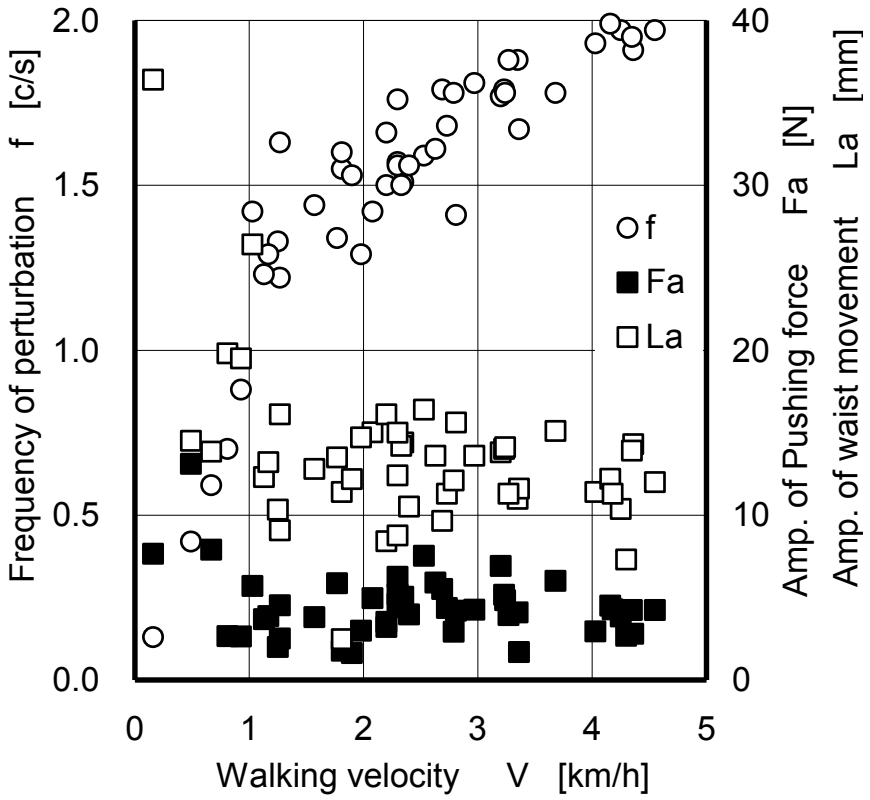

Figure 3-13 Frequency components in pushing force and distance

Relative distance between waist and grips

Figure 3-14 shows the relative distance *d* between participant's waist and grips under the trials in Figure 3-7. The relative distance *d* was about 0.1m when the participants were nearly standing over *R*=80N/(km/h){=288N/(m/s)}. The relative distance *d* increased slightly with the increase of walking velocity under the decrease of the *R*. In nearly natural walking at below *R*=5N/(km/h){=18N/(m/s)}, the relative distance became longer, around 0.2m in all participants. The participant A's distance, however, was comparatively longer than other participant's distances at the walking velocity V_S=1km - 2.5km/h(0.28m/s - 0.69m/s).

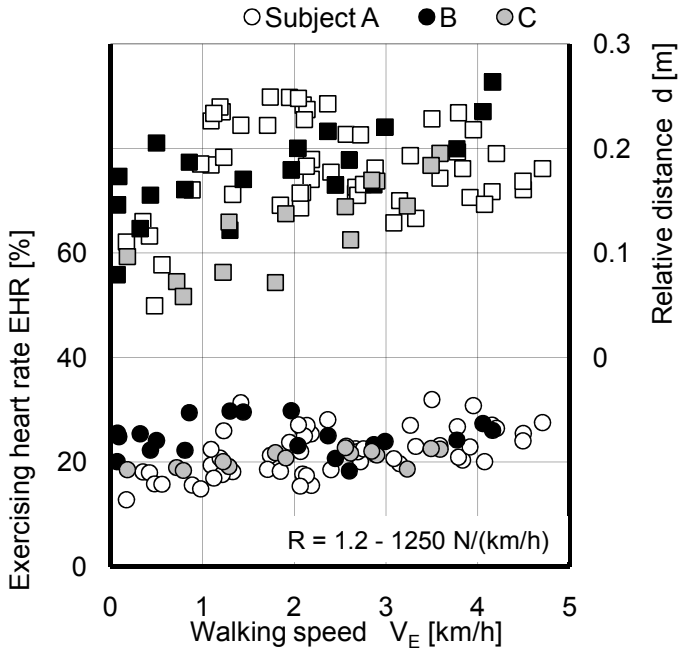

Figure 3-14 Relative distance between waist and grips

Under the results of the autonomous provided capability in propelling $F(t)=\varphi\{v(t)\}$ of Figure 3-7, walking motion was also steady. This study discusses average postures in the propelling task at steady state. Figure 3-15(a) shows the relationship between averaged relative distance *Da* and the walking speed *V*(*t*). These results were measured with the $F(t)=\varphi\{v(t)\}$ in Figure 3-7. Here the *D* is distances from an attendant's waist to wheelchair grips and the *Da* is from attendant's foot. The *D* and *Da* are averaged values in periodic changes caused by two leg walking. On *V*(*t*)<2.0 km/h(0.56m/s) under slow walking range, the relationship *D* < *Da* means that the participants exerted large *F*(*t*) by leaning forward. On the other case of the *V*(*t*)>2.0km/h(0.56m/s), the *D* increased and the *Da* decreased against the increase of the walking velocity *V*(*t*), so it means that the participants choose upright posture in fast walking.

Figure 3-15(b) shows the causal relationship between Δ*D* and Δ*F*, and this is an another experimental result to validate the relationship between the averaged relative distance *D* and the operating point $[F_S,V_S]$. The difference of position Δ*D* is a shifted waist position from the D_E, which is the steady waist position at the operating point under the $F(t)=\varphi\{v(t)\}$. The negative situation in Δ*D* < 0 shows that the participant positions near the grips. The Δ*F* is defined by the equation $\Delta F=F(t)-F_S$. Here, *F*(*t*) and F_S are the propelling forces under the posture conditions of $D_E+\Delta D$ and D_E respectively. The methodology of these experiments for the Figure 3-15(b) was carried out with following instruction; First, after the participant was propelling under the operating point $[F_S,V_S]$, the participant was forced to move the waist position from D_E to $D_E+\Delta D$ without stopping the propelling task. Next, the motor control signal was manually modified to

continue keeping new steady state $[F_S + \Delta F, V_S]$, because the ΔD caused the changes of the propelling force $F(t)$ and the feedback signal of the $F(t)$- F_S. After this adjustment, the differences of force ΔF were measured.

Figure 3-15(b) on the walking velocity V_S < 3km/h(0.83m/s) supposes that the upper arm works as a spring, so the difference of force ΔF would be showed in a next equation 3-18. (beneath ΔL=0 approximately described ΔF=-λ ΔL (λ>0).

$$\Delta F = -k \int \{ v_W(t) - v(t) \} dt \qquad (3\text{-}18)$$

The equation 3-17 can be roughly transformed with ΔD in the range of walking velocity V_S < 3.0km/h(0.83m/s).

$$\Delta F = -k \Delta D \qquad (3\text{-}19)$$

This means that the attendant increases the propelling force in proportion to the waist position near the grips under the difference of position ΔD < 0. In opposite situation ΔD > 0, the attendant generated slight reduced the different of force ΔF under the walking velocity V= 1km/h(0.28m/s) and 3km/h(0.83km/h). However, under the walking velocity 5km/h(1.39m/s), the difference of force ΔF rose steeply in proportion to the further position from the steady position D_E under the operating point $[F_S, V_S]$. This means that the attendant is impossible to regulate the steady waist position under the high walking velocity around 5km/h(1.39m/s). Because once the waist position is unexpectedly shifted to backward under the high walking velocity, the different of force increases, and also the wheelchair velocity increases. This situation would cause the uncontrolled wheelchair acceleration, and the propelling task tends to unstable because of difficult controlling the propelling force. These results suggest to need a prevention measure for aged attendants to prevent from forward fall.

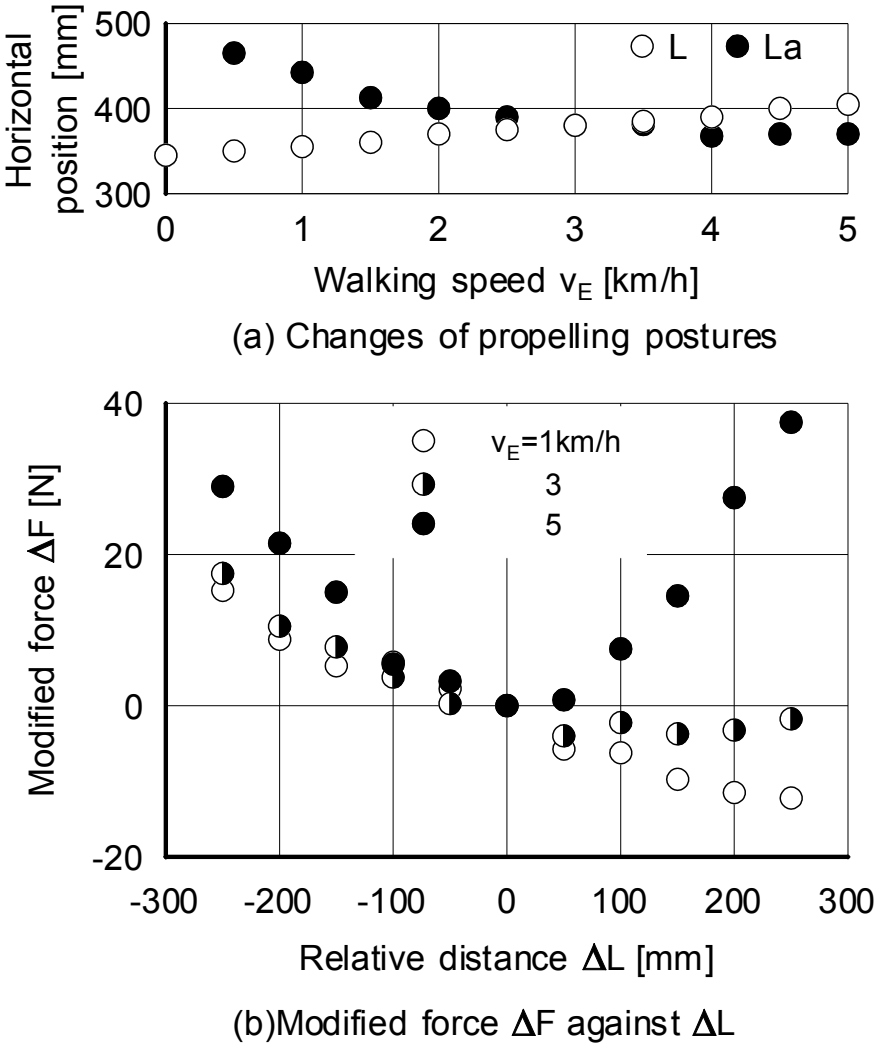

Figure 3-15 Change of operating posture and force against load

Walking pattern under various propelling loads

Based on the walking parameters in Figure 3-4, this section shows walking patterns under various propelling load by the resistance load coefficient R. Figure 3-4 shows typical walking pattern that a right foot started to swing, then touched on the ground while a left foot took one step. One step cycle is defined as the stride period *Dp* from touching on the ground to next touching on single side of foot. The outputs by switches attached side of each attendant's shoes shows touching state(zero) or swinging state(one). The *Dw* is a swinging period in each foot, the *Dt* is the touching period, and the *Db*[=*Db*1+*Db*2] is the double support period. The α, β and γ are the normalised period of *Dw*, *Dt* and *Db* by the stride period *Dp* respectively. These walking parameters were calculated from the outputs by the foot switches under the experiments of the $F(t)=\varphi\{v(t)\}$ in Figure 3-7. Also, the step length *Ls* was calculated from *Ls*=*V*(*t*)/*fc*, here *fc* was cadence obtained by 1/*Dp*. Figure 3-16 shows the changes of the step length *Ls* and the cadence *fc* against the walking velocity *V*(*t*) by the resistance load coefficient *R*. Figure 3-17 shows the change of

the normalised swing period α, touching period β, and double support period γ about the resistance load coefficient *R*. Figure 3-18 provides the relationship between the propelling force and the walking parameters α, β and γ.

Two different trends on the walking pattern in Figure 3-16 and 3-17 can be seen in the ranges divided by the walking velocity *V*=1.2km/h(0.33m/s). The participants chose relatively longer step length *Ls* under the large propelling force in the walking velocity $V(t)$ < 1.2km(0.33m/s). This is because longer step length *Ls* and higher double support period γ, and smaller cadence *fc* are enable to keep body balance steady, so the participant can lean forward to provide large pushing force $F(t)$ with large ground reaction force. Under this condition, the swing period α and the double support period γ were higher, and the touching period β was smaller. This situation means that the participant walked with intermittent steps, which was realised by the slight increased step length *Ls* and the decreased cadence *fc*.

In the range of the walking velocity $V(t)$ > 1.2km(0.33m/s), the participant increased the step length *Ls* as well as the cadence *fc* in proportion to the increase of the walking velocity $V(t)$. Also the swing period α and the double support period γ decreased, and the touching period β increased. In this range, the pushing force $F(t)$ decreased in proportion to the walking velocity $V(t)$ and the double support period γ.

Figure 3-18 shows the changes of walking pattern about the pushing force $F(t)$. The pushing force $F(t)$ became larger when the swing period α and the double support period γ were large and the touching period β was small. The plot of the pushing force $F(t)$ was symmetry at the swing period α and the touching period β were 0.5, and the pushing force $F(t)$ became larger under the walking patten of the touching period $\beta < 1/3$, or the swinging period $\alpha > 2/3$. This walking patten means that the double support period $\gamma > 1/3$. The walking situation appeared in the range of the walking velocity $V(t)$ < 1.2km(0.33m/s) in Figure 3-17. In other walking situation, which is $0<\gamma<1/3$ or $1/2 <\alpha<2/3$, the pushing force $F(t)$ increased in proportion to the swinging period α and the double support period γ. And the propelling force $F(t)$ decreased in proportion to the touching period β on $1/3<\beta<1/2$.

These results suggest that the pushing force $F(t)$ and the walking velocity $V(t)$ have strong relationship based on walking patterns. The participant can generate large pushing force $F(t)$ under steady slow walking velocity $V(t)$ based on the double support period $\gamma > 1/2$ and the swinging period $\alpha > 2/3$. In this walking pattern, the participant choose almost constant step length *Ls* with smaller cadence *fc* to reduce the swing time *Dt* and to increase the double support period γ in the same time. In the case of the double support period $\gamma < 1/3$, the pushing force $F(t)$ decreases largely because the increase of the step

length *Ls* and the cadence *fc* causes large decrease of the double support period γ.

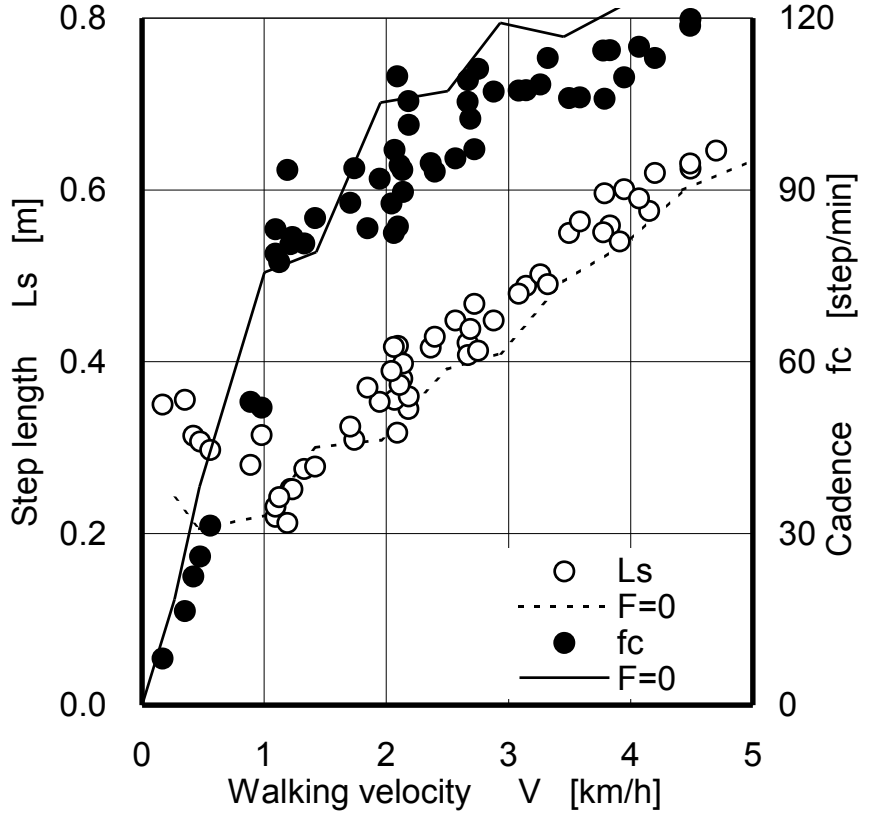

Figure 3-16 Change of step length and cadence against various loads

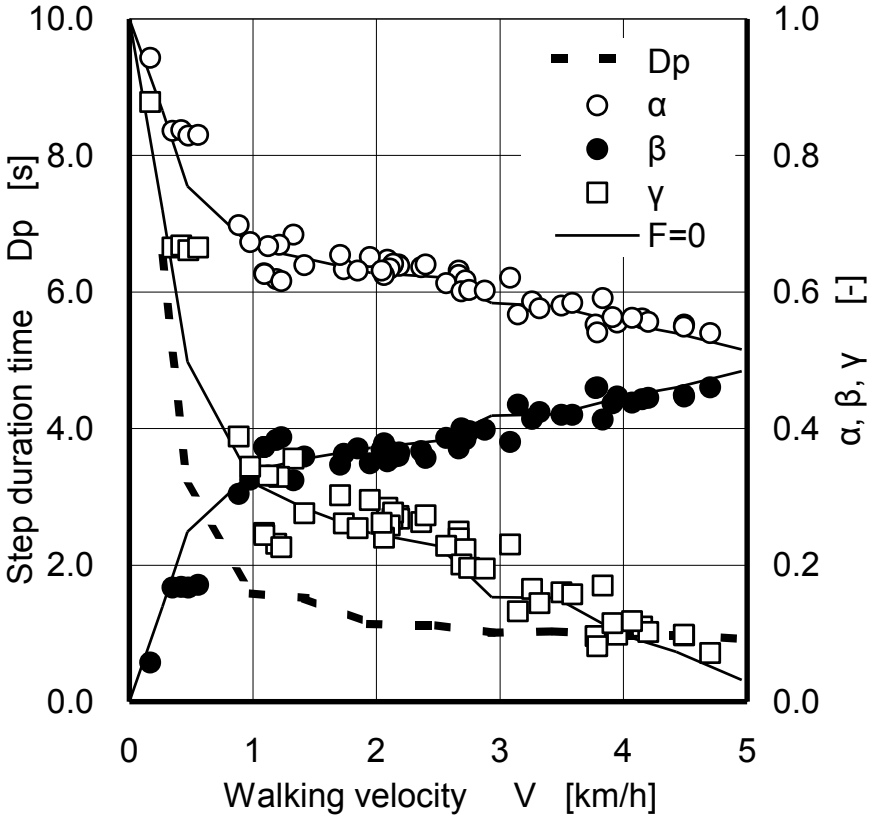

Figure 3-17 Change of walking pattern against various loads

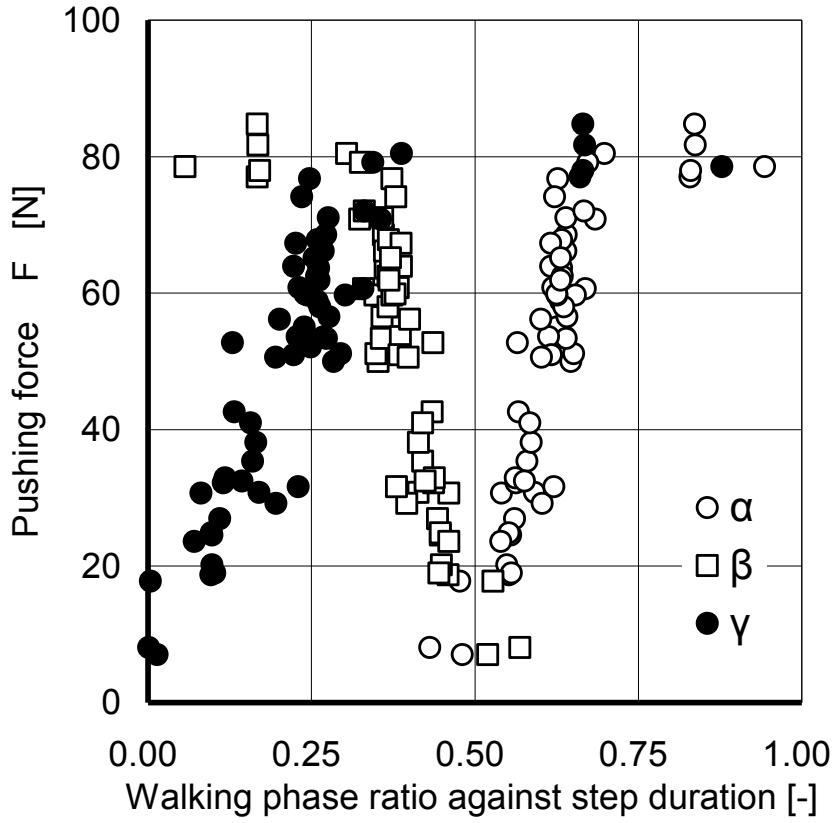

Figure 3-18 Pushing force by walking patten

Single leg force

Figure 3-19 shows the change of the single-leg generated force F_L and normalised double support phase D_b / D_P. The trend of the single-leg generated force F_L and the normalised double support phase D_b / D_P was different by a boarder V_S=1km/h(0.28m/s). Similar trend was appeared in the step length L_S in Figure 3-16 and the stride time D_P in Figure 3-17. In the range of the wheelchair velocity V_S > 1km/h(0.28m/s), the single-leg generated force F_L decreased from 60N to 22N(Participant A). The other participant's F_L, which were smaller than the participant A's F_L, decreased with a similar slope. The normalised double support phase D_b / D_P decreased from 0.35 to 0.1 with the decrease of the resistance load coefficient *R*. The trend in the normalised double support D_b / D_P was very similar in all participants. In the range of the walking velocity V_S < 1km/h(0.28m/s), the single-leg generated force F_L was almost constant 50N(Participant A and B). Participant C's F_L, however, decreased steeply with the increase of the resistance load *R*. The normalised double support phase D_b / D_P sharply increased with the increase of the resistance load coefficient R, and this trend was the similar in all participants.

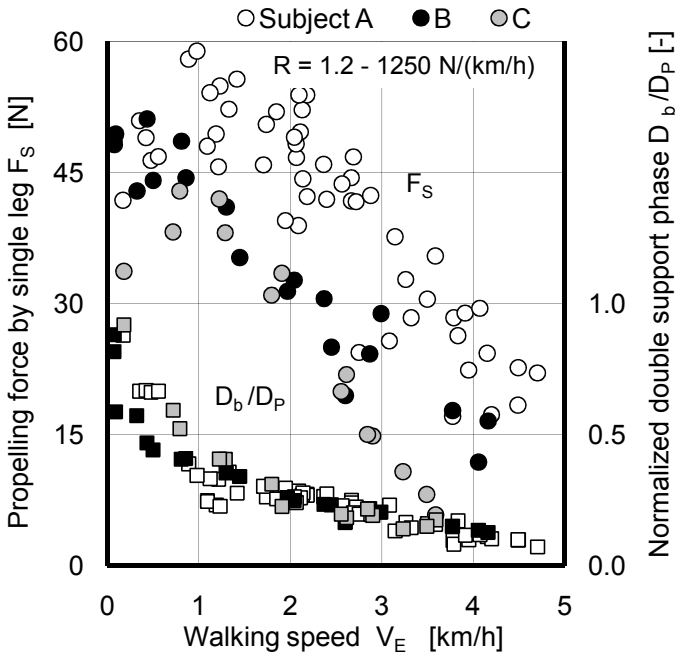

Figure 3-19 Pushing force by single leg

Autonomous provided capability in propelling on slopes

Figure 3-20 shows the autonomous provided capability in ascend-propelling on slopes and Figure 3-21 shows a descend-propelling case, which the propelling forces are pulling forces. On the sloped experiments, the gravity force by wheelchair toward downward direction does not apply to the participants. It means that the participants do not need to exert the pushing/pulling force to support simulated wheelchair weight on the slopes.

With increasing the slope angle θ=0, 4, 8[deg.], the pushing force $F(t)$ decreased because of the increased body weight toward downward direction and the difficulty to lean forward against the slope. On the upward slope, the foot position to touch on the belt in walking was higher than the foot position at starting to swing, so the participant was difficult to move forward the centre of mass of the body. This means that the participant could not use the body weight for pushing. This was validated from the reduction in the walking velocity $V(t)$= 4.3km(1.19m/s) at θ=0deg., 3.9km/h(1.08m/s) at 4deg. and 3.3km/h(0.92m/s) at 8deg. under the situation that the attendant walked naturally with slight gripping without pushing on the treadmill.

On the downward slopes at θ=0, -4, -8[deg.], the participant exerted pulling force $F_P(t)$ for keeping the wheelchair velocity constant to descend. The absolute number of the

pulling force $|F_P(t)|$ decreased exponentially with the increase of the walking velocity $V(t)$, especially a large drop appeared in the range of the walking velocity $V(t)$ < 1km/h(0.28m/s). The curve of the pulling force $|F_P(t)|$ decreased with the increase of the slope angle θ. In the case of $V(t)$<1km/h(0.28m/s), the participant selected stable walking pattern, in which both foot touched the most of the stride time D_P. This walking pattern was able to exert large pulling force $|F_P(t)|$ with leaning backward to shift the centre of mass of the body to back. With increasing the walking velocity $V(t)$, the participant was difficult to exert large pulling force $|F_P(t)|$. This is because the participant could not use the centre of mass of the body effectively under nearly standing position while continuous fast foot moving in walking.

This study found that the participant is able to stop or reduce easily the motion of the attendant propelled wheelchair, with the large pulling force $F_P(t)$ under the range of the walking velocity $V(t)$<1km/h(0.28m/s). In the contrary, with the case of the walking velocity $V(t)$>1km/h(0.28m/s), the regulating wheelchair motion in descending becomes difficult. In addition, the real slopes have the gravity weight toward slopes, and this additional weight makes the attendant harder to control because the participant have to use the most of the pulling force $F_P(t)$ to cope with the gravity weight. Therefore, the propelling load in stopping and reducing wheelchair velocity becomes very high. This finding supposes that assist methods for the emergency stop or the reduction of the wheelchair velocity on downward slope is needed, even though the participants do not need the driving force for the wheelchair because of the gravity acceleration.

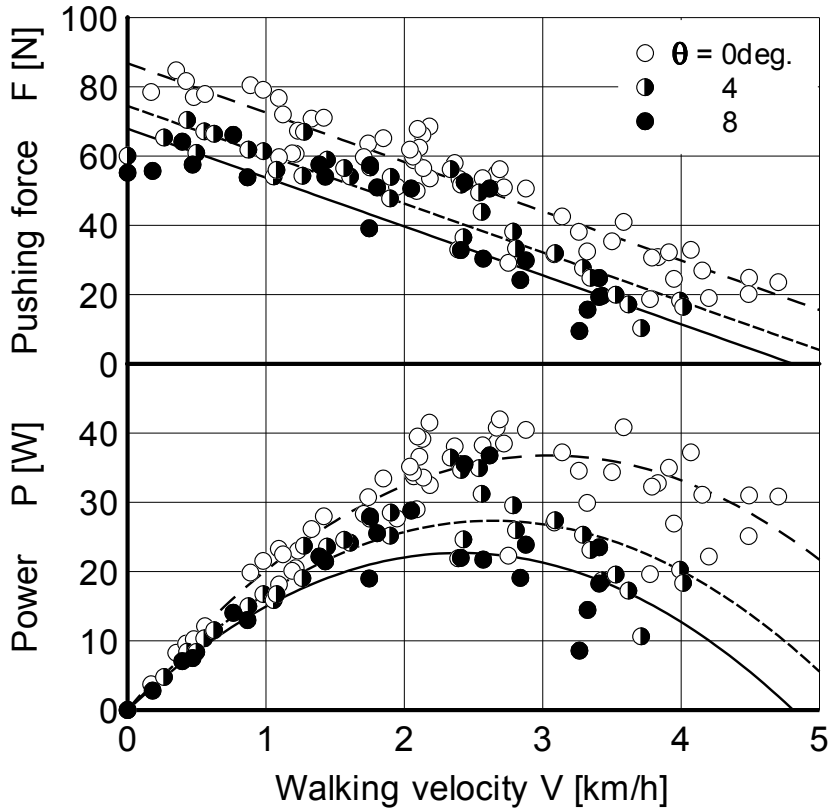

Figure 3-20 Autonomous provided capability in ascend-propelling

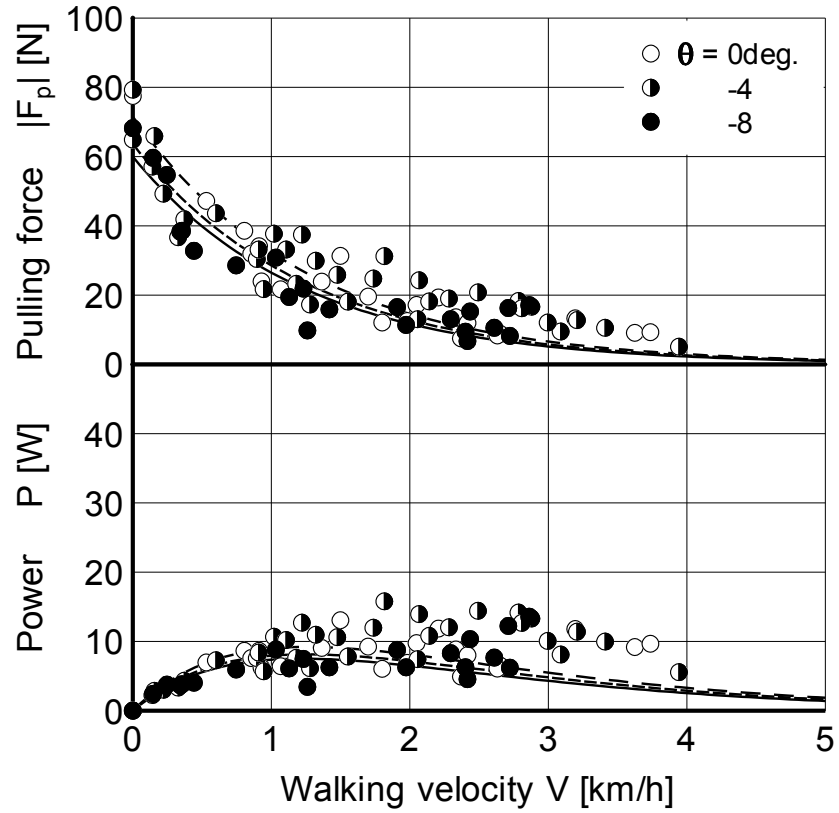

Figure 3-21 Autonomous provided capability in descend-propelling

3-5 Discussions

Autonomous provided capability in pushing

The maximum propelling was difficult to continue over four minutes because of its hardness. On the contrary, the autonomous pushing in Figure 3-7(b) was easy to continue for 20minutes. From comparison between both propelling times, the estimated $F(t)=\varphi\{v(t)\}$ shows the autonomous provided capability in pushing $[F_S, V_S]$ under steady load. This results support the hypothesis 1 in the introduction 3-1.

From the results of the Figure 3-7, the propelling force $F(t)$ decreases in proportion to the increase of the walking velocity $V(t)$ by the increase of the resistance load coefficient R, and the results of these experiments support the hypotheses 2. The simultaneous two task pushing and walking, causes the decline of pushing force with the increase of the walking velocity. The decline rate against the walking velocity was similar between the maximum case in Figure 3-7(b) and the autonomous case in Figure 3-7(a). These results support that the increase of the walking velocity deducts the pushing force in proportion to the walking velocity.

With analogy in a simple electrical system having battery and a register(load), we estimate the attendant capability in propelling with the assumption that the attendant is a battery and the wheelchair is a resister(load). The physical corresponding in the analogy with electric engineering is that the output voltage of the battery is the pushing force F_S, an inner resistance of the battery is the declined slope of the pushing force F_S, an outer resistance is the resistance load by the wheelchair and road surface, and a current of the circuit is the wheelchair velocity V_S. Under this analogy, the pushing force walking velocity relationship by the $F(t)=\varphi\{v(t)\}$ in Figure 3-7(b) can be shown in an equation 3-20. The estimated lines were solved by least square method with the data under the range of the walking velocity V(t) > 1km/h(0.28m/s), in which the data showed linearity.

$$F_S = F_0 - \kappa V_S, \kappa = \frac{dF_S}{dV_S} \tag{3-20}$$

Here, the F_0 is the intercept pushing force at V_S =0. The κ shows an impedance equivalent to the inner resistance. From the trend that the pushing force F_S proportionally decreased with the increase of the wheelchair velocity V_S on the range V_S > 1km/h(0.28m/s), the κ can be defined as constant value. This means that the autonomous provided

capability in pushing $F(t)=\varphi\{v(t)\}$ shows a similar trend by general battery-load systems. With the parameters F_0 and κ, the linear estimated autonomous provided capability in pushing $F(t)=\varphi\{v(t)\}$ is very important for the design of reduced load attendant-propelled wheelchairs. The parameters F_0 and κ would be determined from individual physical parameters, however, the relationship between them are not certain and it is one of our future works. In the range of the walking velocity V_S < 1km/h(0.28m/s), however, the $F(t)=\varphi\{v(t)\}$ is different from the equation 3-19 and the κ has nonlinearity. Under this range, other additional inner resistances would exist because the slope dF_S / dV_S was smaller. This means that the pushing force F_S is less sensitive to the walking velocity V_S on the range with large pushing force F_S. This trend was seen in the results of the participant A and B. Despite the nonlinearity in the slow walking velocity range, the linear estimation of the autonomous provided capability in pushing by the equation 3-19 is very useful to show individual differences.

The force ratio of $F(t)/Fm$ proportionally decreased from 30% to 10% with the increase of the walking velocity $V(t)$. The autonomous provided capability in pushing was very lower than maximum one, so the design to assist the propelling on various road conditions is very important.

Subjective hardness of autonomous provided capability in pushing

The subjective hardness of the autonomous provided capability in pushing in Figure 3-10 was almost under 30%, which means light physical exercising level from the Borg scale. This limit of subjective hardness was common in all participants. This means that the autonomous provided capability in pushing is carried out under light subjective hardness EHR=30%. This results support the hypothesis 3 in the introduction.

Phase difference between pushing force and relative distance

From the time series plots in Figure 3-5 and Figure 3-6, the participant under the large resistance load generated the large pushing force with both legs in the double support phase. Both arms were folded to the whole body near the wheelchair, so the posture of the whole body leaned forward. After the wheelchair moved forward by the maximised pushing force, the participant took a step to move its body forward to continue to propel. That would be the reason why the phase of the pushing force and the distance was opposite. In the light resistance load, the participant was easy to push the wheelchair, so the wheelchair velocity was near to the natural walking. The participant needed relatively

long steps with almost no double support phase, and kept the distance to the wheelchair enough to step freely. In the case, the participant used the body mass for pushing. It means that the participant stepped forward and increase the kinetic energy, then the distance narrowed and the kinetic energy transferred to the wheelchair by both arms. The phase between the pushing force and the distance was opposite in the heavy and light resistance load, also the methodology to generate the pushing force would be different in both cases.

Linearity of attendant-wheelchair model

This chapter proposed the outlined model of the attendant wheelchair system. From the results in the autonomous provided capability in pushing, many linearities were found in the range of walking velocity $V(t)$ > 1km/h(0.28m/s). The transient response in Figure 3-7(a) shows overshoot, and this suggests that the dynamic elements over 2nd order would be included. With the relationship between the difference distance ΔD and the difference force ΔF in Figure 3-15, the attendant wheelchair system would consist of spring and dumping factors in arm functions. These results suggest that the attendant wheelchair system would be assumed as linear system as a first step on the range of the walking velocity $V(t)$ > 1km/h(0.28m/s) V_S

Mechanical power of the autonomous provided capability in pushing

The mechanical power of the autonomous provided capability in pushing in Figure 3-9 had a peak at the walking velocity around 2.5km/h(0.69m/s). From the view of impedance matching, there is a efficient walking velocity to transfer the propelling power to the wheelchair. All participant in this study can transfer the maximum propelling power to the wheelchair at the walking velocity around V_S = 2km/h(0.56m/s), however all participants usually propelled the wheelchair at the walking velocity over 3km/h(0.83m/s) in the overground preliminary tests. From this results, the attendants tend to keep their walking rhythm rather than the efficiency of the power transfer.

Relative distance between waist and grips

The relative distance in Figure 3-14 and 3-15 increased with the increase of the walking velocity. Under higher road resistances, the attendants generated large pushing force at low walking velocity. For generating the large pushing force, the attendants need to lean forward in order to use the body weight effectively. In the range of higher walking

velocity in low resistance load, the attendants do not need to exert large pushing force, so the attendants take upright posture like natural walking. In the range of the walking velocity V_S < 1km/h(0.28m/s), the proportional increase ratio of the relative distance against the walking velocity was almost constant. The differences in the proportional increase ratio among some participants were seen, however the trend of the monotonous increase in the distance was the same. This means that the attendants tend to accelerate the wheelchair at low walking velocity, and generate the large pushing force with leaning body forward. Under lower resistance load, the attendants do not need to accelerate the wheelchair because the walking velocity becomes nearly natural walking velocity.

Single-leg generated force

The single-leg generated force F_L and the walking pattern in propelling had a strong relationship. The series of the result about the walking pattern in Figure 3-16, 3-17, and 3-18, suggest that the walking modes in propelling are classified in two at the walking velocity V_S=1km/h(0.28m/s). In the range of the walking velocity V_S > 1km/h(0.28m/s), the single-leg generated force F_L and the normalised double support period D_b / D_P, decreased with the increase of the step length L_S under the decrease of the resistance load coefficient *R*. In this condition, the stride time D_P was nearly constant. It means that the attendants need to decrease the step length and to increase the double support period. This is because that the generating large leg force in propelling needs stable contact between a foot and the ground, and enoght transient time until full activation in muscles. From this point, the attendants need to increase the leg touch period as much as possible for generating large pushing force. However, the walking rhythm is very important to continue steady two leg walking. To secure the long double support period D_b with keeping the walking rhythm, the attendants take short stride time period D_P. In the range of the walking velocity V_S < 1km/h(0.28m/s) under higher resistance load, the attendants need the normalised double support period over 30% and choose long stride time over 1s to exert the pushing force. The single-leg generated force in the participant A and B, however, became lower than the peak force at the walking velocity V_S = 1km/h(0.28m/s). This is because that the attendants cannot use the inertia force by body movement in pushing at the low walking velocity. The results in Figure 3-19 suppose that suitable walking pattern exists to maximise the single-leg generated force. The walking pattern consisting of the stride time D_P > 1s, the normalised double support period D_b / D_P > 30%, and the step length L_S = 0.3m under the walking velocity V_S = 1km/h(0.28m/s), would maximise the pushing force.

3-6 Conclusions

In this chapter, the outlined signal model of an attendant-wheelchair model was proposed, and confirmed that the autonomous provided capability in pushing can be estimated from the steady state by various resistance loads. This study developed the motorised treadmill to investigate pushing and pulling with walking under steady state with stable resistances load in long time. Our developed treadmill enables to obtain reliable steady state results to evaluate the autonomous provided capability in pushing and pulling. From the results, we found following;

1. The force-velocity relationship of the autonomous provided capability in propelling is a monotonic decreasing function. The attendant generates large propelling force under low walking velocity, however, the propelling force decreases with the increased walking velocity. The attendant autonomously maximises the propelling force and the walking velocity with minimising the subjective hardness, in order to propel long time against resistance loads.

2. The autonomous provided capability in pushing is carried out under exercising heart ratio (EHR) 30%, which shows light subjective hardness to be able to continue over 20min.

3. The provided capability in propelling is determined by the subjective hardness. The attendant can increase the propelling capability in propelling if bearable subjective hardness is increased.

4. In the case of the participant with good strength, the maximum pushing force in the autonomous provided capability is about 80N, which is 10-30% of voluntary maximum pushing force. The maximum mechanical power in the autonomous provided capability is around 30W.

5. For generating large pushing forces, an attendant needs long step length, long stride period and over 30% of double support period in 1 cycle walking.

These findings are very useful to estimate the attendant load to propel attendant-propelled wheelchairs, as well as to apply for the development of the wheelchair with less-load. From the chapter four, we develop more detailed model and identify each element of the model from experiments. After the validation of the model, we develop the assist system for the attendant-propelled wheelchair in the chapter 5. The proposed assist system are designed based on the autonomous provided capability in propelling, which is obtained by this chapter 3.

References

[1]Ayoub, M. M. and McDaniel, J. W., Effect of operator stance on pushing and pulling tasks, AIIE Transactions, Vol. 6, pp. 185-195, 1974

[2]Chaffin, D. B. and Andres, R. O., Volitional postures during maximal push/pull exertions in the sagittal plane, Human factors, Vol. 25, pp. 541-550, 1983

[3]Snook, S.H. and Ciriello, V.M., The Design of Manual Handling Tasks: Revised Tables of Maximum Acceptable Weight and Forces, Ergonomics, Vol. 34, No. 9, pp1197-1213, 1991

[4]R. Andres, "Validation of a biodynamic model of pushing and pulling," *Journal of Biomechanics*, vol. 24, no. 11, pp. 1033-1045, 1991

[5]Kumar, S., The back compressive forces during maximal push-pull activities in the sagittal plane, Journal of human ergology, Vol. 23, pp. 133-150, 1994

[6]M. J. M. Hoozemans, P. P. F. M. Kuijer, I. Kingma, J. H. van Dieen, W. H. K. de Vries, L. H. V. van der Woude, D. J. H. E. J. Veeger, A. J. van der Beek, and M. H. W. Frings-Dresen, "Mechanical loading of the low back and shoulders during pushing and pulling activities," *Ergonomics*, vol. 47, no. 1, pp. 1–18, Jan. 2004.

[7]K. K. Lett and S. M. McGill, "Pushing and pulling: personal mechanics influence spine loads," *Ergonomics*, vol. 49, no. 9, pp. 895–908, Jul. 2006.

[8]W. S. Marras, G. G. Knapik, and S. Ferguson, "Loading along the lumbar spine as influence by speed, control, load magnitude, and handle height during pushing," *Clinical Biomechanics*, vol. 24, pp. 155–163, Jan. 2009

[9]M. Gagnon and S. Beaugrand, "The dynamics of pushing loads onto shelves of different heights," *International journal of industrial ergonomics*, vol. 9, pp. 1–13, 1992.

[10]S. Kumar, "Upper body push-pull strength of normal young adults in sagittal plane at three heights," *International Journal of Industrial Ergonomics*, vol. 15, pp. 427-436, 1995.

[11]M. P. De Looze, K. Van Greuningen, J. Rebel, I. Kingma, and P. P. F. M. Kuijer, "Force direction and physical load in dynamic pushing and pulling," *Ergonomics*, vol. 43, no. 3, pp. 377–390, Mar. 2000.

[12]S. MacKinnon, "Effects of standardized foot positions during the execution of a submaximal pulling task - Ergonomics - Volume 45, Issue 4," *Ergonomics*, 2002.

[13]G. Boocock M, P. Lemon, S. Thorpe, and A. Haslam R, "Initial force and postural adaptations when pushing and pulling on floor surfaces with good and reduced resistance to slipping," *Ergonomics*, vol. 49, no. 9, pp. 801–821, 2006.

[14]S. N. MacKinnon, "Isometric pull forces in the sagittal plane," *Applied Ergonomics*,

vol. 29, no. 5, pp. 319–324, Oct. 1998
[15]S. Herring, “The effects of distance and height on maximal isometric push and pull strength with reference to manual transmission truck drivers,” *International journal of industrial ergonomics*, vol. 37, pp. 685–696, 2007
[16]O. Okunribido, “Ready steady push – a study of the role of arm posture in manual exertions," *Ergonomics*, vol. 51, no. 2, pp. 192-216, 2008
[17]N. J. Seo, T. Armstrong, and J. Young, “Effects of handle orientation, gloves, handle friction and elbow posture on maximum horizontal pull and push forces,” *Ergonomics*, vol. 53, no. 1, pp. 92–101, Jan. 2010.
[18]Hill A.V., "The heat of shortening and dynamics constants of muscles". Proceedings of the Royal Society Series B London, 126 (843), pp.136–195, 1938
[19]Vandewalle, H., Peres, G., Heller, J., Panel, J. and Monod, H., Force-velocity relationship and maximal power on a cycle ergometer: Correlation with the height of a vertical jump, Eur. J. Appl. Physiol., Vol. 56, No. 6, p650-656, 1987
[20]Vandewalle, H., Peres, G., Sourabie, B., Stouvenel, O., and Monod, H., Force-velocity relationship and maximal anaerobic power during cranking exercise in young swimmers. Int. J. Sports Med. Vol. 10, pp439-445, 1989
[21]A. Jaskólska, P. Goossens, B. Veenstra, A. Jaskólski, and J. Skinner, “Comparison of Treadmill and Cycle Ergometer Measurements of Force-Velocity Relationships and Power Output,” *Int J Sports Med*, vol. 20, no. 3, pp. 192–197, Apr. 1999.
[22]A. Rahmani, F. Viale, G. Dalleau, and J.-R. LACOUR, “Force/velocity and power/ velocity relationships in squat exercise,” *Eur J Appl Physiol*, vol. 84, no. 3, pp. 227–232, Mar. 2001.
[23]F. Hintzy, N. Tordi, and E. Predine, “Force–velocity characteristics of upper limb extension during maximal wheelchair sprinting performed by healthy able-bodied females," *Journal of Sports Sciences*, vol. 21, pp. 921-926, 2003.
[24]H. Toji, “Effects of Aging on Force, Velocity, and Power in the Elbow Flexors of Males,” *Journal of physiological anthropology*, vol. 26, no. 6, pp. 587-592, 2007
[25]S. Dorel, A. Counturier, J.-R. Lacour, H. Vandewalle, C. Hautier, and F. Hug, “Force-Velocity Relationship in Cycling Revisited,” *Medicine & Science in Sports & Exercise*, vol. 42, no. 6, p. 1, Dec. 2009.
[26]I. Raj and S. Bird, “Aging and the force–velocity relationship of muscles,” *Experimental gerontology*, vol. 45, pp. 81-90, 2010
[27]Karvonen, M., Kentala, K., and Mustala, O., The effects of training heart rate: A longitudinal study, Annals of Medicine and Experimental Biology Fenn Vol. 35, pp. 307-315, 1957
[28]Alton, F., Baldey, L., Caplan, S., and Morrissey, M. C., A kinematic comparison of overground and treadmill walking, Clinical Biomechanics, Vol. 13, pp. 434-440, 1998

Chapter 4 Modeling Attendant-Wheelchair system

4-1 Introduction

This chapter presents and validates a proposed model of attendant-wheelchair system. In the design of the controller for the powered attendant propelled wheelchairs, the evaluation with various condition of the attendants, wheelchairs, and environments is needed to validate the performances of the controller. The aim of this chapter is to develop the attendant-wheelchair model to simulate the dynamic behaviour in propelling, and the model would be useful to discuss dynamic stabilities related to the safety of attendant, like preventing falling, and required capabilities in various road conditions. Also this model would be useful to the design of environments or low load attendant propelled wheelchairs, traditionally based on experiments with participants.[1 - 8]

In previous studies, the modelling of a human operator in the simple task to track an indication was well established. Abdel-Malek 1988[9] validated the human operator model with experiments. From the results, Abdel-Malek concluded that the model parameters were significant task dependence of the human operator characteristics. It means that the human operator adjusts its dynamic characteristic to distinct tasks. Hess 1990[10] validated the proposed theoretic model of driver steering behaviour. Hess determined the model parameters by a technic derived from the theoretic model. The experimental validation shows the model can produce the similar responses to a simulated lane-keeping driving task on a curving road. In addition, Hess 2009[11] develop the adaptive pilot model to sudden changes in vehicle dynamics.

However, there is few researches to present a model to describe human dynamic tasks. Masani 2006[12] shows the evidence that the proportional-derivative (PD) controller can effectively generate a desired motor command to the body sway position in quiet standing. Masani used an inverted pendulum model by a regulated PD controller to simulate human quiet standing, and validated the model by the experiments with able bodied participants. The PD controller showed a good approximation of the control strategy in quiet standing by able bodied. Unlike the human operator model, the modelling of the human task, like standing, walking, and propelling is very complicated, because the model needed to simulate the strategy in the brain, sensory processing, and body movements about the task. From the conclusion by Abdel-Malek 1988[9], human can adjust its dynamic characteristic to different tasks. From the simplicity of propelling tasks because of be abled to continue longer period with single mind, this study hypothesise that the propelling tasks can be modelled by linear control theory.

Many cases to use mathematical wheelchair models are reported. In recent, Chenier 2011[13] proposed the dynamic wheelchair model to simulate the straight and curvilinear propulsion in manual wheelchairs. This model is suitable for the plane movement in three degrees of freedom. The main elements of the model were the wheelchair's mass and moments, and rolling resistance of each caster and wheel. In this chapter, the movement of propelling was assumed one dimension, so the wheelchair movements in one degree of freedom is enough. Based on various previous studies, this chapter used a centralised mass model with resistance against the ground to describe a wheelchair in straight movements.

This study proposes the attendant-wheelchair model and validate it for evaluating the performances of the assist controller. The proposed attendant-wheelchair model reproduce the attendant's autonomous propelling to maximise propelling force under minimised subjective hardness. The attendant autonomous propelling is determined by the physical strength and preference based on the whole body condition. The wheelchair and environments are vary, so the proposed model was simplified to assume the environments as a resistance load by the wheelchair mass and the road resistances with gravity forces.

Basic idea in modelling is based on the assumption that an attendant is power source, and a wheelchair and environment are a resistance load. This study shows the power curve of the attendant in autonomous propelling. In the modelling, this study mainly focuses on the system under steady state, and the frequency components by two leg walking were treated to average.

The validation of the model was carried out by experiments with the motorised treadmill with grips, which are fixed in the same dimension of a wheelchair. This study used the relative heart rate as an index of the subjective hardness in propelling. This study shows the validated results of the proposed attendant wheelchair model.

4-2 Model of an attendant-wheelchair system

Figure 4-1 shows the outline model of an attendant-wheelchair system. From the investigation of the propelling a wheelchair in the Chapter 2, the attendant continues to generate pushing or pulling force $f_W(t)$ and follows the wheelchair while walking. In the modelling, the important components in the propelling are three parts below;

1. The mechanism of generating pushing or pulling force by the attendant
2. The cushioning components of upper extremity to transfer the generated pushing and pulling force to the wheelchair
3. The physical model of the wheelchair and the road surfaces including slopes.

This study assumed that the attendant has a desired walking velocity $v_D(t)$ in the brain from the discussion in the Chapter 2 and 3. To reduce complexity, the movement of the attendant and the wheelchair was in one dimensional plane, moving forward along with a straight path on the road with slopes, and the attendant and the wheelchair was assumed as concentrated mass systems. The operator "s" in the block diagrams means the laplace operator.

While propelling the wheelchair, the attendant adjusts own walking velocity $v(t)$ to the desired walking velocity $v_D(t)$. The brain of the attendant determines the planned leg force $f_D(t)$ to drive the whole body forward, by regulating the velocity difference $e(t) = v_D(t) - v(t)$ to zero. The planned leg force $f_D(t)$ shown in the equation (4-1) is the output of the brain function $G_{BR}(s)$, which shows the static gain *K* of the musculoskeletal system in the lower extremity.

$$F(s) = K[V_D(s) - V(s)] \tag{4-1}$$

The musculoskeletal system also has a dynamic component defined by the $G_M(s)$, so actual leg force $f_D(t)$ to drive the attendant's whole body is described in the equation (4-2) with the assumption that the gain in the $G_M(s)$ is one.

$$F_D(s) = G_M(s)F(s) \tag{4-2}$$

The attendant has a body mass m driven forward by the force subtraction from the actual leg force $f_D(t)$ to the reactive force $f_W(t)$ by the wheelchair. This force balance is described by the equation (4-3).

$$msV(s) = F_D(s) - F_W(s) \tag{4-3}$$

The actual leg force $f_D(t)$ is transferred from the attendant to the grips of the wheelchair through the cushioning component $G_{AM}(s)$ by both arms. The distance *d*(*t*) and the relative velocity $v_W(t) - v(t)$ are determined by the force difference between the actual

leg force $f_D(t)$ and the attendant horizontal propelling force $f_W(t)$. This study assumed that the cushioning component $G_{AM}(s)$ consisted of the stiffness K and the damping c, as the described equation (4-4).

$$F_W(s) = G_{AM}(s)[V(s) - V_W(s)], \text{ here } G_{AM}(s) = \frac{cs + k}{s} \quad (4\text{-}4)$$

The wheelchair system $G_W(s)$ consisted of the total weight M of the wheelchair including an occupant, and the road resistance force $f_R(t)$, which was defined in the equation (4-6) by the sum of the static resistance f_{R0} and the dynamic resistance $C_R v_W(t)$ from the study by Brauer 1981[14]. From this assumption, the wheelchair system was described as the first order system in the equation (4-5). Here C_R [N/(m/s)] is the proportional coefficient to the wheelchair velocity.

$$V_W(s) = \frac{F_W(s)}{Ms + R} = G_W(s)F_W(s)$$

$$G_W(s) = \frac{K_W}{T_W s + 1}, \text{ here } K_W = \frac{1}{R}, T_W = \frac{M}{R} \quad (4\text{-}5)$$

$$f_R(t) = f_{R0} + C_R v_W(t) \quad (4\text{-}6)$$

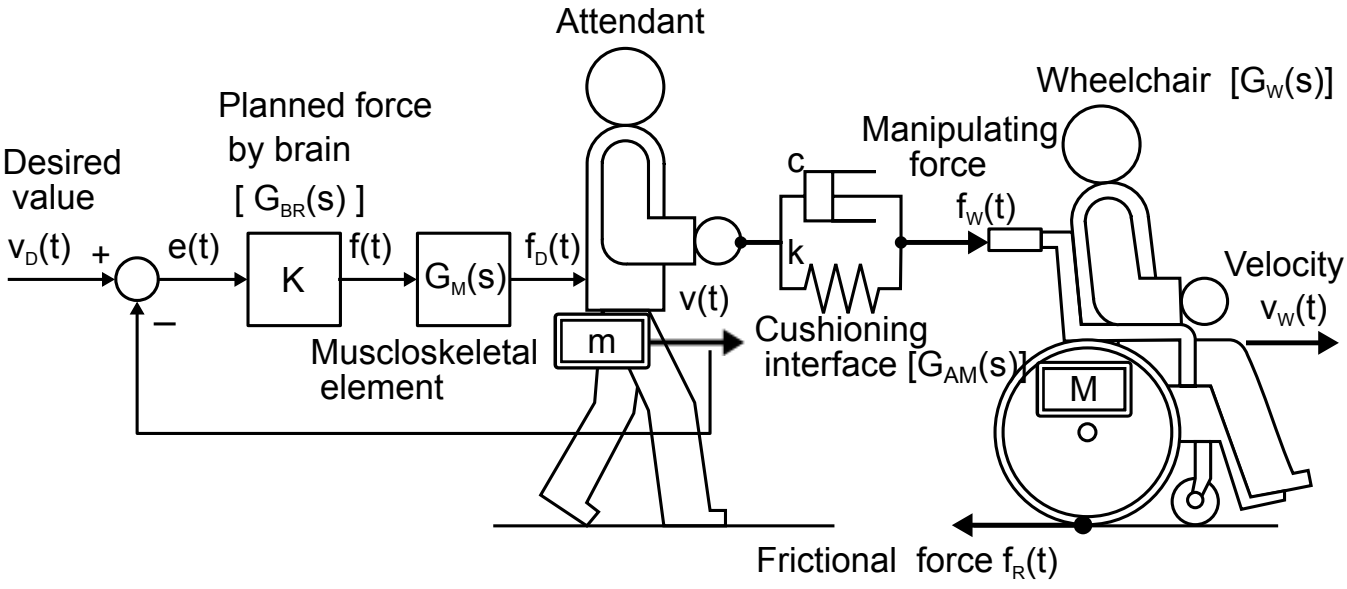

Figure 4-1 Outline of attendant-wheelchair system

The block diagram in Figure 4-2 shows the attendant-wheelchair system with each detailed element. The attendant-wheelchair system had four parts; [A] the brain part to create the planned propelling force, [B] the lower extremity part to move its body forward, [C] the arm part to transfer propelling force from the body to the wheelchair, and [D] the wheelchair and environments. The disturbance force $f_E(t)$ included the downward gravity

force along with slopes and the static road resistance f_{R0}. In this chapter, this study assumed that the wheelchair is on a smooth level surface, so both the parameters f_{R0} and $f_E(t)$ were assumed to be zero because they are negligible numbers under the assumed condition. The dynamic lag element $G_M(s)$ by the equation (4-2) in the part [B] was assumed second order system with a dead time element. The element $G_M(s)$ mainly describes musculoskeletal dynamics. The dotted parts [E] in the part [A] is explained later in 4-6 Validation of the model section. The steady wheelchair velocity $v_{WS}(t)$ in the equation (4-7) was calculated by the final theorem with the transfer function $G(s)$ defined by the desired velocity $v_D(t)$ as an input, and the wheelchair velocity $v_W(t)$ as an output. In this case, the desired walking velocity $v_D(t)$ was assumed to V_M (V_M>0). The parameter with subscript letter "s" means the parameter value under steady state.

$$v_{WS}(t) = \frac{KK_W}{1+KK_W} V_M \tag{4-7}$$

Under the steady state, the relationship between the attendant walking velocity $v_S(t)$ and wheelchair velocity $v_{WS}(t)$, the planned propelling force $f_S(t)$, the actual leg force $f_{DS}(t)$, the propelling force $f_{WS}(t)$, and the road resistance $f_{RS}(t)$, were described in the equations below.

$$v_S(t) = v_{WS}(t)$$

$$v_{WS}(t) = K_W f_{WS}(t) = \frac{f_{RS}(t)}{R} \tag{4-8}$$

$$f_S(t) = f_{DS}(t) = f_{WS}(t) = f_{RS}(t) = C_R v_{WS}(t)$$

From the equations (4-8) with (4-7), the relationship between the attendant walking velocity $v_S(t)$ and the propelling force $f_{WS}(t)$ were described by the Equation (4-9).

$$v_S(t) = V_D - \frac{f_{WS}}{K}$$

$$\Leftrightarrow f_{WS}(t) = F_M - K v_S(t), \text{ here } F_M = KV_D \tag{4-9}$$

From the Equation (4-9), the difference between the attendant walking velocity $v_S(t)$ and the desired walking velocity V_M increased in proportion to the attendant propelling force $f_{WS}(t)$. In opposite, the attendant propelling force $f_{WS}(t)$ decreases monotonically from the F_M with the increase of the attendant walking velocity $v_S(t)$. The F_M was defined as the propelling force at standing $v_S(t)$=0.

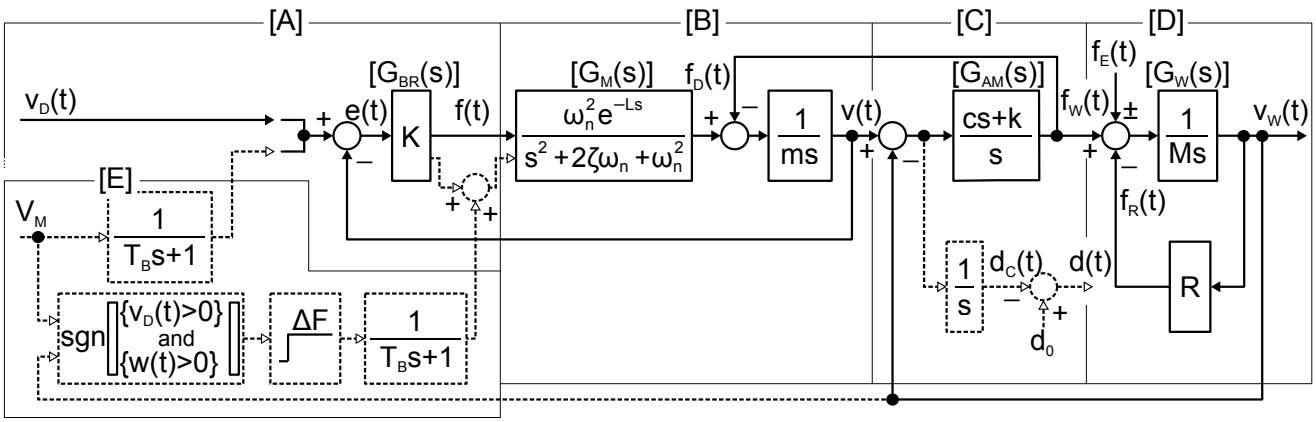

Figure 4-2 Block diagram of the attendant-wheelchair system

4-3 Methodology for indentification

Figure 4-3 shows the developed device based on a motorised treadmill to analyse propelling behaviours. The features of the device are; 1)the participant on this device can propel with grips as the participant do on the ground with a wheelchair, 2)the dynamics of the wheelchair and the road resistance can be given stably to the participant long time. These features enable this study to analyse propelling behaviours precisely and deeply. The device included some part of the block diagram in Figure 4-2. The motorised treadmill had two straight grips, which dimension was the same to the wheelchair. The width and height of the grips were 420mm and 840mm respectively. Each grip had 1-axis load cell, which measurement range was -200N to +200N with time constant 0.6s. The total propelling force $f_W(t)$ was obtained from the sum of both grip forces $f_{WR}(t)$ and $f_{WL}(t)$. The treadmill belt (length: 1450mm, width: 470mm) was driven by an AC servomotor (3.5kW, AC220V) via a front roller (diameter: 63mm). The angular velocity of the front roller was feedback controlled by a motor driver to the input velocity signal. The belt was tensioned well to prevent from any slip between the roller surface and the back of the belt. From this point, the belt velocity $v_T(t)$ was measured by an encoder in the AC servomotor. The oscilloscope in front of the treadmill was used to indicate the needed propelling force, which the participant have to generate in trials. The treadmill had the mechanism of the adjustable inclined base by screws, so that the treadmill reproduced the slope conditions.

With a digital signal processor, the propelling force $f_W(t)(= f_{WR}(t) + f_{WL}(t))$ converted to the belt velocity $v_W(t)$ by $V_W(s) = G_W(s)F_W(s)$ in the equation (4-5) and the part [D] in Figure 4-2. The calculated belt velocity $v_W(t)$ was used as an input signal of the motor driver. The subjective hardness of attendants in propelling was increased by the resistance load $f_R(t)$ from the causal relationship between the propelling force $f_W(t)$ and the wheelchair velocity $v_W(t)$. The coefficient C_R in the resistance load $f_R(t)$ was set by the reciprocal gain $1/K_W$ of the wheelchair component $G_W(s)$. From this system, this device provided reproducible wide range of the resistance load $f_R(t)$ by the gain K_W. In addition, the time constant T_W in the wheelchair component $G_W(s)$ enabled to set the dynamics of the wheelchair system arbitrary. In the case of the pulling force $f_W(t)<0$, the calculation of the belt velocity $v_W(t)$ was used as the absolute value of the propelling force $f_W(t)$ for the input signal of the wheelchair element $G_W(s)$, so that the treadmill belt moved backward for forward walking.

The subjective hardness in propelling was estimated from the heart rate (Yoshioka

1995[15]). In this study, a relative heart rate κ defined by the equation (4-10), was used as the index of the subjective hardness.

$$\kappa = \frac{HR - HR_R}{HR_M - HR_R} \times 100\,[\%] \tag{4-10}$$

Here, the HR was the measured heart rate in the trial, the HR_R was the rested heart rate, and the HR_M was the maximum heart ratio, which was estimated the subtraction from 220 to the participant's age, according to the study by Fox 1971[16]. The heart rate was measured by the strap type of a heart rate sensor (Polar Inc.) rounded the participant's chest.

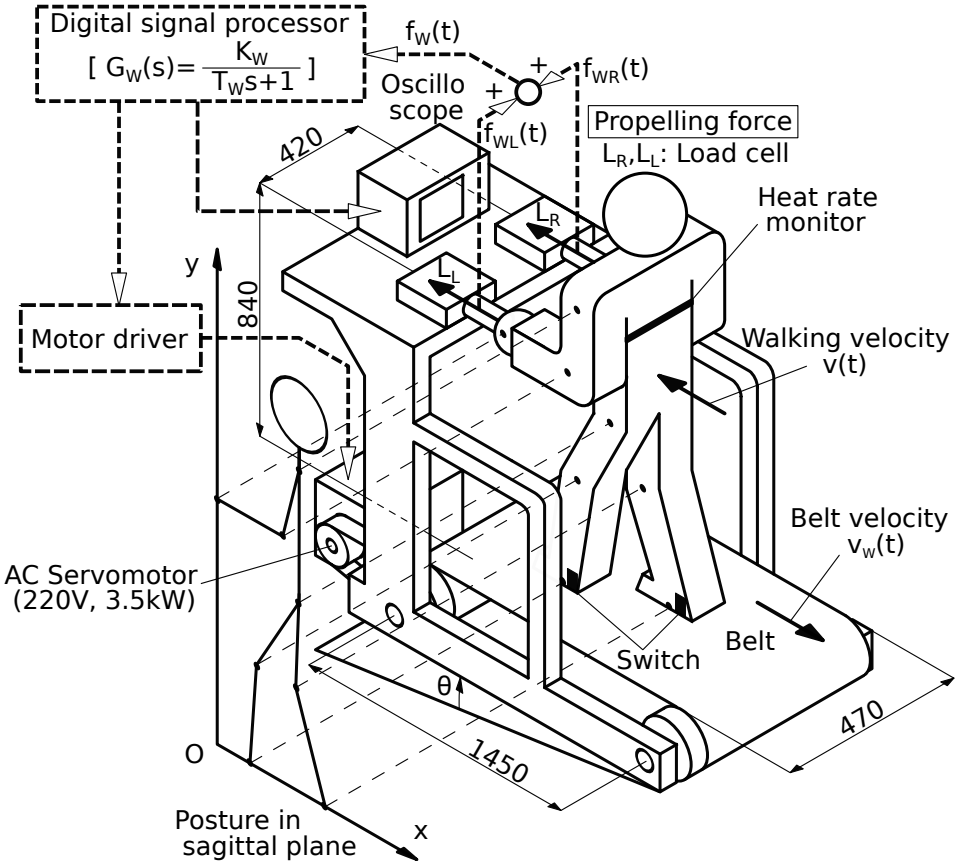

Figure 4-3 Motorised treadmill based propelling motion analyser

Categorise the propelling activities in the trials

Autonomous propelling was discussed in the Chapter 3. In summary, the attendant in the autonomous propelling maximises the walking velocity $v_S(t)$ and the propelling force $f_{WS}(t)$, so that the participant continues the propelling as long as possible under minimising the subjective hardness. The walking velocity $v_S(t)$ and the propelling force $f_{WS}(t)$ in the autonomous propelling depend on the attendant's preference, experiences,

physical strength, and so on. In the trials of the autonomous propelling, this study asked the participants to propel on the treadmill in 20 minutes at steady state, like propelling a wheelchair on the ground long time. The maximum propelling was defined that the participant propeled with maximum propelling force as long as possible voluntarily. In the trial of the maximum propelling, the participant was asked to propel with the maximum force on the treadmill at the steady state within one or two minutes, like propelling a wheelchair in hard, such as on gravel surfaces, steep slopes, and getting over small thresholds.

Participants

Four healthy participants in their 21 to 23 joined this study. The participants had shown no disorder related to human movements. This study gave the detailed procedure of the trials to all participants prior to all trials, and obtained consents. This study shows the series of the results in one participant, because this study focus on the relationship in all components about one attendant, rather than discussing statistic trends by many participants. The represented results in this Chapter 4, were obtained by the male participant, whose descriptions were; age:23years old, height:1.68m, weight:57kb, grip force:42N(right), 37N(left), back force:61N, natural walking velocity V_0=1.17m/s, rested heart ratio HR_R=57bpm, and maximum heart ratio HR_M=197bpm.

Investigation of the base physical strength in propelling

The slope angle of the treadmill had been adjusted to a level before all of trials. In the series trials for each participant, the participant had stood with gripping the bars on the treadmill one minute before starting, then propelled 20 minutes at steady state. After 15 minutes passed, the propelling force $f_W(t)$ and the belt velocity $v_W(t)$ equivalent to the walking velocity $v(t)$, and heart ratio HR were recorded for five minutes. From averaged these recorded parameters, the steady propelling force $f_{WS}(t)$, the steady wheelchair velocity $v_{WS}(t)$, and relative heart ratio κ were calculated. After the end of each trial, the participant rested on a chair in 10 minutes. The maximum period in the trials for one participant was within three hours. The resistance loads $f_R(t)$ in the equation (4-6) were set by the dynamic resistance $Rv_W(t)$ with the static resistance f_{R0}=0. The resistance coefficient $R(=1/K_W)$ was randomly used from $K_W=0.16\times10^{-3}$ to 0.08(m/s)/N in the gain of the wheelchair element $G_W(s)$. With the conversion to the resistance coefficient R, the range was 12.7 to 6250N(m/s). The total weight M of the wheelchair including an

occupant was assumed 100kg.

Posture of the propelling

In the maximum propelling with pushing, there are two propelling styles; 1) The whole body leans forward with straightening arm, so that the attendant effectively applies their weight to horizontal pushing force $f_W(t)$, and 2) With relatively less leaning forward than the case 1), the participant mainly propels by the leg force with the arm placed near the upper body to be enable to stop immediately with the rapid change of the propelling posture. The preliminary experiments showed the maximum propelling force in the case 1) was about 10% more than in the case 2). This study, however, asked the participant to propel with the propelling style under the case 2), because the attendant keeps the propelling style 2) in actual wheelchair propelling to prevent from falling, or any accidents.

4-4 Identification of autonomous propelling and braking

Figure 4-4(a) shows the averaged steady pushing force $f_{WS}(t)>0$ under the condition A_D (autonomous) and M_D (maximum), and the averaged pulling force $f_{WS}(t)<0$ under the A_B (autonomous) and M_B (maximum), in the forward propelling on the treadmill. The propelling forces $f_{WS}(t)$ were plotted with the steady walking velocity $v_S(t)(=v_{WS}(t))$. The plot of the propelling force $f_W(t)$ in Figure 4-4(a) was obtained from averaging the operating point $[f_W(t),\ v_W(t)]$ under the steady state. Figure 4-4(a) also shows the absolute mechanical power P_S under the autonomous pushing A_D and pulling A_B. Figure 4-4(b) shows the relative heart ratio κ at each trial of the autonomous and maximum propelling.

The trajectory by a thin line in Figure 4-4(a) shows the time transition of the operating point $[f_W(t),\ v_W(t)]$ from start to the steady autonomous A_D and maximum M_D propelling conditions under the resistance load $f_R(t)=Rv_W(t)$, R=290N/(m/s). In the beginning of both trajectory of the A_D and M_D, the propelling force $f_W(t)$ increased rapidly to accelerate the wheelchair, then eventually the operating point $[f_W(t),\ v_W(t)]$ stayed steadily on the line of the resistance load $f_R(t)$. The final operation points were determined by the maximised propelling force $f_W(t)$ and the wheelchair velocity $v_W(t)$ under the condition that the participant coped with the resistance load $f_R(t)$ by the autonomous A_D and maximum M_D propelling. The operating point at steady state had a limit cycle, because the propelling force $f_W(t)$ and the wheelchair velocity $v_W(t)$ had frequency components by two leg walking. There were six important findings in Figure 4-4.

1) The propelling force $f_W(t)$ decreased proportionally with the increase of the walking velocity $v_S(t)(=v_{WS}(t))$ under the autonomous propelling in pushing A_D and pulling A_B. This trend was described by the equation (4-9).

2) In Figure 4-4(b), the relative heart ratio κ under the autonomous propelling in pushing A_D and pulling A_B were in the range between 15% and 30%, and this means that the subjective hardness of the propelling was "very light" by the Borg scale.

3) In the maximum propelling in pushing M_D and pulling M_B, the propelling force $f_W(t)$ decreased proportionally with the increase of the walking velocity $v_S(t)$. This trend was similar to the point 1) above. The relative heart ratio κ in the maximum pushing M_D increased between 60%("Hard") and 85% ("Very Hard"). In this condition, the relative heart ratio κ was extract after 30second passed from starting. The subjective hardnesses in

these trials were estimated as "very very hard", even though the times in these trials were short about two minutes, which was very shorter than the time in autonomous steady condition.

4) In the walking velocity $0<v_S(t)<1$m/s, the pushing forces $f_W(t)$ in the autonomous condition A_D were from 30 to 37% of the maximum pushing force in the maximum condition M_D, and the pulling forces $f_W(t)$ in the autonomous condition A_B were from 15% to 1% of the maximum pulling force in the maximum condition M_B. This drop ratio of the autonomous forces by the maximum forces decreased in the range over the walking velocity around 1m/s.

5) The maximum numbers of the absolute mechanical power P_S in the autonomous propelling in pushing A_D and pulling A_B were 24W and 4W respectively. In the maximum propelling, the absolute mechanical powers P_S were 255W(M_D) and 48W(M_B). The absolute mechanical power P_S in the autonomous propelling in pulling A_B dropped about one-tenth to the P_S in the autonomous pushing A_D. This means that the developing an assisting system for pulling would be important for future works.

6) The relative heart ratio κ in the case H_D, which is the middle propelling condition between the autonomous A_D and the maximum M_D propelling, was about 60%, "fairly hard to hard" by the Borg scale. From the comparison among the condition A_D, H_D, and M_D, the force velocity relationship of the propelling force $f_{WS}(t)$ and the walking velocity $v_S(t)$ increased roughly in proportion to the relative heart ratio κ.

Described by the equation (4-9), the monotonic decrease in the propelling force $f_W(t)$ with the walking velocity $v_S(t)$ under the condition A_D, A_B, M_D, and M_B, can be explaind from Figure 4-5. Figure 4-5 shows the cadence α of the condition A_D and A_B, and the standing ratio β defined by the standing period divided by the step time(=60/α). The cadence α increased and the standing ratio β decreased with the increase of the walking velocity $v_S(t)$. To generate the propelling force $f_W(t)$, the attendant needs lower cadence α and higher standing ratio β. From this point, it becomes more difficult to generate the larger propelling force $f_W(t)$ under higher walking velocity $v_S(t)$. That was a reason that the propelling force $f_W(t)$ decreased with the increase of the walking velocity $v_S(t)$. In Figure 4-5, both the standing ratio β in pushing A_D and pulling A_B were similar, however, the cadence α in the pulling A_B showed a steep rise compared with the pushing A_D in the walking velocity $v_S(t)$ <0.25m/s. Under the autonomous propelling in pulling A_B, the participants walked with pulling in the posture of leaning backward with lengthened upper arms to balance their body. This propelling posture needed short and

rapid steps by the higher cadence α, to keep the backward leaned posture.

The propelling condition H_D were reproduced by following steps. The propelling force walking velocity relationship $f_{WS}(t) = 175 - 74.2v_S(t)$ was obtained from the middle line between the A_D and M_D, with the same slope coefficient of the A_D. The operating points on the middle line were selected randomly to cover throughly the velocity range $0 < v_W(t) < 1.25$m/s, then the road resistance $f_R(t)$ was set one by one, so that the selected operating point p was placed on the $f_R(t)$. In the trial to obtain the propelling condition H_D, the participant was asked to adjust the wheelchair velocity $v_W(t)$ to the indicated walking velocity $v_S(t) = V_P$ in the oscilloscope, against each set of the resistance load $f_R(t)$.

From Figure 4-4(a), this study obtained the parameter K and F_M in the equation (4-9). In the pushing cases, the extracted parameters were K =74.2N/(m/s)[A_D and M_D] and F_M =84N[A_D] and 265N[M_D]. In the pulling cases, the extracted parameters were K=-13.1N/(m/s)[A_B], -100.0N/(m/s)[M_B] and F_M=-11.6N[A_B], and -60.0N[M_B].

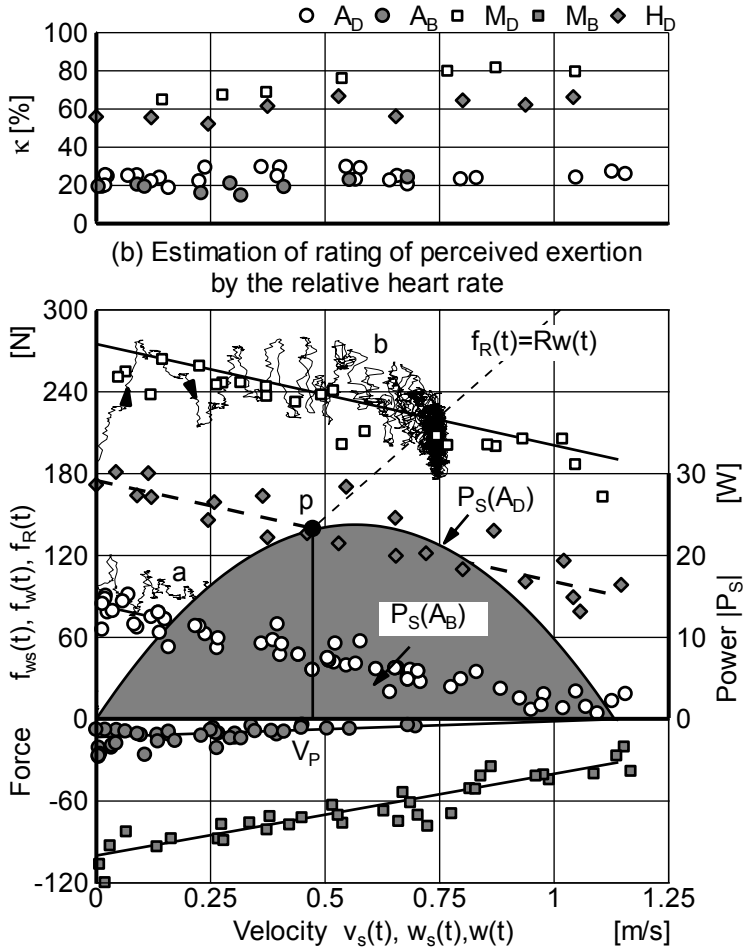

Figure 4-4 Force velocity relationship in Propelling and braking a wheelchair

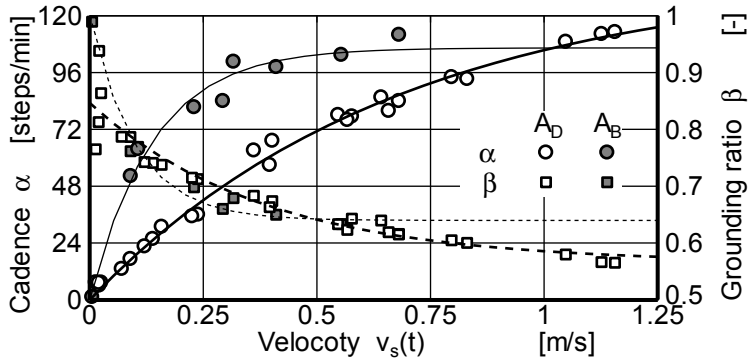

Figure 4-5 Walking pattern in propelling

Autonomous and maximum propelling

In the block diagram of Figure 4-2, this study analysed the autonomous propelling behaviour in pushing ($v(t), v_W(t) \geq 0$) with the desired walking velocity $v_D(t) = V_M > 0$ and the gain $K = K_D (> 0)$ of the planned force element $G_{BR}(s)$. The operations at the summing point in the part [A] and the planned propelling force $f(t)$ were described by next equation (4-11).

$$f(t) = K_D e(t) = K_D \{V_M - v(t)\} \tag{4-11}$$

The equation (4-11) also shows the relationship in steady state, because the element $G_{BR}(s)$ did not have any time lag. The equation (4-11), which provided the steady planned force $f_S(t)$ from the equation (4-8) and the steady propelling force $f_{WS}(t)$ by the equation (4-9), corresponds to the relationship $f_S(t) \sim v_S(t)$ of the steady propelling force and the walking velocity with the gain $K = K_D$. From this point, next equation (4-12) was obtained.

$$f(t) = \begin{cases} 0 & : \quad e(t) < 0 \\ K_D e(t) & : \quad 0 \leq e(t) \leq V_M \end{cases} \tag{4-12}$$

With the regression curve with the equation (4-9) for the autonomous propelling in Figure 4-4(a), the relationship $e(t) \sim f(t)$ provided by the planned force element $G_{BR}(s)$ corresponds to the characteristic of the equation (4-12).

From this point, the control system between the walking velocity $v_D(t)$ and $v(t)$ in the part [A - B] was described as the proportional control system with the gain K_D by the equation (4-12), with the desired walking velocity $v_D(t) = V_M > 0$ and the disturbance force $f_E(t)$. The extracted parameters from Figure 4-4(a) were the walking velocity V_M =1.16m/s, the gain K_D=74.2N/(m/s), and the propelling force intercept f_M=84N. The experiments with other participants suggested that the gain K_D would depend on the

physical strength, and the walking velocity V_M would be similar to the natural walking velocity V_0. In the maximum propelling, the extracted parameters were the gain K_D =74.2N/(m/s) and the propelling force intercept f_M=265N.

Autonomous braking

This study also analysed the planned force element $G_{BR}(s)$ in braking. The $G_{BR}(s)$ described the attendant pulling operation to stop a wheelchair, in other word, the attendant makes the desired walking velocity $v_D(t)$ to zero. The summing point in the block diagram describes the relationship $e(t)=-v(t),(0\le v(t)\le V_M)$. The gain replacement $K=-K_B(>0)$ in the relationship $f_{WS}(t)\sim v_S(t)$ of the propelling force and the walking velocity, provided the equation (4-13) with the same variable replacement in the mentioned section of *Autonomous and maximum propelling* above.

$$f(t)=\begin{cases} f_M-K_Be(t) & : \quad 0\ge e(t)\ge -V_M \\ 0 & : \quad e(t)<-V_M \end{cases} ,(f_M=-K_BV_M) \qquad (4\text{-}13)$$

The extracted parameters from the plot in the autonomous pulling A_B in Figure 4-4(a) were the walking velocity V_M=1.16m/s, the gain K_B=11.6N/(m/s), and the propelling force intercept f_M=-13.1N. The planned force element $G_{BR}(s)$ in braking was non linear. In the maximum braking, the extracted parameters were the gain K_B=60.0N/(m/s) and the propelling force intercept f_M=-100.0N.

4-5 Indentification of dynamic elements

Musculoskeletal dynamics element $G_M(s)$

The musculoskeletal dynamics element $G_M(s)$, which converts from the planned propelling force $f(t)$ to the actual leg force $f_D(t)$, was assumed as a time lag system with its gain = 1. This study identified the musculoskeletal dynamic element $G_M(s)$ by the frequency response method. In the identification experiments, the participants was asked to follow the actual propelling force $f_W(t)$ to the indicated sinusoidal propelling force $f(t)$ on the oscilloscope under the constant walking velocity $v_S(t)$ on the treadmill in Figure 4-3. The indicated propelling force $f(t)$ was assumed to be the simulated planned propelling force in the brain from the negligence of lag time by human visual system. In these experiments, the feedback path from the part [B] to [A] in the attendant-wheelchair system was opened, so that only the musculoskeletal dynamic element $G_M(s)$ was analysed under the condition of the leg propelling force $f_D(t)$ = the actual propelling force $f_W(s)$ by the assumption that the cushioning element $G_{AM}(s)$=1 and the body mass element [1/ms] is zero. To secure this condition, the participant was asked not to move the upper extremity as much as possible. This methodology was used for estimating the stiffness k and the damping c in the cushioning element in the part [B]. These estimations of the k and c were explained later section.

Figure 4-6 shows the frequency response of the actual propelling force $f_W(s)$ with the indicated propelling force $f(t) = 50 + 20\sin\omega t$ [N] under the walking velocity $v_{WS}(t)$=0m/s and 0.83m/s. In Figure 4-6, the plotted circles are the experimental results, and the estimated curves were drawn in lines. The frequency response at the walking velocity $v_{WS}(t)$=0.83m/s was little worse than the response at the walking velocity $v_{WS}(t)$=0m/s, in which the participants took stable posture in standing. Over the frequency 1.6Hz, which corresponded to the cadence α=96step/min under the walking velocity $v_{WS}(t)$=0.83m/s, the attendant was difficult to follow the provided actual propelling force $f_W(s)$ because of small standing ratio β. With a second order system with a dead time L in the equation (4-14), this study did curve fitting to estimate the musculoskeletal dynamics element $G_M(s)$ in the part [B] of the block diagram.

$$G_M(s) = \frac{F_D(s)}{F(s)} = \frac{\omega_n e^{-Ls}}{s^2 + 2\varsigma\omega_n s + \omega_n^2} \tag{4-14}$$

In the later analyses, this study used the parameter L=0.14s, ω_n=6.6rad/s, ς=0.43 as a

typical case. In the case of the walking velocity $v_{WS}(t)=0$, the extracted parameters were L=0.09s, ω_n=8.2rad/s, ς=0.40.

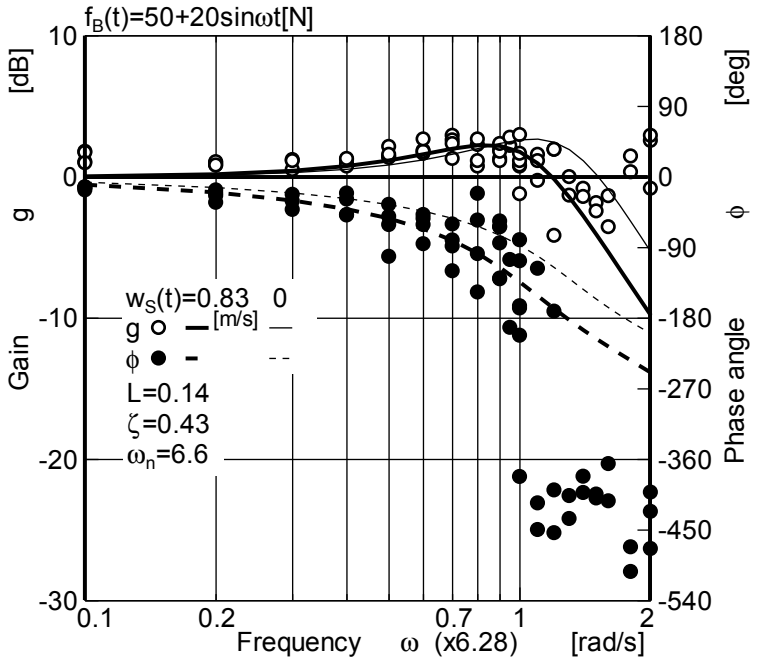

Figure 4-6 Estimation of $G_M(s)$ by frequency response method

Cushioning element $G_{AM}(s)$

This study estimated the stiffness *k*, then the damping coefficient *c* in the cushioning arm element $G_{AM}(s)$, which described the force transferring element from leg propelling force $f_D(t)$ to the actual propelling force $f_W(t)$ at the wheelchair grips by both arms. Figure 4-7 shows the relationship between the propelling force $f_{WS}(t)$ and the distance $d_S(t)$ from the wheelchair grips to the surface of the participant's abdomen, under steady state propelling. The distance *d*(*t*) was measured by a wired distance measuring device, whose tip of the wire was connected to the participant's trousers belt by a small metal hook. In the identification of the stiffness *k*, the trials were done under the condition with the indicated propelling force $20 \le f_{WJ}(t) \le 120$ by 20N step (J=1 to 6) and the indicated walking velocity $v_{WI}(t)$=0.28, 0.56 (I= 1 to 3), and 0.83m/s. Before the identification, the condition $(v_{WI}(t), f_{WJ}(t))$ was selected randomly, then the calculated resistance load coefficient *R* from the equation $R = f_{WJ}(t) / v_I(t)$ was set to the treadmill. The range of the resistance load coefficient *R* was from 24 to 428N/(m/s). The participant was asked to follow the walking velocity $v_W(t)$ to the indicated walking velocity $v_{SI}(t)$ in the oscilloscope by adjusting the propelling force $f_W(t)$. After the propelling became steady, the distance $d_S(t)$ was measured.

From the relationship $d_S(t) \sim f_{WS}(t)$ in Figure 4-7, the propelling force $f_{WS}(t)$ was increased in proportion to the decrease of the distance $d_S(t)$. This behaviour was similar to the mechanical spring in compression. In the range of the distance $d_S(t)$<0.05m, the propelling force by dotted line rose steeply with the decrease of the $d_S(t)$. However, this study simply used a linear straight line to estimate the stiffness of the cushioning arm element $G_{AM}(s)$ by the upper extremity, because the relationship $d_S(t) \sim f_{WS}(t)$ showed a liner trend in the distance $d_S(t)$ > 0.05m. The extracted stiffness in the upper extremity was k=513N/m.

The distance $d_S(t)$ was shortened in which an attendant generated large propelling force $f_{WS}(t)$ under lower walking velocity $v_S(t)$. With the increase of the walking velocity, the propelling force $f_{WS}(t)$ decreased because the attendant was difficult to keep short distance $d_S(t)$ under the longer step length. It means that the attendant needed enough space between the wheelchair and the attendant for steps. Also, the cadence α increased and the posture became nearly straight up. These factors are a reason for the declined propelling force $f_{WS}(t)$ with the increase of the walking velocity $v_S(t)$. From this reason, Figure 4-7 shows that the distance $d_S(t)$ was shorter under larger propelling force $f_{WS}(t)$ and slower walking velocity $v_S(t)$, and the distance $d_S(t)$ was longer under smaller propelling force and faster walking velocity. In the distance $d_S(t)$<0.05m, the participant kept long standing period of both foot to generate large propelling force under the shortened distance $d_S(t)$. This is the reason of the steep rise of the propelling force $f_{WS}(t)$ in the distance $d_S(t)$<0.05m.

The x-intercept of the distance $d_S(t)$ means the natural distance d_0 while the participant stood naturally with gripping before trials. After starting trials, the distance $d(t)$ was shortened by the compression $d_C(t)$. The equation to describe this behaviour is shown next.

$$d(t) = d_0 - d_C(t) \Rightarrow d_C(t) = \int_0^t \left\{ v(\lambda) - v_W(\lambda) \right\} d\lambda \tag{4-15}$$

$$f_W(t) = k d_C(t)$$

Next, the damping coefficient was identified from a transient response of the equation (4-16), which described the relationship between the planned force $f(t)$ and the actual propelling force $f_W(t)$ in the part [B] and [C] in Figure 4-2.

$$F_W(s) = \frac{G_M(s) G_{AM}(s)}{G_{AM}(s) + ms} F(s) \tag{4-16}$$

In the identification of the experiments, the participant was asked to follow the actual propelling force $f_W(t)$ to the indicated step change of the planned propelling force $f(t)$

on the oscilloscope under standing $v_W(t)(=v(t))=0$ on the treadmill. The indicated step changes of the $f(t)$ were between 30N and 80N, and the trials for this identification were repeated many times. Figure 4-8 shows the normalised results of the actual propelling force $f_W(t)$ by the indicated planned force $f(t)$. This study obtained the estimated step response of the equation (4-16) by curve fitting, with the musculoskeletal element $G_M(s)$ and the body mass m and the stiffness k. Finally, this study obtained the damping coefficient c=525N/(m/s) from the curve fitted thick line in Figure 4-8.

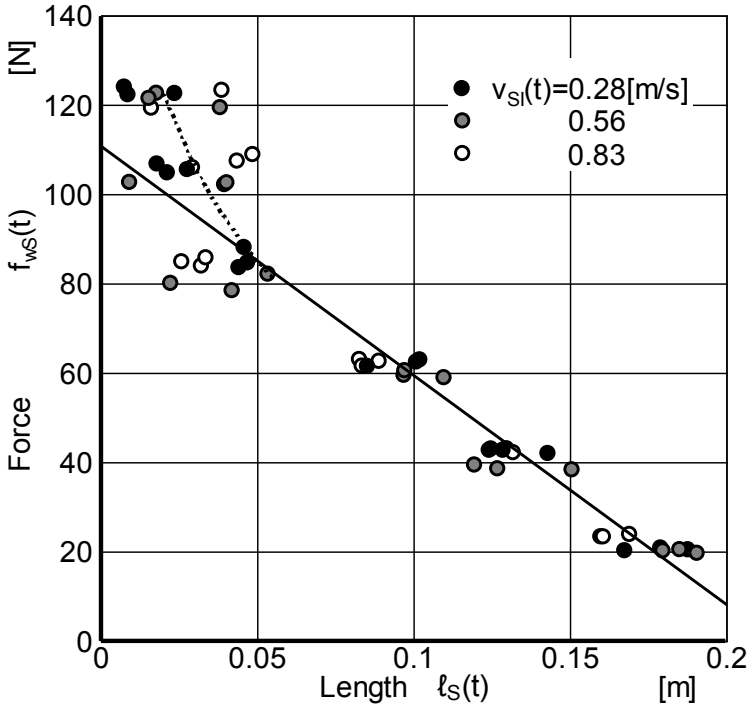

Figure 4-7 Estimation of the stiffness in upper extremity

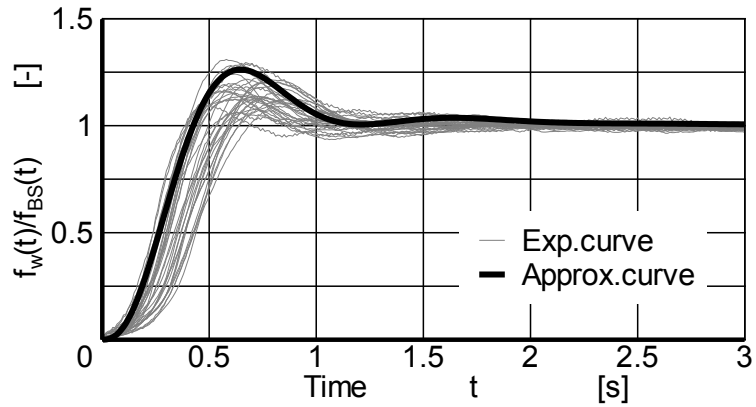

Figure 4-8 Estimation of the damping coefficient c by step response

4-6 Validation of the model

This study validated the attendant-wheelchair model in autonomous propelling on a level, with the two experiments; a)Propelling a wheelchair on the ground, and b)Propelling on the treadmill with simulated wheelchair dynamics and road resistances. The standard road surface used for this validation was an artificial grass surface made of imitated plastic grasses with 30mm height, and its road resistance $f_R(t)$ was simulated by the equation (4-6) with the parameters f_{R0}=57.7N, and R=6.32N/(m/s) estimated from preliminary experiments. The part [E] of the attendant wheelchair model in Figure 4-2 extended to simulate a transient dynamics in starting when the attendant needs larger propelling forces. The part [E] has two component; 1) Generating larger propelling force to accelerate a wheelchair and to identify unknown road resistance $f_R(t)$, 2) Reducing rapid acceleration with turning off the initial hard pushing 1). The part 1) consisted of the excessed propelling force ΔF with the sgn function, which controlled to turn on and off the excessed propelling force ΔF. The part 2) consisted of the first order lag system with a time constant T_B, which was estimated T_B=0.8s from the validation a). The excessed propelling force ΔF=181N was obtained from the difference between the autonomous and maximum propelling at zero walking velocity in Figure 4-4(a).

Figure 4-9 has three types of lines, which shows a) the overground validation: thin line, b) the treadmill validation: dashed thin line, and the calculated results from the model: thick line. Figure 4-9(b) shows time series data in the wheelchair velocity $v_W(t)$ and the propelling force $f_W(t)$, and Figure 4-9(a) shows the trajectory of the operating point $[v_W(t),\ f_W(t)]$. Figure 4-9(a) also has the autonomous propelling relationship $v_{WS}(t) \sim f_{WS}(t)$ by the equation (4-9) in a thick line and the resistance load $f_R(t)$ by the equation (4-6) in a dashed line. Around the cross point between the autonomous propelling relationship and the road resistance, the trajectory in the validation a) stayed in the steady state. This means that the participant regulates autonomously the propelling force and the walking velocity to be suitable for the resistance load. The validation results was well fitted to the calculated results, except the periodic changes at the steady state because the model did not have two leg walking elements. From this validation, the attendant behaviour in propelling a wheelchair could be simulated with the model in Figure 4-2, and the model is useful to analyse the detailed propelling behaviour by various environments.

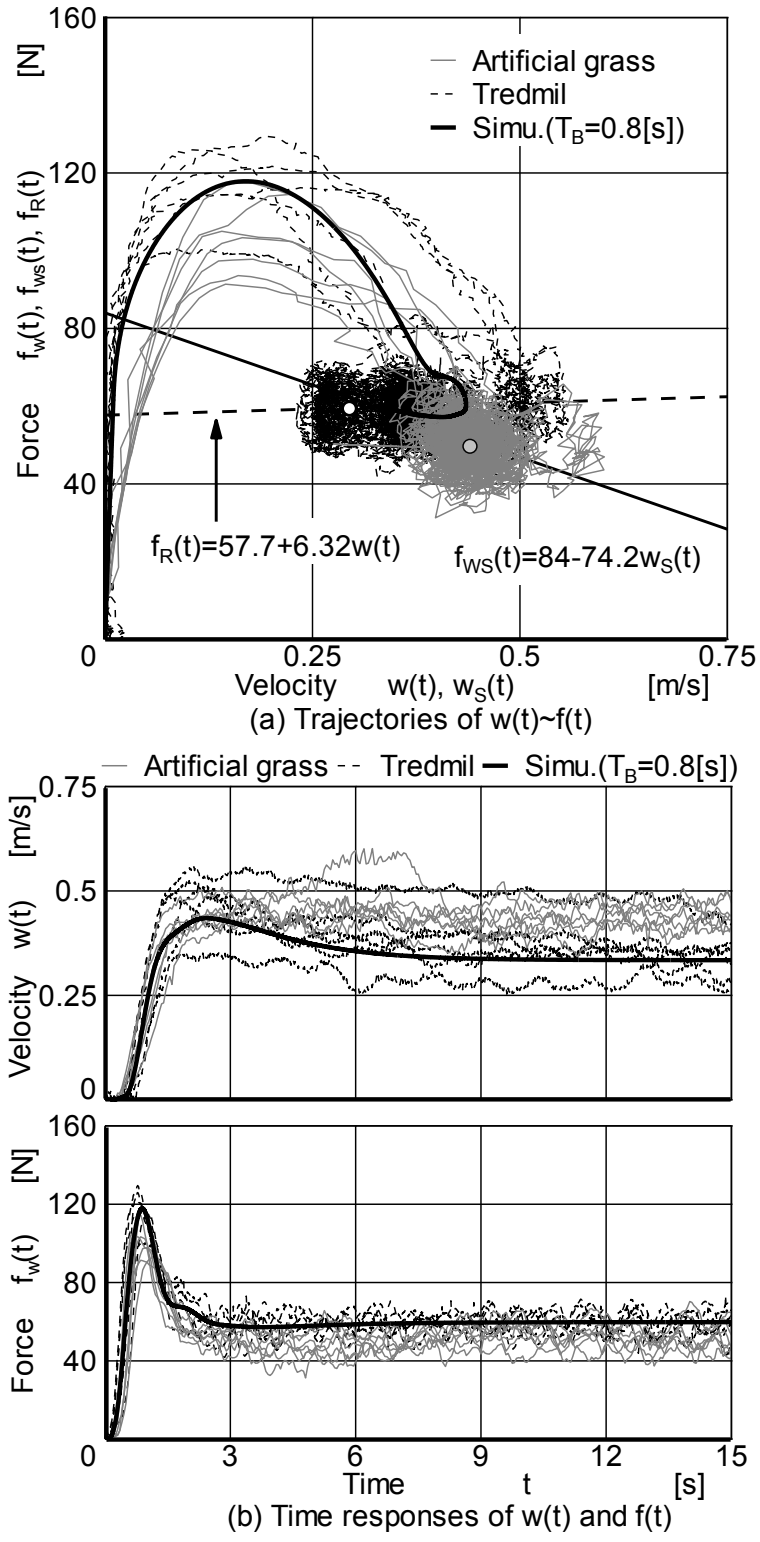

Figure 4-9 Identification of the model
by the overground and the treadmill experiments

4-7 Conclusions

In this chapter, this study proposed the attendant-wheelchair model, and validate it with identified parameters for each element in the model. The proposed model was built upon the analogy of the prime motor and load system. The attendant part had the elements of musculoskeletal dynamics and cushioning arm dynamics, and the wheelchair part had the mechanical dynamics of wheelchairs in straight moving on longitudinal slopes. From the experiments for validation of the model on the artificial grass surface at a level, our findings are below.

1) The proposed attendant-wheelchair model can simulate the attendant behaviour well. This suggest that the proposed model is very useful for estimating an attendant's propelling hardness on various resistance load, such as rough surface, gap and threshold.

2) The propelling force - walking velocity relationship of attendants dominates main steady state in the model. The transfer functions of other elements become 1 under steady state, so the attendant steadily propels a wheelchair at the operating point, at which attendant's force velocity relationship and wheelchair's resistance load are the same.

3) The dynamics of the musculoskeletal system can be described as the second order system with lag element. However, the identification suppose that the human cannot follow force change over 1 Hz while walking.

4) The arm function can be described as a parallel spring and damper system. The results shows the arm stiffness and dumping coefficient are linear.

These findings contribute to improve the attendant-propelled wheelchairs, and to develop effectively the assist controller for a powered attendant-propelled wheelchair.

References

[1]Strinberg, L. and Petersson, N.F., Measurement of Force Perception in Pushing Trolleys, *Ergonomics*, No.15, pp. 435-438, 1972

[2]Yumiko, Y., The optimum inclination of a ramp for the transport of a loaded wheelchair by the assistant (in Japanese), *Acta Scientiarvm V aletvdinis Universitatis Praefectvralis Ibarakiensis : ASVPI*, Vol. 2, pp. 53-59, 1997

[3]Al-Eisawi, K.W., Kerk, C.J., Congelton, J.J., Amendola, A.A., Jenkins, O.C. and Gaines, W., Factors affecting minimum push and pull forces of manual carts, *Applied Ergonomics*, No.30, pp. 235-245, 1999

[4]Jansen, J.P., Hoozemans, M J.M., van der Beek, A.J. and Frings-Dresen, M.H.W., Evaluation of ergonomic adjustments of catering carts to reduce external pushing forces, *Applied Ergonomics*, No.33, pp. 117-127, 2002

[5]Horiuchi. K., Aoki, K., Measuring propelling force of walking auxiliary car (in Japanese), *Ningen Kogaku(Japanese Journal of Ergonomics)*, No. 39-1, pp. 38-41, 2003

[6]Akira, K. and Kouji, M., Effects of a Difference in Body Weight between a Wheelchair User and an Assistant of Wheelchair Propulsion (in Japanese), *Journal of Physical Therapy Science*, Vol.17， No.4, pp. 249-252, 2002

[7]Shinji, I., Shuichi, K., Hideto, T., Kenji, H. and Shigeru, K., Evaluation method for sidewalk unevenness based on wheelchair traveling load (in Japanese), *Doboku Gakkai Ronbunshuu E*, Vol.62, No.2, pp. 295 ~305, 2006

[8]Satosi, M., Akihiro, M., Yousuke., M. and Takashi, N., The application and quantification of physcial strain during wheelchair locomotion on a slope (in japanese), *Doboku Gakkai Ronbunshuu D*, Vol.62, No.3, pp. 401~416, 2006

[9]A. Abdel-Malek and V. Z. Marmarelis, “Modeling of task-dependent characteristics of human operator dynamics pursuit manual tracking,” Systems, Man and Cybernetics, IEEE Transactions on, vol. 18, no. 1, pp. 163–172, 1988.

[10]R. A. Hess and A. Modjtahedzadeh, “A control theoretic model of driver steering behavior,” IEEE Control Syst. Mag., vol. 10, no. 5, pp. 3–8, 1990.

[11]R. A. Hess, “Modeling Pilot Control Behavior with Sudden Changes in Vehicle Dynamics,” Journal of Aircraft, vol. 46, no. 5, pp. 1584–1592, Sep. 2009

[12]K. Masani, A. H. Vette, and M. R. Popovic, “Controlling balance during quiet standing: proportional and derivative controller generates preceding motor command to body sway position observed in experiments,” Gait Posture|9416830, vol. 23, no. 2, pp. 164–172, 2006.

[13]F. Chenier, P. Bigras, and R. Aissaoui, “A new dynamic model of the manual

wheelchair for straight and curvilinear propulsion," presented at the Rehabilitation Robotics (ICORR), 2011 IEEE International Conference, pp. 1–5, 2011

[14]Brauer, R.L. and Voegtle, P. J., Wheelchair rolling resistance, *American Society of Mechanical Engineers Applied Mechanics Division*, Vol.43, pp. 267-270, 1981

[15]Yoshioka, T. et al, Exercising level of mid-high aged people on walking based on relative heart ratio (in Japanese), *Osaka Kyoiku Daigaku Kiyo, 03, Shizen Kagaku Oyo Kagaku(Memoirs of Osaka Kyoiku University, Ser. 3, Natural Science and Applied Science)*, No. 43-2, pp. 159-165, 1995

[16]Fox, S.M., Naughton, J.P., Haskell, W.L., Physical activity and the prevention of coronary heart disease, Ann Clin Res., Vol. 3, pp404–443, 1971

Chapter 5 Design of assistive system for attendant-propelled wheelchair

5-1 Introduction

Attaching powered assisting devices to the wheelchair is one of the best solutions to reduce the propelling load. The powered attendant propelled wheelchair has load cells mounted at the grips to measure the propelling force of attendant, and the assistive force is generated by electric motors, which power either an auxiliary wheel or the two rear wheels directly. The assisting controller calculates the assisting force from the propelling force at the grips. This basic mechanism was proposed by Abel 1991[1]. Abel tested three types of drive system to provide power assistance for attendant propelled wheelchair. From user trials on test track simulating outdoor conditions, participants favoured a two-motor drive system with force sensing handles, and attendants with the proposed assist system can successfully negotiate most outdoor conditions, without overexertion.

For assisting control for the attendant propelled wheelchair, many types were proposed. Kakimoto 1997[2] proposed model based assist control for attendant propelled wheelchairs. The power assist is contorled as if a lightweight wheelchair was operated on solid flat surfaces. Kakimoto validated the proposed assist control by experiments, and found his assist control reduced effectively the attendant propelling forces. Kitagawa 2004[3] proposed an omni-directional transport wheelchair. The desired motion of the wheelchair was estimated by fuzzy algorithm, from the operational forces by an attendant in the grips back of the wheelchair. The omni-directional movement was realised by four omni-wheel motors. Katsura 2004 proposed a powered attendant propelled wheelchair based on the adaptive force control. This adaptive control with reaction torque observer estimated reaction force from environment, then control both wheel motors to follow the attendant intention, which appears in both operating forces at grips back of the wheelchair. Ren 2007[4] developed a power assisted mobile vehicle based on torque observer. This vehicle can be driven as a human-guided powered mobile vehicle without measurements in human forces. The controller is designed from the Lagragian model of the vehicle with a torque observer using the Lyapunov stability theorem. The torque observer was applied to estimate external human forces.

For assistive powered manual wheelchair, Cremers 1989[5] introduced a basic idea of the pushrim activated power assist wheelchair. Cremers proposed and validated the hybrid powering combined with arm force and electric power in order to reduce necessary arm forces in pushing manual wheelchair by pushrim. After this, the pushrim activated power assist wheelchair became popular, and many control strategies were proposed. Hata

2003[6] proposed a control strategy to prevent from tumbling backward for pushrim-activated power assist wheelchair. The control strategy with an observer estimated the position of the centre of mass and decreased an assist ratio to prevent from tumbling backward. Seki 2005[7] also proposed the compensation system of the disturbed torque from uneven road surfaces for power assisted wheelchairs. The disturbance observer estimated the difference of the driving torques on both wheels, and minimum jerk trajectory control improved the drivability of powered assisted wheelchairs. Seki 2005[8] proposed the assist system to improve the drivability in straight and circular path. The proposed balanced assisted torque was determined from the ratio of the user pushing torque between both wheels. The results show the improvement of the drivability. Seki 2006[9] proposed the step climbing control for powered assisted wheelchair based on driving mode switching. This study used two control systems for the front casters and rear wheels while climbing to change the control rules. Petersson 2007[10] proposed the assist controller without force sensors in the pushrims. The controller was based on a simple PD structure, to tune easily to fit a certain user. One parameter in the assist controller adjusts the amplification of the user's force, and the another one determines the lasting time of the propulsion assist. Tashiro 2008[11] proposed an assist system without force sensors. The assist controller estimated pushing torques by the observer with the signal of the reaction torque in the motor, then generated the assist forces. Seki 2009[12] developed the regenerative braking control scheme for powered assisted wheelchairs. The back electromotive force of the motor in a wheel was applied to the step-up chopper circuit to generate the braking force while driving the wheelchair on downhill. Oonishi 2010[13] proposed the assist method to use the EMG signal in adductor pollicis muscle, which is activated by gripping hand rim when a user pushes a manual wheelchair. Oonishi estimated the pushing torque from the EMG signal of the adductor pollicis muscle. The disturbance by uneven surfaces and inclined slope in all orientations, decreased the drivability in the power assisted wheelchairs. Seki 2011[14] proposed a fuzzy algorithm based on an adaptive control in order to improve low drivability in the assistive driving on large disturbance roads.

In addition, the assessment of the pushrim activated power assist wheelchair by disabled user were investigated. Cooper 2001[15] evaluated pushrim-activated power assisted wheelchair(PAPAW) for metabolic energy cost during propulsion. The results show the user with the PAPAW had a significantly lower oxygen consumption and heart rate when compared with a manual wheelchair at different speeds. Cooper 2002[16] studied performance assessment of a PAPAW control system. The control system reduced peak torque by over 50% and the contact time on the rim was nearly doubled. Somer 2003[17] introduced the case study in the usage of the PAPAW for a patient with the mid level (C5 or C6) tetraplegia. The patient became independent in propelling the PAPW over

variety of surfaces for long distance at functional speeds, and in ascending and descending ramps. Fitzgerald 2003[18] examined the usage of the PAPAW in a real world setting and to characterise the driving habit of manual wheelchair users. Significant differences in usage were not seen between the personal manual wheelchair and the PAPAW. Levy 2004[19] tested whether a prototype variable ratio PAPAW would decrease effort and perceived exertion. The results showed that the prototype was associated with lower heart rate, lower perceived exertion, and reduced electromyopgraphic activity in 5 of 8 muscles. Of the 11 participants, 10 found the prototype to be "very easy" or "easy" to push on level and inclined surfaces. Algood 2004[20] studied to determine differences in metabolic demands, stroke frequency, and upper extremity as well as joint range of motion in propulsion of the PAPAW propulsion and traditional manual wheelchair. The participant with tetraplegia joined this study. The PAPAWs reduce the energy demands, stroke frequency, and overall joint ROM, compared with traditional manual wheelchair. Also Algood tested to assess the relative merits of the PAPAW for people with tetraplegia. Algood found that four obstacle conditions (carpet, dimple strips, up a ramp, up a curb cut) were rated as significant easy to complete with the PAPAW. Haubert 2005[21] compared energy expenditure and propulsion characteristics in person with spinal cord injury propelling their own wheelchairs and three commercially available PAPAWs. The results shows that the PAPAWs reduced the oxygen consumption, however the maximised self-selected propulsion velocity and minimised oxygen cost varied. Best 2006[22] tested the hypothesis that the usage of the PAPAW provides a wider range of wheelchair skills than the use of a manual wheelchair. The results show the skills needed higher forces on pushrim were performed more easily with the PAPAW, but the skills to require greater control were performed with the manual wheelchair. The PAPAW may be helpful in the case to require more wheel torques, however the additional torque appears to be disadvantage in the case to require greater control. Karmarkar 2008[23] studied to determine and compare performances of the PAPAW (iGLIDE, e-motion, Xtender) on US national standard. The results shows all PAPAWs performed equally on the slopes of 3 and 6 degree in forward and rearward direction. Nach 2008[24] studied the effect of the PAPAW in the energetics and perceptual responses to steady state and intensity graded wheelchair propulsion in the persons with paraplegia and tetraplegia with chronic shoulder pain. Nach found that the use of the PAPAW reduced in Oxygen consumption, heart rate, and perceived exertion by RPE(Borg scale). The propelled distances were significantly increased. Ding 2008[25] studied the impact of the PAPAW among individuals with tetraplegia. Ding recorded the mobility level, such as daily distance traveled, averaged speed, accumulated driving time so on. The results show the participants used the powered wheelchair at a similar frequency to manual wheelchairs. The traveled distances in both wheelchairs were almost same, however, the averaged speed in the powered

wheelchair was significantly faster then manual wheelchairs.

The control rule commonly used is simple that the assisting force is proportional to the propelling force(Cremers 1989[5]). This type of assist controller is called as a proportional assist control. The proportional assist control calculates the assistive force form the production of the assist gain ratio and the operating force by a user. Other controllers have also been proposed such as the one that uses the reference wheelchair model to realise a mathematical light weighted wheelchair (Kakimoto 1999[26]). Also, the assisting control system without measuring attendant force has also been proposed(Tashiro 2008[27]). Morbi 2011[28] introduced the assistive device control strategy to provide intermittent assistance with capable of encouraging user effort during assistive device use. This system is based on the impedance control and aimed at developing an effective assist-as-needed control strategy suitable for use with assistive devices.

With increasing the combined desires for securing safety on propulsion with saving electric energy under reducing the load of propulsion effectively, simple proportional controller hold problems to cover these demands. The previous proposed assist control using mathematical techniques succeed in increasing the manoeuvrability of the wheelchairs. However, they do not optimise the relationship between assisting force and individual capability in order to reduce energy expenditure of the attendant, a topic that is growing in popularity as an area where control systems can aid society. Elderly people's pushing force is very variable, which makes it difficult to adapt current control system parameters to the individual's capability.

This study focuses on the individual propelling performance, and propose an assisting control method based on the individual force velocity relationship. The force velocity relationship is well used to evaluate individual exercising performance, especially cycling (Vandewalle 1987[29], Sargeant 1994[30]). In Chapter 3, this study measured steady force velocity performance of attendant propelling on a motorised treadmill.

Our proposed assisting controller generates the assisting force when the attendant propelling force exceeds an assisting boundary defined by a force velocity relationship. From this assisting rule, our proposed force velocity (FV) assistive system uses attendant propelling power up to the assisting boundary. The assisting boundary is easy to adjust to the individual propelling performance. Also by using assisting force only when it is needed the amount of electrical energy used is reduced and, further, the attendant is able to use pushing the wheelchair as a form of moderate, controlled exercise to keep healthy. The FV assist system also applies for training machines, rehabilitation systems and power assisting devices.

In this paper, we tested the performance of the assisting controller based on force velocity relationship using simulation, then validate it with experiments. The simulation used the attendant wheelchair model with the parameters determined in Chapter 3 and 4.

5-2 Powered attendant propelled wheelchair

Figure 5-1 shows typical powered attendant propelled wheelchairs. The assistive system, which generates assisting forces by electric motors, reduces the physical hardness in the propelling a wheelchair by the attendant. The two types of the assistive system are commonly developed and available in the market; The type (A) has two motorised rear wheels in both sides, instead of two basic wheels. The electric motor at each side drives the rear wheel via reduction gears. In other way, the type (B) has an auxiliary motorised wheel bottom of the wheelchair, and the motorised wheel is driven by an electric motor with reduction gears. The power of the electric motors are vary from 60W for each wheel to 100W for one auxiliary wheel. The comparison between the type (A) and (B), the price of the type (A) is higher than the type (B), however, the looking is very similar to the manual wheelchairs. Basically no slip between driven wheels and the ground is occurred in the type (A), however, the type (B) has a problem about slipping in the auxiliary wheel sometimes because of the shortage of normal force at the auxiliary wheel. The type (B) also has a problem such as, narrow foot space for attendants, and impossible to fold the wheelchair without detaching the motorised auxiliary wheel.

However, the mechanism for the assisting control in both types is the same. The force sensors in the grips back of the wheelchair measure attendant operating forces, and the assisting controller calculates assistive forces and indicate it to the electric motors. The type (A) needs synchronisation between both side wheels in some cases like driving straight. Wheelchair velocity is commonly measured from a rotary encoder in the electric motors.

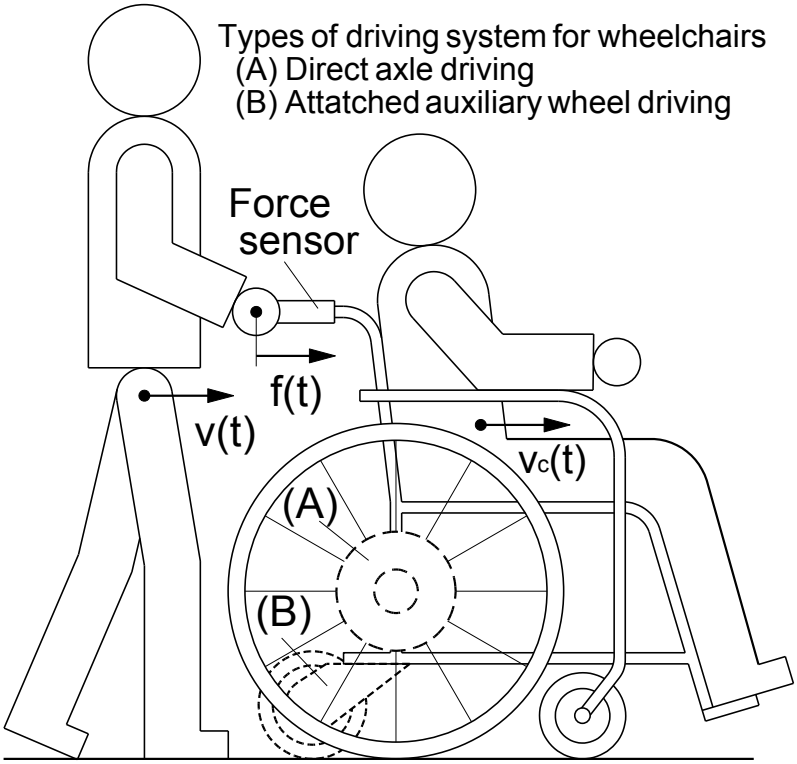

Figure 5-1 Typical powered attendant propelled wheelchair

5-3 Design of assistive system based on attendant model

From previous studies and products in the market, there are mainly three types of the assist controller for powered attendant propelled wheelchairs. In the first products at early stage, the attendant drove the wheelchair by manual switches to be on and off of electric motors. Wheelchair velocity was commonly controlled by a feedback system. Recent products of powered attendant propelled wheelchairs are driven by attendant propelling forces measured at the grips back of the wheelchair. In this section, various assist controllers to use attendant forces in previous studies are explained, then our proposed model based controller by an attendant force velocity relationship is introduced. In the comparison of the assist controllers, this section focuses on forward propelling, such as a propelling by pushing at a level, and ascending on slopes.

Threshold assist controller

Figure 5-2 shows the assist controller to generate certain assistive force when the propelling force is generated over a threshold force. The block diagram in the figure shows the mechanism of this assist control. The propelling force of the attendant basically drives the wheelchair, and the assistive force generated by the assist controller also drives the wheelchair. The total driving force of the wheelchair is the sum of the attendant propelling force and the assistive force by the electric motor. The summing point in the diagram prior to a wheelchair element describes the summation in these forces. With the threshold assist controller, the attendant have to drive by their forces under the threshold force F_T. The assist controller generates the assistive force when the pushing force by attendants is over the threshold force F_T, and the summing point with the propelling force and the threshold force F_T provides this function. In this system, the constant assistive force F_A is employed and outputted to a motor diver with a time lag system to prevent from rapid acceleration. Under the threshold force F_T, the threshold assist controller does not generate any assistive forces.

The lower figure shows the function of the threshold assist system. The horizontal axis is the resistance load, which is mainly determined by a wheelchair mass and road resistances. The vertical axis is the propelling force by attendants. Without assisting at the steady state, the attendants need to generate the propelling force in equal to the resistance load. With this assist system, the assistive force supports attendant's pushing above the threshold force F_T. In the real system, the attendant and the electric motor have time lag elements, so the actual attendant pushing force with this assist controller exceeds the

threshold force in the transient phase. The simplified rule to generate the assist force in the threshold assist controller is described by the equations (5-1) below.

$$f_A(t) = \begin{cases} F_A & : \quad F_T < f_W(t) \\ 0 & : \quad 0 < f_W(t) \le F_T \end{cases} \tag{5-1}$$

A superior point in this system is simpleness. However, this system has a problem that the assist force is too sufficient or too insufficient in some cases, because the constant assistive force is generated when the assist system is on. Under this situation, the attendants need to modify their propelling force to compensate surplus and deficit in driving forces. This matter provides imbalance feeling to attendant in various conditions of wheelchair weights and road resistances.

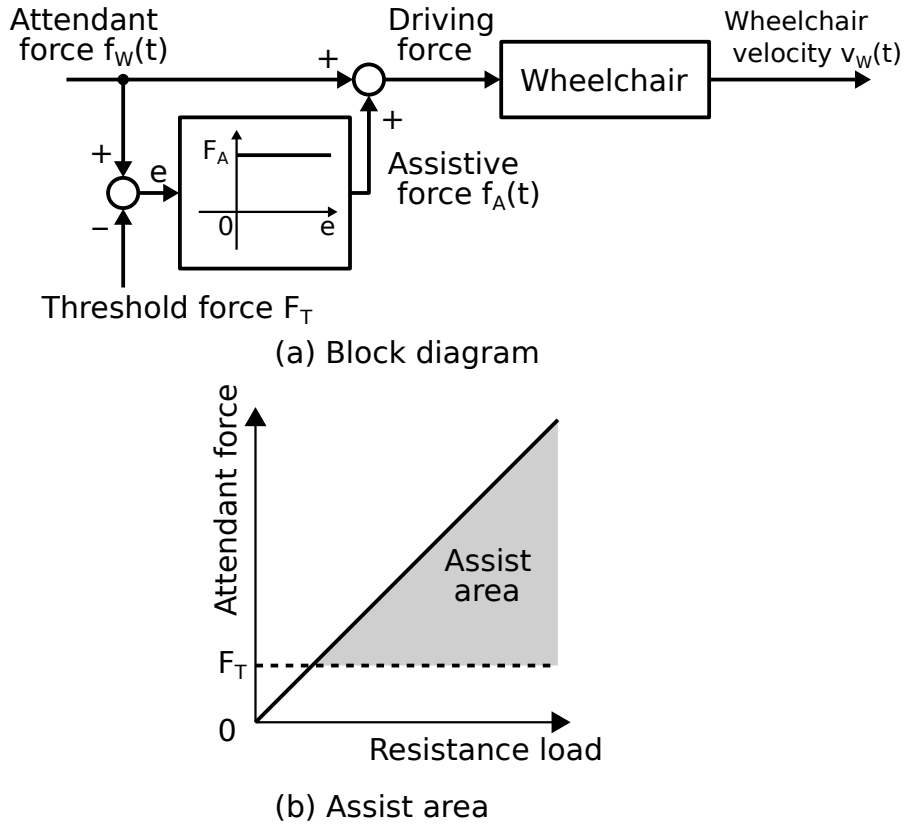

Figure 5-2 Threshold assist controller

Proportional assist controller

Figure 5-3 shows the proportional assist controller. This assist controller has the same part to calculate a force difference between the threshold force F_T and the attendant propelling force. The assistive force is calculated from multiplying the force difference by an assist gain K_P, which is commonly used constant number around one. For example, the

assist gain "1" means that the generated assistive force is equal to the attendant force, and the assist gain "2" means that the assistive force is twice. The assistive force in the proportional controller is described in the equation (5-2).

$$f_A(t) = \begin{cases} K_P(f_W(t) - F_T) & : \quad F_T < f_W(t) \\ 0 & : \quad 0 \le f_W(t) \le F_T \end{cases} \tag{5-2}$$

Figure 5-3(b) shows the assist region for the attendants. The attendant needs the propelling force in proportion to the road resistance in steady state. The attendant can relatively feel the wheelchair mass and road resistance by force feedback from the wheelchair. Also the assistive force in the proportional controller is reduced, compared with the threshold assist controller. It means the proportional controller has less energy consumption than the threshold assist controller.

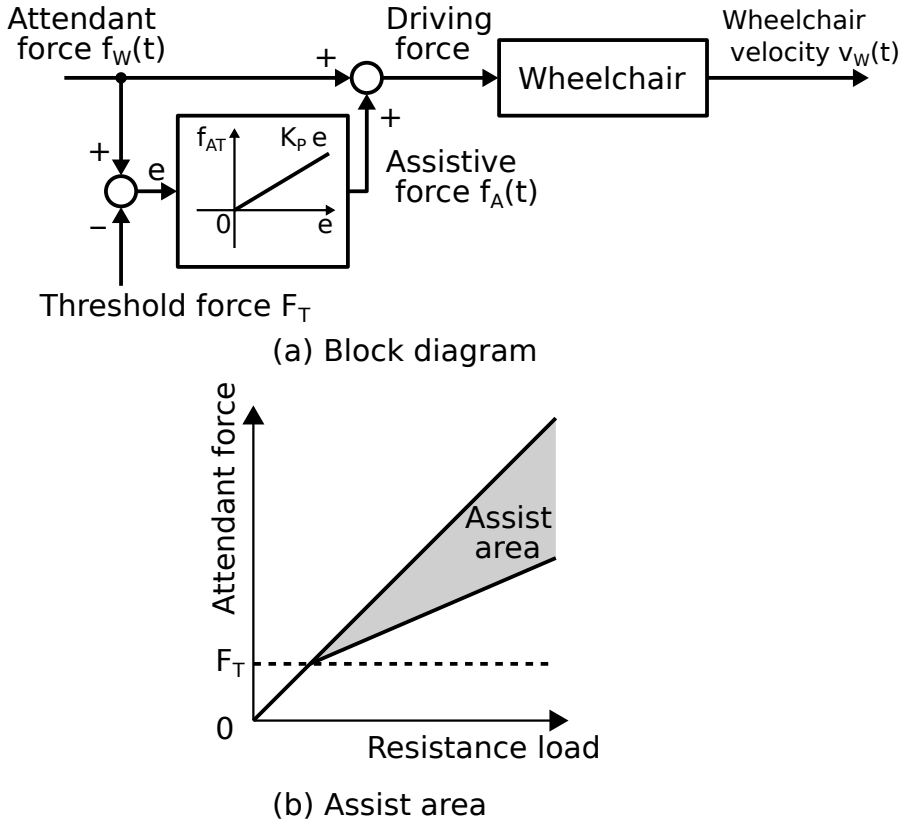

Figure 5-3 Proportional assist controller

Model Based assist controller by a desired wheelchair model

Figure 5-4 shows a wheelchair model based assist controller. This assist controller compensates attendant propelling force for reducing difference between actual movements and calculated movements by the desired wheelchair model. The wheelchair model used as standard is built from wheelchair dynamics with low road resistance, such as flat

smooth surface, and the light wheelchair mass. With this assist system, the attendant alway feel to propel the desired wheelchair typically modelled by light weight and flat smooth surface on a level, even though actual wheelchair is heavy weighted and on slopes. This system is realised with the block diagram in Figure 5-4(a). The desired wheelchair model provides the desired wheelchair velocity from the attendant force. With the difference between actual wheelchair velocity and the desired wheelchair velocity, this assist controller calculates insufficient driving force for the attendant to correspond actual wheelchair movements to modelled one. The actual wheelchair is driven by the total force in the sum of the attendant force and the assistive force for the compensation. Finally, the actual wheelchair can be driven as the desired wheelchair model, and the needed attendant force is equal to the force to drive the modelled wheelchair. The assistive force by a simple model based assist controller is described in the equation (5-3).

$$f_A(t) = K_M(v_{WM}(t) - v_{WA}(t)), v_{WM}(t) = \int_0^t w_M(t-\tau) f_W(t) d\tau \qquad (5\text{-}3)$$

Here, K_M is the gain of the assist controller, and $w_M(t)$ is a weighting function of the desired wheelchair model. The desired wheelchair velocity $v_{WM}(t)$ is calculated from the convolution integral between the weighting function $w_M(t)$ and the attendant force $f_W(t)$.

The assistive area in this system shows in Figure 5-4(b). Typical light resistance load is also shown as a thick line in monotonic increase. In propelling condition above the thick line, the assist controller generates the compensating force for the attendant. In other words, the needed attendant force to drive the actual wheelchair in any situation is basically under the thick line. However, the attendant cannot feel the wheelchair weight and road resistance by force feedback. Also the design of the desired wheelchair model should depend on attendant's physical strength and propelling performances.

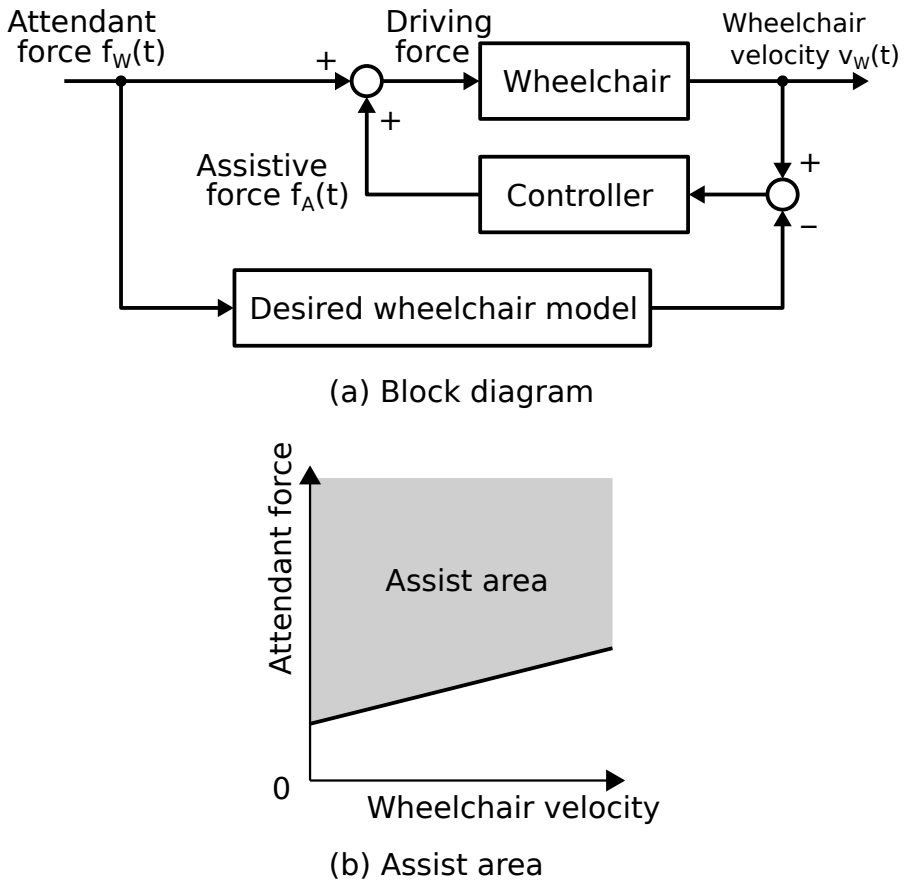

Figure 5-4 Model based assist controller
by a desired wheelchair model

Model based controller by attendant force velocity relationship

This study proposes a model based assist controller with the attendant force velocity relationship. From the chapter 2, 3, and 4, this study shows the attendants have a force velocity relationship and it depends on the physical strength of the attendants. The state-of-art in this method is that the powered wheelchair with this assist control estimates individual attendant hardness, and generates assistive forces when the attendant needs to assist under high subjective hardness. The block diagram of this system in Figure 5-5(a) is similar to the model based control in Figure 5-4, however, this system is designed based on the attendant force velocity relationship, which describes an autonomous relationship between maximised bearable propelling forces and wheelchair velocities under minimised subjective hardness by the attendant. From the comparison between the maximised bearable force and actual attendant force, the assist controller generates the assistive force in proportion to this force difference. If the actual propelling force is under the maximised bearable force, the assist controller does not generate any assist forces, because the attendant is easy to generate the propelling force long time up to the maximised bearable force. The simplified this assist system is explained by the equation (5-4).

$$f_A(t) = \begin{cases} K_{FV}(f_B(t) - f_W(t)) & : \quad f_W(t) > f_B(t) \\ 0 & : \quad f_W(t) \le f_B(t) \end{cases} \qquad (5\text{-}4)$$

$$Here, f_B(t) = f_M - K_D v_W(t)$$

The parameters f_M and K_D, which are determined by the experiments in Chapter 3 and 4, are the intercept and the slope of the attendant force velocity relationship respectively.

With this assist system, the assist forces are only generated in which the attendant propelling condition is over the autonomous force velocity relationship as shown in grey area of Figure 5-5(b). This means that the powered assistive force comes in which the attendant feel hard to propel, and the attendant propels the wheelchair naturally while the attendant propelling condition is under the autonomous force velocity relationship. This mechanism reduces the electric energy consumption for assist, and persuades the attendant to use their physical strength as much as possible, as well.

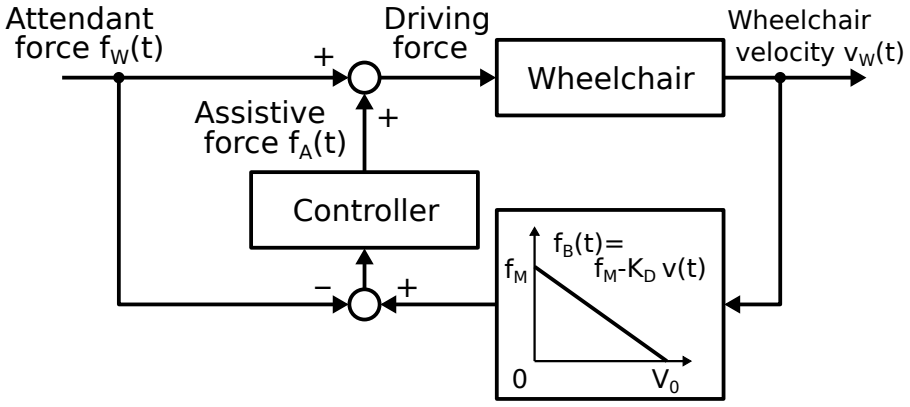

(a) Block diagram

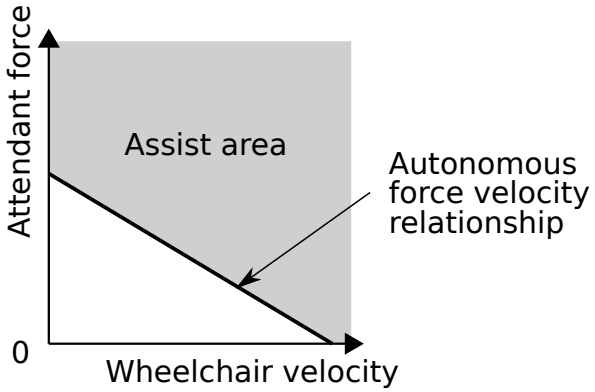

(b) Assist area

Figure 5-5 Model based controller by the model of an attendant force velocity relationship

Assist control based on force velocity relationship

Figure 5-6 shows a block diagram of the attendant and powered wheelchair system

used in this study. The assist system in the centre part in Figure 5-6 shows the assisting system based on the force velocity relationship. In this study, this assist controller is called as a force velocity (FV) assist controller. The FV assist system has two inputs; one is the attendant propelling force $f_W(t)$ and the other is the wheelchair velocity $v_W(t)$. The assist boundary force $f_B(t)$ is determined by the wheelchair velocity $v_W(t)$.

$$f_B(t) = f_M - K_D v_W(t) \tag{5-5}$$

Here, f_M is an intercept value of the force velocity relationship and K_D is the reducing ratio in proportion to the wheelchair velocity. The assistive force $f_A(t)$ with an assist gain K_{FV} is calculated by the equation (5-6).

$$f_A(t) = \begin{cases} K_{FV}(f_B(t) - f_W(t)) & : \quad f_W(t) > f_B(t) \\ 0 & : \quad f_W(t) \le f_B(t) \end{cases} \tag{5-6}$$

This equation means the controller generates the assistive force $f_A(t)$ when the attendant propelling force $f_W(t)$ exceeds the assist boundary force $f_B(t)$. When the attendant force $f_W(t)$ is lower than the assist boundary force $f_B(t)$, the assistive force becomes zero because a half wave rectification element connected to the assist gain *K* converts negative numbers to zero. In Figure 5-5(b), the area above the assist boundary force generates the assistive force $f_A(t)$, however the area below the assist boundary force does not generates any assistive forces.

The wheelchair model employed a one-dimensional simple mechanical system in the equation (5-6). The wheelchair model had two elements; the total mass *M* including an occupant weight and rolling resistance $f_R(t)$ including bearing resistances. This study assumed that the body frame of a wheelchair was rigid, and inertial moments of front casters and rear wheels could be neglected because of its smallness compared with the mass of the wheelchair and occupant. Air drag resistance was also neglected in this wheelchair model.

$$M \frac{dv_W(t)}{dt} = f_T(t) - f_E - f_R(t) \tag{5-7}$$

Here, *M* is the total wheelchair mass including the occupant, and $f_T(t)$ is total propelling force, which is the sum of the attendant force $f_W(t)$ and the assistive force $f_A(t)$. f_E is the additional load due to gravity in the case of the wheelchair on slopes. This study assumed that the rolling resistance $f_R(t)$ was described as a simple linear function in the equation (5-8).

$$f_R(t) = R_0 + R v_W(t) \tag{5-8}$$

Here, R_0 is the static force at $v_W(t)$=0. The coefficient *R* is the increase ratio of rolling resistance by wheelchair velocity. The additional load f_E by gravity is described in the

equation (5-9).

$$f_E = Mg\sin\theta \tag{5-9}$$

Here, f_E shows a downward longitudinal factor of gravity force due to the slope with the angle θ.

This study used the attendant model in Chapter 4 to estimate controller performances by the FV assist system. The parameters in the attendant model were evaluated from experimental results shown in Chapter 4.

In the block diagram with f_M=0 and K_D=0, the assist system works with a proportional controller having an assist gain K_P. In this case, the assisting force $f_A(t)$ is calculated by the equation (5-10). This study used this function to compare between our proposed FV assist control and the proportional assist control.

$$f_A(t) = K_P f_W(t) \tag{5-10}$$

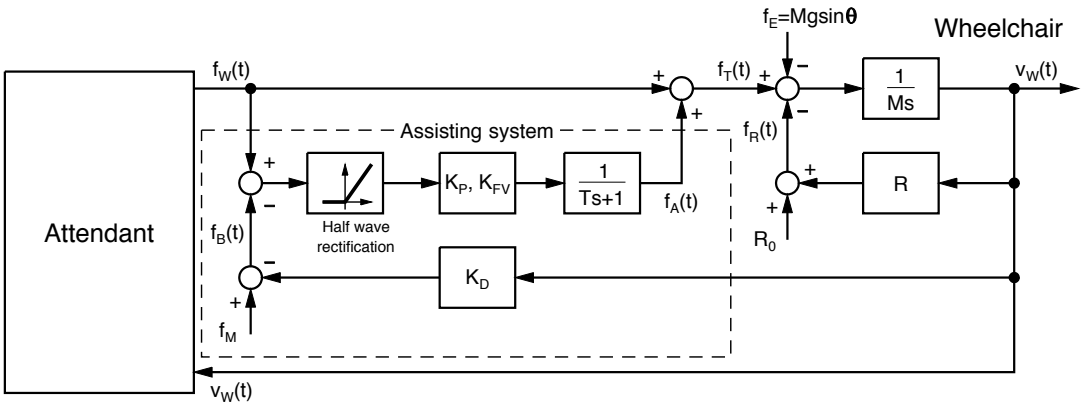

Figure 5-6 Model based control by attendant force velocity relationship

Simulation methodology to evaluate the control performance in the assist systems

From the results of Chapter 4, this study calculated the attendant propelling behaviour using the model. By simulation with the model, this study shows the difference between the FV assist control and the proportional control.

The autonomous propelling capability in Chapter 4 was used as the assist boundary force in the FV assist control. The equation of the assist boundary force was defined as $f_B(t) = 84.6 - 74.2v_W(t)$[N], so the parameters in the assist boundary force were f_M =84.6N and K_D=74.2N/(m/s). The road resistance was estimated from other experiments, which measured propelling force at various wheelchair velocities to be kept constant by visual feedback on UCL Pamela facility. Under steady constant velocities, the measured propelling force is equal to the rolling resistance. The estimated road resistance was $f_R(t) = 11 + 22v_W(t)$[N]. For the comparison between the FV and P assist controllers in simulation and experiments, the external force $f_E = 42$N is set to simulate gravity force

on the slope. The assist gain K_P and K_{FV} in the assist system were used from 0 to 4. The performance of the assist controllers were evaluated by the maximum and steady attendant propelling forces, and maximum and steady assistive forces.

Simulation based evaluation for the assist controllers

Figure 5-7 shows the comparison between the FV and proportional assist about maximum and steady attendant forces and maximum and steady assistive forces. These simulation results were obtained from the calculation with the model in Figure 4-2 and Figure 5-6 by MATLAB. This plot shows how maximum and steady attendant and assistive forces changes with the assist controller gain K_P and K_{FV}. The condition of the gain K_P or K_{FV}=0 shows the results without assist controls. The thickness of the lines shows type of controllers; thick lines are for the FV assist control and thin lines are for the proportional assist control. The continuous lines at each assist control are for steady forces, and the dotted lines are for maximum forces.

With the additional road resistance condition $f_E = 42\,\mathrm{N}$, the steady forces of the FV assist control at operating points did not change from 60N with the increased assist gain K_{FV}, however, the steady assistive forces in this case were zero, because the FV assist control does not generate the assistive forces in the situation that the attendant's force is under assist boundary force $f_B(t)$. In other words, the propelling under the assist boundary force continues long time about 20 minutes because of light subjective hardness. In the maximum forces of the FV assist control, the attendant force decreased 6N(K_{FV}=2) from 101N without assist control. In the case of the proportional assist control, both maximum and steady forces in the attendant decreased sharply 24N(steady: K_P=1) from 60N and 30N(maximum: K_P=1) from 101N by the increase of the assist gain K_P, compared with the FV assist control. In opposite, both maximum and steady assistive forces increased sharply 34N (steady: K_P=1) and 68N(maximum: K_P=1) from 0N without assist control.

From the comparison between the FV and the proportional assist control, the assistive force by the proportional control is the excess of the autonomous propelling capability, which consists of maximised propelling force and wheelchair velocity under minimised subjective hardness. The autonomous propelling capability is defined and validated in Chapter 3 and 4. The comparison means that the attendant does not need excess assistive forces, and the FV assist control would achieve to provide sufficient assist to attendants as well as to reduce electric energy consumption. This study validates the performance of the FV assist control by experiments in next section.

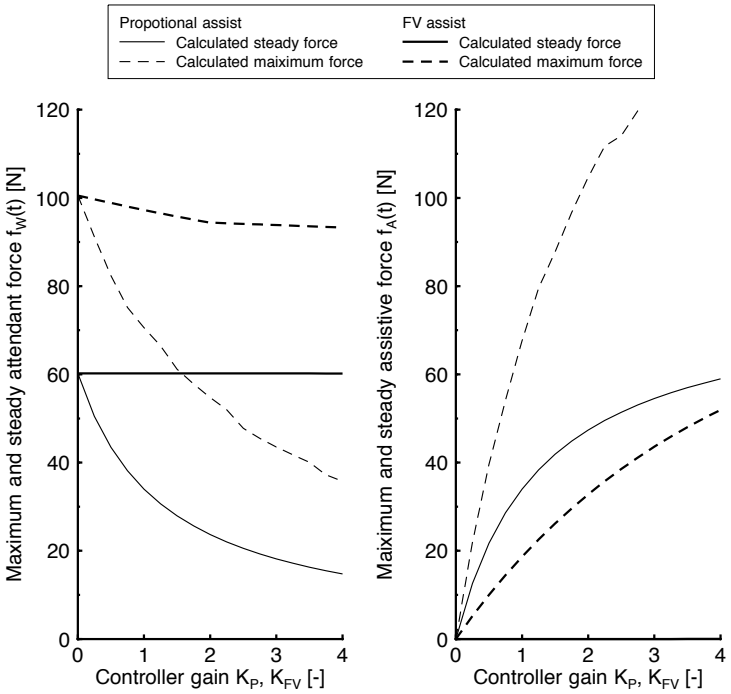

Figure 5-7 Simulation based comparison of assist controllers

5-4 Methodology for validation

The powered attendant propelled wheelchair in Figure 5-8 was developed for this study. This powered wheelchair had partly the same dimensions and specification of the instrumented wheelchair in Chapter 2. The same parts that this study used for the powered wheelchair, were the basic dimensions and structure of the wheelchairs by NHS in UK, the two straight grip with six-axis load cell by AMTI, and the wheel velocity measurement by the rotary encoder. The detail of these components was mentioned in Chapter 2. The powered wheelchair had two additional parts from the instrumented wheelchair; One was the motorised rear wheels, and the another was the assist control system.

The motorised rear wheel at each side in Figure 5-9 consisted of a DC electric motor (RE50: 200W, maxon motor ag) with a reduction gear head (GP52C(19:1), maxon motor ag), chain drive system, and a sprag bearing between the motor shaft and the driving sprocket. The diameters of the sprockets were 67mm(Driving) and 134mm(Driven), and the reduction ratio is 2:1. The chain type was 06B1, which width was 6mm. The driven sprocket was fixed to the rear wheel tightly. The torque generated by the DC motor was transferred from the motor shaft to the rear wheel by the chain system. The final reduction ratio was 38:1. The sprag bearing was used between the motor shaft and the driving sprocket to prevent from braking under no assist forces that the attendant forces were smaller than the assist boundary force.

The DC motors in both sides were controlled by two motor driver (ADS50/10, maxon motor ag) with shunt regulator (DSR70/30, maxon motor ag) in Figure 5-10. The general power supply 24V, 20A(480W) was used to drive the two DC motors. The motor driver controlled current flows to the motor in order to regulate motor torques. The torque constant of the DC motors was 38.5(mNm/A). The generated motor torques were measured from the multiplication of the current flow by the torque constant. The current flow was measured from the output signal from the motor driver.

The assist control by the attendant force velocity relationship was implemented by LabView. The assist system by LabView had the assisting control system and the recording system, and this code was originally developed for this study. The assisting control system worked with the block diagram in Figure 5-6, and its panel screen in Figure 5-11 provided a user interface to modify the control parameters and realtime graphs for experiments. The changeable assist parameters in this system were the assist gain K_P and K_{FV}, the time constant T, and the assist boundary force consisted of the intercept f_M and the slope K_D. The recording system had the same function of the instrumented wheelchair in Chapter 2, and some additional features were implemented for recording motor torques

and output signals from the assist controller. The sampling time in the assist control and the recording system was 100Hz.

The total weight of the powered wheelchair was 47.45kg. This study used steel weights instead of an occupant, the same way in Chapter 2. The weight conditions in this study were implemented with rounded steal weights placed on the seat of the wheelchair. Each steal weight was about 10kg.

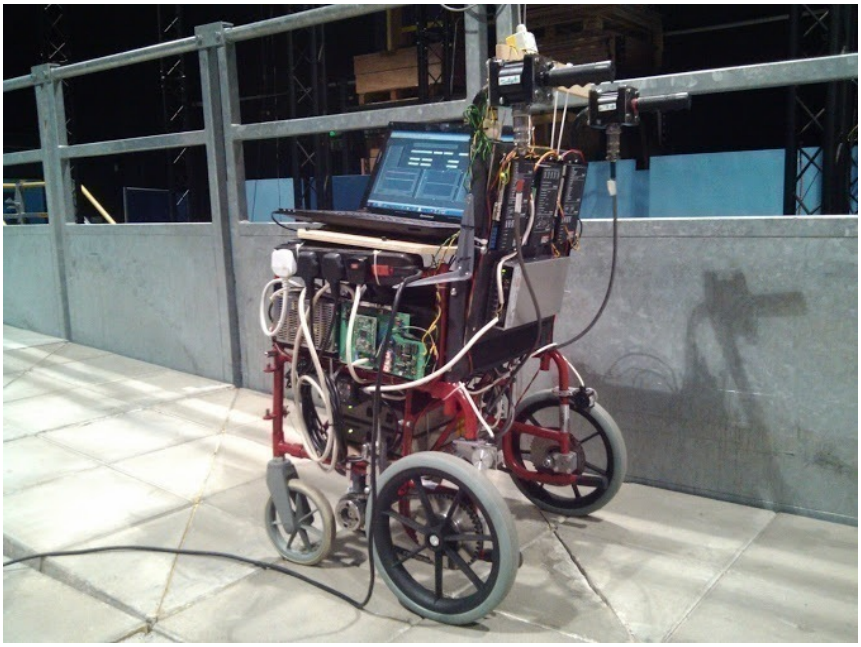

Figure 5-8 Over view of the powered attendant propelled wheelchair

Figure 5-9 Motorised rear wheel

Figure 5-10 Motor driver and power supply

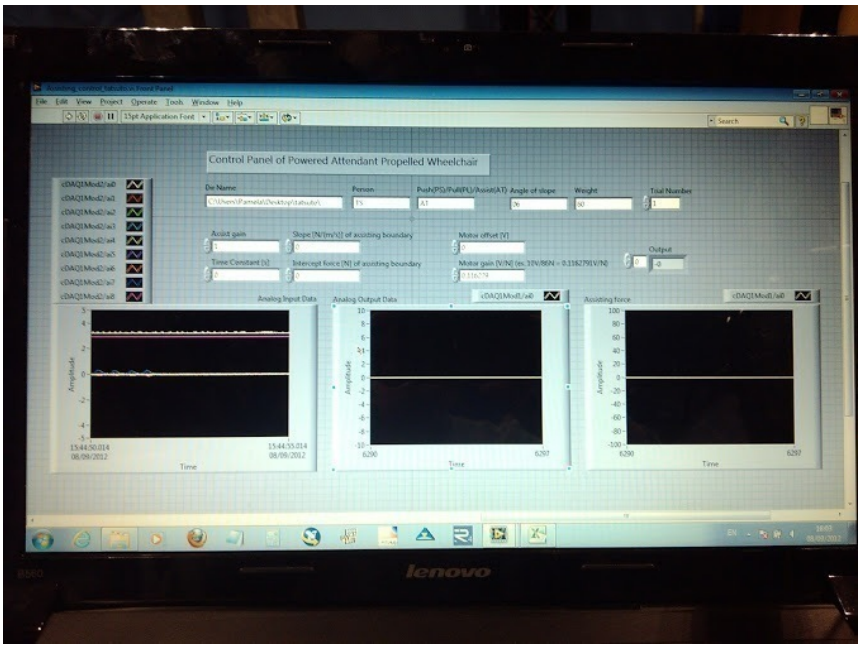

Figure 5-11 Assist controller by LabView

This study used for three longitudinal slopes and a flat lane in the Pedestrian Accessibility Movement Environment Laboratory(PAMELA) facility of University College London. The PAMELA platform has 57 of surface modules, which can reproduce various height and oriented slopes by five oil cylinders to support the surface 1200mm x 1200m from the ground. The surface material can be replaced to many types of real kerbs and road surfaces. In this study, typical concrete pavers in UK footway, which consists of 400mm x 400mm tiles, were used as the surface material.

For the validation of the powered attendant propelled wheelchair, the slopes 3.6deg. (6.5%) was set in the PAMELA platform, and the length in the slope was 4.8m. The length of the flat lane was 7.2m.

The measurements of the attendant propelling at a level and on the upward slope θ =3.6deg. were carried out on three additional weight conditions W (+0.0, +30.5, and +61.0kg). The base weight M of the powered wheelchair was 47.45kg, so maximum weight condition in the wheelchair was 108.4kg. The additional resistance loads from the flat condition were calculated from the equation (2-1). From the equation (2-1), the additional resistance loads f_E in this study are shown in Table 5-1.

Table 5-1 The additional resistance load f_E by weight W and slope angle θ

Additional resistance load f_E [N]	**Slope angle θ [deg. (%)]**	
Additional weight W [kg]	0 (0)	3.6 (6.5)
0.00	0	29.2
30.50	0	48.0
61.05	0	66.8

This study tested two types of the assist controller; the proportional (P) assist controller and the force velocity relationship model based (FV) assist controller. The P assist controller in Figure 5-3 generates the assistive forces from the multiplication of the attendant forces by the assist gain. The FV assist controller in Figure 5-5 generates the assistive forces in the case that the attendant force is exceeded the assist boundary force. The assist forces in the FV assist was calculated from the multiplication of the assist gain and the force difference between the actual attendant force and the assist boundary force. At each trial set by the weight W and slope angle θ, this study tested the controller performance with the assist gain K_P=1 and 2 for the P assist control, and the K_{FV}= 1 to 4 by step 1 for the FV assist control. The time constant T of the first order lag system in the assist controller inserted between the assist gain and the motor driver, and it set as 0.1s because muscle response time from visual feedback is 200ms to 400ms. In the trials of the FV assist control for each participant, the intercept f_M and the slope K_D of the participant force velocity relationship, were obtained from the 25% of the force velocity relationship in the results of Chapter 2. Because the comparison of the participant force velocity relationship in the overground in Chapter 2 and in the treadmill in Chapter 3 supposed that the 25% of the force velocity relationship in Chapter2 corresponded to the result in Chapter 3. Also the 25% of the maximum force velocity relationship is fatigue

resistant(Sargeant 1994[28]), which means the attendant can continue propelling a wheelchair with minimised fatigue. The trials at each resistance load condition were carried out with this order; 1) Without assist control, 2) With the P assist control, 3) With the FV assist control.

The slope conditions were used with this order; 1) The slope angle θ=3.6deg., 2) At a level. The order of the additional weight W at each slope condition was from heaviest +60kg first, then reduced the weigh W=30kg to zero. Before each trial on the slope, the wheelchair was placed so that the rear wheels were positioned at the edge between the slope and level surface. The orientations of the front casters were set to straight toward heading into a traveling lane. The participant waited with slightly gripping the both straight bars behind of the wheelchair, then started to propel after a "go" sign, which was made after starting the recording. Before all of trials, the participant was asked to propel a wheelchair naturally at steady speed, not vigorously, and to imagine as if a person was sitting the wheelchair and you were in charge of transferring the person by the wheelchair safely. After finishing propelling, the participant stopped and standed still without gripping the bars until the recording was stopped. All combinations in the assist control and the resistance load for one participant was carried out within two hours.

Three participants in aged from 27 to 44 without any movement disorders took part in this study. All participants were male and they also took part in the study in Chapter 2. The averaged height of all participant was 172cm, and averaged weight was 69 kg.

5-5 Results of validation by experiments

Figure 5-12 shows the time series plot of the participant propelling a wheelchair with and without the assist controls. The upper graph shows the horizontal propelling force, the middle graph shows the wheelchair velocity, and the lower graph shows the assistive force by electric motors. These graphs were for the participant one as a representative example, and the resistance load was set by the weight W=60kg and the slope angle θ=3.8deg. In the beginning, the participant pushed hard to accelerate the wheelchair at the starting, then the participant reduced pushing force and finally the wheelchair velocity became steady. This propelling behaviour was similar to all participant's cases in all situation without and with the P and FV assist controls. This means that all participant could adapt to all of assist controls without problems.

Without assist system, described as a dashed line, the participant needed to generate the propelling force 95N at maximum in the beginning, then the participant reduced the propelling force after the participant noticed the wheelchair acceleration was enough. After five seconds passed, the wheelchair velocity became steady around 0.4m/s with the propelling force 65N. The propelling force had frequency components caused by two leg walking. The maximum propelling forces with the P and FV assist controls were reduced around 48N(P assist) and 75N(FV assist) compared with the maximum propelling force 95N without assist systems. The steady propelling force with the assist systems also were reduced around 32N(P assist) and 43N(FV assist) from the propelling force 65N without assist systems. The wheelchair velocities with and without the assist systems, however, were similar to 0.4m/s at steady state. The wheelchair acceleration at the beginning without assist systems was slower than with the assist systems. The wheelchair accelerations with the P and FV assist controls were similar.

The assistive force in the lower graphs showed the difference between the P and FV assist controls. In the beginning, the P assist system generated the assistive forces just after the propelling force was generated. However the FV assist generated the assistive forces after the attendant propelling force was over the assist boundary force. This is the reason why the assistive force in the FV control lagged compared with the assistive force in the P control. At the steady state, the assistive forces in the P control generated around 38N continuously, and the assistive force in the FV control generated lower around 25N with frequency components.

Figure 5-13 shows the trajectory of the time series plots in Figure 5-12. The P assist control generated the assistive forces from the lower attendant propelling forces, however the FV control generated the assistive force after the participant propelling force exceeded over the assist boundary force. The operating point P_{NA} without assist systems was around

the propelling force $f_W(t)$=67N at the wheelchair velocity 0.33m/s. The operating points by the assist systems were placed near the assist boundary force. However the operating point P_{FV} by the FV assist control was slightly higher from the assist boundary force because the perturbation by two leg walking in propelling force caused switching electrical motors repeatedly beneath the assist boundary force, and the participant increased propelling force unconsciously to avoid these switching because of unpleasant propelling feeling.

Figure 5-14 shows the mechanical power of the participant propelling and the motor driving by the assist systems. The attendant mechanical power in the upper graph increased after the wheelchair was accelerated, then became steady state gradually. The steady attendant mechanical powers were about 20W(without assist), 14W(With the FV assist control), and 12W(With the P assist control). The motor mechanical powers with assist systems in the lower graph increased after the wheelchair was accelerated, then became steady state after four seconds passed. The steady motor powers were 13W(the P assist control) and 9W(the FV assist control).

With various resistance load and the assist gain by both assist systems, this study focused on the maximum and steady force and power by the participants, and the maximum and steady assist force and power by the electric motor. Also the steady wheelchair velocities were focused.

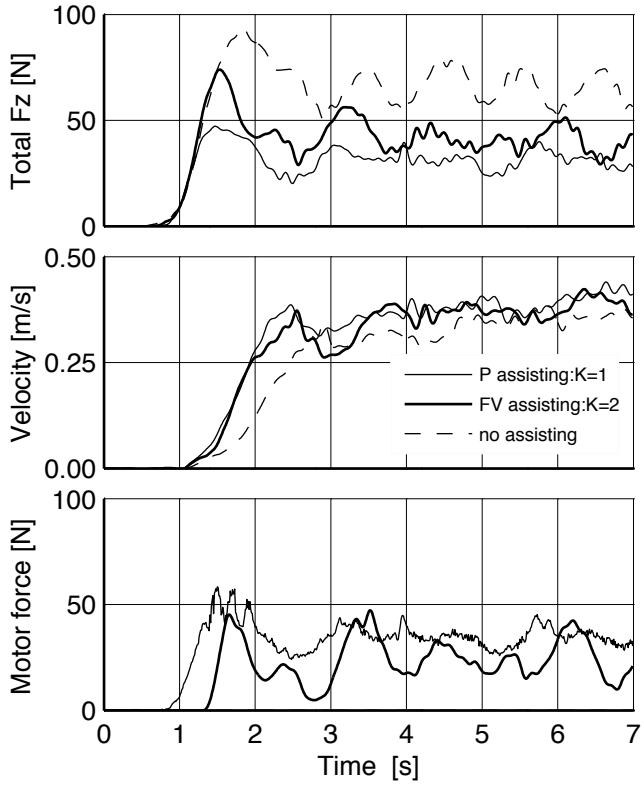

Figure 5-12 Typical time series plot of the attendant propelling with and without the P and FVRMB assist controls.

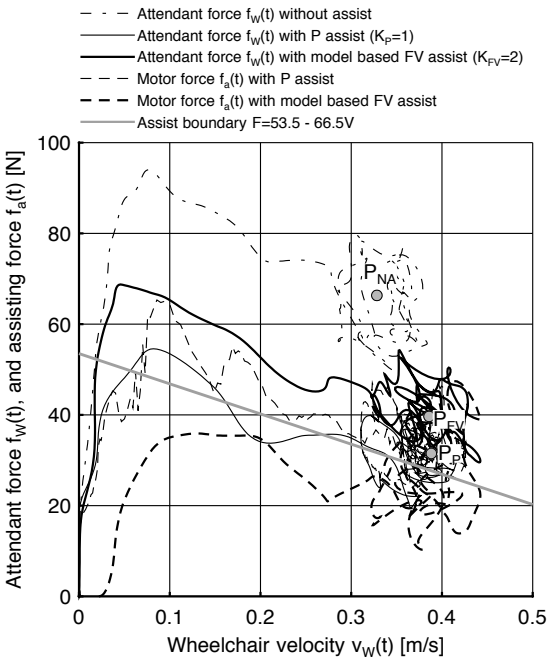

Figure 5-13 Typical trajectories of the attendant propelling with and without the P and FV assist controls.

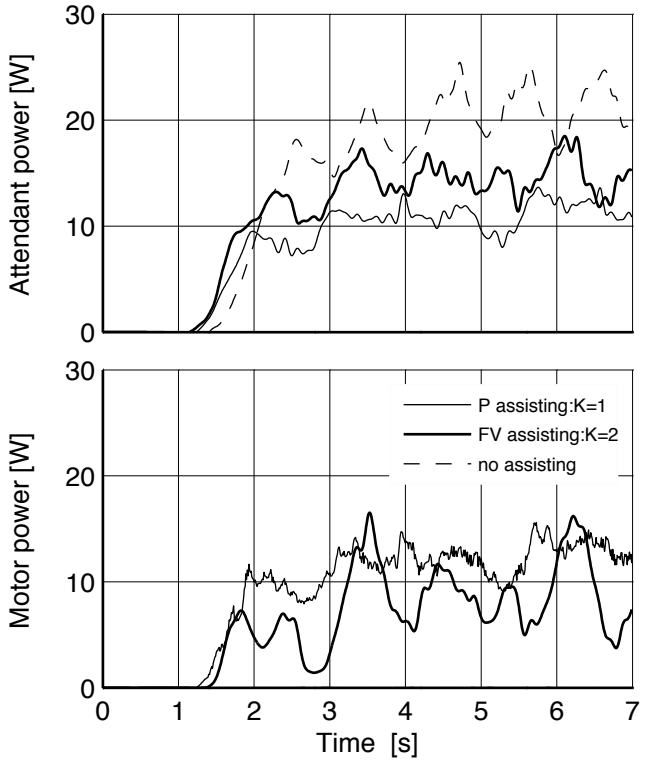

Figure 5-14 Mechanical power in the attendant and the electric motor

5-5-1 Results at steady state

Figure 5-15 shows the attendant horizontal force at steady state with and without the assist systems, under various resistance loads. The upper graph shows the attendant horizontal force without and with the proportional(P) assist control, and the lower graph shows the attendant horizontal force without and with the force velocity relationship model based(FV) assist control. The resistance forces in the horizontal axis were obtained from the attendant horizontal forces without the assist systems at steady state, and the circle markers under the assist gain K=0 in upper and lower graphs shows the same resistance load as well as the attendant horizontal forces without assist systems. All participants were plotted together to focus on the function of the assist systems. The assist gain K in the P assist control means $K=K_P$, and $K=K_{FV}$ in the FV assist control. These arrangements are the same in the series of graphs in this Chapter.

The P assist control reduced the attendant horizontal force by the assist gain K; a half force (K=1) and one-third force (K=2) against various resistance load. With the FV assist control, the attendant propelling forces under around 30N were almost same forces without assist systems, however the attendant forces decreased to around 40N in which the attendant horizontal force (K=0) was 63N. With the increased K, the attendant horizontal force decreased from 43N (K=1) to 28N (K=4) at the maximum resistance load around 64N.

Figure 5-16 shows the vertical force with and without assist systems. The averaged vertical forces of all participant were different, for example, the participant one kept the vertical force around -10N against the resistance load, but other two participant had different trends that the vertical forces were under -20N, and increased to around -40N without assist, with the increased resistance load. In the P assist control, these two participants dropped the vertical force with the increased assist gain K, however, the dropped values were smaller in the FV assist control. Figure 5-17 shows the averaged distance between the participant and the wheelchair, without and with assist systems. The averaged distances of all participant were different and similar tread in the attendant vertical force in Figure 5-16. One participant almost kept around 200mm, but other two participants widened the distance from around 130mm at the resistance load 10N to 150mm at 65N. The distances with and without assist systems were almost same.

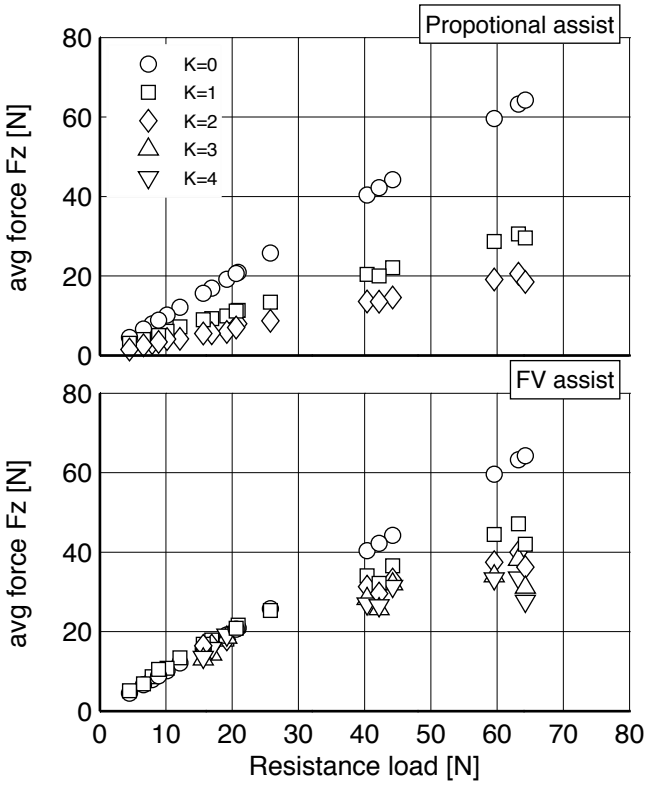

Figure 5-15 Averaged attendant horizontal force Fz at steady state

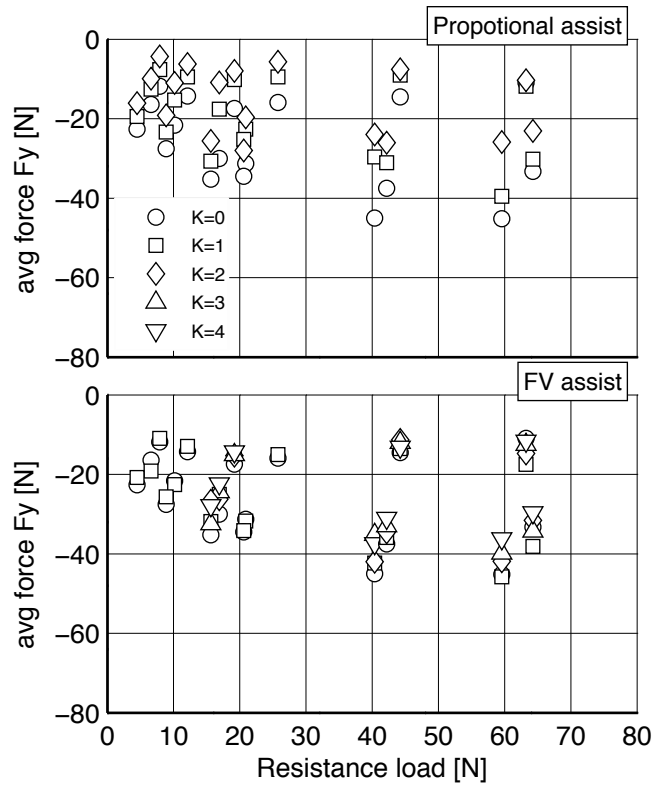

Figure 5-16 Averaged attendant vertical force Fy at steady state

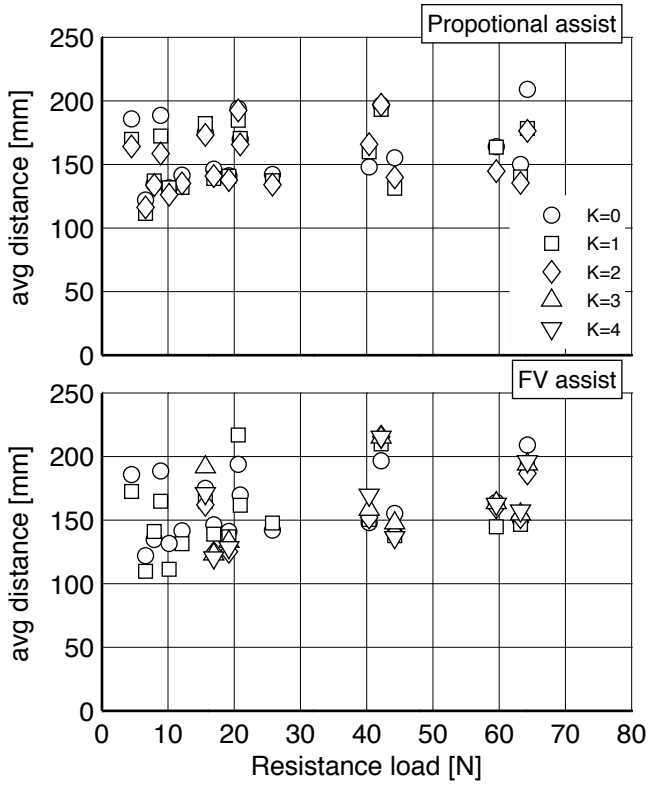

Figure 5-17 Averaged distance at steady state

Figure 5-18 shows an averaged attendant mechanical power at steady state. Without assist, the maximum attendant mechanical powers were 20W at the resistance load by the weight W=60kg and the slope angle θ=3.8deg. With the P assist control, the attendant mechanical powers decreased to half (K=1) and one-third(K=2) against the resistance load, and this trend was similar to the horizontal propelling forces in Figure 5-15. With the FV assist control, the attendant mechanical powers in all of assist gain K were similar until 10W to the power without assist systems, however, the power with the FV assist control dropped from the resistance load over 40N. The increased assist gain K reduced the attendant mechanical power more, however, the decrease of the attendant mechanical powers was not proportional to the assist gain K. At the maximum resistance load, the maximum attendant mechanical powers in the P assist control were around 12W(K=1) and 8W(K=2). The FV assist control cases were 16W(K=1), 15W(K=2), 14W(K=3) and 13W(K=4).

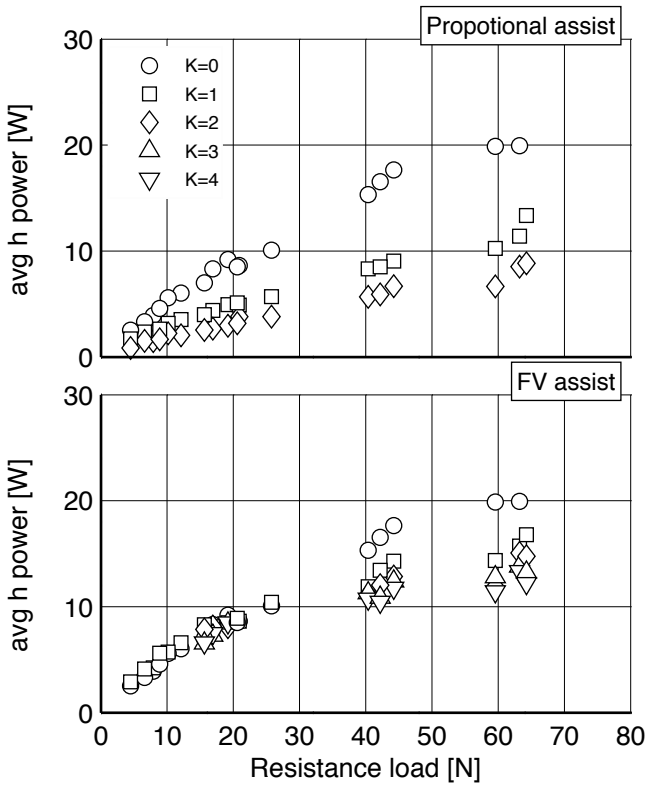

Figure 5-18 Attendant mechanical power in propelling at steady state

Figure 5-19 shows the averaged wheelchair velocities at steady state, with and without assist systems. The wheelchair velocity without assist systems dropped from 0.6m/s to 0.35m/s with the increase of the resistance load. With the assist systems, the decrease of the wheelchair velocity were smaller with the increase of the assist gain *K* in both assist systems, and the decrease of the wheelchair velocity by the P assist control was smaller than the decrease by the FV assist control. All participant showed a similar trend.

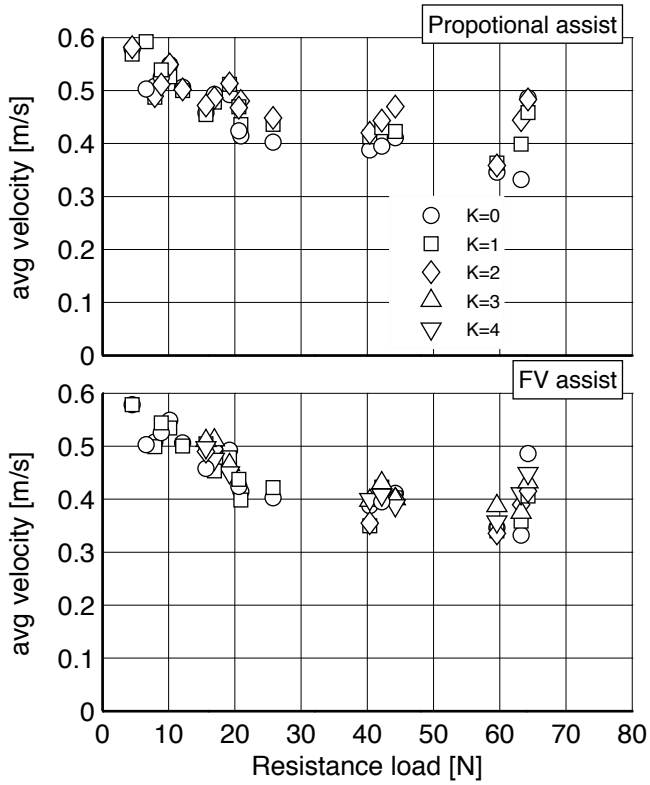

Figure 5-19 Averaged wheelchair velocity at steady state

Figure 5-20 shows the assistive forces by the electric motors at the steady state. The maximum assistive forces were about 41N(K=1) and 37N(K=2) with the P assist control. The assistive forces with the FV assist control, were 30W(K=4), 28W(K=3), 24W(K=2) and 20W(K=1). The assistive forces with the P assist control increased from low resistance load, however, the assistive forces with the FV assist control were almost zero until the resistance load 30N, and increased proportionally with the increase of the resistance load over 30N.

Figure 5-21 shows the assist mechanical powers by the electric motor. The maximum powers with the P assist control were about 20W(K=2) and 14W(K=1). The FV assist control cases were 14W(K=4), 12W(K=3), 9W(K=2), and 7W(K=1). The trend against the resistance load in the P and FV assist controls were similar to the tread of the assistive forces in Figure 5-20. The assistive powers by the P assist control increased proportionally with the increase of the resistance load, and the assistive powers by the FV assist control were almost zero until the resistance load 30N, and increased proportionally with the increase of the resistance load over 40N.

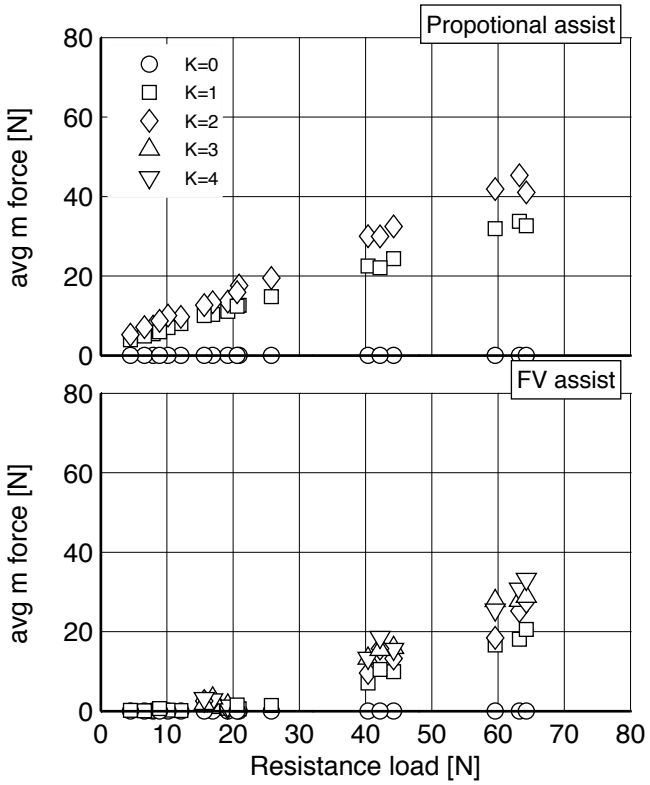

Figure 5-20 Assist forces at steady state

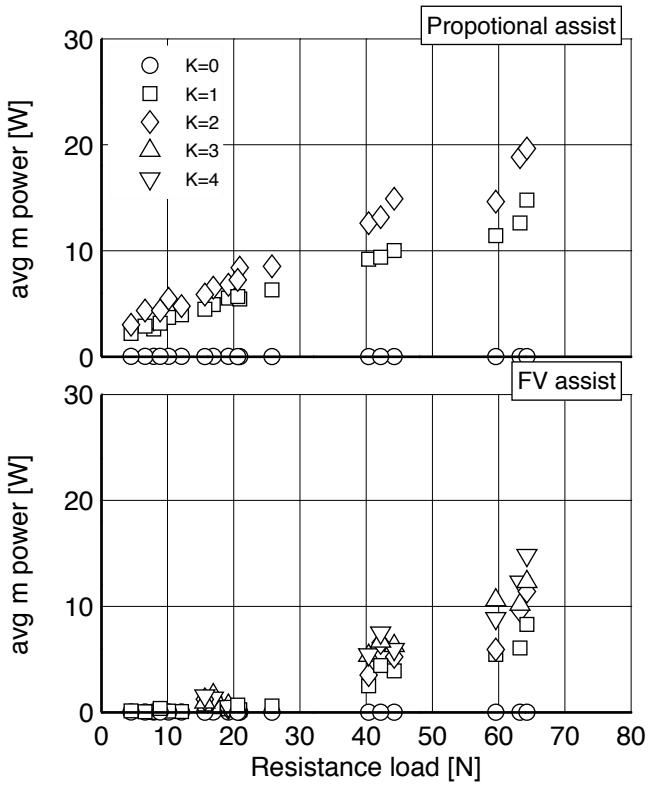

Figure 5-21 Assist mechanical power at steady state

5-5-2 Results at maximum points

This study also focused on the assist performances at maximum conditions. Figure 5-22 shows the attendant horizontal force at the maximum conditions. The resistance loads in horizontal axis in Figure 5-22 were used from the maximum attendant horizontal forces at each participant without assist systems. This arrangement is the same in all of graphs in this section to show the assist performances at the maximum conditions. Other arrangements are the same in the 5-4-1 section to show the results at stead state.

The maximum horizontal forces reached to 103N without assist systems. The P assist control reduced the attendant forces to 58N at K=1 and 40N at K=2. The maximum conditions were affected by the dynamic elements in the attendant and the wheelchair, so the horizontal force was not equal to the resistance load. This is why the attendant forces with the P assist control K=1 were not half of the maximum attendant force without assist systems. The attendant horizontal forces with the P assist control decreased in maximum force about over 25N, with the increase of the maximum forces. The attendant horizontal forces with the FV assist control were almost equal to the force without assist systems, up to the maximum horizontal force 60N, and decreased from the force without assist systems, over the maximum horizontal forces 60N. The maximum attendant horizontal forces roughly limited around 70N with the FV assist control in any assist gain K conditions.

Figure 5-23 and Figure 5-24 shows the vertical force and the distance at maximum horizontal force respectively. The treads in the vertical force and the distance at maximum condition were similar to the results at steady condition. The participant one kept low vertical force around -20N, and the vertical forces in other two participant increased from around -20N at lower maximum horizontal force to -60N at higher maximum conditions. Under high maximum condition, the P assist control reduced the vertical forces about 10N at K=2, and the FV assist control reduced for 10N at K=4. The decrease of the minimum vertical forces and the minimum distances started from lower maximum conditions under the P assist control, however the decrease by the FV assist control appeared over maximum conditions 60N.

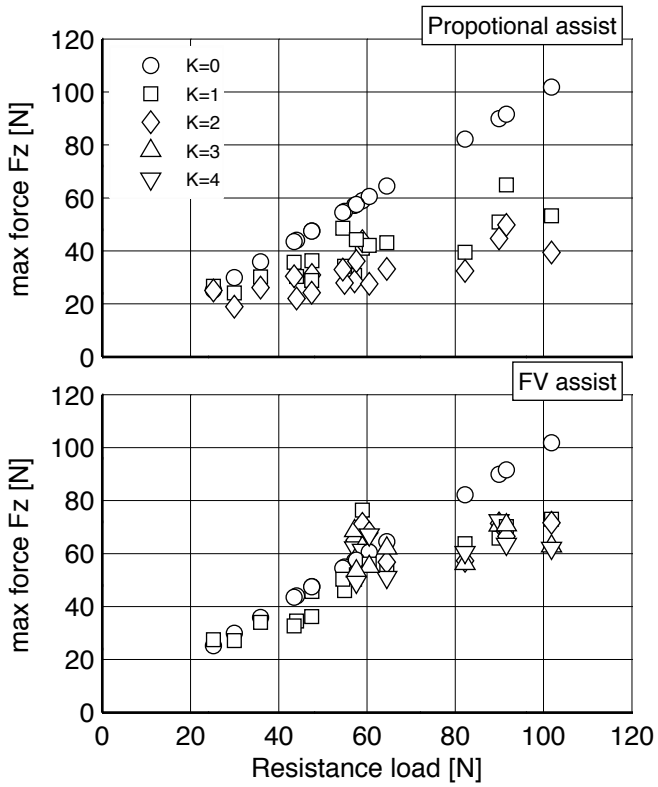

Figure 5-22 Attendant horizontal force at maximum condition

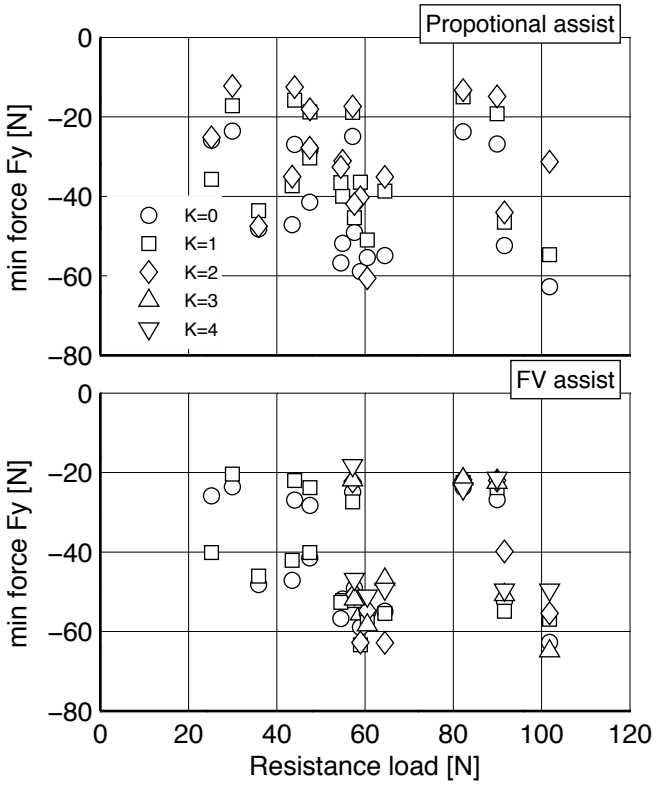

Figure 5-23 Attendant vertical force at maximum conditions

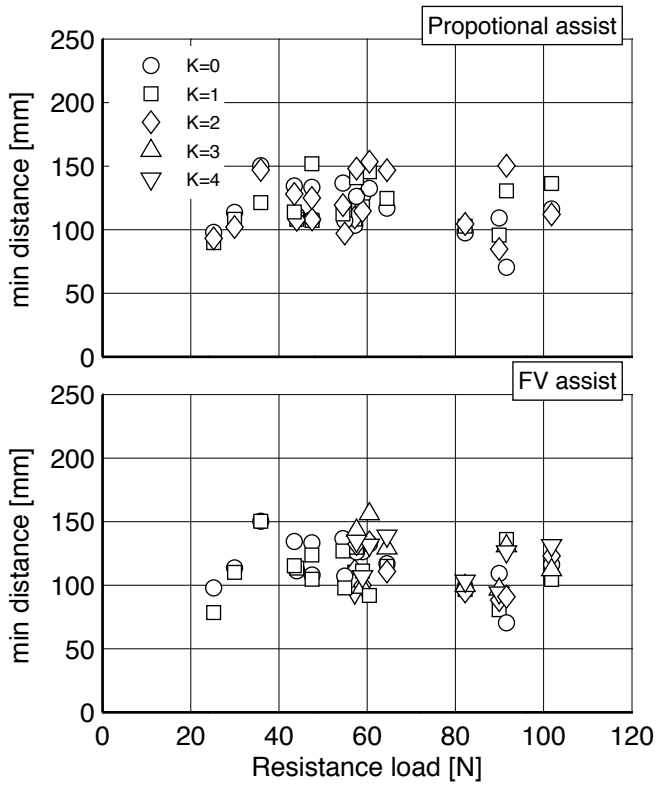

Figure 5-24　Distance at maximum conditions

Figure 5-25 shows the attendant mechanical power at maximum conditions. The maximum power reached to about 25W at higher maximum conditions. The attendant mechanical power with the P assist contorl decreased to 15W (K=1) and 12W (K=2). The attendant power with the FV assist control decreased to around 18W at any K conditions. The decrease of the attendant power with the P assist control appeared from lower maximum condition about 25N, however the decrease of the power with the FV assist control appeared over maximum condition about 60N.

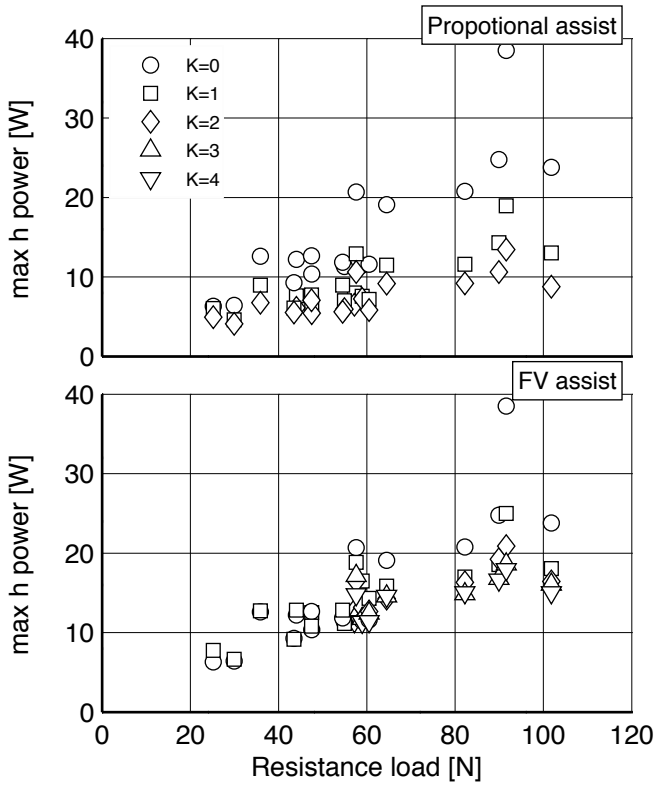

Figure 5-25 Attendant mechanical power at maximum conditions

Figure 5-26 shows the maximum assistive force at maximum horizontal force conditions. The assistive forces by the P assist control were generated from the lower maximum conditions, and the maximum assistive force reached to 90N(K=2) and 65N(K=1). The assistive forces by the FV assist control were mainly generated over 60N of maximum conditions, and the assistive forces under 60N of maximum conditions were under 10N. The assist gain K increased the assistive forces up to 80N(K=4), 75N(K=3), 55N(K=2), and 38N(K=1).

Figure 5-27 shows the maximum assistive power at maximum horizontal force conditions. The tread in maximum assistive power was the same as the assistive forces in Figure 5-26. The maximum assistive power with the P assist control reached to around 28W(K=2) and 18W(K=1), and the maximum power with the FV assist control also reached to around 25W(K=4), 22W(K=3), 20W(K=2), and 10W(K=1). The assistive powers with the P assist control generated from lower maximum conditions, however the assistive powers with the FV assist control mainly generated over 60N of maximum conditions. Under 60N of maximum conditions, the assistive powers by the FV assist control were under 5W.

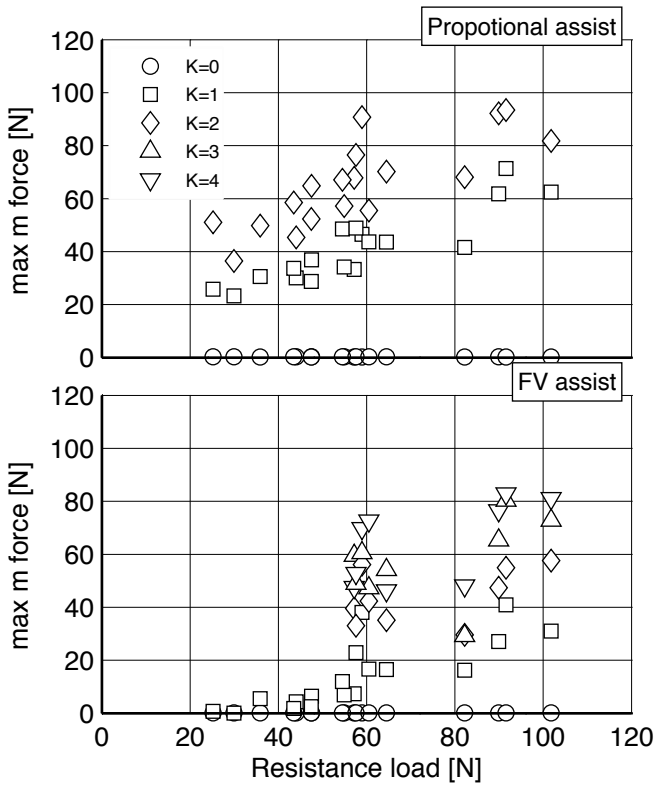

Figure 5-26 Maximum assist force at maximum conditions

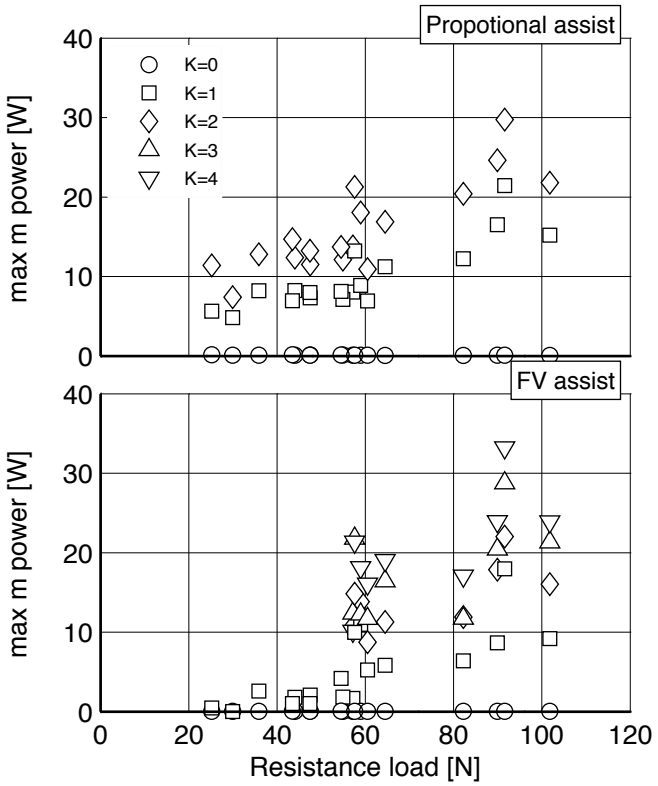

Figure 5-27 Maximum assist power at maximum conditions

Figure 5-28 shows the maximum wheelchair acceleration against the resistance load. The trend in the P and FV assist control was similar, except the cases in very light resistance load about 5N. The maximum wheelchair acceleration without assist systems in

light resistance load around 10N was 9mm/s, then decreased to 6.5mm/s with the increase of the resistance load. The P assist control increased the maximum wheelchair acceleration up to 10mm/s at higher resistance loads, from the condition without assist systems. Also the maximum wheelchair acceleration reached up to 11mm/s at low resistance load about 5N. The FV assist control increased the maximum wheelchair acceleration up to 9m/s at higher resistance loads, and also increased the wheelchair acceleration up to about 10mm/s at lower resistance loads. The increased wheelchair accelerations by the P assist were larger than the accelerations by the FV assist control.

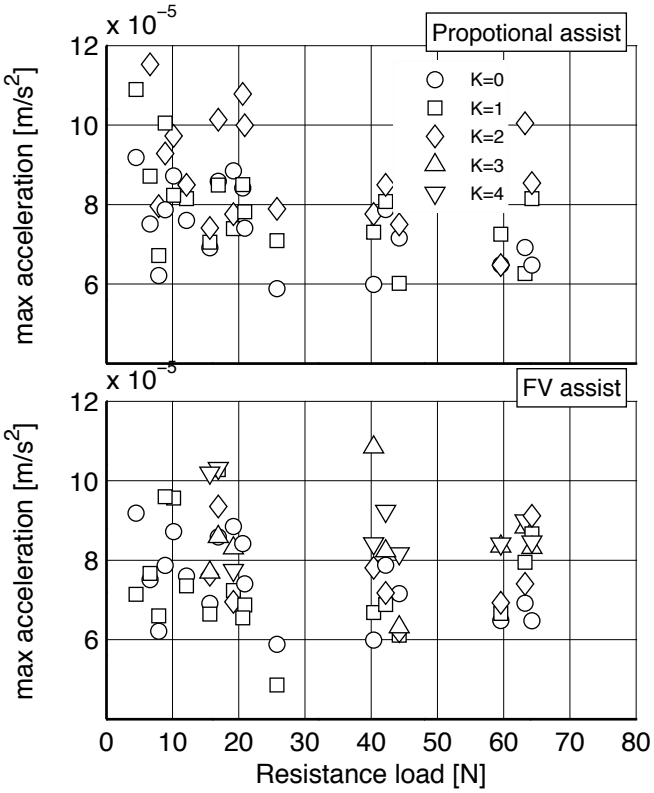

Figure 5-28 Maximum wheelchair acceleration against the resistance load

5-5-3 Comparison of assist control

Figure 5-29 shows validation results to compare between the FV and P assist control systems. Figure 5-29 is based on the simulation results in Figure 5-7, and has experimental results of assist systems. In the graph, the resistance load $f_R(t) = 11 + 22v_W(t)$ [N] was used for emulating the road resistance of the concrete surface in PAMELA facility. For the comparison between simulation and experiments, the external force $f_E = 42\,\mathrm{N}$ is set to simulate gravity force of the wheelchair on the slope 3.6deg. The participant in the model and experiment is different, however, the comparison is worth to show because the attendant behaviour is determined by the road resistance, which is common between simulation and experiments.

The results by the P assist control in white circles(steady) and squares(maximum) were well fitted to the simulation results in the attendant and assistive forces, even though the participants were different. It means that the proposed model in Chapter 4 well described the attendant-wheelchair systems. In contrary, the results of the FV assist control in black circles and squares had over 20N(K>2) difference from simulation results. However, the constant trend in the assist gain K>2 was similar between simulation and experiment despite the number of forces were different.

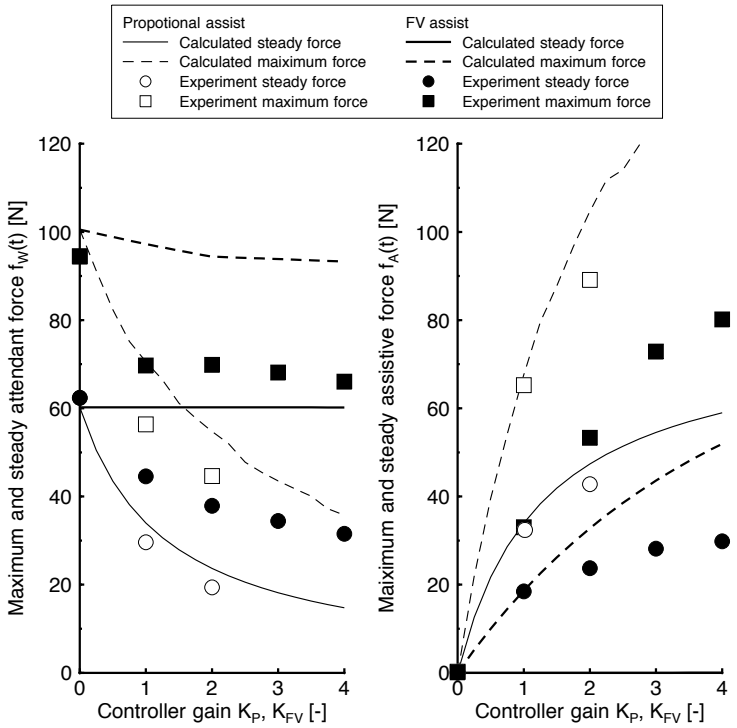

Figure 5-29 Validation of assist systems

5-6 Discussions

This study tested the performance of the assisting controller based on the force velocity relationship, and compared the controller performance with the proportional assist controller. In the tests, this study used simulation methodologies based on the model in Chapter 4, and developed the powered attendant propelled wheelchair system with the proposed FV assist system in Figure 5-6. From the comparison between with and without assist systems in Figure 5-12, the participants without assist systems need large force to accelerate the wheelchair at the resistance load in the condition of the weight W=60kg and the slope angle θ=3.6deg. However, the assist systems helped the participant to accelerate the wheelchair easily.

From the summarised results in Figure 5-29, the proposed FV assisting system worked well in line with the control rule that the assist system generates assistive force in the case the attendant needs propelling force over the assist boundary force. This feature provides superior low energy consumption in the FV assist control compared with the P assist control, because the attendant propelling force under the assist boundary can continue with light subjective hardness similar to walking. The assistive force in the maximum condition in the FV assist control was inferior to the force in the P assist control, however, the actual feelings in the FV(K=2) and the P(K=1) assist controls were similar in all participant from hearing after all of trials. The participants would not mind the shortage at maximum situation, because the period in that case commonly short time like at starting. Most part of propelling period carries out in steady state, so the feeling in steady propelling would be important for the attendant. The difference between the results in simulation and experiment in the FV assist control would be based on the perturbation of the propelling force by two leg walking. The frequency components by the FV assist control at the steady state in Figure 5-12, were caused by the switching between on and off adjacent the assist boundary force. The model in Chapter 4 did not include the element of two leg walking, and the lack of this element did not generate any assistive forces at steady state. However, the participant had actual assistive forces in the FV assist control, and would be avoid unconsciously the switching area because of unpleasant propelling feeling, even though the sprag bearings in both motorised wheels to prevent from braking by dropping the assistive forces. In the future works, we will investigate this problem to improve the performance in the FV assist control.

Comparison between the P and FV assist controls

With the comparison between the P and FV assist control, the FV assist control don't

provide the assist forces under the assist boundary by the attendant force velocity relationship. The assistive forces in Figure 5-18 and the assistive powers in Figure 5-21 shows clear difference in control behaviours between the P and the FV assist control. The FV assist control clearly reduces the energy consumption for assisting, compared with the P control. This is because the FV assist control provide the assist forces in which the attendant propels hard over the autonomous force velocity relationship. The autonomous force velocity relationship, which was explained in the detail in Chapter 3, is defined as the propelling condition to be able to continue long time under the maximised power and minimised subjective hardness based on physical fatigue. The attendant powers with the P assist control in maximum conditions were reduced more than the powers with the FV assist control. The P assist control proportionally generates the assistive forces from low resistance loads, so the P assist control reduces the attendant power in proportion to the resistance load. However the motor power by the P assist control increases more than by the FV assist control.

The minimum distances and the minimum vertical forces with the FV assist control were slightly improved by the assistive force, over 60N of the maximum horizontal forces. The decrease in both parameters in the P assist control were larger than in the FV assist control. This is because the P assist control reduced the horizontal forces more than the FV assist control, so the attendant under the P assist control do not need to generate large horizontal force by leaning forward using the body weight for pushing.

From the participants feeling about the assist systems, the assist gains K=2 and 3 by the FV assist control were natural and light, and the K=1 by the P control was similar. The smaller assist gain K caused the increase of the heaviness in propelling, however, it is clearly lighter than the cases without assist. In opposite, the larger assist gain K causes too light feeling, and the participants need to propel carefully to prevent from the rapid movement by unexpected sudden large pushes, which are generated by the disturbance of walking balances.

For the healthy attendant, the FV assist control is better than the P assist control, in terms of keeping minimum exercise and reducing the energy consumption. However, some attendant in aged with weak physical strength would prefer the P assist control, because the assistive forces were generated from low resistance load, and well reduced the high resistance load effectively.

5-7 Conclusions

This study tested the performance of the assisting controller based on the force velocity relationship, and compared the controller performance with the proportional assist controller. From the summarised results, the proposed FV assisting system worked well in line with the control rule that the assist system generates assistive force in the case the attendant needs propelling force over the assist boundary force. This feature provides superior low energy consumption in the FV assist control compared with the P assist control, because the attendant propelling force under the assist boundary force can continue with light subjective hardness similar to walking. The actual feelings in the FV(K=2) and the P(K=1) assist controls were similar in all participant from hearing after all of trials.

The FV assist control would be very useful to add a assistive system to the attendant propelled wheelchair as well as manual wheelchairs, hand cycles, and rehabilitation systems to control patients's load in line with rehabilitation progress.

References

[1]E. Abel, T. Frank, G. Boath, and N. Lunan, "An Evaluation of Different Designs of Providing Powered Propulsion For Attendant Propelled Wheelchairs," *Proceedings of Annual International Conference of the IEEE Engineering in Medicine and Biology Society*, vol. 13, no. 4, pp. 1863–1864, 1991

[2]A. Kakimoto, H. Matsuda, and Y. Sekiguchi, "Development of Power-Assisted Attendant-Propelled Wheelchair," *Proceedings of Annual International Conference of the IEEE Engineering in Medicine and Biology Society*, pp. 1875–1876, 1997

[3]H. Kitagawa, T. Nishigaki, T. Miyoshi, and K. Terashima, "Fuzzy Power Assist Control System for Omni-directional Transport Wheelchair," *Proceedings of the 2004 IEEE/ RSJ International Conference on Intelligent Robots and Systems (IROS)*, vol. 2, pp. 1580–1585, 2004

[4]T. J. Ren and T. C. Chen, "Modelling and control of a power-assisted mobile vehicle based on torque observer," *IET Control Theory Appl.*, vol. 1, no. 5, p. 1405, 2007.

[5]G. B. Cremers, "Hybrid-powered wheelchair: a combination of arm force and electrical power for propelling a wheelchair.," *J Med Eng Technol*, vol. 13, no. 1, pp. 142–148, 1989.

[6]N. Hata, Y. Koyasu, H. Seki, and Y. Hori, "Backward Tumbling Control for Power-Assisted Wheelchair based on Phase Plane Analysis," *Proceedings of Annual International Conference of the IEEE Engineering in Medicine and Biology Society*, pp. 1594–1597, 2003

[7]H. Seki, T. Sugimoto, and S. Tadakuma, "Novel Straight Road Driving Control of Power Assisted Wheelchair Based on Disturbance Estimation and Minimum Jerk Control," *Proceedings of the Fourtieth IAS Annual Meeting Conference Record of the 2005 Industry Applications Conference*, vol. 3, pp. 1711–1717, 2005

[8]H. Seki, T. Sugimoto, and S. Tadakuma, "Straight and Circular Road Driving Control of Power Assisted Wheelchair Based on Balanced Assisted Torque," *Proceedings of the 31st Annual Conference of IEEE Industrial Electronics Society*, p. 6, 2005

[9]H. Seki, T. Iijima, H. Minakata, and S. Tadakuma, "Novel Step Climbing Control for Power Assisted Wheelchair Based on Driving Mode Switching," *Proceedings of the IECON 2006 - 32nd Annual Conference on IEEE Industrial Electronics*, pp. 3827–3832, 2006

[10]D. Petersson, J. Johansson, U. Holmberg, and B. Astrand, "Torque Sensor Free Power Assisted Wheelchair," *Proceedings of the Rehabilitation Robotics ICORR 2007. IEEE 10th International Conference*, pp. 151–157, 2007

[11]S. Tashiro and T. Murakami, "Step Passage Control of a Power-Assisted Wheelchair

for a Caregiver," *IEEE Trans. Ind. Electron.*, vol. 55, no. 4, pp. 1715–1721, 2008

[12]H. Seki, K. Ishihara, and S. Tadakuma, "Novel Regenerative Braking Control of Electric Power-Assisted Wheelchair for Safety Downhill Road Driving," *IEEE Trans. Ind. Electron.*, vol. 56, no. 5, pp. 1393–1400, May 2009.

[13]Y. Oonishi, Sehoon Oh, and Y. Hori, "A New Control Method for Power-Assisted Wheelchair Based on the Surface Myoelectric Signal," *IEEE Trans. Ind. Electron.*, vol. 57, no. 9, pp. 3191–3196, 2010.

[14]H. Seki and A. Kiso, "Disturbance road adaptive driving control of power-assisted wheelchair using fuzzy inference," *Proceedings of the Engineering in Medicine and Biology Society,EMBC, 2011 Annual International Conference*, pp. 1594–1599, 2011

[15]R. Cooper, S. Fitzgerald, and M. Boninger, "Evaluation of a pushrim-activated, power-assisted wheelchair, " *Archives of Physical Medicine and Rehabilitation*, vol 82, pp. 702-708, 2001.

[16]R. A. Cooper, T. A. Corfman, S. G. Fitzgerald, M. L. Boninger, D. M. Spaeth, W. Ammer, and J. Arva, "Performance assessment of a pushrim-activated power-assisted wheelchair control system," *IEEE Trans. Contr. Syst. Technol.*, vol. 10, no. 1, pp. 121–126, 2002.

[17]M. F. Somers and S. Wlodarczyk, "Use of a Pushrim-activated, Power-assisted Wheelchair Enhanced Mobility for an Individual with Cervical 5/6 Tetraplegia," *Journal of Neurologic Physical Therapy*, vol. 27, no. 1, p. 22, 2003.

[18]S. G. Fitzgerald, J. Arva, R. A. Cooper, M. J. Dvorznak, D. M. Spaeth, and M. L. Boninger, "A Pilot Study on Community Usage of a Pushrim-Activated, Power-Assisted Wheelchair," *Assistive Technology*, vol. 15, no. 2, pp. 113–119, Dec. 2003.

[19]C. Levy, J. Chow, M. Tillman, and C. Hanson, "Variable-ratio pushrim-activated power-assist wheelchair eases wheeling over a variety of terrains for elders," *Archives of Physical Medicine and Rehabilitation*, vol. 85, pp104-112, 2004.

[20]S. Algood, R. Cooper, and S. Fitzgerald, "Impact of a pushrim-activated power-assisted wheelchair on the metabolic demands, stroke frequency, and range of motion among subjects with tetraplegia, " *Archives of Physical Medicine and Rehabilitation*, vol. 85, pp. 1865-1871 , 2004.

[21]L. L. H. MPT, P. S. R. PhD, C. J. N. DPT, and S. J. M. PhD, "Comparison of Energy Expenditure and Propulsion Characteristics in a Standard and Three Pushrim-Activated Power-Assisted Wheelchairs," *Topics in Spinal Cord Injury Rehabilitation*, vol. 11, no. 2, pp. 64–73, Jan. 2005.

[22]K. L. Best, D. R. L. Kirby, C. Smith, and D. A. MacLeod, "Comparison between performance with a pushrim-activated power-assisted wheelchair and a manual wheelchair on the Wheelchair Skills Test," *Disability and Rehabilitation*, vol. 28, no. 4, pp. 213-220, 2006.

[23]A. Karmarkar, R. Cooper, H. Liu, and S. Connor, “Evaluation of Pushrim-Activated Power-Assisted Wheelchairs Using ANSI/RESNA Standards,” *Archives of Physical Medicine and Rehabilitation*, vol. 89, pp1191-1198, 2008.

[24]M. Nash, D. Koppens, and M. van Haaren, “Power-Assisted Wheels Ease Energy Costs and Perceptual Responses to Wheelchair Propulsion in Persons With Shoulder Pain and Spinal Cord Injury" *Archives of Physical Medicine and Rehabilitation*, vol. 89, pp2080-2085, 2008.

[25]D. Ding, A. Souza, R. A. Cooper, S. G. Fitzgerald, R. Cooper, A. Kelleher, and M. L. Boninger, “A Preliminary Study on the Impact of Pushrim-Activated Power-Assist Wheelchairs Among Individuals with Tetraplegia,” *American Journal of Physical Medicine & Rehabilitation*, vol. 87, no. 10, pp. 821–829, Oct. 2008.

[26]Akira Kakimoto, Hideo Matsuda, and Yukio Sekiguchi, "Development of power-assisted attendant propelled wheelchair", Japan Society for Precision Engineering, vol. 65, no. 8, pp. 1126-1130, 1999(in Japanese)

[27]S. Tashiro and T. Murakami, “Step Passage Control of a Power-Assisted Wheelchair for a Caregiver,” *IEEE Trans. Ind. Electron.*, vol. 55, no. 4, pp. 1715–1721, 2008.

[28]A. Morbi, M. Ahmadi, A. D. C. Chan, and R. Langlois, “Comparing continuous and intermittent assistance controllers for assistive devices,” *Proceedings of the Robotics and Automation (ICRA), 2011 IEEE International Conference*, pp. 4651–4656, 2011

[29]H. Vandewalle, G. Peres, J. Heller, and J. Panel, “Force-velocity relationship and maximal power on a cycle ergometer,” *Eur J Appl Physiol*, vol. 56, pp. 650–656, 1987

[30]A. Sargeant, “Human Power Output and Muscle Fatigue,” *Int J Sports Med*, vol. 15, no. 3, pp. 116–121, Mar. 1994.

Chapter 6 Conclusions

This study focused on the individual propelling performance by force velocity relationship, and validated a proposed assisting control method based on the individual force velocity relationship. The force velocity relationship is well used to evaluate individual exercising performances, especially cycling. This study defined the individual force velocity relationship as the sustainable physical performance that an attendant maximises operating force under minimising subjective hardness.

A proposed assistive controller in this study generates assistive forces when the attendant propelling force exceeds an assist boundary force defined by the individual force velocity relationship. From this assisting rule, the proposed assistive system uses attendant propelling power up to the assist boundary force. The assist boundary force is easy to adjust to the individual propelling performance. Also by using assistive forces only when it is needed, the energy consumption in this system is reduced, and further, the attendant is able to use pushing the wheelchair as a form of moderate, controlled exercise to keep healthy. The main objectives in this studies were below.

1) Investigate the actual propelling load in the attendant propelled wheelchair on flat surface and longitudinal slopes, by operating forces, wheelchair velocity, walking pattern and each joint load. (Chapter 2)

2) Investigate the autonomous force velocity relationship in propelling on a motorised treadmill, by operating forces, walking velocity, walking pattern, postures, and heart rate. (Chapter 3)

3) Develop and validate an attendant-wheelchair model to design the assist controller. (Chapter 4)

4) Design and validate the assist as needed control with a powered attendant propelled wheelchair on real environments. (Chapter 5)

In Chapter 2, this study investigated required capability of propelling an attendant-propelled wheelchair in ascending and descending on longitudinal slopes, against the resistance load by the wheelchair weight and the slope angle. The participants need to exert pushing/pulling force equivalent to the resistance load under steady wheelchair velocity. The participants choose wheelchair velocity to match individual physical strength. In the comparison between the joint torque in the upper and lower extremity, the pushing force in ascending and the pulling force in descending are mainly generated by the ankle and knee.

From the estimated relationship between the pushing force and the wheelchair velocity,

this study can easily estimate the attendant load from the mechanical power and energy on the ascending works. The descending cases were vary, so we would need to investigate pulling cases deeply in future experiments with increased number of participants.

In Chapter 3, the outlined signal model of an attendant-wheelchair model was proposed, and confirmed that the autonomous provided capability in pushing can be estimated from the steady state by various resistance loads. This study developed the motorised treadmill to investigate pushing and pulling with walking under steady state with stable resistances load in long time. Our developed treadmill enables to obtain reliable steady state results to evaluate the autonomous provided capability in pushing and pulling. From the results, we found following;

1. The force-velocity relationship of the autonomous provided capability in propelling is a monotonic decreasing function. The attendant generates large propelling force under low walking velocity, however, the propelling force decreases with the increased walking velocity. The attendant autonomously maximises the propelling force and the walking velocity with minimising the subjective hardness, in order to propel long time against resistance loads.

2. The autonomous provided capability in pushing is carried out under exercising heart ratio (EHR) 30%, which shows light subjective hardness to be able to continue over 20min.

3. The provided capability in propelling is determined by the subjective hardness. The attendant can increase the propelling capability in propelling if bearable subjective hardness is increased.

4. In the case of the participant with good strength, the maximum pushing force in the autonomous provided capability is about 80N, which is 10-30% of voluntary maximum pushing force. The maximum mechanical power in the autonomous provided capability is around 30W.

5. For generating large pushing forces, an attendant needs long step length, long stride period and over 30% of double support period in 1 cycle walking.

These findings are very useful to estimate the attendant load to propel attendant-propelled wheelchairs, as well as to apply for the development of the wheelchair with less-load. From the chapter four, we develop more detailed model and identify each element of the model from experiments. After the validation of the model, we develop the assist system for the attendant-propelled wheelchair in the chapter 5. The proposed assist system are designed based on the autonomous provided capability in propelling, which is obtained by this chapter 3.

In Chapter 4, this study proposed the attendant-wheelchair model, and validate it with identified parameters for each element in the model. The proposed model was built upon the analogy of the prime motor and load system. The attendant part had the elements of musculoskeletal dynamics and cushioning arm dynamics, and the wheelchair part had the mechanical dynamics of wheelchairs in straight moving on longitudinal slopes. From the experiments for validation of the model on the artificial grass surface at a level, our findings are below.

1) The proposed attendant-wheelchair model can simulate the attendant behaviour well. This suggest that the proposed model is very useful for estimating an attendant's propelling hardness on various resistance load, such as rough surface, gap and threshold.

2) The propelling force - walking velocity relationship of attendants dominates main steady state in the model. The transfer functions of other elements become 1 under steady state, so the attendant steadily propels a wheelchair at the operating point, at which attendant's force velocity relationship and wheelchair's resistance load are the same.

3) The dynamics of the musculoskeletal system can be described as the second order system with lag element. However, the identification suppose that the human cannot follow force change over 1 Hz while walking.

4) The arm function can be described as a parallel spring and damper system. The results shows the arm stiffness and dumping coefficient are linear.

These findings contribute to improve the attendant-propelled wheelchairs, and to develop effectively the assist controller for a powered attendant-propelled wheelchair.

In Chapter 5, this study tested the performance of the assisting controller based on the force velocity relationship, and compared the controller performance with the proportional assist controller. From the summarised results, the proposed FV assisting system worked well in line with the control rule that the assist system generates assistive force in the case the attendant needs propelling force over the assist boundary force. This feature provides superior low energy consumption in the FV assist control compared with the P assist control, because the attendant propelling force under the assist boundary force can continue with light subjective hardness similar to walking. The actual feelings in the FV(K=2) and the P(K=1) assist controls were similar in all participant from hearing after all of trials.

With findings of autonomous individual force velocity relationships, this study successfully showed desired performance of the proposed assist controller based on the force velocity relationship. From the summarised results, the proposed assistive system worked well in line with the control rule that the assistive system generates assistive forces as the attendant needed propelling force over the assist boundary force. This feature provides superior low energy consumption in the proposed assistive system compared with the common proportional assist controls, because the propelling force by attendants

under the assist boundary force can continues under light subjective hardness similar to walking. The actual feelings by attendants with the proposed assistive system were similar to the proportional assist control.

The proposed assist control in this study would be very useful to add an assistive system to the attendant propelled wheelchair as well as manual wheelchairs, hand cycles, and rehabilitation systems to control patients's load in line with rehabilitation progress.

Appendix

A. Road resistance and autonomous manual wheelchair pushing

Introduction

The users of manual wheelchairs have many possibilities of injuries in shoulders and elbows because of repetitive long use. One solution to reduce this problem, the position of rear axle is changed by user's demands based on subjective comfortableness or the clinician's prescription based on user's body sizes in upper extremity. There are two directions to change the position of the rear axle; horizontal and vertical. The change of these two directions means the change of relative distance from shoulder to hand rim. The relative distance is one of important factor for propelling because the propelling performance is determined by the length of upper arms.

The trajectory to push the hand rim is consists of continuous points and directions to push force along with a bar, which assumes one of short pieces of hand rim. The comfortableness of propelling is determined by the easy points and directions of exerting force within hand's reach. The moving velocity and its direction of hand rim is also important because the propelling task consists of gripping on with generating force and off with retrieving hand position for next propelling. In addition, the change of the distance between shoulder and hand rim by seat position or rear axle position means the change of road resistance at each wheel, because the normal forces at each wheel are changed by the centre of mass (COM) in wheelchairs. The propelling capability and road resistance is changed by seat position or rear axle position. But the contribution level of two factors to the total mobility in wheelchairs is not well known.

The horizontal seat position affect the position of centre of mass in wheelchair. Asahara[1] studied the horizontal position of centre of mass during manual wheelchair propulsion with four horizontal axle conditions. Asahara found that the distance between the centre of mass and axle positions significantly decreased with the forward axle position in propulsion on the flat level floor. In addition, the road resistance in wheelchairs is changed by horizontal seat position or rear axle position, because the changed mass distribution cause each wheel's normal force, which is proportional to rolling resistance at each wheel. Brubaker[2] showed rough reduction ratio in road resistance by increased rolling resistance by normal load under two condition; wheels and casters, and main

wheels only. The experiments in the paper was insufficient to calculate the reduction ratio by the COG of wheelchairs. Also the reason from physical views was not shown.

The propelling capability depends on the relative distance from shoulder to hand rim. The relative distance is determined by relative distance in horizontal and vertical. Also the individual body sizes of upper extremity, such as shoulder height from seat and arm length, also affect horizontal and vertical relative distance from shoulder to hand rim. Boninger[3] studied the effect of rear axle position relative to the shoulder on push rim biomechanics with 40 subjects in individual dimensions of upper body. The position of rear axle was prearranged by users or clinicians for daily use. Of the subjects, the group in a shorter vertical distance between the rear axle and the shoulder and a more forward axle position was correlated with improvement in wheelchair propulsion biomechanics. This result shows that some manual wheelchair users or clinicians likely set the seat position backward and downward.

In the lower vertical direction in seat adjustment, the grip range of hand rim increases. The study by van der Woude[4] showed lower vertical position of the seat is better performance to propel in mechanical efficiency, oxygen cost, push range and duration, and motion. But too lower position leads wrist injuries. Wei[5] showed that during wheelchair propulsion, seat height was found to be a critical factor affecting the temporal parameters of movement and wrist kinematic properties of the subjects. Wrist joint angles and wrist flexion-extension range of motion all varied according to seat height. Observations and statistical analysis of the results provided useful information.

In the horizontal direction in seat adjustment, the capability in shoulder and elbow joints depend on its joint angle is important factor. In addition, the angle range in joints is also important. Masse[6] studies that the pattern of propulsion was investigated for five male paraplegics in six seating positions. The seat positions consist of a combination of three horizontal rear axis positions at two seating heights on a racing wheelchair. Masse found that with lower seat positions, less EMG activity was recorded than for higher seat positions. Of the six seat positions, the backward seat with low position was found to have the lowest pushing frequency. Mulroy[7] studied that the effect of fore-aft seat position on shoulder joint kinetics. In the backward seat position, the plus component of the resultant force in shoulder joint was significantly lower at free propelling condition without road resistance. The seat-posterior position displayed increased internal rotation moment, decreased sagittal plane power absorption, and increased transverse plane power generation. The investigation provides that a posterior seat position reduces the plus component of the shoulder joint resultant force.

Also theoretical approaches tried to solve the optimum seat position. Richter[8]

showed a quasi-static wheelchair propulsion model was developed to investigate the mechanism by which seat position affects propulsion biomechanics. From the result of calculation with the model, the effect of seat position on push angle was found to be directly affected by the length of the position vector from the hub of the wheel to the shoulder length. Also decreasing hub to shoulder length was found to increase push angle, decrease push frequency, decrease shoulder torque and increase elbow extension torque. Sasaki[9] defined an ellipsoid to describe dynamic manipulating forces under various hand positions in three dimensional space. These results showed easiness and hardness to exert static propelling force by hand position.

Some studies showed backward seat position, or forward position of rear axle gives better propelling condition, because the rolling resistance in wheelchairs decreases and the propelling load also decreases. But which factors of the rolling resistance or the propelling load contribute to the total mobility of wheelchair, is not well know.

In this paper, we focus on the arrangement in horizontal seat position for better mobility and drivability of wheelchairs. The simple relationship between a user and a wheelchair assumed as an electric motor and a load. On the first step, we proposed and validate a model of the rolling resistance of wheelchairs by horizontal seat position as a load. On the second part, we estimate propelling capability by horizontal seat position as an electric motor. Our hypothesis is that for better mobility and drivability of wheelchairs, the contribution level of decreased rolling resistance by horizontal seat position is larger than the increased propelling capability.

The first part of the rolling resistance in wheelchairs proposes the model of the user-wheelchair system by horizontal seat position. The proposed model focuses on static change of road resistance by horizontal seat position. The dynamics change at each wheel by propelling does not include in the model, because the change of load by propelling is small. The rolling resistance of wheelchairs is determined by sum of each rolling resistance at casters and wheels. The experiments to identify the rolling resistances at a caster and wheel were carried out. These results show the validation of the proposed model first. The change of rear axle positions gives the similar effect to the change of COM in wheelchairs. The effect of rear axle is also discussed.

The second part of the propelling capability by horizontal seat position showed the estimation the static and dynamic propelling capability by horizontal seat position. The propelling force shows intermittent rise of the propelling torque, caused by the repeat dynamic behavior of hand on and off to propel. Under the propelling period, the wheelchair is accelerated by averaged(static) propelling torque, then the releasing period in hands-off, the wheelchair is decelerated by road resistance. To measure the static

propelling capability, an autonomous propelling capability was measured as an electric motor performance. The autonomous propelling means that the propelling is unconsciously regulated in steady state for long time along with user's body performances. The estimation of dynamic propelling capability was carried by the trails to control push on and off along with indication. The indication was set to keep impulse constant.

The static and dynamic propelling capability and road resistance determine the mobility and drivability in wheelchairs. This results help users and clinicians to set up wheelchair seating in horizontal position.

Propeosed human-wheelchair model

Define of symbols in the system

M: Manual wheelchair with the user mass

X_G : Horizontal position of the COG

N_f : Front normal force

N_r : Rear normal force

$R_f(v)$: Front resistant force

$R_r(v)$: Rear resistant force

$v(t)$: Horizontal wheelchair velocity

X_S : Horizontal seat position

Y_S : Vertical seat position

L : Horizontal distance between front and rear wheel axis

g : gravity constant

μ_f : Coefficient of rolling resistance in front caster

μ_r : Coefficient of rolling resistance in rear pneumatic tire

R_H : radius of hand rims

R_W : radius of rear wheel

R_d : radius of road drum

β: reduction ratio for road roller

$\tau(t)$: Propelling torque

T: Averaged propelling torque by propelling cycle

$\omega(t)$: rim angular velocity

Ω: averaged rim angular velocity by propelling cycle

The assumption for the model is following. The wheelchair is described as a mass point, because the structure of the wheelchair is rigid. The user of the wheelchair is also described as an another point of mass, because the changed distribution by user's hands in propelling is very small. Both front casters and rear pneumatic tires are always contacted on the ground. The wheelchair moves straight forward and the road surface are performed on flat surface in a level. No dynamic change of front and rear wheel load is assumed to simplify the model.

The planar model of wheelchairs is shown at the Figure 1(a). The total mass of wheelchair's body and user's weight is *M*. The mass *M* is concentrated at the point of COG. The origin of the coordinate system is at the rear axis in planar plane. The seat position $S(X_S, Y_S)$ determines the point of COG. However, in the model, the vertical position Y_S is neglected to simplify the model for the discussion of the effect on horizontal seat adjustment. The normal forces at each front caster and rear wheel are steady parameter N_f and N_r respectively. The N_f and N_r are determined by the COG position. The block diagram of the system is shown by the Figure 1(b). The user exerts the propelling torque τ(t) by wheelchair velocity v(t). The torque $\tau(t)$ is converted to the driving force of the wheelchair by dividing the rear wheel radius R_W. The driving force is detected by the total road resistance of wheelchairs, then the remaining driving force accelerates the wheelchair. In the wheelchair propelling, the user regulates the wheelchair velocity by own body performance. In this paper, the regulating unconsciously the wheelchair velocity by user's body performance was defined as autonomous propelling. We assume that the user propel wheelchairs autonomously in daily wheelchair use. The equation of kinetic motion is described by the equation (1) below.

$$M\frac{dv(t)}{dt} + R(V) = \frac{\tau(t)}{R_W} \tag{1}$$

Here, the $R(V)$ is functioned as the force of the road resistance. The detail of the road resistance $R(V)$ is below.

$$R(V) = 2(\mu_f(V)N_f + \mu_r(V)N_r) \tag{2}$$

The normal forces N_f and N_r are assumed as the constant because the mass movement of upper extremity is small. The total road resistant $R(V)$ is depend on front and rear normal force N_f and N_r.

Also along with vertical axis in the model, there is the equilibrium between wheelchairs's weight and front and rear normal forces. The equilibrium of the normal

force and gravity force of the wheelchair is shown below.

$$N_f + N_r = Mg \tag{3}$$

From the assumption of contacting all wheels on the ground, the equilibrium of moments at the rear axle is described below.

$$MgX_G = N_f L \tag{4}$$

Here, the L shows the horizontal distance between front and rear axis. If the position of rear axis changes, the L also changes. Finally, the normal force Nf and Nr is solved from Eq. (3) and (4)

$$N_f = MgX_G / L\,,\ N_r = Mg(1 - X_G / L) \tag{5}$$

The user, human being consists of many parts of body with mass. However under the assumption that the upper extremity movement does not affect the change of the normal force Nf and Nr, the horizontal position of centre of gravity X_G is determined from seat position. We defined a function $S(X_S)$ to show the relationship between horizontal centre of gravity X_G and seat position X_S. The function $S(X_S)$ is needed to solve from experiments.[1]

$$X_G = S(X_S) \tag{6}$$

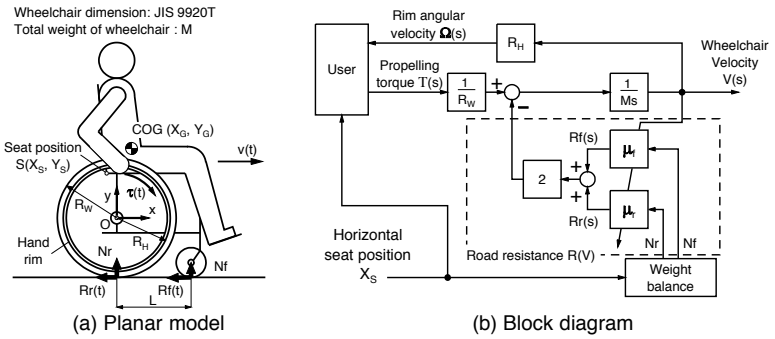

(a) Planar model (b) Block diagram

FIg. 1 Model of self-propelling wheelchair with horizontal seat position

Experiment device and method

Figure 2 shows the device to measure the rolling resistance of front polyurethane casters and rear pneumatic wheels. This device has three wheels, one front wheel and two rear wheels. The target wheel for the measurement of rolling resistance is the two rear wheels in the device. The rear wheels of the device can be replaced to front casters or rear wheels of wheelchairs. The front wheel of the device is the same rear pneumatic wheel of the wheelchair. The direction of front wheel of the device is fixed at straight angle to allow drive only straight forward. First, the rolling resistance of rear pneumatic wheel was determined by the device with three rear pneumatic wheels. Next, the rolling resistance of front caster was determined by the device with one rear pneumatic wheel of wheelchairs at front and two front casters at rear. The normal load of rear wheels of the device can be adjusted by the additional mass weight on the bottom place of the device.

The rotary encoder synchronizing the rotation of the front wheel detects the velocity of the device. The force sensor detects the pushing force and the indicator mid of both force sensor shows the velocity of the device to adjust the device velocity at constant.

This experiments to measure the rolling resistance at the caster and the rear wheel of the wheelchair were carried out by person. The instruction for the measurement of rolling resistances was following. The person pushed the device at constant velocity with continuously checking the device velocity from the indicator. The indicated velocity to the person was increased from 0 to 1.25m/s by 0.14m/s step. The air pressure of the rear pneumatic tires of the wheelchair was set as 0.3MPa.

First experiment was started with three rear wheels of wheelchairs for solving the rolling resistance at one wheel. The total road resistances were measured by sum of both left and right force sensors. Then the rolling resistance at one rear pneumatic wheel can be solved by division of the total resistance force by three, because the device has three same rear pneumatic wheels of the wheelchair. Then change the rear wheel of the device to the front polyurethane casters of wheelchairs, then the same experiments were carried out. The rolling resistance of the front casters at rear of the device, was solved to subtract the one rolling resistance at rear pneumatic wheel from the total resistance force, then divide the remaining resistance force by two, because of two rear casters in the device.

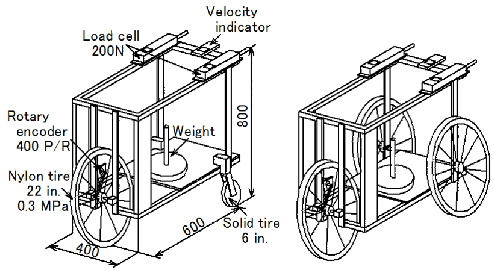

(a) front casters (b) Rear wheels

Fig.2 The device to measure rolling resistance

The device to measure propelling performance is shown on the figure 3. The device consists of the wheelchair with a torque sensor in right side and motorized road rollers. The rear wheels of the wheelchair are set mid on the two road rollers. The front casters of the wheelchair were replaced to rotational joints. The angle of the wheelchair is set at a level. The right side of the hand rim has a torque sensor to detect propelling torque. The two road rollers were driven by AC servo motor via reduction pulley 2/3. The horizontal seat position X_S can be set from -100mm to 100 mm on horizontal direction. The origin of position was fixed at the rear axle in planar plane. The initial standard seat position $S(X_S, Y_S)$ is $S(0,\ 100\text{mm})$. The angle of back rest of the seat is 105deg. The weight of wheelchair is 21kg and subject's weight is 67kg, so the total mass M is 88kg. The control of motor has two modes. One is the mode to control indicated velocity constantly under the switch S_1 to the point C_f. Under the constant velocity mode, the two road rollers were controlled with feedback at indicated rotational velocity. This mode used for investigating dynamics propelling performance to follow the indication of the monitor in front of the wheelchair with the closed switch S_2. Another mode on the switch S_1 to the point C_S, simulates the dynamic characteristic of wheelchairs to measure the autonomous propelling performance with the opened switch S_2. Under the simulated wheelchair mode, the rotational velocity of the motor is controlled by the output signal of the transfer function $G_W(s)$. From the equation (1) and (2) with the assumption $R(V) = RV$, the transfer function $G_W(s)$ is shown by next equation (7).

$$G_W(s) = \frac{K}{Ts+1} \tag{7}$$

Here the time constant $T = M / R$ and the gain $K = 1/R$.

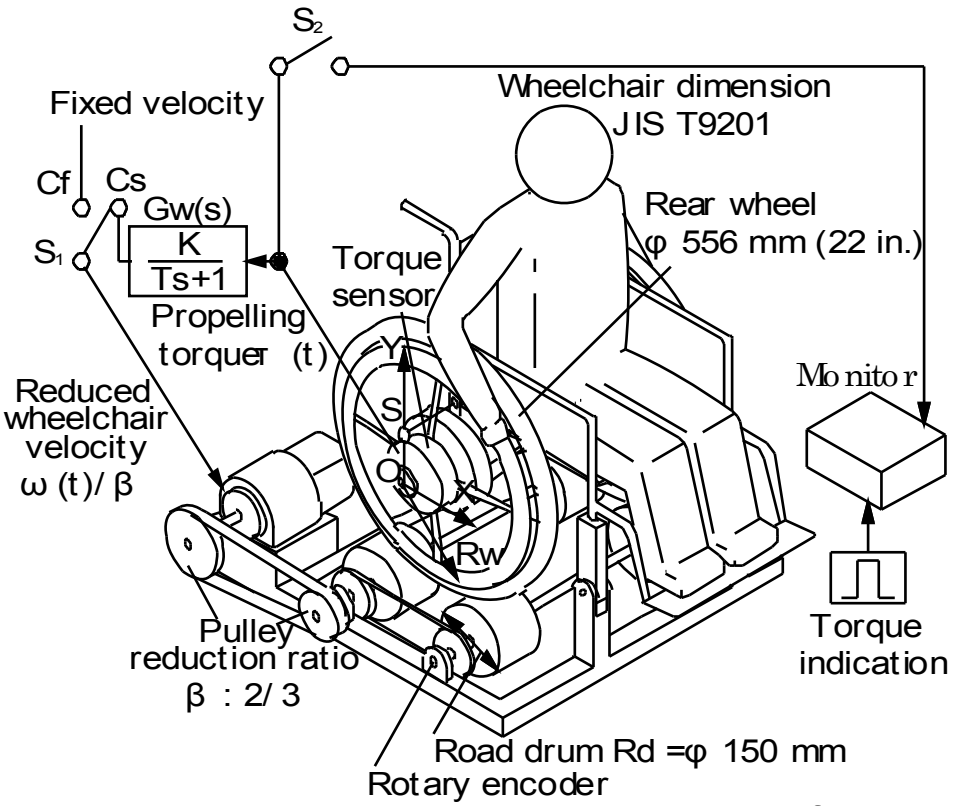

Fig.3 The device to measure propelling performance

We carried out two types of investigation to measure propelling performance by the horizontal seat positions X_S = −50, 0 and 50mm; autonomous(static) propelling and dynamic propelling.

The first experiments was to measure the difference of autonomous propelling performance by horizontal seat positions. To measure the autonomous propelling performance, the switch S_1 of the experimental device was set to the point C_S. The transfer function $G_W(s)$ calculated the rotational velocity of the motor and indicated the motor velocity to the motor controller. The measurement of the autonomous propelling is performed to solve the operating points one by one respective to the various propelling resistances. The operating point is that the averaged propelling torque is equal to the propelling resistance under steady state. Unconsciously the user of wheelchairs detects various propelling resistance by road surfaces, and regulate the propelling torque determined by the user's body performance to continue the propelling task. The measurement of the autonomous propelling was carried out along with following steps; 1. Set the propelling resistance 1/*K* from 0.2 to 250 Nm/(rad/s) randomly. 2. The subject starts propelling and continues propelling 5min. 3. After 3min passed and under the confirmation that the propelling is under steady state, the recording data is started until 5min passed from the start of each trial. 4. The subject rest well for 20min until the heart

ratio drop to the value at rest. 5. Repeat from step 1 until all of the propelling resistance 1/ *K* were tested.

The subjective hardness of propelling is measured by Exercising Heart Ratio (*EHR*) based on Borg scale[9]. The *EHR* shows subjective hardness of propelling based on individual body performance in each subject. The monitor of heart ratio attached the chest of subjects, and detects R-R intervals. Then the heart ratio were converted from the R-R interval, and the *EHR* was solved from the equation (8) below [10]. The maximum heart ratio was determined by simple calculation with age of each subject [10].

$$EHR = \frac{HR - HR_{REST}}{HR_{MAX} - HR_{REST}} \tag{8}$$

Next, the investigation of dynamic propelling performance measured the accuracy of dynamic push on and off the hand rim. The subjects were indicated pulses by the monitor in front of the wheelchair. The pulses are created by digital signal processor so that the width of the pulses is constant 0.3s. The height of the pulse shows the value of the torque that the subject have to exert, also the actual torque that the subject exert was shown as an another line on the monitor. Before the experiment, the subject is instructed to push on and off the hand rim along with the indicated pulses on the monitor. The interval time P of the pulses on all trials is fixed as 1.5s, because of keeping the impulse of the propelling torque constant through all trials. The indicated torques as a high of the pulses were 5, 10 and 15Nm. The rollers velocity was set from 0.5 to 4.0m/s by 0.5m/s. After the sign to the subject, each trial starts for 30s. The subject start to propel along with the pulse after the sign, then 10s passed, the recording of the data carried out until 30s passed.

The subject is employed only one subject because this paper focuses on the balance between the propelling capability and road resistance respective to horizontal seat positions. The details of the subject is following; Age: 21. Height:163cm, Weight: 66kg, Height from seat surface to shoulder: 570mm, Upper arm length from shoulder to wrist: 590mm, Length from shoulder to elbow: 260mm. The subject are healthy and have never experienced related to any motor diseases. The subjects are informed the detail of this studies well before the trials. The subjects had the right to stop the experiments when the subjects feel something uncomfortable.

Results and discussion

The figure 4 shows the change of normal force of front N_f and rear N_r, and the COG position against horizontal seat positions. The normal force N_f and N_r was measured by the load cells under each wheel, then averaged both front loads and both rear loads respectively. The load measurements from $X_S = -100$ to 100mm by 25mm step, were carried out the wheelchair with the subject at a level surface. The horizontal position X_G of the COG was calculated by the equation (5) with the wheel base L=0.38m. At the standard horizontal seat position X_S=0, the front normal force N_f was 230N and the rear normal force N_r was 205N. At the X_G=190mm, half distance of the wheelbase *L*, the front and rear normal force were the same as a half of the total weight 421N. The COG at the seat position X_S=0 was placed on 30mm forward from mid of *L*. The N_f proportionally decreased along with the backward seat position X_S. In opposite, the N_r proportionally increased with the backward X_S position. The relationship X_G=*S*(X_S) between horizontal seat position and the COG position was estimated a line function X_G =179+0.844 X_S. The horizontal position X_G of the COG and the wheel base L determined the normal force Nf and Nr by the equation (5). With the equation (5), the normal force N_f and N_r can be solved any type of wheelchairs. The wheel base *L*, which is the distance between front and rear axles, is determined by the horizontal rear axle position. The horizontal seat position Xs does not affect the wheel base L, but the horizontal COG position X_G changes by the X_S. From the figure 4, the rear positioned seat position reduced the normal force N_f at the front casters and increased the normal force N_r at the rear wheels.

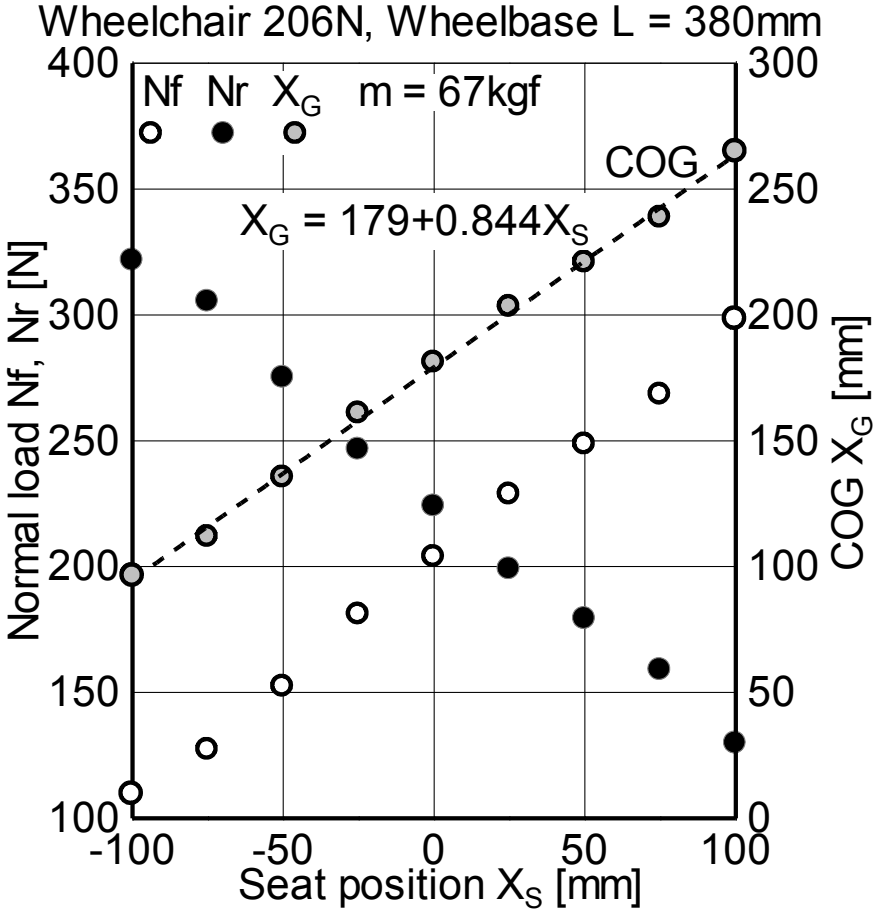

Fig.4 Relationship between seat position and load, COG

The figure 5 shows the coefficient of friction μ_f and μ_r respective to velocity. The μ_f and μ_r were solved to divide the rolling resistance at one wheel by normal force N_f and N_r respectively. From the comparison with both the coefficients between front μ_f and rear μ_r, the slope of the both line by velocity was similar, but the intercept of the μ_f at the front caster was six times higher than the intercept of the μ_r at the rear wheel. This means that the rolling resistance at the front polyurethane caster is six times higher than the rolling resistance at rear pneumatic wheel, under the same normal force. In the figure 5, the maker points of triangle show the measured total resistance of the wheelchair with X_S =0 at asphalt surface. The dotted line is calculated by the planar model at the figure 1. Both experimental and calculated road resistance correspond well. So the total resistance of wheelchair is determined by the normal force N_f and N_r. In addition, the backward seat position moves the horizontal position of COG backward, so finally the N_r increases and the N_f decreases. The coefficient μ_f of the front caster is six times higher than the μ_r, so backward seat position reduces the total resistance of wheelchair.

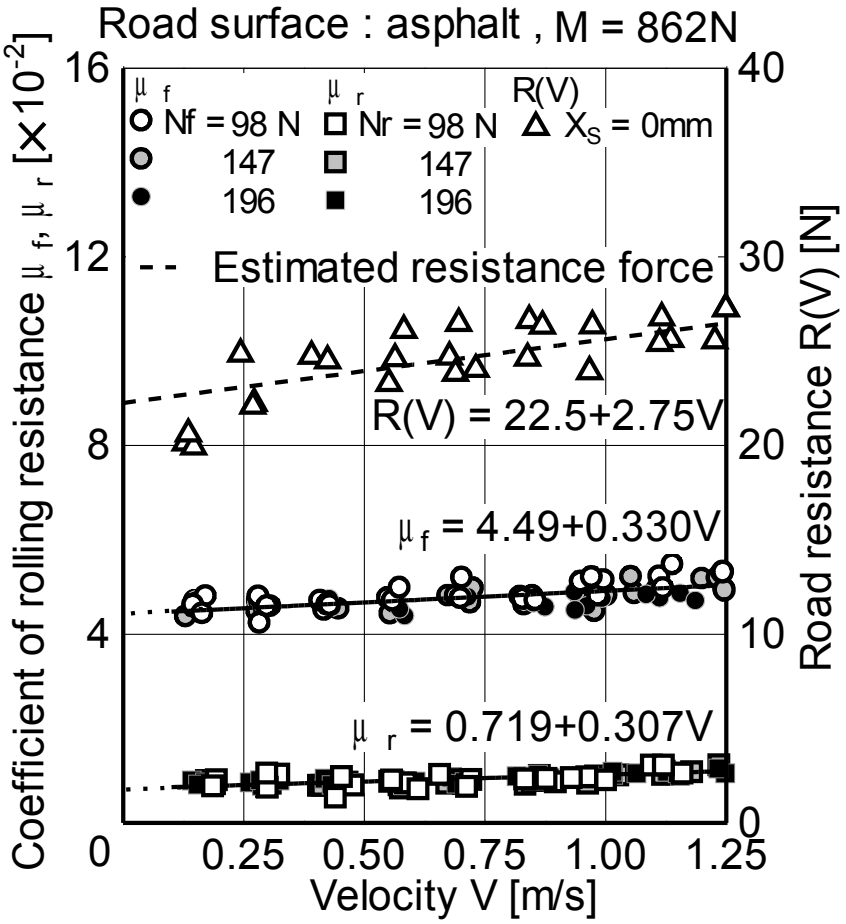

Fig.5 The coefficient of rolling resistance

Figure 6 shows the propelling behaviors under the autonomous propelling. For focusing on the difference of propelling torque by horizontal seat positions, the graphs in the figure 6 were cut out only duration in propelling. In the propelling torque curve, the important factors are the rising slope, the peak part in propelling torque, the maximum holding angle and end of the holding angle. Theses factors determine the shape of propelling toque and so we focus on the difference of these three factors in the graph.

The first point is the rising slope in the propelling torque. At the large propelling resistance R=20Nm/(rad/s), the propelling torque rose sharply against holding angle. Under the large propelling resistance, the subject could hand on and push the rim easily because the rim angular velocity was slow around 0.2rad/s. The rising slope in the propelling torque dropped along with the decrease of the propelling resistant torque 1/*K*. This means that the subject became difficult to hand on and push the rim because the decrease of the 1/*K* increases the rim angular velocity. In horizontal seat position, no typical difference can be seen on the rising slope of the propelling torque.

The second point is the peak shape in the propelling torque. The propelling torque at 1/*K*=20Nm/(rad/s) were almost kept at the flat level around 15Nm against the holding angle.

The holding angle at maximum propelling torque on 1/*K*=20Nm/(rad/s), was around 40deg. Also the holding angles at the maximum point by other 1/*K* conditions, were nearly similar holding angle at 40deg. The shapes of the peak part in propelling torque also were similar, but the only propelling torque in the 1/*K*=4.0Nm/(rad/s), has round shape. In horizontal seat position, no typical difference can be seen on the peak shape of propelling torque.

The third point is the holding angle from start to end. At the large propelling resistance 1/*K*=20Nm/(rad/s), the subject likely grasped the rim angle about −3deg. earlier timing than the other condition of propelling resistance 1/*K*. The end of holding angle became most large angle around 80deg. at the large propelling resistance 1/*K*. Along with the decrease of the 1/K, the holding angles at start were increased and the angle at end were decreased. This means that the holding range decreased along with the decrease of the propelling resistance 1/*K*. The horizontal seat position slide the holding range along with the relative position between the shoulder and a rim.

The reason of the difference in four factors is that the high propelling resistance at low rim angular velocity is easy to grasp and exert the muscle forces, then continue to exert the propelling torque in high level easily. At the end of holding angle, the subject easy to release the hand from the rim and carried out the return motion because the low rim angular velocity gives small inertia to the hand. In opposite, the low propelling resistance at high angular velocity is difficult to grasp the rim at high velocity, then difficult to keep high propelling torque, and also difficult to release the hand from the rim.

The wheelchair acceleration by holding angle on the duration of propelling at high propelling resistance 1/*K*=20Nm/(rad/s), is small because the propelling torque for acceleration was deducted by the large propelling resistance. At the low propelling resistance 1/*K*=0.4Nm/(rad/s), the acceleration of wheelchair also small, because the propelling torque was small because of difficulty of propelling at high rim angular velocity. The medium propelling resistance shows good acceleration of wheelchair, because the balance between propelling torque and resistance is better than other conditions. This result shows that the difficulty of propelling torque is proportional to the increase of the angular velocity of hand rim. The acceleration of wheelchair by holding angle is determined by the balance between propelling torque and resistance.

Figure 7 shows that the summary of the autonomous propelling. The horizontal axis is averaged angular velocity Ω and the vertical axis is averaged propelling torque T against various propelling resistance 1/*K* from 0.2 to 250Nm/(rad/s). In the high propelling resistance 1/*K*=250Nm/(rad/s), the propelling torque was high about 17Nm, but the rim angular velocity was low 0.15rad/s. Along with the decrease of the propelling resistance 1/

K, the propelling torque decreased and the angular velocity increased. All of *EHR* values showed constant value about 20%, so every trials were carried out under the light exercising condition, which means to continue about 20min.[9] Small difference by horizontal seat position in the the graph of propelling torque - angular velocity, can be seen. The propelling torque in the seat position X_S =0 and X_S=-50mm were the same, but the torque on X_S=50mm was smaller than other conditions. The thick line in the graph shows an estimated curve for all of data, because the difference by horizontal seat positions was small. This line means the performance curve as electric motors. The mechanical power of propelling torque were calculated by multiplying the averaged torque T with the averaged angular velocity Ω. All of the mechanical powers against seat positions had maximum points at around 0.7rad/s of rim angular velocity. The maximum values of X_S=0 and -50 were similar, and both value slightly larger than the value at the X_S=50. The large mechanical power means that the energy of the user's propelling effectively transfer to wheelchairs. The *EHR* of the subject was similar at all propelling torques in any horizontal seat positions, so the propelling torque at around 0.7rad/s of rim angular velocity was the most effective to transfer the propelling energy to wheelchairs. This results show that the effect of horizontal seat position to the autonomous propelling was very small. And the hardness from the *EHR* was similar in all horizontal seat positions. This means that human being well regulate to move their upper arms to adjust the different condition. Also there is the effective propelling condition to transfer the propelling energy to wheelchairs.

This result of the autonomous propelling has limitation that only one health subject. The autonomous propelling depends on the body performance, so the well trained and exercised SCI subjects would show the better performance in the autonomous propelling.

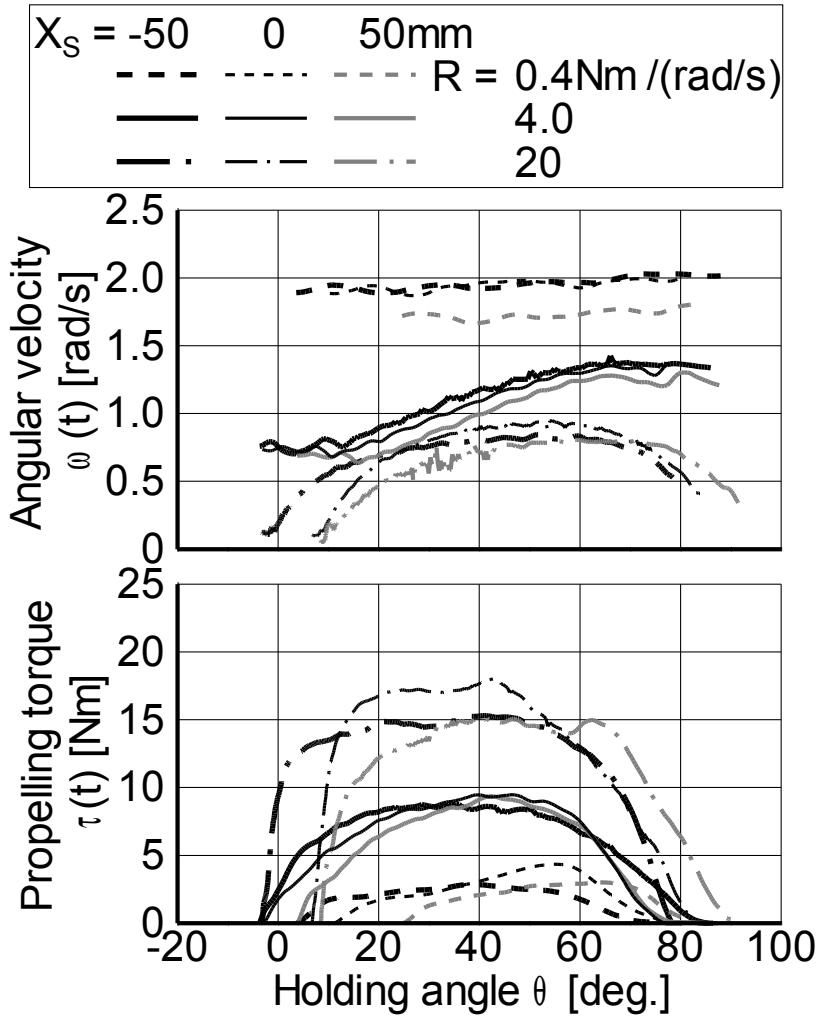

Fig.6 Autonomous propelling against holding angle θ

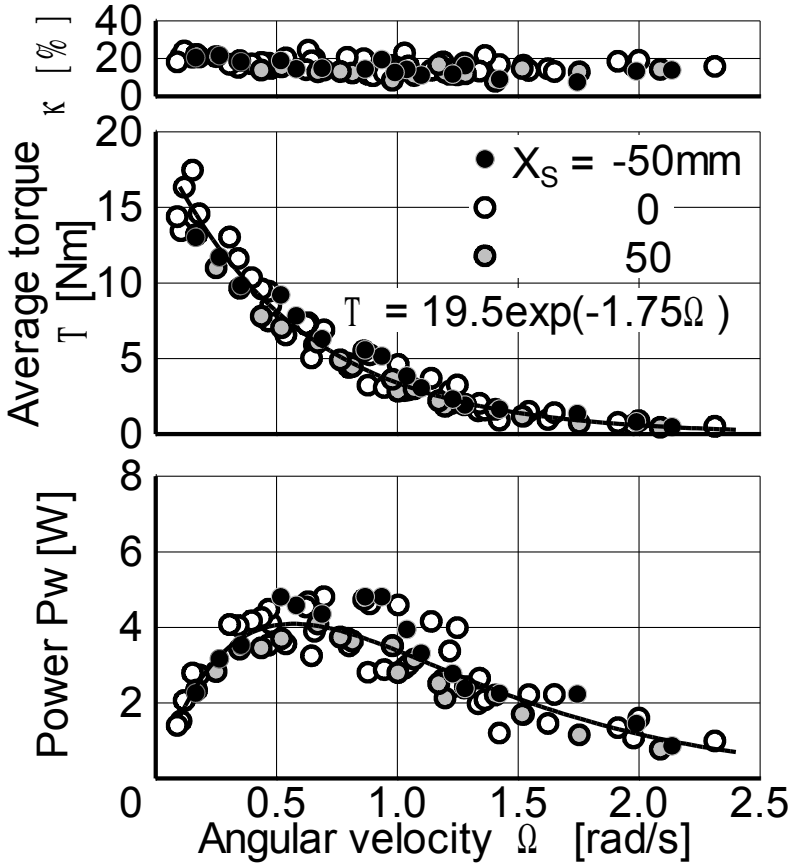

Fig.7 Human self-directive characteristics

Figure 8 shows the time response of indicated propelling. The propelling torques were intermittently exerted by indicated pulses. The figure 8 is one of example from all results, the exerting part of indicated propelling at torque 10Nm and rim angular velocity 2.0rad/s. The dotted line in the graph shows indicated pulse. There are three trajectories; X_S =-50, 0 50. At the condition of X_S=0, there are two trajectories in the different of indicated rim angular velocity 0.5 and 4.0rad/s. The upper part of the graph is the holding angles respective to each conditions lower part of the graph. About the horizontal seat positions, the trajectories of indicated propelling torque were similar, though the subjects used different range of holding angles. But the trajectories of propelling showed the differences against the rim angular velocity. At the low velocity 0.5rad/s, the subject exerted propelling torque along with the indicated pulse, though the delay of rising time occurred. The lag time from the time when pulse indicated, is similar about 0.16s at all conditions. The subject was indicated not to expect next timing of pulses, but to make action for propelling after the pules indicated. In the increase of the rim angular velocity, the time responses at push on were delayed and exerted propelling torque was short time. At the beginning stage of pushing, the subject needs to grasp the rim and exerts the muscle force quickly. This task is very difficult to be done in short time. In opposite, the releasing is relatively easier than the pushing, because the time to relax fingers from grasping is

expected to be shorter than the time of pushing. About the impulse of propelling torque, the impulse the subject transfer to the wheelchair became small at high rim angular velocity 4.0rad/s.

The figure 9 shows the change of impulse of forced propelling torque at the combinations of indicated torque 5, 10, 15Nm and horizontal seat positions X_S = -50, 0 50mm, respective to the rim angular velocity. In the graph, the horizontal dotted line shows indicated impulse 1.5Nms(0.3s x 5Nm), 3.0Nms(0.3s x 10Nm) and 4.5Nms(0.3s x 15Nm). On the low rim angular velocity 0.5rad/s, the exerted impulse of propelling torque was similar to the indicated impulse, but the exerted impulse start to decrease over rim angular velocity 1rad/s. The decreasing ratio of exerted impulse is rapid near Ω=1.0rad, then likely became the same value. At the Ω = 4.0rad/s, the decreased impulse became about 60% of indicated impulse. In another view of horizontal seat positions, the impulses of propelling toque showed the similar decrease along with averaged rim angular velocity. The difference between horizontal seat positions was smaller than the decrease against the rim angular velocity. This is because the task of grasping hand rim and exert propelling torque against rim velocity is the most difficult. The horizontal seat position has effect to the task of propelling, but the human being is good at using their hand with hand's reach even if there is difficult situations.

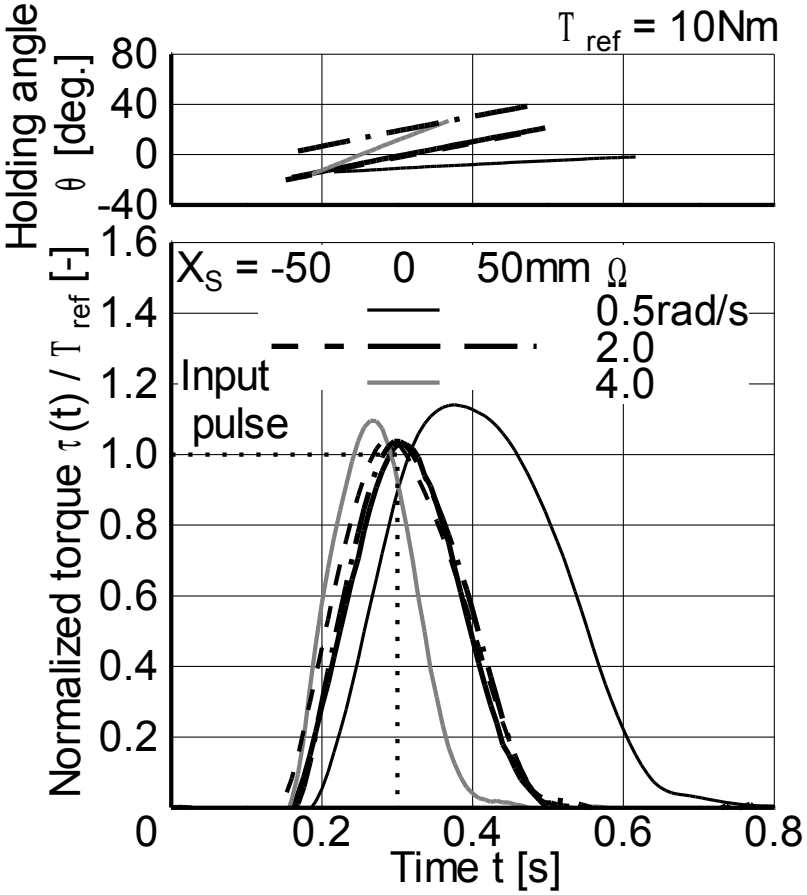

Fig.8 Normalized torque by reference torque

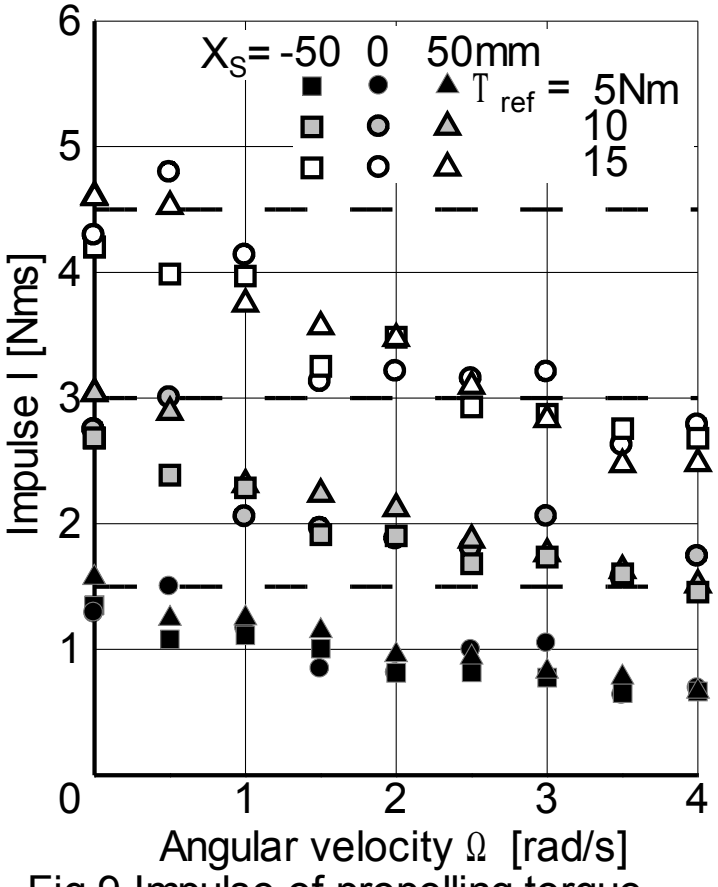

Fig.9 Impulse of propelling torque against pushrim angular velocity

The figure 10 shows the validation of reduction of hardness in propelling by horizontal seat positions. The two type of propelling conditions were tested; indicated velocity in propelling and autonomous propelling. For these validation, the device in the figure 3 was employed with various horizontal position. The road resistance in the device was also set along with horizontal seat positions. At the propelling condition under indicated velocity 2rad/s and 3rad/s, the *EHR* proportionally reduced along with the decrease(backward) of the seat position X_S. At the condition in autonomous propelling, the averaged autonomous velocity of the wheelchair increased along with the backward horizontal position X_S under the same *EHR*. From these validation, the reduction of hardness in propelling decreases proportionally along with the backward position X_S, because the main factor of reduction is the reduction of road resistance by horizontal seat position.

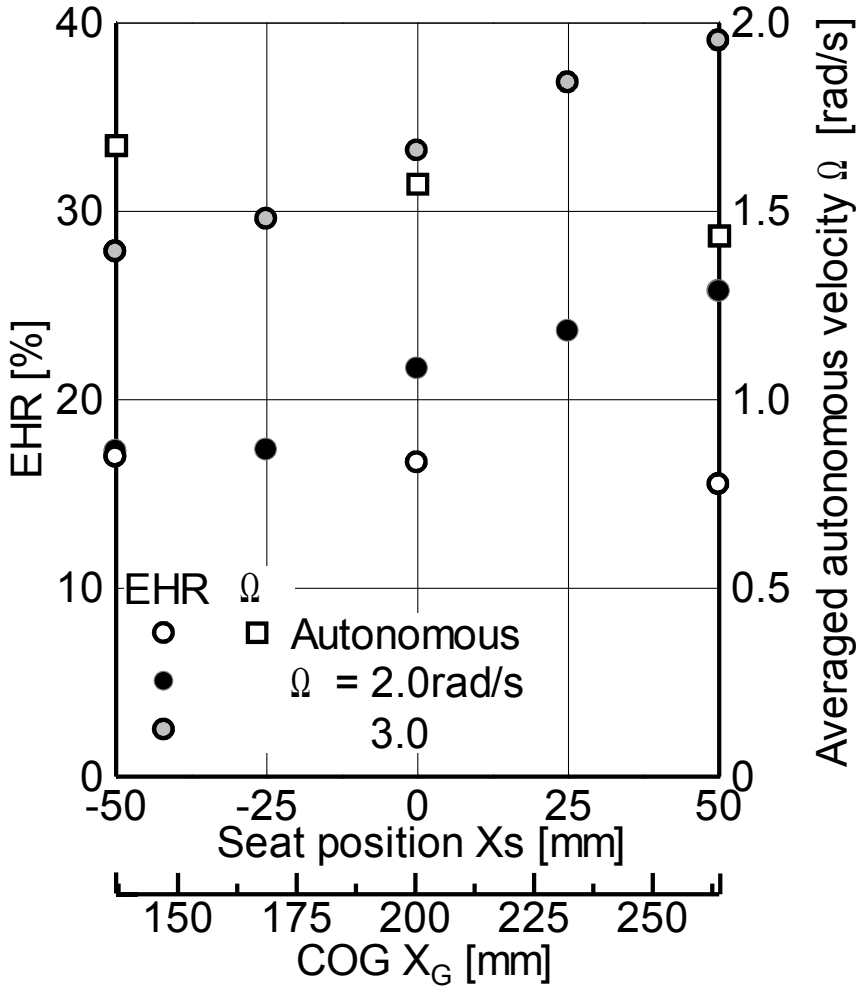

Fig.10 Validation of load reduction by seat positions

Conclusions

This paper focuses on the arrangement in horizontal seat position for better mobility and drivability of wheelchairs. The important factors to determine the mobility and drivability of wheelchairs, are mainly propelling capability and road resistance by horizontal seat position.

The total road resistance of wheelchairs is determined by the normal force N_f and N_r. The backward seat position moves the horizontal position of COG backward, in addition the N_r increase and N_f decrease. The coefficient μ_f at the front polyurethane caster on asphalt surfaces is six times higher than the μ_r at the rear pneumatic wheel, so backward seat position reduce the total road resistance of wheelchairs.

On the investigation of autonomous propelling, the autonomous propelling in backward position X_S=-50 and standard X_S=0 was the same and small higher than the propelling capability at forward position X_S=50. And the hardness in propelling based on the *EHR* was similar in all seat positions. This means that the autonomous propelling in the backward seat position is better than in the forward position. Also there is the effective propelling velocity to transfer the propelling energy to wheelchairs. On the indicated propelling investigation, the difference between horizontal seat positions was smaller than the decrease against the rim angular velocity. This is because the task of grasping hand rim and exert propelling torque against rim velocity is the most difficult. The horizontal seat position has effect to the task of propelling, but the human being is good at using their hand with hand's reach even if there is difficult situations.

From the validation of the total effect of horizontal seat positions, the reduction of hardness in propelling decreases proportionally along with the backward seat position X_S, because the road resistance of wheelchairs is reduced by backward horizontal seat position. Finally, the factors to determine the wheelchair mobility and drivability by horizontal seat positions, are the COG position and the angular velocity of hand rims. The angular velocity cannot be fixed at constant, so only effective factor to be able to adjust is the backward COG position, which reduces the resistance force at the front caster effectively.

References

[1]Asahara, S., Yamamoto, A., Method for the Determination of Center of Gravity during Manual Wheelchair Propulsion in Different Axle Positions, J. Phys. Ther. Sci., Vol. 19(2007), pp57-63

[2]Brubaker, C.E., Wheelchair prescription: analysis of factors that affect mobility and performance, Journal of Rehabilitation Research and Development Vol. 23, No. 4, pp19-26, 1986

[3]Boninger, M. L., Baldwin, M., Cooper, R. A., Koontz, A., Chan, L., Manual Wheelchair Pushrim Biomechanics and Axle Position, Arch Phys Med Rehabil, Vol. 81(2000), pp 608-613

[4]Van der Woude LHV, Veeger DJ, Rozendal RH, Sargeant TJ, Seat height in handrim wheelchair propulsion, Journal of Rehabilitation Research and Development Vol. 16, pp31-50, 1992

[5] Wei, S., Huang, S., Jiang, C., Chiu, J., Wrist kinematic characterization of wheelchair propulsion in various seating positions: implication to wrist pain, Clinical Biomechanics, Vol. 18, No. 6 (2003), pp S46-S52

[6]Masse, L. C., Lamontagne, M., O'Riain, M.D., Biomechanical analysis of wheelchair propulsion for various seating positions, Journal of Rehabilitation Research, Vol. 29, No. 3(1992), pp12-18

[7]Mulroy, S.J., Newsam, C. J., Gutierrez, D. D., Requejo, P., Gronley, J. K., Haubert, L. L., Perry, J., Effect of Fore-Aft Seat Position on Shoulder Demands During Wheelchair Propulsion: Part 1. A Kinetic Analysis, The journal of Spinal Cord Medicine, Vol. 28, No. 3(2005), pp 214-221

[8]Richter, W.M., The effect of seat position on manual wheelchair propulsion biomechanics: a quasi-static model-based approach, Medical Engineering & Physics, Vol. 23 (2001), pp707-712

[9]Sasaki, M., Iwai, T., Obinata, G., Miyazaki, K., Miura, H., Shimada, Y., Kiguchi, K., Analysis of Wheelchair Propulsion and Hand Force Pattern Based on Manipulation Ability of the Upper Limb, Transaction of the Japan Society of Mechanical Engineers, Series C, Vol. 74, No. 732(2007), pp2279-2286 (in Japanese)

[10]Borg, G, Perceived Exertion as an indicator of somatic stress, Scandinavian journal of Rehabilitation Medicine 1970, 2(2), 92-98

[11]Karvonen M. et al. The effect of training on heart rate. A longitudinal study. Ann Med Exp Biol Fenn Vol. 35, pp307-315

B. Autonomous hand cranking

Introduction

Hand-cranking devices have been developed over the last 20 years (1). Hand-cranking offers an alternative form of propelling a wheelchair from the more traditional handrim propulsion. Hand-cranking has been shown to be more efficient than handrim propulsion(2,3). This could mean a reduction in upper limb injury for manual wheelchair users. Therefore, hand-cranking devices have increased in popularity both as a means of wheelchair propulsion and also as a means of keeping fit.

Hand-cranking systems form part of commercially available hand-cycling systems, or which there are two main types currently on the market; one is a 'detachable type' for daily use and the other is a 'recumbent' sports type, which is popular for sports activity. The detachable type consists of a pair of cranking handles, a driving chain with sprockets, reduction gears and a driving wheel. The unit can firmly attach and easily detach to the frame of wheelchair. It attaches to the wheelchair by raising the front casters; therefore, there are three contact points with the ground: the two rear wheels and the front wheel of the handcycle unit. In order to power the wheelchair the user simultaneously cranks with both arms, this power is transmitted to the wheels via reduction gears, at the same time the user steers the front wheel. So the front wheel of a handcycle unit has two functions; to drive and steer the wheelchair. The direction of the front wheel is fixed by the user's arms, and the front wheel has self aligning torque, which allows handcycles to give stable driving conditions over 4.5m/s. Therefore it is better suited for longer and faster journeys than traditional handrim propulsion. Many wheelchair users have begun to use a handcycle device for longer journeys, then detach the handcycle unit and use their handrims to get about indoors.

As handcycle users use the system for journeys which take a long time and are far away the vast majority of handcycling occurs under sub-maximal and steady cranking condition. This period excludes starting and stopping. Under sub-maximal conditions, the users autonomously regulate their own cranking torque and angular velocity against road resistance to continue cranking without fatigue based on user's cranking performance.

Autonomous cranking is a repetitive process and so repetitive loads are put on the shoulder and elbow joints. Repetitive loads have been linked to chronic pain in the shoulder and elbow joints(4). The risk of injury of the upper limbs for manual wheelchair users is particularly debilitating as it can leave them without a form of independent mobility. The first step in preventing injury to the shoulder and elbow joints is to

understand their performance during autonomous steady cranking. The angle, angular velocity and torque on each joint are important measures to investigate joint functions. From the view of mechanical engineering, the mechanical power on each joint also gives important index of hardness. Also, the gear ratio of handcycles should be properly designed according to the individual performance on autonomous cranking for the prevention of joint injuries.

In the previous studies related to arm cranking, the common purposes are to investigate effective cranking conditions. Power(5) investigated the effects of increasing work ratio and speed of movement on efficiency during steady-state arm crank ergometry. Goosey-Tolfrey(6) carried out investigation of crank length and cadence on mechanical efficiency in hand cycling under fixed cadence. Goosey-Tolfrey found 180mm crank length to be better than 220mm on mechanical efficiency by wheelchair dependent, high performance athletes. These experiments were carried out a recumbent style handcycle with magnetic flow ergo-trainer, which consists of a roller with variable road resistance. Van der Woude(7) also carried out an investigation of mechanical efficiency of handcycling using a motorised treadmill at a constant velocity under the asynchronic and synchronic conditions with varying gear ratios. Van der Woude showed synchronic arm use is more efficient than asynchonic.

There have also been a number of studies in recent years investigating the use of hand cranking for preventing joint injuries. Faupin(8) focused on the kinetic motion of upper extremity while cranking. Faupin showed the maximum and minimum joint angles on shoulder, elbow and wrist by inverse kinematics of 3D simulated cranking motion using an ergometer at 70rpm. Faupin also showed the change of joint angles against upward, downward, forward and backward cranking position.

This paper reports the joint toque and power in the shoulder and elbow under autonomous cranking, which means natural sub-maximal cranking style that can be seen in every-day handcycling. The joint torques are calculated in the sagittal plane by inverse analysis of the cranking torque and angular velocity. The model assumes the upper extremity to be massless and the shoulder to be fixed during cycling. The condition of autonomous cranking for experiments was made by a motorised cranking device. The cranking device can detect cranking torque, position and angular velocity. The angular velocity was controlled by simulated road resistance and mass of handcycle according to a simple model of handcycling, which is described in section 2. Also this device can change crank length and crank centre position. This paper focus on non-athlete cranking and subjects are all healthy, non-wheelchair users.

Shoulder and elbow joint power are calculated throughout the cranking cycle. Joint power is seen as a measure of how hard the joint has to work as it represents the rate of energy production. By knowing where the peaks occur in the power curves, mechanical

solutions can be developed to reduce these peaks, which in turn would reduce the hardness of the task on the wheelchair user. The results of this study can also be used to help inform correct cranking position for individuals.

Planar model of handcycles

In order to measure autonomous cranking performance, a model must be developed of handcycling. The purpose of this model is to understand the motion of the wheelchair given the input torque by the user into the handcycling system and the resistive loads which act on a wheelchairs motion. This model is then used to control the motorised crank angular velocity based on the input torque. This model is developed in the plane of motion (sagittal plane) and so is 2-dimentional as this paper focuses on only straight driving. The planar model of the handcycle is shown in Figure 1 (a). The input cranking torque $\tau(t)$, generated by the person driving the handcycle is transferred via a hand crank on the top of handcycle unit. The crank sprocket, which rotates with the hand crank, transfers cranking torque to the drive sprocket with reduction ratio β via the driving chain. The driving torque transferred by the drive sprocket is converted to the driving force $f(t)$ by the wheel radius R_W. In this paper, the handcycle's mass is assumed to be a concentrated mass. The total mass including the wheelchair, handcycle unit and driver are defined as M. The velocity $v(t)$ of the handcycle is found by solving the resulting differential Eq.(1) from the planar model shown in Figure 1 (a)

$$M\frac{dv(t)}{dt} = f(t) - Rv(t) \tag{1}$$

In Eq. (1), $Rv(t)$ is the ideal resistance force of the front and rear wheels, R is the ideal rolling coefficient, $f(t)$ is the force applied by the wheelchair user, M is the wheelchair system mass and $dv(t)/dt$ is the acceleration of the system.

The block diagram of the handcycle model is shown in Figure Figure 1(b). In the block diagram, the road resistance acts as the load torque, and this is described at the summing point of $\tau(t)/\beta$ and $R_W Rv(t)$. The whole transfer function $G_H(s)$ of input $\tau(t)$ and output $v(t)$ is shown in Eq.(2), below.

$$G_H = \frac{\Omega(s)}{\mathrm{T}(s)} = \frac{1}{R_W^2(Ms+R)} = \frac{K}{Ts+1} \tag{2}$$

Here, $T = M/R$, and $K = 1/RR_W^2$. With the transfer function $G_H(s)$ of Eq.(2), the motorised cranking device can simulate the results of changes to handcycle mass, road resistance, gear ratio and front wheel radius on the torque and angular velocity during autonomous cranking. The parameter $1/K$ describes the total load torque at the crank handle.

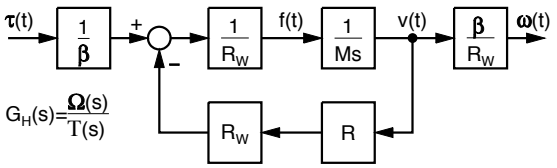

(b) Block diagram of modeled handcycles

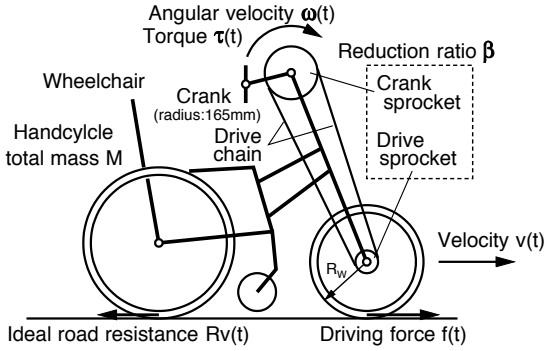

(a) Planar model of handcycles

Figure 1 Planar model of handcycles

Experimental system

Figure 2 shows the experimental system to measure autonomous cranking performance. The crank can only be cranked using the subject's right arm; there is no left side crank. Subjects sit on the chair with a 90-degree back. The crank centre is fixed on a pillar directly in front of the chair. Horizontal and vertical positions of the centre of the crank can be adjusted by the horizontal and vertical position of the chair. The crank length is adjustable, but only one length (165mm) was tested. This is the same length as a commercially available handcycle system. The grip of the crank arm is vertical in nature, which is the same style as the handcycles. The crank has a counter weight on the left-hand side to counter the weight of the crank handle. The torque meter set between the crank and the motor detects the cranking torque of the subjects and the rotary encoder detects the crank angle and angular velocity of crank rotation. The zero position of the crank angle α(t) is made when the crank handle is in the horizontal plane and the end of the crank arm is nearest the subject . The rotation of crank is clockwise, i.e. away from the subject, as it would be in every-day hand cycling.

The motor rotates the crank handle according to the output of the transfer function $G_H(s)$. $G_H(s)$ simulates the various conditions of handcycles including the handcycle mass itself; the device can simulates inertia of mass in cranking. For example, the cranking is heavier at the start, then as the velocity increases, which causes the crank to save kinetic energy and thus have inertial rotation of the crank increases, the cranking will become less heavy.

How hard subjects found hand-cranking ('hardness' of cranking) is measured using the Exercising Heart Rate (*EHR*), which is based on Borg's Perceived Rate of Exertion Scale(9). The *EHR* shows subjective hardness of cranking based on the individual performance of each subject. The *EHR* is calculated using by attaching a heart rate monitor to the chest of subjects, and detecting the R-R intervals. Then the heart rate ratio was calculated by time, and the *EHR* was solved using Eq. (3)(10).

$$EHR = \frac{HR - HR_{REST}}{HR_{MAX} - HR_{REST}} \tag{3}$$

The maximum heart rate is determined by simply deducting a subject's age from 220(11).

The joints, which contribute to cranking, are the shoulder and the elbow in planar motion i.e. when cranking in a straight line. Both joint torques were estimated with a planar massless two link arm model, shown in Figure 2. The two link arm model did not include the wrist joint, because the torque in the wrist joint was expected to be very smaller than the torque in the shoulder and the elbow. The grip bars allow rotating

respective to the sagittal plane, so that the wrist joint keeps a constant angle. When cranking is relatively slow and the subject's hands are fixed to the grip, the effect of upper arm and forearm mass, both become negligible. The shoulder position is assumed as fixed at one point and to be a rotational joint in the sagittal plane. The cranking position detected from the rotational sensor gives the wrist position. According to the upper arm model shown in Figure 2, the elbow position can be solved by simple geometry. In addition, the elbow angle is constrained due to it being a hinge joint and therefore must be from 0 to 150°. The shoulder and elbow torque are calculated using Eq. (4) and (5). These equations are formulated based on the assumptions stated above and where τ_1 is the torque at the shoulder and τ_2 is the torque at the elbow.

$$\tau_1 = \frac{\tau(t)}{R_C} L_1 \sin(\alpha + \theta_1) + \tau_2 \tag{4}$$

$$\tau_2 = \frac{\tau(t)}{R_C} L_2 \sin\{\alpha + (\theta_1 + \theta_2)\} \tag{5}$$

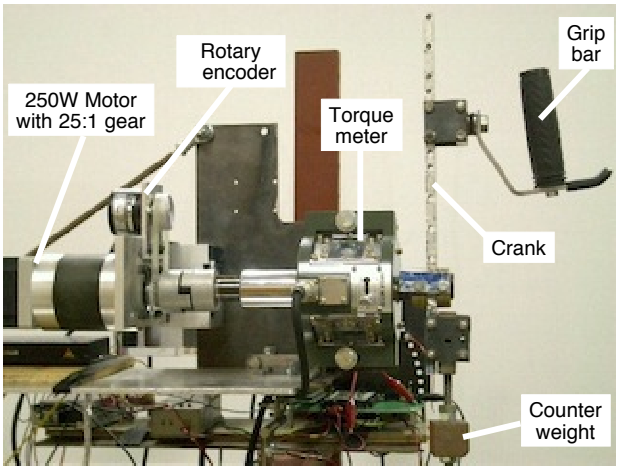

(b) Front view of experimental device

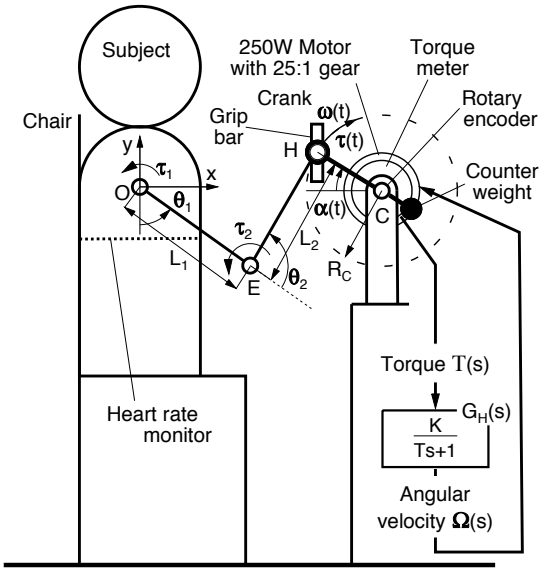

(a) Planar model of cranking and signal flow

Figure 2 Experimental device for hand cranking

Methodology of experiments

Prior to the trials, the seat position for all subjects was adjusted mid of maximum and minimum rotation from the adjustable range of the German made detachable handcycle. Determined seat position is assumed as normalised shoulder position, which is the same position normalised by the arm length of each subject. The normalised distance between the crank centre and the shoulder position was 0.61 in all subjects. The arm length for normalisation is used the length from shoulder to centre of the wrist. Each subject before each trial sat on the seat and was asked to relax, then the experiments started by an audible signal. In advance, the subjects were instructed how best to crank in natural style for a long time. Also the subjects were instructed to crank with their backs against the back of the chair. This prevents them from using trunk muscles, so that the cranking situation is more representative of patients with a spinal cord injury who do not have trunk control. The cranking of the device was done using only the right hand and the left hand was put on the knee during the trials. The cranking direction is clockwise from right side of view, and thus the same direction as hand cycling. After the subject starts cranking, the torque sensor detects the cranking torque, then the transfer function $G_H(s)$ simulates the physical movement of the handcycle, it calculates the velocity $v(t)$ and indicates $v(t)$ to the driving motor. The motor, which provides the power to rotate the crank with simulated inertia and resistance, is a 250W DC motor. While cranking, the subject regulates the crank torque against the angular velocity $\omega(t)$ of the crank according to each subject's physical performance. To prevent from fatigue and the decrease in concentration to the trials, each trial lasted 3 minutes, then each subject rested for about 10 minutes until their heart rate returned to what it had been at rest. Data recording for this study started after 2 minutes 30 seconds had passed from the start of each trial. We confirmed the cranking condition and heart rate in all subjects were almost constant after 3 minutes passed, in the prior trial with 15 minutes. After this time each participant had achieved a state of steady cranking. The experiment was carried out with seven different resistances ($1/K$): 0.24, 0.60, 1.5, 3.2, 7.0, 15, 37Nms/rad. The resistance coefficient 1/K was randomly set before each trial. The gain K of the transfer function $G_H(s)$ was set as 1 and the time constant T was set as 1s, because the $G_H(s)$ also works as low-pass filter to smooth rotation of the motorised crank.

All subjects were trained on real handcycles with the same crank position prior to all trials. Subject details are shown in Table 1. All subjects were healthy and had no previous history of muscle injury to the upper limbs or back. The dominant hand of all subjects is the right side.

In advance of the trials, the details of the study were explained to each participant and

they were asked if they had any questions, before they agreed to take part. Participants were told the experiment could be stopped at any time and were instructed to inform the experimenter if they became ill or fatigued. The maximum time of experiments for each subject in the same day was limited to three hours.

Table 1 Specification of participants

Participants	A	B	C
Height [cm]	161	169	172
Weight [kg]	55	66	56
Age	21	20	20
Upper arm length L_1 [mm]	255	210	280
Fore arm length L_2 [mm]	310	315	320
Shoulder position O(x, y) [mm]	(328, 97)	(305, 90)	(349, 103)
Maximum around upper arm [mm]	286	261	245
Maximum around fore arm [mm]	251	260	250
Body fat percentage [%]	25	17	10
Grip force (right side) [N]	304	392	431
Rest heart rate [bpm]	70	63	66
Sports activity	Rarely	Occasionally	Often

Results

Figure 3 represents the time behavior of the crank torque $\tau(t)$ and angular velocity $\omega(t)$ for $1/K$=37 and 3.2Nms/rad. A full crank cycle is occurs when the crank arm rotates through 360°. When the resistance was high ($1/K$=37Nms/rad), all subjects produced higher values of torque throughout the first half of the crank cycle. However, in the second half of the cycle, the torque was reduced noticeably with a minimum occurring at approximately 270°. After the experiment each subject said they had difficulty applying torque to the crank at its lowest position i.e. at around 270°. The Angular velocity is very slow at around 0.2m/s, and there is deviation caused by perturbation of the cranking torque. The resistance coefficient $1/K$ of load torque is high at $1/K$=37Nms/rad, so the subject had to exert a high torque in order to crank against this load torque. Subject A was weaker than the other subjects, causing their cranking torque and angular velocity to be lower than the results for the other subjects.

On the relatively lower load resistance of $1/K$=3.2Nms/rad, the cranking torque became lower and the cranking velocity became higher than the previous high load condition. In this condition, the cranking has inertia rotation, so the subjects don't need to generate vigorous cranking torque. With this low resistance setting it can be seen that there is a relatively large cranking torque is from crank position 0 to 250° and the period was wider than the period at large $1/K$. However, the cranking torques in subject A were nearly constant against the crank angle, though subject A's torque curves in other conditions $1/K$ showed similar tendency in $1/K$=37Nms/rad.

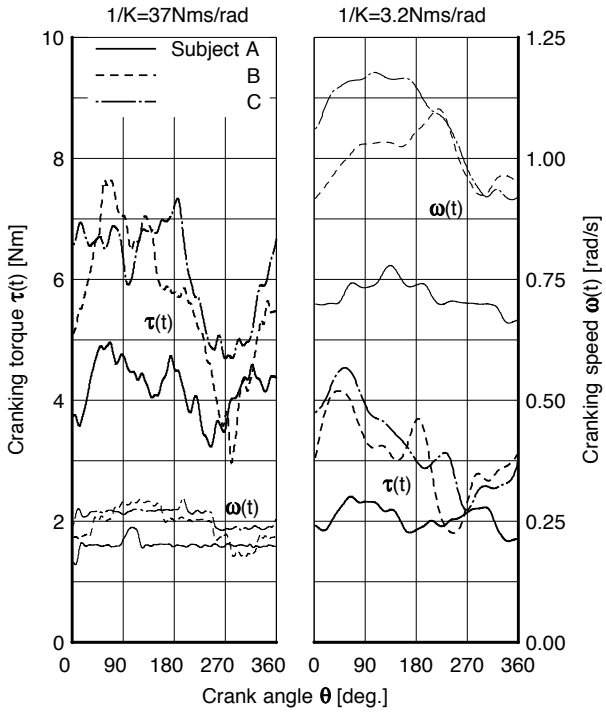

Figure 3 Time responses against crank angle

Figure 4 shows the stick picture of cranking posture with estimated elbow positions, which have been solved using geometry. The rotating task was achieved using the possible joint angle orientations of the shoulder and elbow. Both joints periodically collaborate to carry out the cranking task. From this stick picture, there are flexion and extension motions on both shoulder and elbow joints. Figure 5 shows the detailed functions on both joints. Figure 5(a) shows example joint angle, angular velocity and joint torque (estimated using Eq. (4) curves for the shoulder and elbow. Figure 5(a) shows the case of subject B under the load torque $1/K$=3.2Nms/rad. The overall elbow range of motion was from 48 to 154° and the shoulder range was -23° to 83°. The angular velocity of the elbow, which was calculated from the movement of the elbow position, was from -1.6 to 1.5rad/s, and the range of angular velocity on the shoulder was from -1.5 to 2.9rad/s. The movements of the shoulder and elbow were periodical, which means each joint both flexed and extended. The change point from extension to flexion at the elbow was identified by the change of sign of the angular velocity was at 157°, and the reverse change of direction was at 338°. The changes of rotational direction at the shoulder occurred at 125° and 318°. The range of motion of the joints in subjects A and C were almost the same, despite the lengths of forearm and upper arm being different for each participant.

Both joint torque at the shoulder and elbow were calculated from the measured cranking torque and its position using Eq. (4). The range of shoulder and elbow torque was -10 to 2.8Nm and -6.5 to 5.4Nm respectively. The maximum torque at the shoulder occurred when it was extended, which correlates to the minimum torque applied to the hand crank shown in Figure 5. This point of maximum shoulder torque and minimum hand-cranking torque occurs at which was the point when the hand crank was furthest away from the person. The maximum shoulder torque when in flexion occurred at around 0°; when the hand crank was nearest the shoulder. The maximum elbow torque in extension occurs around crank angle 75° and the torque curve was almost flat around this angle. When in flexion the maximum was around 250° and its shape around this maximum point was a gentle curve.

The joint powers for the shoulder and elbow are shown in Figure 5(b). The joint power produced by both joints show periodical changes during one cranking cycle. This means that each joint works both as a motor and as a brake periodically. The maximum shoulder power appeared at crank angle 187 during concentric motion of shoulder. The minimum shoulder power, which occurs when the shoulder works as brake in eccentric motion, was around crank angle 78°. The maximum elbow torque was 66° and minimum power was at 190°. When the shoulder works as a motor, the elbow works as a brake, this occurs at the maximum torque points in one cranking cycle. In the same way when the elbow works as a motor, the shoulder works as a brake. The shape around the maximum point of shoulder

power at 180° shows a sharp rise and drop. The total power at the shoulder and elbow were about twice that of the cranking power. This is because the arm has two degrees of freedom, but the cranking has one degree of freedom, so there is redundancy. The efficiency, which is defined as cranking power divided by total joint power, was almost 0.5% on one cranking cycle.

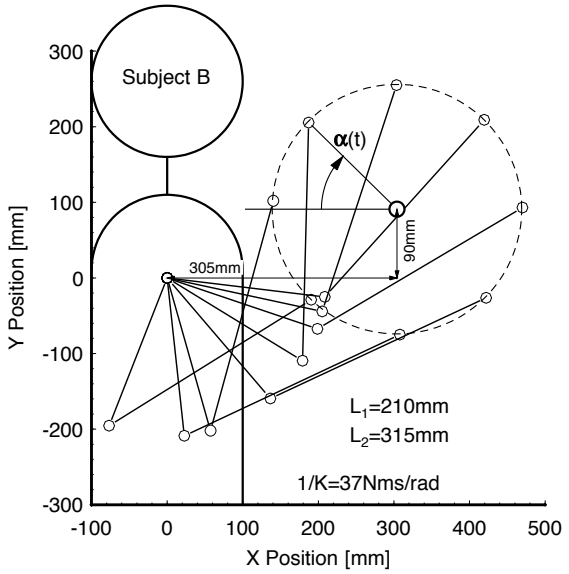

Figure 4 Stick figure of cranking behaviour

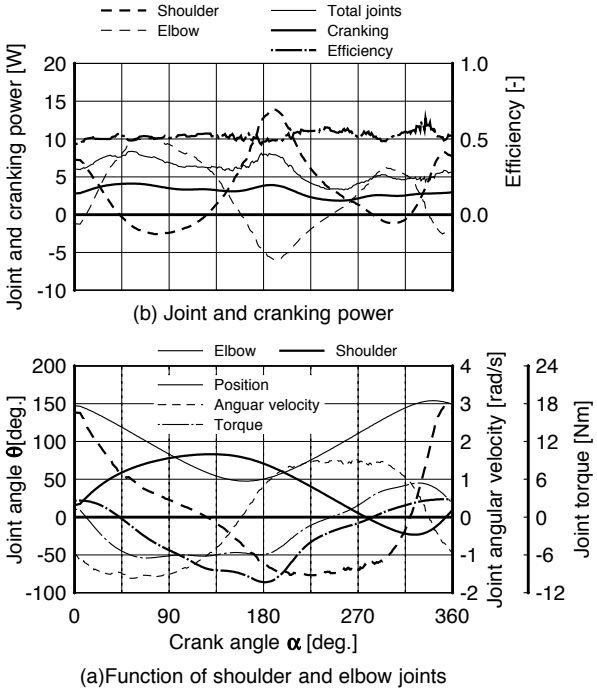

Figure 5 Joint functions at 1/K=3.2Nm/rad
(Subject B's case)

The autonomous cranking torque is shown in Figure 6(a). Averaged cranking torque T and angular velocity Ω were calculated from one cranking cycle shown in Figure 5. The

cranking torque of all subjects has the same tendency: high torque was exerted against high load torque and the cranking torque proportionally decreased along with the decrease of load torque. The dotted lines are estimated lines for each subject with a simple straight line. In these experiments, subject C produced the largest torque (6.5Nm) at the maximum load coefficient $1/K$=37Nms/rad, and subject A produced the minimum torque (3.7Nm).

The *EHR* of all subjects are shown in Figure 6(a). The *EHR* shows subjective exercise intensity, for example, *EHR*=0%: Nothing at all, 10%: Very easy and 20%: Easy. The *EHR* for all subjects is lower than 10%, which means that the autonomous cranking task was a relatively easy task physiologically for all subjects. The *EHR* of all subjects increased along with the decrease of load torque from $1/K$=37 to 0.24Nms/rad.

Maximum and minimum torque during one cranking cycle is shown in Figure 6(b). Maximum torque refers to the maximum torque during flexion and minimum torque refers to the maximum extension torque. The shoulder of subject B exerted a maximum extension torque of -19Nm against high load torque. The maximum shoulder extension torque was about four times larger than the maximum flexion torque of 5.1Nm. At the elbow, the maximum flexion torque (9.8Nm) and the maximum extension torque (-12Nm) were almost the same in magnitude, though the sign was opposite. The maximum torque during flexion and extension at the shoulder and elbow decreased along with the increase of crank angular velocity Ω, because the autonomous cranking torque T decreased. Although only one subject is shown here the tendencies for maximum flexion and extension torque of the other subjects were similar. The maximum flexion and extension torque for subject A were 4.7Nm and -14Nm at the shoulder and 8.4Nm and -8.7Nm at the elbow. For subject C the maximum flexion and extension torques were 7.5Nm and -22Nm at the shoulder, 9.7Nm and -13Nm at the elbow.

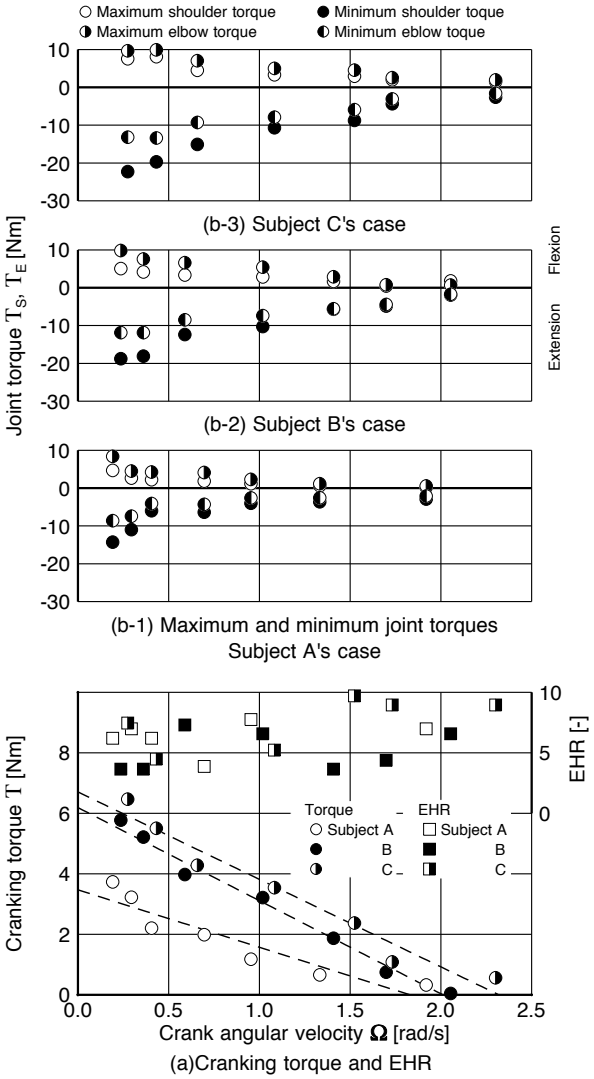

Figure 6 Autonomous cranking

The mechanical power during autonomous cranking for all subjects is shown in Figure 7(a). The maximum cranking power appears around 1.0rad/s for subjects B and C. Subject A's power was the smallest in this experiment. The dotted line shows the calculated power by estimated torque line in the Figure 6(a). The largest maximum power is 3.8W at 1.1rad/s for subject C.

The maximum joint powers when the muscles are eccentrically contracting (lengthening) and when they are concentrically contracting (shortening) are showed in Figure 7(b). Therefore, minimum joint power correlates to maximum eccentric power. The maximum concentric power of the shoulder and elbow were over three times larger than the joints' maximum eccentric power. The concentric maximum shoulder power (13W) occurs when the crank angular velocity is around 1.0rad/s, this coincides with the maximum point of autonomous cranking power. The eccentric maximum power of the shoulder was -3.3W, which is smaller than the concentric power of shoulder. The concentric and eccentric maximum elbow powers were 13W and -5.6W respectively. Again the maximum powers occur with a cranking speed of 1.0rad/s. The maximum

concentric and eccentric power tendencies of subjects C were similar to those shown here for subject B. The maximum concentric and eccentric powers were 4.1W and -0.82W at shoulder (subject A), 4.6W and -1.6W at elbow (subject A), 14W and -2.1W at shoulder (subject C), 12Nm and -3.9Nm at elbow (subject C).

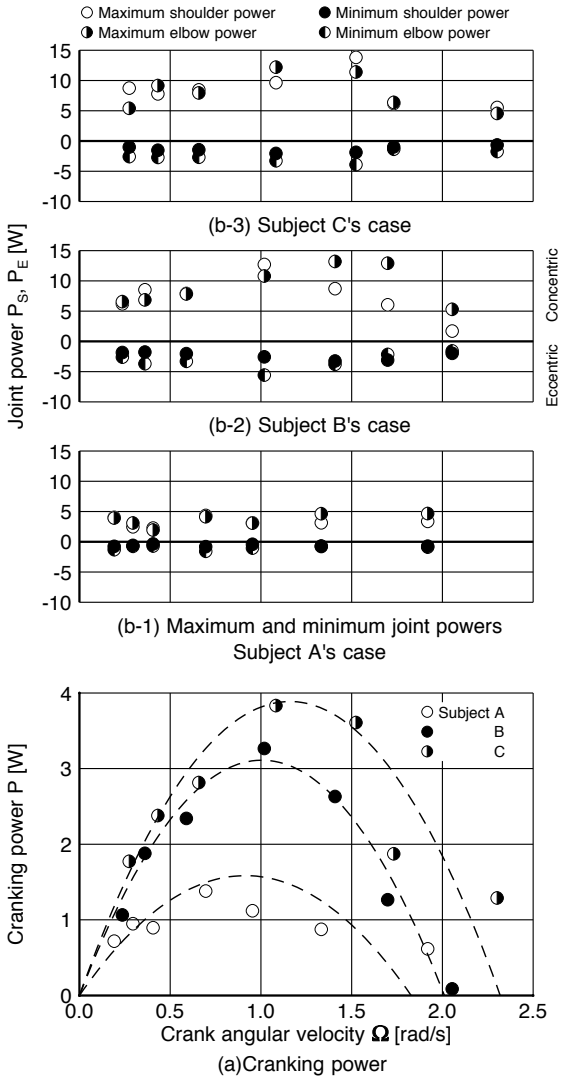

Figure 7 Autonomous cranking power

Discussions

When the cranking position was around 270°, all subjects' torque became lower than each average torque. According to the Bober's investigation(12), the static maximum joint torque depends on its joint angles. The static torque also depends on how much flexion and extension is being applied by the muscles surrounding a joint at any given angle. The main joints to generating cranking torque are the shoulder and the elbow. From Figure 5, it can be seen for subject B that the angular range of the shoulder motion is from -23° to 83° and the elbow range of motion is from 48° to 154°. When the elbow joint goes beyond 90°, the flexor torque decreases steeply as the flexor angle increases. This is one reason for the drop in cranking torque around a crank angle of 270°. A second reason is that the elbow angle ranges from 90°- 100° at around 250° of crank angle (see Figure 4). In this geometry the elbow is unable to generate cranking torque, in other words, only shoulder joint generate cranking torque. This is because the elbow is a hinge joint, which is only capable in this orientation of flexing inwards towards the centre of the crank, or extending away from the centre of the crank.

The cranking performance of subject A is lower than other subjects. Subject A has rarely participated in sports activities and has a small right-hand grip force. Due to their low grip force, it is expected that subject A is generally less strong than the other subjects. This helps to explain their relatively low levels of performance seen in Figure 6(a) and Figure 7(a). In these figures the cranking torque and power of subject A is lower than the performance of other subjects. Subject A's *EHR*, see Figure 6(a), showed similar levels compared with the other subject's *EHR*. Therefore, it can be concluded that subjects regulate the amount if torque applied to the hand-crank in accordance with their overall body performance, which includes their cardiovascular system. This automatic regulation, referred to as 'autonomous cranking' is very important as it allows people to travel long distances without tiring excessively. Overuse injury occurs due to the effects of repetitive force, leading to micro-trauma in the muscles, which in turn triggers the inflammatory process and results in swelling and pain(4). In this report, cranking is identified as a repetitive task, which is powered by the elbow and shoulder joints, therefore these joint were the focus of this study. The maximum torque in flexion and extension, and maximum power on each joint are important. Figure 6(b) and Figure 7(b) show the maximum joint function during autonomous cranking. It can be seen in Figure 5, 6(b) and 7(b), that the shoulder is working very hard when the cranking angle is at 180°. This is because the hand position is furthest away from the shoulder. Also, the elbow is very weak over 100° of flexion angle, which results in increased work done by the elbow from cranking position 270° to 70°. Previous studies, have not documented the maximum joint torque and power

in this repetitive task. This study has shown that during hand cranking both joints must work hard at different angles and this may explain why some users of hand cycles complain of shoulder pain sometimes. There are two relatively simple ways to reduce the maximum power needed to be produced by the shoulder and elbow during hand cranking; adjust the cranking position, and the cranking length. A further way would be to ensure the correct setting of the gear ratio for each person. Larger crank length gives a longer lever arm, which allows for higher torque generation, but the amount of exercise necessary would increase. Therefore, it may be difficult for people who are less fit. However, it has been shown that for those who are fit a longer crank arm increases mechanical efficiency. Conversely a smaller crank is better for increasing heart-rate, and so better for those trying to get more aerobically fit, but it is more difficult to generate crank rotation with. The effect of these adjustments in relation to the torque produced by the shoulder and elbow needs further investigation in future studies.

In this paper, there are some limitations, which are stated here: 1) Only on length of crank (165mm) is used in this study. The measurement of autonomous cranking performance with other crank lengths should be investigated to determine the effect of crank length and crank centre position on performance. 2) The model used by this study did not include wrist joint because of simplicity. The investigation by a three-link model with masses is needed in future studies. 3) This study did not measure maximum voluntary force, because the cranking task is dynamic, it is difficult to measure eccentric and concentric performance of the shoulder and elbow joints. However, this should be done in future studies 4) The subjects were all young healthy males and a larger and more diverse subject set is needed in future studies. 5) Subjects were instructed not to use their trunk muscle to lean forward, however, it is small movements were detected during the study, which were unable to be quantified.

Conclusions

This paper has successfully demonstrated that the designed hand cranking system can be used to measure the load on the shoulder and elbow joints under different load conditions during autonomous cranking. From the results it can be seen that subjects regulate their own autonomous cranking performance according to their body performance and subjective exercising heart rate. The largest maximum power produced was 3.8W at 1.1rad/s by the subject who regularly participates in sports activity. The shoulder is working very hard at a cranking angle of 180°. This is because the hand position on the tip of crank is furthest from the shoulder. Also, the elbow is very weak over 100° flexion angle, so the elbow is working at its hardest between a cranking angle of 270° and 70°. Adjusting the cranking position and cranking length would reduce the repetitive maximum power on the shoulder and elbow. The proper setting of gear ratio for individual performances also would reduce overuse injury on shoulder and elbow. When the cranking position was around 270°, all subjects' torque became lower than each average torque.

References

[1]Nag,P.K., Malvankar,M.G., Pradhan,C.K., Chatterjee,S.K., Panikar,J.T., Performance evaluation of lower extremity disabled people with reference to hand-cranked tricycle propulsion, Appl. Ergon., Vol. 13 (1982), pp171-176

[2]Glaser,R.M., Sawka,M.N., Brune,M.F., Wilde,S.W., Physiological responses to maximal effort wheelchair and arm crank ergometry., J. Appl. Physiol., Vol. 48 (1980), pp1060-1064

[3]Troop,H., Samuelsson,K., Jorfeldt, L., Power output for wheelchair driving on a treadmill compared with arm crank ergometry, J. Sports Med., Vol. 31 (1997), pp41-44

[4]Herring SA, Nilson KL, Introduction to overuse injuries, Clin Sports Med, Vol. 6 (1987), pp225-239

[5]Powers,S.K., Beadle, R.E., Mangum,M., Exercise efficiency during arm ergometry: effect of speed and work rate, J. Appl. Physiol., Vol. 56 (1984), pp495-499

[6]Woude,L.H.V. van der, Bosmans,I., Bervoets,B., Veeger,H.E.J., Handcycling: different modes and gear ratios, J. Med. Eng. and Tech., Vol. 24 (2000), pp242-249

[7]Goosey-Tolfrey, V. L., Alfano, H., Fowler, N., The influence of crank length and cadence on mechanical efficiency in hand cycling, Eur J Appl Physiol, Vol. 102 (2008), pp189-194

[8]Faupin, A., Gorce, P., The effects of crank adjustments on handbike propulsion: A kinematic model approach, Int J Ind Ergo, Vol. 38 (2008), pp577-583

[9]Borg, G, Perceived Exertion as an indicator of somatic stress, Scandinavian journal of Rehabilitation Medicine Vol. 2, No. 2 (1970), pp92-98

[10]Karvonen, M., Kentala, K., and Mustala, O., The effects of training heart rate: A longitudinal study, Annals of Medicine and Experimental Biology Fenn Vol. 35 (1957), pp307-315

[11]Fox, S.M., Naughton, J.P., Haskell, W.L., Physical activity and the prevention of coronary heart disease, Ann Clin Res., Vol. 3 (1971), pp404–443

[12]Bober, T., B. Pietraszewski, et al, Predictive torque equations for joints of the extremities." Acta of Bioengineering and Biomechanics Vol. 4, No. 2 (2002), pp49 - 60

Acknowledgements

I would like to thank the following people without whom this thesis would never have been written, and also the process would not have been as much fun.

Firstly to Former Professor Hironobu Uchiyama, whose enthusiasm, guidance and support throughout my research activities with Kansai University have been incredible, especially given the numerous other commitments he has had during this time. In particular I would like to thank him for giving me the space, time and devices to develop my research topics, but also for providing many advices to shape this thesis.

I have also received invaluable help from a number of academic staff and student at Kansai University(KU). I would like to thank Professor Hideo Utsuno for his much valued advices and patience in improving this thesis to be understandable more clearly. I would like to thank Professor Kentarou Kotani, and Professor Hiroshi Tani, for providing valuable suggestions to this thesis and presentation carefully at the final stage. Also I would like to thank Associate Professor Junichi Kurata and Yoshihiro Murakami for supporting my research activities in KU, as well as to thank many talented previous Msc and Bsc students who joined and helped research projects in this thesis.

A great thank you must also go to Professor Nick Tyler, Catherine Holloway and Derrick Boampong at University College London(UCL), who helped significantly in the experiments with the attendant propelled wheelchair in longitudinal slopes at the Pedestrian Accessibility Movement Environment Laboratory(PAMELA), and in the development of the powered attendant propelled wheelchair while I stayed at UCL for one year from October 2011 by overseas research scholars programme in Maizuru National College of Technology(MNCT).

The experiments in this thesis would not have been possible without the fantastic support I have received from many previous Msc and Bsc students at KU, and the staff at PAMELA, Derrick Boampong, Harry Rostron and Kim Morgan. Their time, effort and ideas got me through some problems-thanks you very much. I'd also like to thank factory staffs at KU and Ian Seaton at UCL for their help in manufacturing the components that I needed, often at incredibly short notice.

I also owe a big debt of gratitude to my colleagues and friends from MNCT. I had a great pleasure to work with you all. A special mention must be given to staffs at Department of Mechanical Engineering for their friendship and kindness. I had been very lucky to have shared my time with such a lovely and interesting bunch of people at MNCT.

I am also very grateful to all those who took the time to participate in my experiments.

Also, of course to my parents Naoyuki and Kiyoko, who have always supported me in

all my long endeavours.

And finally to Ayako, for the numerous sacrifices she has made to help me produce this. Thank you.